

UNIVERSIDADE FEDERAL DE OURO PRETO - ESCOLA DE MINAS  
DEPARTAMENTO DE ENGENHARIA CIVIL  
PROGRAMA DE PÓS-GRADUAÇÃO EM ENGENHARIA CIVIL

**QUALITATIVE INVESTIGATION OF THE PERFORMANCE OF A  
STRUCTURAL MEMBRANE ROOF PROJECT**

**PHD THESIS IN CIVIL ENGINEERING**

Area of study: steel construction

Author

Eliana Ferreira Nunes

Advisers

Prof. Dr. João Batista Marques de Sousa Junior

Prof. Dr. Bernd Baier

Co-adviser

Prof<sup>a</sup> Dra. Arlene Maria Sarmanho Freitas

Ouro Preto, October 2012.

N972q

Nunes, Eliana Ferreira.

Qualitative investigation of the performance of a structural membrane roof project [manuscrito] / Eliana Ferreira Nunes - 2012.

241f.: il. color.; grafs.; tabs.

Orientadores: Prof. Dr. João Batista Marques de Sousa Júnior.

Prof. Dr. Bernd Baier.

Coorientadora: Prof<sup>a</sup> Dr<sup>a</sup> Arlene Maria Sarmanho Freitas.

Tese (Doutorado) - Universidade Federal de Ouro Preto. Escola de Minas. Departamento de Engenharia Civil. Programa de Pós Graduação em Engenharia Civil.

Área de concentração: Construção Metálica.

1. Metallic structures - Teses. 2. Structural membranes - Teses.  
3. Structural optimization - Teses. 4. Performance strategies - Teses.

I. Universidade Federal de Ouro Preto. II. Título.

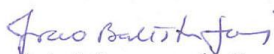
CDU: 624.014:624.074

Catálogo: sisbin@sisbin.ufop.br

# INVESTIGAÇÃO QUALITATIVA DA EFICIÊNCIA DE UM PROJETO DE COBERTURA EM MEMBRANA ESTRUTURAL

**AUTORA: ELIANA FERREIRA NUNES**

Esta tese foi apresentada em sessão pública e aprovada em 16 de outubro de 2012, pela Banca Examinadora composta pelos seguintes membros:



Prof. Dr. João Batista Marques de Sousa Jr. (Orientador / UFOP)



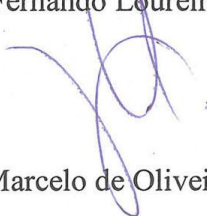
Profa. Dra. Arlene Maria Sarmanho Freias (Orientadora / UFOP)



Prof. Dr. Bernd Baier (Orientador / U.Duisburg-Essen)



Prof. Dr. Luiz Fernando Loureiro Ribeiro (UFOP)



Prof. Dr. Ruy Marcelo de Oliveira Pauletti (USP)



Prof. Dr. Athail Rangel Pulino Filho (UNB)



## ACKNOWLEDGEMENTS

Prof. Dr João Batista, for the opportunity to do this work, for the guidance, great support, confidence and for sharing knowledge about the finite element method.

Prof Dra Arlene, the co-guidance, motivation and support in constructive process studies.

Prof Dr Bernd Baier, the receptivity, the analysis and reflections proposed, guidance, confidence and motivation, and great support throughout the period of the internship abroad, which all went beyond the knowledge and experience transmitted, guiding the refinement of surfaces geometry and analysis.

Dr Reinhold Koenen, the receptivity, the willingness and orientation in numerical and experimental analysis, and for sharing great knowledge and experience.

Mr Klaus Saxe (Essen Labor), for valuable suggestions and support in experimental analysis. Mr Thomas Homm (Essen Labor), for information and suggestions on conducting the material tests.

Dr Baeck, for the receptivity and suggestions.

Dr Henor de Souza (DEARQ) and Dra Katie Novack (DEQUI) for information.

PROPEC coordinators (Pos-graduation program of civil engineering) and Federal University of Ouro Preto (UFOP), for supporting on research development.

Professors Marcílio and Ricardo (UFOP), Prof. Ruy (USP) and Róvia (representative student) for supporting doctoral sandwich selecting process.

Prof. Menkenhagen, head of Department of Civil Engineering University Duisburg-Essen (UDE) and Laboratory for Lightweight structures Essen (Essen Labor), for the receptivity and for providing favorable conditions for the development of this work, as well as resources to experimental tests.

Fapemig, Gorceix Foundation and Capes, for the resources that made it possible for this research to be carried out, including membrane constructive work study, and technical cooperation between the UFOP (Universidade Federal de Ouro Preto) and UDE (University Duisburg-Essen).

COPPE-RJ, on behalf of Vinicius Oliveira, for the kindly assignment of Densalfa software used in this investigation.

Mr Robert Schwetz, Mr Paolo Giugliano, Mr David Holten and Mrs Renate Müller (Mehler Technologies), for receptivity, material data, detailed presentation of material production procedures and assignment for material sample tests.

Mr Harry Buskes (Carpro), for friendship, discussions of system performance criteria, presentation of manufacturing procedure and gentle preparation of materials for tests.

Mr Wolfgang Rudolf-Wittrin (Ceno-tec), for sharing valuable knowledge and experience about the design and manufacturing procedures and presentation of conducted work

Mr Murat Devecioglu, (Verseidag), for the receptivity, material data and for presentation of material production procedures.

Architect Nicolai Kugel, for interview and for sharing valuable work process.

Celio Firmo, for friendship, wisdom, motivation, support and challenging questions.

Dietrich Wischhoff (Tensitex) for friendship, discussions during the development of this work, willingness and for sharing great knowledge and experience.

Architects Siegbert Zanettini and Erika Bataglia (Zanettini Architecture) and Gilberto Gabriel and Gustavo Alves (Ruy Rezende Arquitetura) for great support on carrying out membrane design/ constructive work studies. Engineers Prof Ruy M. Pauletti, Prof<sup>a</sup> Heloísa Maringoni and Nelson Fiedler (Fiedler-Tensoestrutura), for willingness and encouragement to share their work processes, great knowledge and experience.

Construction and Assembly team of Petrobras, especially Rafael Carneiro, João Marcelo Vieira Desirée, Erika Batista; CNC/Consórcio Novo Cenpes team, especially Antônio Passos, Magrini, Henry Mouta and Tarcisio; and Confidere team: especially Marco Antonio Philipe Coutinho, Ozana Viana by trust, for information and support during membrane constructive works studies.

The masters of the air, responsible for the assembly of membrane roofs, for sharing their knowledge and experience.

Patricia and Tatiana, for friendship, and great support translating this work.

Mrs Abigail for revising the Portuguese version of this work.

Carmen, Claudio, Luciana, Andrea and Kislá the great support during this work. Maria Ana, Daniele and Eliane, the affection and great support during membrane constructive work study.

Mrs Pasch, Mrs Monreal, friends Johannes, Kai, Yusuf, Shamila and Somayeh and most especially to Zelina, Jörn, Claudia and Christopher, for the great support during the internship abroad.

And all those somehow supported the development of this work.

Most especially to my dear parents and siblings, for their unconditional, silent and loving support, and God, for enlightening my paths.

## **ABSTRACT**

This paper provides a qualitative investigation about the structural performance of the membranes, surface structures (with double curvature in opposite directions) with minimum thickness and weight, which absorb forces in form of tensile stresses in its own plane, considering two aspects: structural and design procedure. Initially, it involved the analyses of lightweight structure buildings and the observation of constructive work process in membrane roofs. These investigations allowed identifying strategies that contribute to achieve optimum system performance and the challenges encountered along the stages of designing and building. They also guided the qualitative analysis of the performance of a structural membrane roofing project, i.e., a particular situation, as example. This qualitative analysis was developed in two stages, guided by experimental and numerical data. The first stage involved the optimization procedure of the structural system under load action. This analysis showed that the flexible system performance is a result of the three-dimensional stability of the structural system (arrangement and geometry of all components), membrane surface stiffness (membrane geometry), as well as the cooperation of all components in pre-tension state. The second stage comprised the experimental investigation of the membrane material behaviour within the structure context in order to analyze the flattened membrane geometry. Such evaluation enabled to verify the difference between the theoretical model (shape of equilibrium) and the actual shape (consisting of flat panels), enabling the proper adjustment of the surface geometry so that the final shape can reveal not only the path of the forces, but also the best use of the material. The investigations, analyses and working procedure here adopted broadened the understanding of this system pointing possibilities to increase its performance and to minimize failures during the preliminary stage of design.

**Keywords:** structural membranes, performance strategies, membrane material, optimization process, membrane material testing.



# CONTENTS

<b>1</b>	<b>INITIAL CONSIDERATIONS</b>	<b>21</b>
1.1	INTRODUCTION AND BACKGROUND .....	21
1.2	OBJECTIVES AND RESEARCH HYPOTHESIS .....	23
1.3	METHODOLOGY .....	23
1.4	ORGANIZATION OF WORK .....	24
<b>2</b>	<b>LIGHTWEIGHT STRUCTURES - OVERVIEW</b>	<b>25</b>
2.1	HISTORICAL CONTEXT .....	25
2.2	CONSTRUCTION SYSTEM .....	30
2.3	PRINCIPLES OF THE SYSTEM .....	33
2.4	STRATEGIES THAT GUIDE THE OPTIMUM PERFORMANCE OF THIS SYSTEM .....	36
2.4.1	OBSERVATION AND ANALYSIS OF BUILDINGS	36
2.4.2	STRATEGIES OR RULES IDENTIFIED	54
2.5	MEMBRANE MATERIAL .....	63
2.5.1	MEMBRANE MATERIAL CHARACTERISTICS	63
2.5.2	MOST USED MATERIALS	66
2.5.3	MATERIAL BEHAVIOR	72
2.6	DESIGNING PROCESS .....	75
2.6.1	FORMFINDING – FORCE DENSITY METHOD	77
2.6.2	NUMERICAL ANALYSIS – FINITE ELEMENTS METHOD	79
2.6.3	PATTERNING PROCESS	79
2.7	CHALLENGES OF DESIGNING AND CONSTRUCTION PROCESS IN BRAZIL .....	82
2.7.1	MEMBRANE ROOFS DESCRIPTION	83
2.7.2	MANUFACTURING AND ASSEMBLY PROCEDURES	84
2.7.3	WORK PROCEDURES AND ITS CHALLENGES	88
<b>3</b>	<b>CASE STUDY</b>	<b>93</b>
3.1	1 <sup>ST</sup> STAGE OF QUALITATIVE ANALYSIS .....	94
3.1.1	STRUCTURAL CONCEPT OF THE PROJECT THAT GUIDES ANALYSIS	94
3.1.2	VARIABLES THAT GUIDE THE PROJECT PERFORMANCE ANALYSIS	96
3.1.3	INVESTIGATED CASES (VARIABLES) AND EVALUATED MODELS	97

3.1.4	FORM FINDING AND ANALYSIS PROCEDURES OF THE MODELS	102
3.1.5	DATA/ PARAMETERS THAT GUIDES THE SIMULATION OF THE MODELS	106
3.1.6	INTERPRETATION AND ANALYSIS OF THE MODELS	120
3.1.7	1 <sup>ST</sup> STAGE OF QUALITATIVE ANALYSIS - CONSIDERATIONS	182
<b>3.2</b>	<b>2<sup>ND</sup> STAGE OF QUALITATIVE ANALYSIS / EXPERIMENTAL .....</b>	<b>183</b>
3.2.1	BIAXIAL TEST	185
3.2.2	SEAM BIAXIAL TEST	197
3.2.3	UNIAXIAL SEAM TESTS	206
3.2.4	CONSIDERATIONS OF 2 <sup>ND</sup> STAGE OF QUALITATIVE ANALYSIS	212
<b>4</b>	<b>FINAL CONSIDERATIONS</b>	<b>213</b>
<b>5</b>	<b>REFERENCES</b>	<b>219</b>
	APPENDIX A – PROJECT INFORMATION	225
	APPENDIX B – WIND DIRECTIONS	227
	APPENDIX C – MAPPING OF PRESSURE COEFFICIENTS	228
	APPENDIX D – ANCHOR POINTS OF MODELS	231
	APPENDIX E – DIMENSIONS OF SUPPORT SYSTEM COMPONENTS	232
	APPENDIX F – PRELIMINARY EVALUATION OF SUPPORT SYSTEM COMPONENTS	233
	APPENDIX G – INFORMATION OF EXPERIMENTAL TESTS	238
	APPENDIX H – METHOD DENSITY FORCE (EQUATIONS)	239
	APPENDIX I – ISOBAR LINES OF CP, TESTED MODELS	240

## LIST OF FIGURES

Figure 2.1-1 – Black tent of the Middle East, Velaria, Chapiteau .....	25
Figure 2.1-2 – Shukhov radio tower - Views: external, internal, Rússia (1896) .....	26
Figure 2.1-3– External View and model of the Raleigh Arena, North Carolina, 1952 .....	27
Figure 2.1-4 – Forms of equilibrium.....	27
Figure 2.1-5 – Olympic Stadium, Munich (1972) .....	28
Figure 2.1-6 – Fröttmaning station – Munich, 2004 .....	30
Figure 2.1-7 – Allianz Arena, Munich, 2005 .....	30
Figure 2.2-1 – Cable nets/ membranes (double curvature in opposite directions): forms of equilibrium ....	31
Figure 2.2-2 – Principal curvatures: $r_1$ and $r_2$ and Gaussian curvature (K) of curved surfaces.....	32
Figure 2.2-3 – Soap bubble (a), soap film (b); behavior of the anticlastic membranes (c).....	33
Figure 2.3-1 – Optimization process of structures: physical models, drawings and image of tree .....	34
Figure 2.3-2 – How six bars can be connected: they may form two or four triangles. ....	35
Figure 2.3-3 – Tensegrity made from: prism (a) and octahedron (b); Tensegrity arch (c) .....	35
Figure 2.4-1 – Roof of courtyard - History Museum of Hamburg .....	37
Figure 2.4-2 – <i>Exhibition hall</i> , Hückelhoven .....	39
Figure 2.4-3 – RheinEnergie Stadium, Köln .....	40
Figure 2.4-4 – RheinEnergie Stadium, Köln .....	41
Figure 2.4-5 – Imtech Arena (Volksparkstadion), Hamburg .....	42
Figure 2.4-6 – Imtech Arena (Volksparkstadion), Hamburg .....	43
Figure 2.4-7 – Retractable roof, Castle Kufstein.....	44
Figure 2.4-8 – Retractable roof, Castle Kufstein.....	45
Figure 2.4-9 – <i>New Waldstadion</i> , Frankfurt/ Main .....	46
Figure 2.4-10 – <i>New Waldstadion</i> , Frankfurt/ Main .....	47
Figure 2.4-11 – Rothenbaum Tennis Stadium, Hamburg .....	48
Figure 2.4-12 – Rothenbaum Tennis Stadium, Hamburg .....	49
Figure 2.4-13 – Ice rink ( <i>Eisbahn Stellingen</i> ), Hamburg.....	50
Figure 2.4-14 – Ice rink ( <i>Eisbahn Stellingen</i> ), Hamburg.....	51
Figure 2.4-15 – Olympic stadium, Munich .....	52
Figure 2.4-16 – Roof - courtyard of the company IHK, Würzburg .....	53
Figure 2.4-17 – Roof - courtyard of the company IHK, Würzburg .....	54
Figure 2.4-18 – Structural system analysis - shells and frame/suspension bridge structure .....	55
Figure 2.4-19 – Structural system analysis - surface membrane roof and cable net roof.....	56
Figure 2.4-20 – Membrane arrangement (investigated roofs) .....	57
Figure 2.4-21 – (a-d) Ridges and valleys; (e-h) Highs and low points.....	58
Figure 2.4-22 – Seam and fittings .....	58
Figure 2.4-23 – Geometry and arrangement of the supporting system components.....	59
Figure 2.4-24 – Anchor points of components.....	61
Figure 2.4-25 – Progressive capacity of lightweight structures support large forces with smaller mass.....	62
Figure 2.5-1 – Material structure (fabric + PVC coating) .....	63
Figure 2.5-2 – (a) Thread/ yarn structure; (b) Graph: breaking length of fibres .....	64
Figure 2.5-3 – (a-b) Polyester fabric weaving and PVC coating process .....	65
Figure 2.5-4 – Woven fabrics ( <i>plain e atlas</i> ): thread direction and arrangement .....	66
Figure 2.5-5 – Light transmittance of coated fabric (a, b, c) and foil (d) .....	71
Figure 2.5-6 – (a) Non-linear behavior; (b) Inelastic behavior .....	72
Figure 2.5-7 – Thread curves: (a) weft; (b) warp .....	73

Figure 2.5-8 – Fabric behavior – thread directions: 90°, 0° e 45° .....	73
Figure 2.5-9 – Different strains in the fabric directions .....	73
Figure 2.5-10 – (a) <i>Creep</i> (fluência); (b) <i>Relaxation</i> .....	75
Figure 2.6-1 – Elastic behavior of the bar element: individually and as a part of a cable net. ....	77
Figure 2.6-2 – Form of equilibrium fulfilling vertical equilibrium .....	78
Figure 2.6-3 – Density force method and soap film behavior .....	79
Figure 2.6-4 – Patterning process .....	80
Figure 2.6-5 – Seam detail - areas with less deformation.....	81
Figure 2.6-6 – Types of seam.....	81
Figure 2.7-1– Membrane roof of the Convention center: aerial view; support system.....	83
Figure 2.7-2 – Support system of the Convention center (vertical section) .....	83
Figure 2.7-3 – Membrane roof of the Courtyard .....	84
Figure 2.7-4 – Surface manufacturing procedure – Courtyard roof .....	84
Figure 2.7-5 – Surface assembly procedure – Courtyard roof.....	86
Figure 2.7-6 – Surface assembly procedure - Convention center roof .....	87
Figure 2.7-7 – Connections of saddle shape modules (rigid edge) proposed by engineer Prof Ruy Pauletti ....	88
Figure 2.7-8 – Connections of double inverted cone shape (flexible edge) proposed by Tensitex.....	89
Figure 2.7-9 – Cutting patterns of the membrane roof of the Convention center .....	89
Figure 2.7-10– Support system of the membrane roof of the Convention center – proposed changes.....	90
Figure 2.7-11 – Adjustments of the membrane roof of the Courtyard.....	90
Figure 2.7-12 – Supporting system inaccuracy – roof of the Convention center .....	91
Figure 2.7-13 – Supporting system inaccuracy – roof of the Courtyard.....	91
Figure 3.1-1 – Original model – A1: plan, 3D views, lateral section.....	94
Figure 3.1-2 – Original model – A1: support system (masts + spatial support system) .....	95
Figure 3.1-3 – Original model – A1: plant and vertical section. ....	95
Figure 3.1-4 – Original model – 3D view and details of masts.....	96
Figure 3.1-5 – 1 <sup>st</sup> stage of the qualitative analysis of the performance of the project .....	97
Figure 3.1-6 – 1 <sup>st</sup> Case: number of masts (investigated variable) - A1, B1, C1 models.....	98
Figure 3.1-7 – Cable configuration that holds the spatial support system (e.g. A1model) .....	98
Figure 3.1-8 – 2 <sup>nd</sup> Case: cable configuration (investigated variables ) - A2.40°, B2.30°, C2.24° models ...	99
Figure 3.1-9 – 2 <sup>nd</sup> Case: cable configuration (investigated variable) - B2.60° and C2.48° models.....	99
Figure 3.1-10 – 2 <sup>nd</sup> Case: angle between the pair of cable defined by one module of internal membrane ..	100
Figure 3.1-11 – 2 <sup>nd</sup> Case: angle between the pair of cable defined by two modules of internal membrane	100
Figure 3.1-12– 3 <sup>rd</sup> Case: geometry of the internal membrane (investigated variable).....	101
Figure 3.1-13 – 3 <sup>rd</sup> Case: geometry of the external membrane (investigated variable).....	101
Figure 3.1-14 – Physical models (scales 1/1500, 1/200, 1/100) of A1 model.....	103
Figure 3.1-15 – Information (nodes, net elements and pre-tension) for defining the form of equilibrium..	103
Figure 3.1-16 – Superposing cable nets (computational models) and physical model .....	103
Figure 3.1-17 – Form finding and simulation of models – work steps.....	105
Figure 3.1-18 – Wind pressures acting on the surface geometry .....	108
Figure 3.1-19 – Models (R215, R30, R475) used as a reference to the case study. ....	110
Figure 3.1-20 – Isobar lines' graphs of Cp* (color) - models: R215, R390, R47 .....	111
Figure 3.1-21 – Angles and sectors of the Model A1 for mapping pressure coefficients .....	113
Figure 3.1-22 – Wind directions (global and local) - external surface models A, B, C .....	114
Figure 3.1-23 – Mapping of wind pressure coefficients (direction -Y).....	114
Figure 3.1-24 – Structure anchor points; restraints considering local coordinates, e.g. A1model .....	119
Figure 3.1-25 – Wind directions.....	120

Figure 3.1-26 – Von Mises stress – A1, B1, C1 (wind: -Y; -Y2).....	124
Figure 3.1-27 – Von Mises stress – A1, B1, C1 (rain + wind: -Y; -Y2).....	124
Figure 3.1-28 – Maximum stress trajectories - external membrane – A1, B1, C1 (wind: -Y; -Y2) .....	125
Figure 3.1-29 – Minimum stress trajectories - external membrane – A1, B1, C1 (wind: -Y; -Y2) .....	125
Figure 3.1-30 – Maximum stress trajectories - internal membrane – A1, B1, C1 (wind: -Y; -Y2) .....	126
Figure 3.1-31 – Maximum stress trajectories - int. membrane – A1, B1, C1 (material allowable stress)..	126
Figure 3.1-32 – Minimum stress trajectories - internal membrane – A1, B1, C1 (wind: -Y; -Y2) .....	126
Figure 3.1-33 – Small compression areas observed only at the top of the surface – A1, B1, C1 .....	127
Figure 3.1-34 – Displacements - support system – A1, B1, C1 (wind: -Y; -Y2) .....	127
Figure 3.1-35 – Displacements – external membrane – A1, B1, C1 (wind: -Y; -Y2).....	128
Figure 3.1-36 – Displacements - internal membrane – A1, B1, C1 (wind: -Y; -Y2).....	128
Figure 3.1-37 – Von Mises stress – A1, B1, C1 (wind directions: -X, Y, -Y, -Y2) .....	130
Figure 3.1-38 – Von Mises stress – A1, B1, C1 (rain + wind directions: -X, Y, -Y, -Y2) .....	131
Figure 3.1-39 – Maximum stress trajectories - external membrane – A1, B1, C1 (wind: -X, Y, -Y, -Y2)...	132
Figure 3.1-40 – Minimum stress trajectories - ext. membrane – A1, B1, C1 (wind: -X, Y, -Y, -Y2) .....	133
Figure 3.1-41 – Maximum stress trajectories - internal membrane – A1, B1, C1 (wind: -X, Y, -Y, -Y2)....	134
Figure 3.1-42– Maximum stress trajectories - A1, B1, C1 (material allowable stress).....	135
Figure 3.1-43 – Minimum stress trajectories - int. membrane –A1, B1, C1 (wind: -X, Y, -Y, -Y2) .....	136
Figure 3.1-44 – Support system displacements – A1, B1, C1 (wind: -X, Y, -Y, -Y2) .....	137
Figure 3.1-45 – External surface displacements – A1, B1, C1 (wind: -X, Y, -Y, -Y2) .....	138
Figure 3.1-46 – Internal surface displacements – A1, B1, C1 (wind: -X, Y, -Y, -Y2) .....	139
Figure 3.1-47 – Von Mises stress – A1, B1, C1 (wind: -Y; -Y2).....	142
Figure 3.1-48 – Von Mises stress – A2-40°, B2-30°, C2-24°; B2-60°, C2-48° (wind -Y; -Y2).....	142
Figure 3.1-49 – Maximum stress trajectories - external membrane – A1, B1, C1 (wind -Y; -Y2) .....	143
Figure 3.1-50 – Max. stress - ext. membrane – A2-40°, B2-30°, C2-24°; B2-60°, C2-48° (wind -Y; -Y2)	143
Figure 3.1-51– Minimum stress trajectories - external membrane – A1, B1, C1 (wind -Y; -Y2) .....	144
Figure 3.1-52 – Min. stress - ext. membrane – A2-40°, B2-30°, C2-24°; B2-60°, C2-48° (wind -Y; -Y2).....	144
Figure 3.1-53 – Maximum stress trajectories - internal membrane – A1, B1, C1 (wind -Y; -Y2) .....	145
Figure 3.1-54 – Max. stress - int. membrane – A2-40°, B2-30°, C2-24°; B2-60°, C2-48° (wind -Y; -Y2)..	145
Figure 3.1-55 – Minimum stress trajectories - internal membrane – A1, B1, C1 (wind -Y; -Y2) .....	146
Figure 3.1-56 – Min. stress - int. membrane – A2-40°, B2-30°, C2-24°; B2-60°, C2-48° (wind -Y; -Y2).....	146
Figure 3.1-57 – Support system displacements– A1, B1, C1 (wind -Y; -Y2) .....	147
Figure 3.1-58 – Support system displacements – A2-40°, B2-30°, C2-24°; B2-60°, C2-48° (wind -Y; -Y2) .	147
Figure 3.1-59 – External membrane displacements – A1, B1, C1 (wind -Y; -Y2).....	148
Figure 3.1-60 – Ext. membrane displacements – A2-40°, B2-30°, C2-24°; B2-60°, C2-48° (wind -Y; -Y2)	148
Figure 3.1-61 – Internal membrane displacements - A1, B1, C1 (wind -Y; -Y2).....	149
Figure 3.1-62 – Int. membrane displacements - A2-40°, B2-30°, C2-24°; B2-60°, C2-48° (wind -Y; -Y2) ...	149
Figure 3.1-63 – Angles between cables, applied pre-tension; load path .....	151
Figure 3.1-64 – Von Mises stress – A2-40°, B2-30°, C2-24° .....	152
Figure 3.1-65 – Von Mises stress – B2-60°, C2-48° .....	153
Figure 3.1-66 – Maximum stress trajectories – external membrane – A2-40°, B2-30°, C2-24° .....	154
Figure 3.1-67 – Maximum stress trajectories - external membrane – B2-60°, C2-48° .....	155
Figure 3.1-68 – Minimum stress trajectories - external membrane – A2-40°, B2-30°, C2-24° .....	156
Figure 3.1-69 – Minimum stress trajectories - external surface – B2-60°, C2-48° .....	157
Figure 3.1-70 – Maximum stress trajectories - internal surface – A2-40°, B2-30°, C2-24° .....	158
Figure 3.1-71 – Maximum stress trajectories - internal surface – B2-60°, C2-48° .....	159
Figure 3.1-72 – Minimum stress trajectories - internal surface – A2-40°, B2-30°, C2-24° .....	160

Figure 3.1-73 – Minimum stress trajectories - internal surface - B2-60°, C2-48° models .....	161
Figure 3.1-74 – Support system displacements – A2-40°, B2-30°, C2-24° .....	162
Figure 3.1-75 – Support system displacements – B2-60°, C2-48° .....	163
Figure 3.1-76 – External surface displacements – A2-40°, B2-30°, C2-24° .....	164
Figure 3.1-77 – External surface displacements - B2-60°, C2-48° .....	165
Figure 3.1-78 – Internal surface displacements – A2-40°, B2-30°, C2-24° .....	166
Figure 3.1-79 – Internal surface displacements - B2-60°, C2-48° models .....	167
Figure 3.1-80 – Schematic representation of changes in edge cable curvature of the surface .....	169
Figure 3.1-81 – Von Mises stress – B2-30°, B2 <sub>int</sub> and B2 <sub>int-ext</sub> (wind -Y2) .....	169
Figure 3.1-82 – Maximum stress trajectories - external membrane – B2-30°, B2 <sub>int</sub> and B2 <sub>int-ext</sub> (wind -Y2)..	170
Figure 3.1-83 – Minimum stress trajectories - external membrane – B2-30°, B2 <sub>int</sub> and B2 <sub>int-ext</sub> (wind -Y2)..	170
Figure 3.1-84 – Maximum stress trajectories - internal membrane – B2-30°, B2 <sub>int</sub> and B2 <sub>int-ext</sub> (wind -Y2)..	171
Figure 3.1-85 – Minimum stress trajectories - internal membrane – B2-30°, B2 <sub>int</sub> and B2 <sub>int-ext</sub> (wind -Y2)..	171
Figure 3.1-86 – Support system displacements – B2-30°, B2 <sub>int</sub> and B2 <sub>int-ext</sub> (wind -Y2) .....	172
Figure 3.1-87 – External membrane displacements – B2-30°, B2 <sub>int</sub> and B2 <sub>int-ext</sub> (wind -Y2) .....	172
Figure 3.1-88 – Internal membrane displacements — B2-30°, B2 <sub>int</sub> and B2 <sub>int-ext</sub> (wind -Y2) .....	173
Figure 3.1-89 – Von Mises stress - B2 <sub>int</sub> e B2 <sub>int-ext</sub> models.....	174
Figure 3.1-90 – Maximum stress trajectories - external surface - B2 <sub>int</sub> e B2 <sub>int-ext</sub> models.....	175
Figure 3.1-91 – Minimum stress trajectories - external surface - B2 <sub>int</sub> e B2 <sub>int-ext</sub> models.....	176
Figure 3.1-92 – Maximum stress trajectories - internal surface - B2 <sub>int</sub> e B2 <sub>int-ext</sub> models.....	177
Figure 3.1-93 – Minimum stress trajectories - internal surface - B2 <sub>int</sub> e B2 <sub>int-ext</sub> models.....	178
Figure 3.1-94 – Support system displacements – B2 <sub>int</sub> e B2 <sub>int-ext</sub> models .....	179
Figure 3.1-95 – External surface displacements - B2 <sub>int</sub> e B2 <sub>int-ext</sub> models .....	180
Figure 3.1-96 – Internal surface displacements - B2 <sub>int</sub> e B2 <sub>int-ext</sub> models .....	181
Figure 3.2-1 – Qualitative analysis of the performance of a project: 1 <sup>st</sup> e 2 <sup>nd</sup> stages.....	184
Figure 3.2-2 – Parameters and procedures evaluated in the experimental stage.....	184
Figure 3.2-3– Biaxial test; material PES/PVC.....	185
Figure 3.2-4 – Test equipment - Essen laboratory for lightweight structures,UDE .....	185
Figure 3.2-5 – Cutting patterns of external and internal surfaces of B2 <sub>int-ext</sub> model .....	186
Figure 3.2-6 – Maximum stress (a) and minimum stress (b) – external membrane B2 <sub>int-ext</sub> model (-Y2) .....	187
Figure 3.2-7 – Maximum stress (a) and minimum stress (b) – internal membrane B2 <sub>int-ext</sub> model (-Y2) .....	187
Figure 3.2-8 – Calculation of elastic constants calculation .....	192
Figure 3.2-9 – Crimp interchange .....	194
Figure 3.2-10 – Compensation of flat panels .....	196
Figure 3.2-11 – Cutting patterns´ angles of external and internal surfaces (A2-40°, B2 <sub>int-ext</sub> e C2-48°) ...	198
Figure 3.2-12 – Seam biaxial tests – angles between panels evaluated: 0°, 4° e 8° .....	198
Figure 3.2-13 – (a) Reference points and lines marked in the specimen; (b) seam/ overlap of panels ....	199
Figure 3.2-14 – Threads´ direction related to seam and applied loads direction .....	200
Figure 3.2-15 – Seam biaxial test - comparison of tests - angle between panels: 0°, 4° .....	204
Figure 3.2-16 – Seam biaxial test - comparison of tests - angle between panels: 4°, 8° .....	205
Figure 3.2-17 – Specimen detail.....	207
Figure 3.2-18 – Uniaxial seam test - specimens after tests .....	207
Figure 3.2-19 – Uniaxial seam test, temperature: + 23°C.....	208
Figure 3.2-20 – Uniaxial seam test, temperatures: (a) +70°C; (b) -10°C .....	210
Figure 3.2-21 – Uniaxial seam test (temperature +23°C) - failure detail of the specimens.....	210
Figure 3.2-22 – Uniaxial seam test (temperature -10°C) - failure detail of the specimens.....	210
Figure 3.2-23 – Uniaxial seam test (temperature +70° C) - failure detail of the specimens.....	211

Figure 4-1 – Work preliminary procedure and new work steps .....	216
--	-----

## LIST OF TABLES

Table 2.5-1 – Technical characteristics of materials.....	69
Table 3.1-1 – Characteristics and pre-tension applied to the surfaces in form finding .....	104
Table 3.1-2 – Material (type 3 and type 4) data.....	106
Table 3.1-3 – Table with the tangential stiffness of technical membranes .....	107
Table 3.1-4 – Characteristics of the models R215, R390 and R475 and wind direction.....	110
Table 3.1-5 – Limit values of $C_p^*$ (mean values resulted) – tested models.....	111
Table 3.1-6 – Pressure coefficients and dynamic pressure applied to models .....	112
Table 3.1-7 – Maximum stress at membrane surface .....	117
Table 3.1-8 – Parameters for analysis and comparison of the study models - applied pre-tension.....	118
Table 3.1-9 – Load steps and pre-tensioning applied to components of the study models .....	121
Table 3.1-10 – Ratio mass / area of each study model .....	121
Table 3.1-11 – Displacements (system support/ membranes) of the study models (wind and rain actions) 122	122
Table 3.1-12 – Pre-tension applied to the support system cables – 1 <sup>st</sup> case.....	123
Table 3.1-13 – Ratio mass/area of models – 1 <sup>st</sup> case .....	123
Table 3.1-14 – Pre-tension applied to the support system cables – models of the 1 <sup>st</sup> and 2 <sup>nd</sup> cases.....	140
Table 3.1-15 – Ratio mass/area total – models of the 1 <sup>st</sup> and 2 <sup>nd</sup> cases .....	141
Table 3.1-16 – Pre-tension applied to the support system cables – B2-30°, B2int e B2int-ext models ...	168
Table 3.1-17 – Ratio mass/ area – A1, B2-30°, B2int e B2int-ext models .....	169
Table 3.2-1 – Biaxial test – load ratio applied in the material directions .....	188
Table 3.2-2 – Evaluation of elastic constants in cycles of maximum load applied to structure .....	191
Table 3.2-3 – Biaxial seam test – load ratio applied in material directions .....	199
Table 3.2-4 – Seam biaxial tests - material deformation .....	200

## LIST OF DIAGRAMS

Diagram 3.2-1 – Biaxial test - reference values of applied loads in the material directions (warp/ weft) ..	189
Diagram 3.2-2 – Force-time (biaxial test) in material directions: warp and weft .....	190
Diagram 3.2-3 – Force-elongation time (biaxial test) in material directions: warp and weft.....	190
Diagram 3.2-4 – Elongation-time (biaxial test) .....	195
Diagram 3.2-5 – Seam biaxial test – load values applied.....	199
Diagram 3.2-6 – Biaxial seam test – angle between panels: 0° .....	202
Diagram 3.2-7 – Biaxial seam test – angle between panels: 4° .....	202
Diagram 3.2-8 – Biaxial seam test – angle between panels: 8° .....	203
Diagram 3.2-9 – Biaxial seam test – comparison between tests .....	203
Diagram 3.2-10 – Uniaxial seam test, temperature: +23°C .....	208
Diagram 3.2-11 – Uniaxial seam test, temperature: -10°C.....	209
Diagram 3.2-12 – Uniaxial seam test, temperature: +70°C .....	209

## SYMBOLS

Ag	gross sectional área
Ae	net sectional area
Cp*	pressure coefficient (total or resultant)

$C_p$	pressure coefficient
$E$	modulus of elasticity
$E_1 ; E_2$	elastic modulus of warp direction and weft direction
$F_y$	specified minimum yield stress
$F_e$	elastic buckling stress
$F_{cr}$	critical stress
$K$	Gaussian curvature
$M_n$	nominal flexural strength
$N_0$	material allowable strength
$P$	transversal pressure
$P_n$	nominal axial strength
$P_u$	required axial strength
$S$	elastic modulus section
$S_h, H_x$	horizontal component of tensile force
$S_1, S_a$	internal tensile force in the bar element
$S_1$	topographic factor
$S_2$	roughness factor
$S_3$	statistical factor
$T_1 ; T_2$	tensile forces
$V_1 ; V_2$	vertical component of tensile force
$V_k$	characteristic wind velocity
$V_o$	wind speed
$Z$	plastic modulus section
$a$	final length – considering coordinates XYZ
$\cos x$	cosine (x)
$d ; y ; \emptyset$	diameter
$f_{u,k}$	seam breaking strength
$h$	height
$I$	moment of inertia
$k$	buckling coefficient
$k_1 ; k_2$	principal curvatures
$l$	initial length; member length
$m$	mass
$p_x$	external tensile forces
$q$	force density
$r$	radius of gyration
$r_1 ; r_2$	radii of principal curvatures
$t$	thickness
$z, u$	vertical displacements
$\alpha, \beta$	angles
$\Delta\varepsilon$	strain range
$\Delta x$	projected length of cables (axis x)
$\Delta\sigma$	stress range
$\varepsilon$	strain
$\varepsilon_1 ; \varepsilon_2$	strains in the warp and weft directions
$\lambda$	slender parameter
$\rho$	density
$\pi$	mathematical constant
$\sigma_1 ; \sigma_2$	tensile stress
$\nu_{21} ; \nu_{12}$	Poisson ratio

*To my family, my friends and everybody, with no exception.*



*It is not the material but how it is used that matter – a Chinese old saying.*

*(YU, 2012)*



# 1 INITIAL CONSIDERATIONS

## 1.1 INTRODUCTION AND BACKGROUND

The subject of this thesis, structural membranes, is based on the concept of surface structures with minimum thickness and weight, which absorb only forces in the form of tensile stresses in its own plane, and whose three-dimensional stability is a result of the geometry (double curvature) and tautness. These fall within the field on tensile structures when classified according to their internal stress state, in the group of flexible systems according to their behaviour, as space systems considering its morphological classification, and lightweight structures when considering their own weight (PAULLETI, 2003).

These structures work together with the support system (masts, cables, truss, arcs, etc.), normally in steel, in a joint and continuous way and in a tensile state of stress. This association has enabled the development of structures capable of spanning large distances with low weight, high strength, fast construction time and reusability which became a trend in architecture and engineering.

The weight reduction lowers the cost and increases the adaptability of the building, allowing multiple uses and greater application of them (ROLAND, 1973). Thus, these structures have been widely used in complex buildings with large spans, such as large roofs of stadiums, airports, amphitheatres, auditoriums and subway stations, among others. They stand out in their use as retractable structures and as temporary structures with easy assembly, great adaptability to different places, as the accommodations for emergencies. These structures are also observed in multilayer membrane, filled with gas, used as roofing or cladding of façades, or filled with mineral wool, in order to provide thermal insulation for the building.

These structures are characterized by high complexity presenting great challenges to design and constructive procedures. They are flexible when compared to rigid-type systems such as shells. Besides that, they present large displacements under load action. Also, they present non-linear geometric behavior, making it difficult to be analyzed by traditional methods and processes.

The material used for membranes treated herein as structural fabric, presents high efficiency (high strength and low weight). However, it displays a complex behavior under tensile forces and needs to be verified by testing.

The wind is generally considered the critical loading of these lightweight structures generating significant suction forces, except for buildings located in areas with high snow load. This information require testing in wind tunnels, that provides the appropriate values of the coefficients of wind pressure, which are necessary for structural analysis (FOSTER; MOLLAERT, 2004).

Furthermore, membranes such as steel support system are prefabricated. The manufacturing results from patterning process, which involves the flattening of the three-dimensional surface. So these surfaces, compounded by flat panels joined by seam, are just mounted and tensioned on site, which restricts major changes.

In Brazil, architects and engineers deal with the typical challenges of this system, the uncertainties of the evaluated data (material and wind loads) and the limitations of the numerical programs used. There are still few publications in this area and lack of technical recommendations that ensure quality control of these structures and the technical work of the teams involved in design and construction.

Because of these uncertainties and limitations, it is usual to adopt simplifications in numerical simulations, according to the behaviour of the material, loads, as well as the stages of patterning process. However, these simplifications generate methodological flaws in design procedure, making the analysis less accurate. These methodological flaws are added to the inaccuracies of constructive elements, hindering constructive accuracy and performance of these structures.

These considerations highlight the motivations and justifications for investigating the efficiency of a project, trying to understand the strategies used to achieve the structural efficiency of the system and the procedures that enable diminishing the methodological flaws of this preliminary stage of work, in order to contribute to improve the performance (structural and building) of these structures.

This work is also a result of the cooperative project between Federal University of Ouro Preto (UFOP, Ouro Preto, Brazil) and University Duisburg-Essen (UDE, Essen, Germany), as well as the support of architects, engineers, and manufacturing companies of structural membranes enabling integrate knowledge and experience from different fields: architecture, engineering and materials.

## **1.2 OBJECTIVES AND RESEARCH HYPOTHESIS**

This work investigates the performance of structural membranes (with double curvature in opposite directions) within the following contexts: structural (system configuration and membrane material behaviour) and the design process.

It searches parameters or strategies that guide the optimal performance of the system; and procedures that contribute towards the improvement of the system, to minimize the methodological flaws of the preliminary stage of work and the differences between the theoretical model and the real structure.

It starts with the assumption that the efficiency of these structures is derived from the geometry of all system components (membrane and support system) and their cooperative work in tensile state; in addition from the geometry of the membrane resulted from patterning process.

Thus, this hypothesis involves two investigations. Initially, it analyzes the influence of the geometry of membrane and the structural system arrangement in system performance, regarding the membrane as a continuous spatial surface. Afterwards, it analyzes the influence of the geometry of the membrane compounded by joined flat panels, and so, it considers that the understanding and evaluation of the material behavior are essential to minimize the differences between theoretical and real models.

## **1.3 METHODOLOGY**

The initial stage of the work covered the literature review, investigation of design and constructive work of membrane roofs and technical visits. This approach involved the observation of the research object in site, increasing the perception of it, and made it possible to integrate the theoretical support and scientific critical analysis of the object under investigation, forming the basic knowledge that underlies this research.

The investigation of design and constructive work covered observation, recording and analysis of membrane roofs under construction in Brazil, investigating the challenges of these stages of work. The technical visits involved the observation, recording and analysis of lightweight structure buildings in Germany, seeking to identify strategies for achieving system efficiency. Technical visits to manufacturers of materials were also carried out, seeking the understanding of the production stages of the material.

To demonstrate the hypothesis of this work within the structural context and the design process perspective, it was conducted a qualitative analysis of the performance of a structural membrane roofing project. This analysis was performed in two stages, guided by numerical and experimental data.

The first stage involved the procedure in which the structural project set was optimized. It covered modelling and simulation (preliminary analysis) of the structural system (composed by membranes and system support) under load actions, using the Force Density Method and Finite Element Method. The wind loads, used in simulated models, were based on the wind pressure calculation NBR 6123 (ABNT 1988) and the results of wind tunnel tests on tensile structures performed by Vilela (2011).

The second stage comprised the experimental investigation of the membrane material for analysis of the geometry of the flattened membrane resulted from patterning process. The tests were performed at Essen laboratory for lightweight structures -UDE.

## **1.4 ORGANIZATION OF WORK**

This paper is organized into four parts. The first part includes the introduction of the whole thesis: introduction and explanation of the subject; objectives and hypothesis that guides this research.

The second part includes an overview of lightweight structures and the knowledge that underlies this research. It presents the historical context, the characteristics and principles of this system, as well as the analysis of lightweight structure buildings in Germany and the strategies that contribute to achieve optimal system performance. It describes the characteristics and behaviour of membrane materials, highlighting the most used ones. Afterwards, it discusses the design process of these structures and some work methods. Later, it points out the challenges and failures encountered in the stages of designing and building in Brazil.

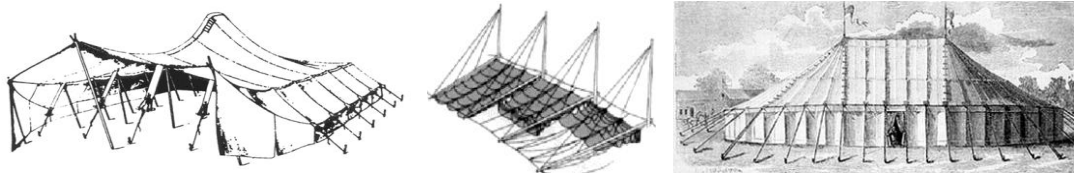
The third part presents a qualitative analysis of the efficiency of a project carried out in two steps. In the first step it was assessed the influence of the system support and the geometry of the membrane on the system performance under the action of loads. In the second step it was assessed the influence of the geometry of the flattened membrane on the system performance. This stage was guided to the experimental analysis of the material. The fourth part presents the final considerations of the thesis: the conclusion of this work and its contributions.

## 2 LIGHTWEIGHT STRUCTURES - OVERVIEW

### 2.1 HISTORICAL CONTEXT

Structural Membranes are referred to tents found in earlier times of civilization. These lightweight and mobile constructions stand out as one of the first spontaneous forms of housing built by man, being used to this day by nomadic peoples. The tents were introduced into Western culture by Persian armies, being transmitted to the Greeks and later the Romans (PAULETTI, 2003). It is also important to emphasize the retractable roof made by the Romans for sun protection on internal courtyards and theatres, called *velaria*, which according to Otto et al., (1972), they were constructed, extended and retracted by sailing boats (Figure 2.1-1).

Figure 2.1-1 – Black tent of the Middle East, Velaria, Chapiteau



Sources: KOCK, 2004, p.23; JOTA; PORTO, 2003, p.5; FOSTER; MOLLAERT, 2004, p.26.

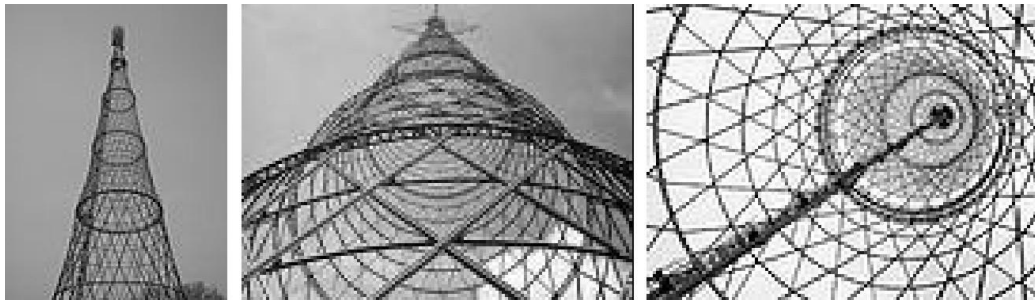
However, this form of construction evolved little since the Romans until the late eighteenth century, being used in urban cultures as temporary or mobile coverings, for accommodation of military campaigns, parties and public events. The lack of development of these single curvature surfaces can be explained by their instability to wind and strength limitation of the fabric and the connections (FOSTER, 1994).

According to Baier (2010), the first fabrics used in construction as tents were made of wool thread (sheep, goat) and fibres such as flax and hemp. Cotton has only been cultivated in Asia and South America in the late sixteenth century, enabling its use for clothing and buildings. However, the shift of craftsmanship production of fabrics for industrial production only happened right after the invention of the spindle and loom, i.e., in the late eighteenth century, with the invention of the spinning jenny and the power loom which revolutionized the textile production.

With industrialization, the development of weaving and the expansion of the railroads, from 1860, the fabric roofs have become widely used in modern travelling circuses (fabric roofs on linen canvas or hemp) in the United States and Europe, as shown in Figure 2.1-1, (FOSTER, 1994 *apud* PAULETTI, 2003).

However, the ideas and modern applications of suspended roofs with double curvature in opposite directions with small pressure were observed only in the late nineteenth century, with the work of engineer Vladimir Shukhov (1853-1939). According to Linkwitz (1999), the space surfaces, consisted of flexible metallic nets, which were proposed by Shukhov, were generated by the displacement of parallel straight and reversed lines in space, directed by directrix curves (Figure 2.1-2).

Figure 2.1-2 – Shukhov radio tower - Views: external, internal, Rússia (1896)

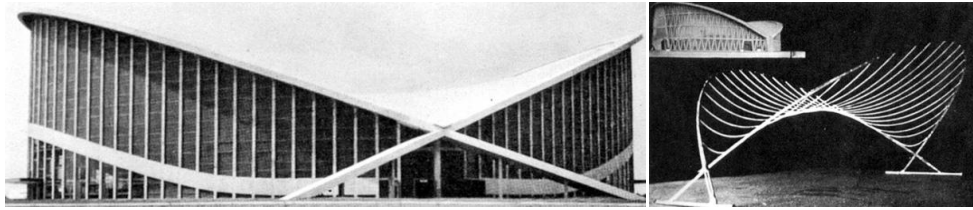


Source: SHUKHOV\_TOWER..., 2010.

This basic concept, which allows freeform drawn was also widely used by the architect Antoni Gaudí (1852-1926) in the coverage of the Sagrada Familia Church in Barcelona, and by the architect/engineer Félix Candela (1910-1997) to develop concrete hyperbolic shells. The free forms in concrete or wood can be set independently of the flow of forces acting on them; however, under the effect of its self-weight and external loads, they are subjected to bending and require certain thickness and/ or steel reinforcement (LINKWITZ, 1999).

In 1952, the first significant experience in roofing using cable net for large spans was registered with the design for the Raleigh Arena, North Carolina, USA, by architect Matthew Nowicki and engineers Severud Fred and William H. Deitrick (OTTO; TROSTEL, 1969). This cable net roof has introduced the principle of pre-tension surfaces of double curvature in opposite directions, providing great stability against aerodynamic loads, drawing the attention of architects and engineers from around the world (Figure 2.1-3).

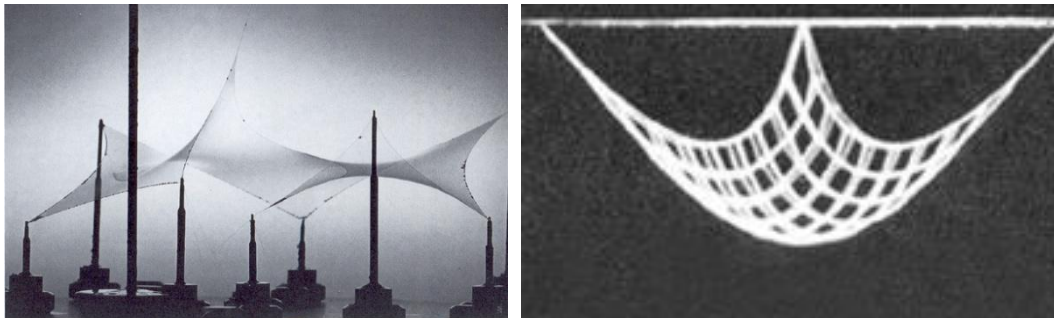
Figure 2.1-3– External View and model of the Raleigh Arena, North Carolina, 1952



Source: OTTO; TROSTEL, 1969, p.56, p.21.

However, according to Addis (1994), until the 50s, these structures were limited to catenary or hyperbolic paraboloid curves, because there was not a design procedure that enabled the development of structures based on forms of equilibrium. These follow the path of the forces acting on them, such as the cable net under pre-stress or freely suspended by its anchor points and the soap film (minimum surface) (Figure 2.1-4). The forms of equilibrium are defined by differential equations, and originally could only be revealed with the help of physical models, whose research had as precursor architect Prof. Dr. Frei Otto.

Figure 2.1-4 – Forms of equilibrium.



Soap film model; cable net suspended freely by their anchor points.

Source: OTTO, 1990, p.7.7; Adapted from OTTO; TROSTEL, 1969, p.29.

According to Rodríguez (2005), Prof. Dr. Frei Otto opened a new field of knowledge with his thesis *Cubiertas Colgantes* (Das Hängende Dach) in 1958, based on the theory of cables and suspension bridges, motivated by the properties of the catenary curve and the structural systems consisted of spatial meshes and tensile membranes.

Later, as a director of the Institute for Lightweight Structures (IL), University of Stuttgart (1964-1992), he investigated the structural forms, with small-scale experimental models. These studies were conducted by interdisciplinary teams of architects, engineers and biologists and were based on the lightweight principle. They were developed from the observation of the physiology of animals, shapes and

structures of nature, seeking to identify the consumption of matter and energy of these systems (LEWIS, 2003). Among his works it stands out the structures of the Olympic Complex, Munich (1972), which marks the beginning of modern tensile structures engineering (DREW, 1979 *apud* PAULETTI, 2003), as shown in Figure 2.1-5.

Figure 2.1-5 – Olympic Stadium, Munich (1972)



(image by author)

These studies provided an understanding of the qualitative behaviour of these structures and the development of real models. They also made it possible for engineers in the late '60s to create mathematical and computer models to simulate the geometry and non-linear behaviour of three-dimensional curves. According to Addis (1994) *apud* Nunes (2008), the tensile structures caused a revolution in building culture in the '60s: it nourished the development of engineering and the research on new materials, motivated by new designing methods developed by architects and engineers.

Frei Otto's research and development of technologies of hot air balloons in France in the late eighteenth century, and the 1st International Colloquium on Pneumatic Structures in 1967 stimulated the development of pneumatic structures, having its golden days in Expo'70 in Osaka.

The development of materials technology can be observed only in the second half of the twentieth century, making it possible to replace easily decay materials (fur and natural fibres) by synthetic fibres or foils of high performance, durability, reliability and safety to fire (KOCH, 2004).

According to Baier (2010), fabrics made with natural fibres, when compared with the current synthetic ones, absorb more moisture, are heavy, flammable,

susceptible to mildew, rot, dirt, even under the use of repellents and flame retardants, which also interferes with its durability. Thus, with the discovery of synthetic fibres (Nylon in 1938 and Polyester in 1947) and demanding of durability, mechanical strength and standardization of material properties, there is occurred the reduction in the use of natural fibres in construction. Moreover, the progressive development of other synthetic fibres and plastic products influenced the change in small-scale manufacturing to large global industrial production, and improved the quality and characteristics of materials used in today's membranes constructions.

Noteworthy are the structural fabrics of polyester coated with PVC, used since the 50s, the fibreglass coated with Teflon (PTFE), used from the 70s (HUNTINGTON, 2003), as well as the translucent ETFE foil, used from the 80s.

These high quality materials, with its minimal weight and stiffness, developed according to a structural logic that makes them slightly deformable under load action, as they are guided by concepts such as the double curvature and surface pre-stress, so that under load action, there are just the initial stress decreases (RODRÍGUEZ, 2005).

The combination of these structural fabrics to steel structures, mostly, has enabled its application to permanent structures, capable of spanning large distances with low weight, as well as retractable and temporary structures. It favours this approach: patterning, standardization and pre-fabrication of steel structure and development of high resistance connections that facilitate adjustment, joint and assembly of components.

The retractable structures allow altering their shape within a relative short time, and the use of open and closed features. These structures are associated with folding or sliding mechanisms.

The temporary coverings can be disassembled and carried in small volumes such as nomadic tents. They allow mobility and adaptability to different sites and activities, as a reversible intervention on the site.

These structures with minimum thickness are most suitable as open roofs allowing air flow and velocity (BAIER, 2010) or associated with conventional constructions, so that the membrane can act as a passive filter to the environment, creating a pleasant microclimate and integrating different spaces (Figure 2.1-6).

Figure 2.1-6 – Fröttmaning station – Munich, 2004



Arquitetos: Bohn Architekten, Munich (image by author)

These structures are also observed in multilayer membranes filled with air or insulating material, and translucent ETFE foils filled with air used as, for example, the cladding of façade and roof of Allianz Arena (Figure 2.1-7). The system promotes greater control of thermal conditions within the building and reduces mechanical ventilation (heating or cooling) costs. However, multilayer membranes reduce the translucency during daytime (CHILTON *et al.*, 2004).

Figure 2.1-7 – Allianz Arena, Munich, 2005



Architects: Herzog &amp; De Meuron, Basel; Eng.: Arup GmbH, Berlin and Sailer Stepan und Partner, Munich (image by author)

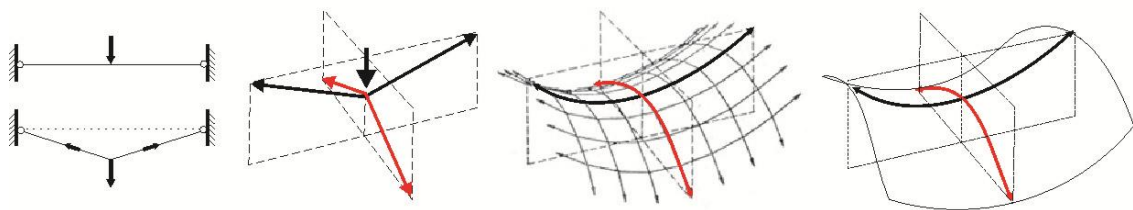
## 2.2 CONSTRUCTION SYSTEM

The membrane is a continuous two-dimensional surface – two significant dimensions, with a very small third one (thickness) – with minimum weight, that is, one flexible surface whose three-dimensional stability and ability to withstand loads result from its geometry (double curvature) and pre-stress state or tautness.

These structures exhibit behavior similar to cable nets: they take up shapes according to the forces that act on it. They perform as active form or form of equilibrium, and support loads by reactions in the form of tensile stresses in its own plane (Figure 2.2-1).

These surfaces work jointly and continuously with the system support, which involves the tensile flexible elements (cables), elements under combined flexure-axial forces (masts, beams, arches, frames) and/ or tensile and compression elements/ systems (trusses, tensegrity systems).

Figure 2.2-1 – Cable nets/ membranes (double curvature in opposite directions): forms of equilibrium



Source: Adapted from ROLAND, 1973, p.15.

According to Knippers *et al.* (2011), the geometry of the membrane surface is defined by its principal curvatures and the Gaussian curvature (Figure 2.2-2). The principal curvatures describe the magnitude and direction of the curvature, the minimum and maximum at one point on a surface. They result from the intersection of perpendicular planes to the tangent plane of the curved surface at the considered point. The principal curvatures ( $k_1$  e  $k_2$ ) correspond to the inverse of the radii of curvature ( $k_1=1/r_1$ ). The direction of curvature is indicated by values, values over zero indicate the curve toward the observer (convex), and values below zero indicate the curve in the opposite direction to the observer (concave). Thus, the Gaussian curvature is a measurement of the surface curvature, i.e., the product of the principal curvatures ( $K = k_1 \cdot k_2 = 1/r_1 \cdot 1/r_2$ ).

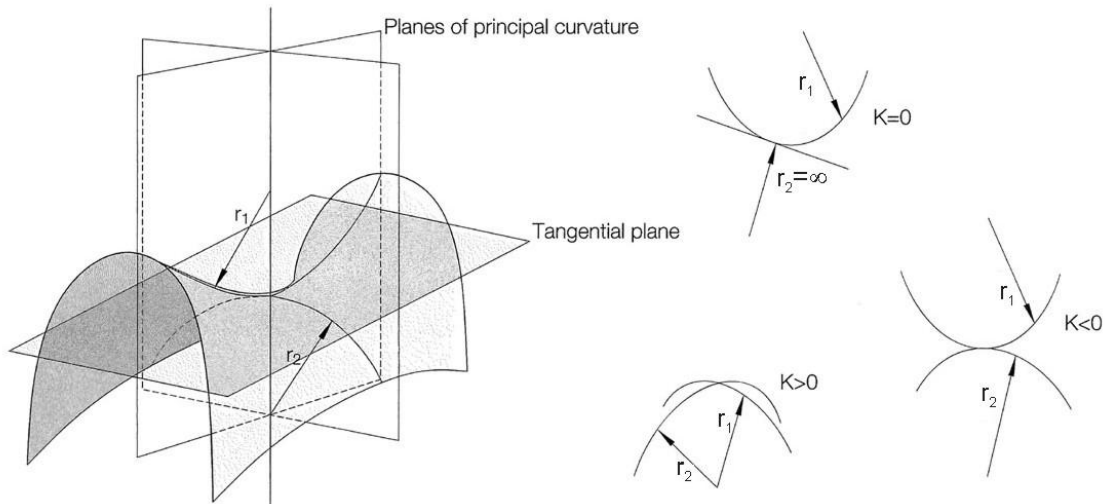
When these curvatures are oriented in the same direction, that is, when the centres of these curvatures are on the same surface side, they are called synclastic curvatures and the Gaussian curvature is positive ( $K > 0$ ). They are pneumatic structures stabilized applying pneumatic or hydraulic pressure in volume.

When the curvatures are oriented in opposite directions to each other and produce a warping effect to the surface, they are referred as anticlastic curvatures, and the Gaussian curvature is negative ( $K < 0$ ). These are stabilized by applying pre-stress in the plane of the membrane at its boundaries. When radii of principal

curvatures are equal, the surface stress is uniform (constant in all directions), forming a minimal surface (minimum surface area), as obtained with the soap film.

On the surfaces of a single curvature, as cylinders and cones, one of the curvature radii goes to infinity. Then, the Gaussian curvature is zero.

Figure 2.2-2 – Principal curvatures:  $r_1$  and  $r_2$  and Gaussian curvature ( $K$ ) of curved surfaces.

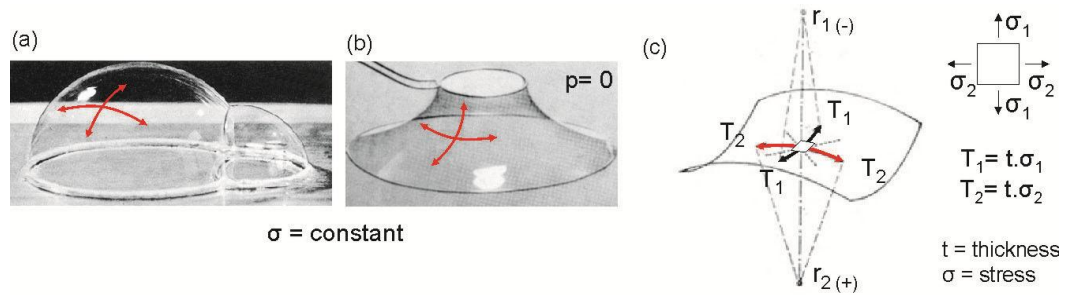


Source: adapted from KNIPPERS *et al.*, 2011, p.136.

The work carried out independently by Young (1805) and Laplace (1806), also considered to express the membrane, shows that the difference between inner and outer pressure across the curved fluid surface ( $p$ ) is directly proportional to the surface stress ( $\sigma$ ) and inversely proportional to the surface radii ( $r_1$ ;  $r_2$ ) that occur in planes perpendicular to each other, [ $p = \sigma (1/r_1 + 1/r_2)$ ]. In case of soap film (idealized membrane with anticlastic or plane surface), the stress ( $\sigma$ ) is constant and the pressure ( $p$ ) is zero, so the equation is reduced ( $1/r_1 + 1/r_2 = 0$ ), (LEWIS, 2003). It can be said that the membrane stress field is similar to the state of plane stress, but across a curved surface; the membrane withstand loads by the double curvature of the surface, according to the relationship of tensile forces ( $T_1$ ;  $T_2$ ) in the principal directions (orthogonal directions to each other, in which the curvature radii are maximum or minimum) and principal curvature radii ( $r_1$ ;  $r_2$ ), ( $T_1/r_1 + T_2/r_2 = 0$ ), (PAULETTI, 2007), as shown in Figure 2.2-3.

Thus, surfaces that have small curvature (large radii) require large pre-tension forces to stabilize them, while the surfaces that present greater curvature (smaller radii) are lighter structures. Therefore, the curvature radius changes the geometric stiffness of the surface and can help to minimize its deflection (change of shape geometry).

Figure 2.2-3 – Soap bubble (a), soap film (b); behavior of the anticlastic membranes (c)



Source: (a,b) adapted from OTTO; TROSTEL, 1967, p.13; OTTO; TROSTEL, 1969, p.70; (c) adapted from ROLAND, 1973, p.15; adapted from PAULETTI, 2007.

## 2.3 PRINCIPLES OF THE SYSTEM

According to Lewis (2003), the membranes have as reference structural forms that follow the lightweight principle i.e., forms that have the least amount of material, high stability and overall strength.

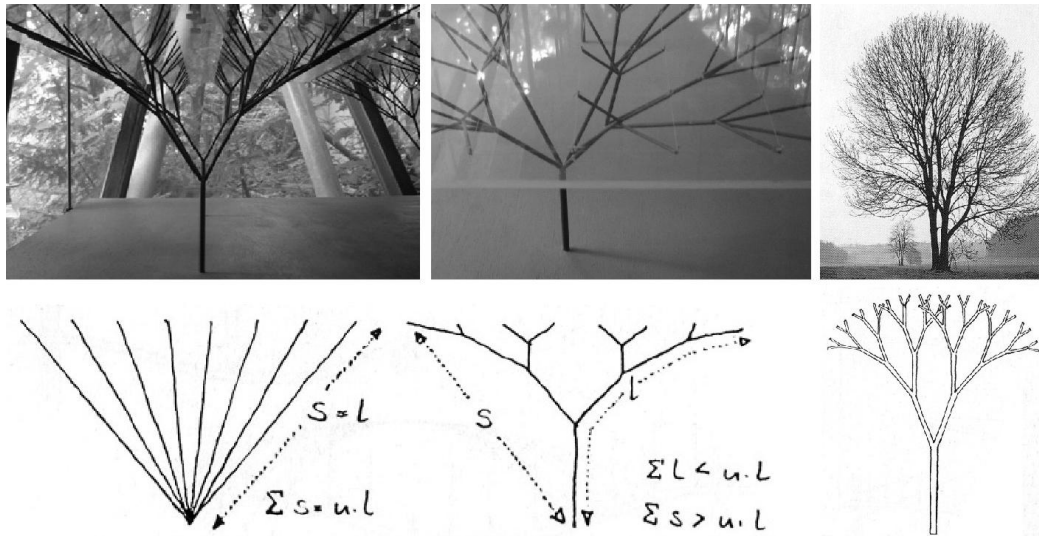
So to understand the behaviour of these structures it is important to know the principles behind this system. Noteworthy are the studies by Prof Dr Frei Otto, together with his study group, and Buckminster Fuller. Both sought to understand how the structures of nature maximize its stability and resistance and how this knowledge can contribute to the improvement of structures.

### *Frei Otto – Lightweight principle*

The lightweight principle, according to *et al.* (1997), is associated with the load-bearing capability of an object or structure, as well as its capability to transmit relatively large forces with little mass over a certain distance. Moreover, the mass of an object or a structure depends on the shape, the material used, the type of load acting in it, how it is applied, and the structural arrangement. Thus, the knowledge of the relationship between mass, force and form sets the fundamentals of light structures and allows understanding that lightweight is rarely accidental.

This principle results from a process of optimization of structures, i.e., the improvement of the geometry of the building components and the way they are organized in order to reduce the mass itself and to support the most critical load combinations (Figure 2.3-1). Therefore, it is considered one of the bases of the evolution of natural and technological objects.

Figure 2.3-1 – Optimization process of structures: physical models, drawings and image of tree



Source: physical model from Institute for Lightweight Structures and Conceptual Design - ILEK, University of Stuttgart (image by author); OTTO *et al.*, 1990, p.2.38, 2.40 (image of tree and drawings).

This process of refinement and selection has its roots in nature, as it can be seen in the shells and trees. According to D'Arcy Thomson (D'ARCY THOMSON, 1917 *apud* LEWIS, 2003), the shells grow smoothly, without changing its shape and in an asymmetrical way. Such growth is characterized by a geometric progression and can be represented as a logarithmic spiral.

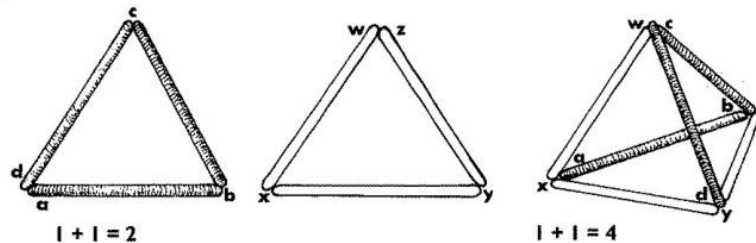
The trees, according to Mattheck (MATTHECK, 1990 *apud* LEWIS, 2003), are highly optimized living structures. Characterized by minimum weight, they can withstand all relevant loads by large movements. Furthermore, load changes are compensated by adaptive growth, and in the case of failure of a branch, it is clear that the regeneration process minimizes the area of the wound surface. These characteristics refer to the minimum area and constant tension, and can also be observed in the soap films (Figure 2.2-3b). These surfaces, also considered idealized membranes, take up the configuration of minimum potential energy which means minor action. Thus, as the potential energy is minimum, they present stable configuration.

### *Buckminster Fuller - Synergy*

Buckminster Fuller investigated how to arrange the components in pursuit of greater efficiency, i.e., the relationship between geometry and the forces acting on the structural system components and their overall behaviour. He observed that the performance of the components (parts) when they work together and simultaneously exceeds its individual performance (parts or sub parts).

According to Baldwin (1933), for B. Fuller, the unexpected action of associated elements (whole) amplifies the performance of individual parts and can be defined as synergy, being observed in geometry, configuration of chemical components and nature. In chemistry, there is the example of the performance of the alloy of chrome-nickel-steel. This exhibits ten times the tensile strength of its weakest component thereof and six times the resistance of its strongest component, being much greater than the sum of the resistances of all its components. In geometry, there is the example of how six bars can be connected. These may form two or four triangles, as flat shapes or a volume (tetrahedron) as the bars are arranged synergistically (Figure 2.3-2).

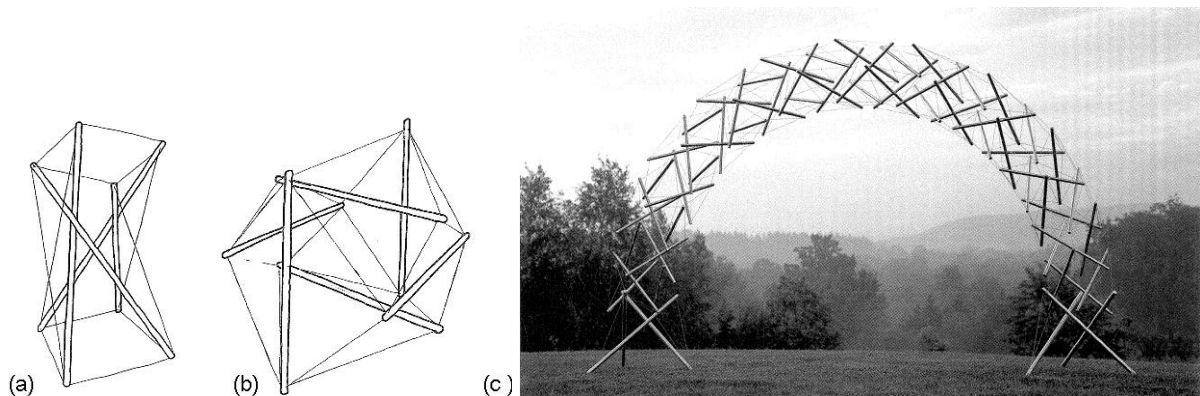
Figure 2.3-2 – How six bars can be connected: they may form two or four triangles.



Source: BALDWIN, 1933, p.68.

Among his inventions, the space system composed of discontinuous compressed bars, embedded in a continuous cable net forming a stable volume in space, called *Tensegrity* can be highlighted (Figure 2.3-3). In this system the structure can be organized more economically using small components and prioritizing the use of components working under tensile forces.

Figure 2.3-3 – Tensegrity made from: prism (a) and octahedron (b); Tensegrity arch (c)



Source: (a,b) REBELLO, 2000, p.136; (c) GOMES JÁUREGUI, 2007, p.118 (courtesy of image by Bob Burkhardt, Mascit y Kenneth Snelson).

## 2.4 STRATEGIES THAT GUIDE THE OPTIMUM PERFORMANCE OF THIS SYSTEM

After understanding the principles behind this system, the question arises: how to achieve optimal performance or efficiency of this system?

Thus, it was proposed the analysis of constructed buildings, i.e., membranes and cable nets roofing, grid shell and wooden shell covered by glass and membrane, as well as steel supporting system covered by translucent tiles.

The selection of these buildings aimed to do a qualitative evaluation of the performance of the structural membrane in the context of the lightweight structures.

The first stage of this research involved observing in site buildings, taking photographs, making sketches (not to scale) and analysing structural concept proposed of the selected buildings, according showed in this work. Then, the strategies or rules used by architects and engineers for these structures achieve great performance were identified. The analysis of some of these buildings and the strategies identified are presented, as it follows (sections 2.4.1 e 2.4.2).

### 2.4.1 OBSERVATION AND ANALYSIS OF BUILDINGS

*Roof of the courtyard - History Museum of Hamburg History, Hamburg, 1989*

*Architects: von Gerkan, Marg und Partner, Hamburg; Engineers: J. Schlaich, R. Bergermann*

The roof of the inner courtyard of this Museum complies two rectangular areas with different dimensions (L-shaped); it is made up of two cylindrical shells, whose junction has a dome shape (double curvature), as shown in Figure 2.4-1.

The curved surfaces system, known as *grid shell* is formed by the combination of a flat grid with hinged joint and a stressed cable network, then covered in laminated glass plates. The grid is composed of steel bars<sup>1</sup> (solid) of similar length with connections that rotate around its axis. These connections allow the bars to adapt to the surface geometry, forming square meshes (cylindrical area) and rhombus-shaped meshes (dome). The ends of these bars are connected with diagonal cables continuously pre-tensioned, increasing the rigidity of the shell and preventing the bending.

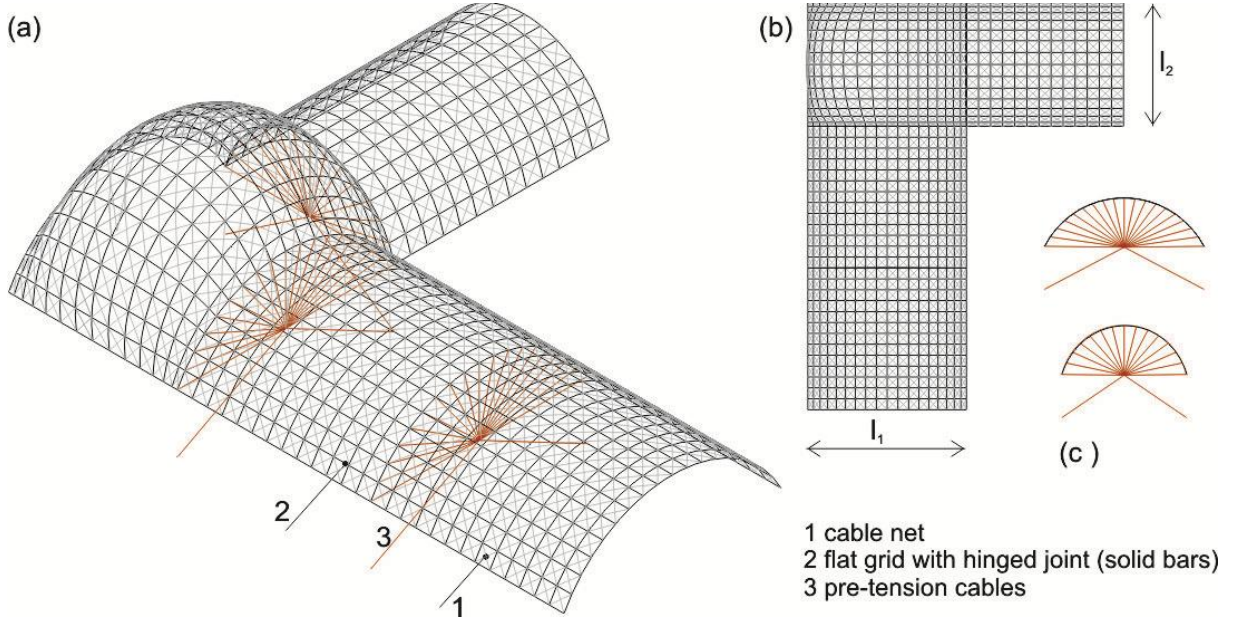
Besides the combination of two mesh with different behaviours, cables (tension) and bars (compression), it was observed that the cylindrical arches have

---

<sup>1</sup> Steel bars (117x 60 x 40 mm), according Schlaich and Bergermann (2003).

tensile cables (radial cables under pre-tension) to control the arch deformation and to eliminate horizontal reaction.

Figure 2.4-1 – Roof of courtyard - History Museum of Hamburg



(a, b) 3D views, plant syst. support (drawing), (c, e) pre-tension cables, (d) internal view, (e) tensile cables, (f) roof support (sketches and images by author)

*Exhibition hall, Hückelhoven, 1996, (2800m<sup>2</sup>)*

*Architects:: Prof Dr Bernd Baier, Leo Graff, Aachen; Engineers: Prof Dr Wilfried Führer, Prof Friedhelm Stein, Ulrich Kosch, Aachen.*

The roof of the Exhibit Hall in Hückelhoven (base approx. 42 x 96m) is composed of five saddles (paraboloids), being supported by four large three-hinged wooden arches which are anchored on concrete pillars, spanning distances of approximately 42m, as shown in Figure 2.4-2.

On these three-hinged arches there are slender wooden purlins (cross section: 20x10cm), which bow as suspended cables working only under tensile forces and defining the surface geometry (anticlastic curvature). Furthermore, the ends of these three-hinged arches are tensioned by boundary arches compound of wood and steel. Thus, the thin wooden shell with anticlastic curvature working under pre-tension, presents membrane behaviour, it only absorbs forces in the form of tensile stresses in its own plane.

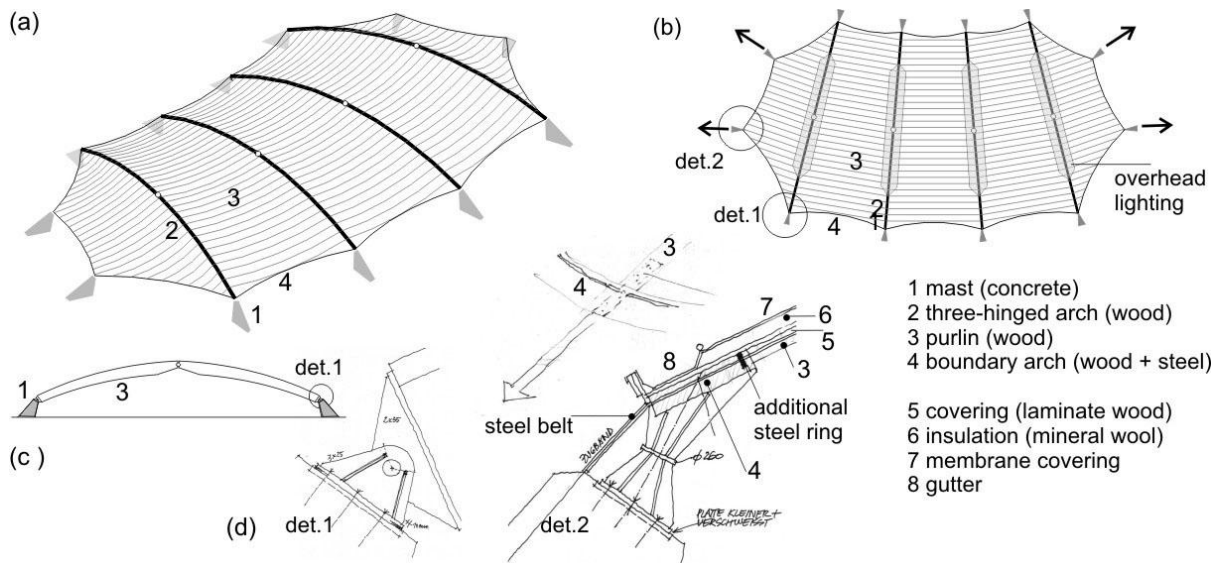
As this exhibition hall is a closed environment, it presents acoustic insulation, as well as ventilation and overhead lighting, aiming at optimal internal temperature control. Therefore, the purlins support the laminated wooden shell (which has a protective film against moisture) and the thermal and acoustic insulation (mineral wool mattresses), as well as the overhead lighting and ventilation structure. The outer roof is made of PVC- polyester<sup>2</sup> membrane (which was welded on site).

This Exhibit Hall was rewarded in 1994 with International GLULAM Award and 1996 with Holzbaupreis Nordrhein-Westfalen.

---

<sup>2</sup> PVC/polyester: membrane material compounded by polyester fabric coated by PVC, section 2.5.2.

Figure 2.4-2 – Exhibition hall, Hückelhoven



(a, b, c) 3D view, plan and vertical section syst. support; (d- det1, h)) anchoring of the three-hinged arch; (d- det2, f) points of pre-tension of the edge arch; (e) external side view; (g) internal view; (i) overhead lighting on three-hinged arch, (j, k) three-hinged arch and purlins; (f, i, j, k) images by author; (g, h) photos: Friedhelm Thomas, Krefeld (*Informationsdienst Hols*, 1996); (a, b, c) sketches by author; (d1 e d2) drawings by Prof Dr Baier.

*RheinEnergie Stadion, Köln, 2003*

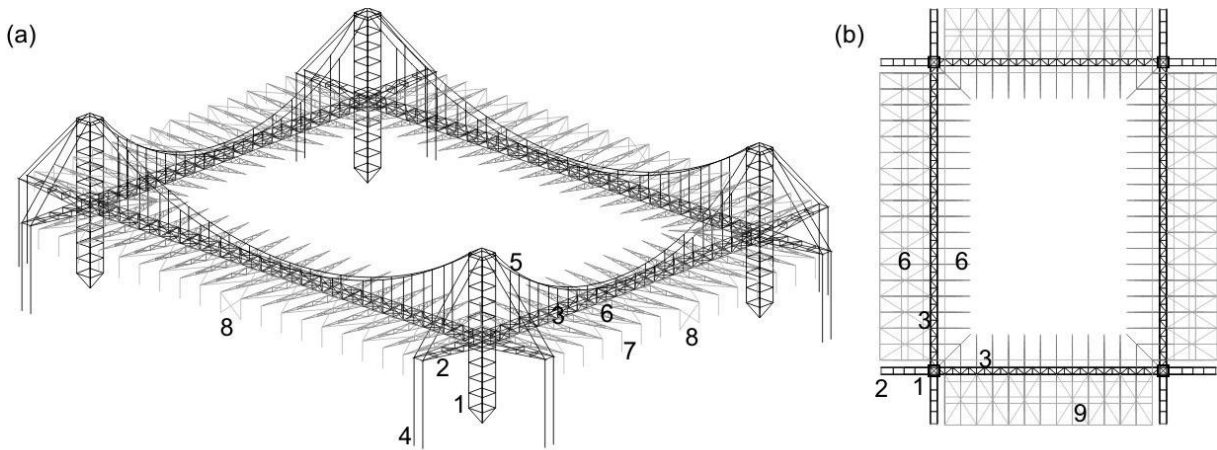
Architects: von Gerkan, Marg und Partner; Engineers: Schlaich Bergermann und Partner, Stuttgart

This stadium in Köln presents rectangular base. The concrete bleachers are positioned on each side of the polygon and covered with metal and translucent tiles, (Figure 2.4-3 and Figure 2.4-4).

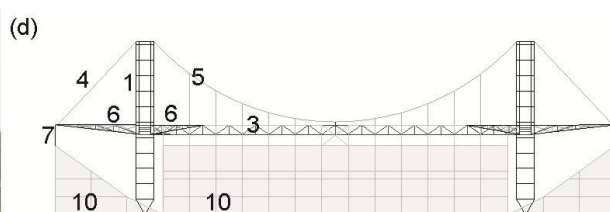
The arrangement of the roof support system in steel is remarked by the combination of systems: frames and suspension bridge structure. The masts, (with hollow cross section, compounded by the arrangement of tubular profiles) located at the corners of the polygons, are linked to large truss beams forming four large frames. However, such large truss beams are also suspended by cables as a bridge, minimizing the bending. Moreover, the quadrangular cross section gives the beam torsion stability.

The masts are hinged and had truss arms, which are held and pre-stressed by cables at the top of the mast and base, reducing the buckling length and increasing its structural stability.

Figure 2.4-3 – RheinEnergie Stadion, Köln



- 1 mast (hollow section) with hinge
- 2 truss arm
- 3 truss beam
- 4 pre-tension cable
- 5 cables
- 6 cantilever truss
- 7 tubular profiles
- 8 bracing (vertical plane)
- 9 bracing (horizontal plane)
- 10 concrete bleachers



(a) 3D view, (b) plan and vertical section of the system support; (c) front view; (sketches and image by author).

This large suspended truss beam hold cantilever truss beams (comprised of steel profiles and cables) that support the steel tiles. This large suspended truss beam also supports the gutter for collecting water/ snow from roofs.

In order to withstand wind suction, the ends of the cantilever truss beams, which support the steel tiles, are held by slender tubular profiles to the concrete bleachers structure, also allowing the connection between the steel structure and the bleachers concrete structure. These cantilever truss beams are braced. There are also bracing in the vertical plane, between the tubular profiles, in the central part of the external faces of the stadium.

Figure 2.4-4 – RheinEnergie Stadium, Köln



(a) internal view; (b) roof of the bleachers; (c) mast; (d,e) detail of tubular profiles; (f, g) anchors of the mast and cables (images by author).

*Imtech Arena (Volksparkstadion), Hamburg, 1998*

Architects; Mos Architekten; Engineers: SBP Engineers

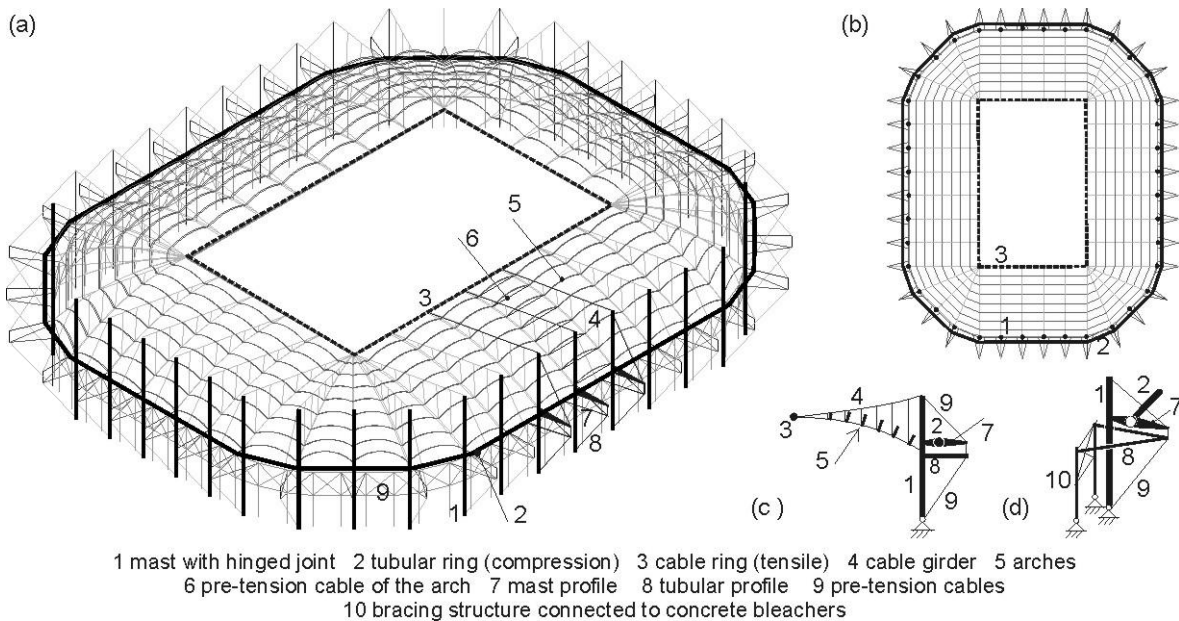
This stadium in Hamburg presents polygonal base, composed of 40 segments. The bleachers are made of concrete and covered by surface membrane roof (PVC / polyester), supported by steel profiles and cables (Figure 2.4-5, Figure 2.4-6).

The roof supporting system is compound of cable girders<sup>3</sup> positioned perpendicularly to the polygon faces, connected to the tensile inner ring and tubular masts (which are connected to the compressing outer ring), showing similar behaviour to a bicycle wheel or spoked wheel.

The lower cables of such beams support tubular arches. These arches have pre-tensioned cables, allowing eliminating the horizontal reaction. Furthermore, the tubular arches and the lower cables support saddle-shaped modules of the roof. The cable girders divide the roof in 40 modules. Each module is divided into eight modules in the form of saddles, totalizing 320 saddles.

The masts are hinged connected to their base plates and have lateral bracing (profile with variable transversal section held by pre-stressed cables to the top and base of the mast), reducing the buckling length and increasing its stability. These cables are also jointed to tubular arms that are connected to the steel bracing frame that involves the concrete bleachers.

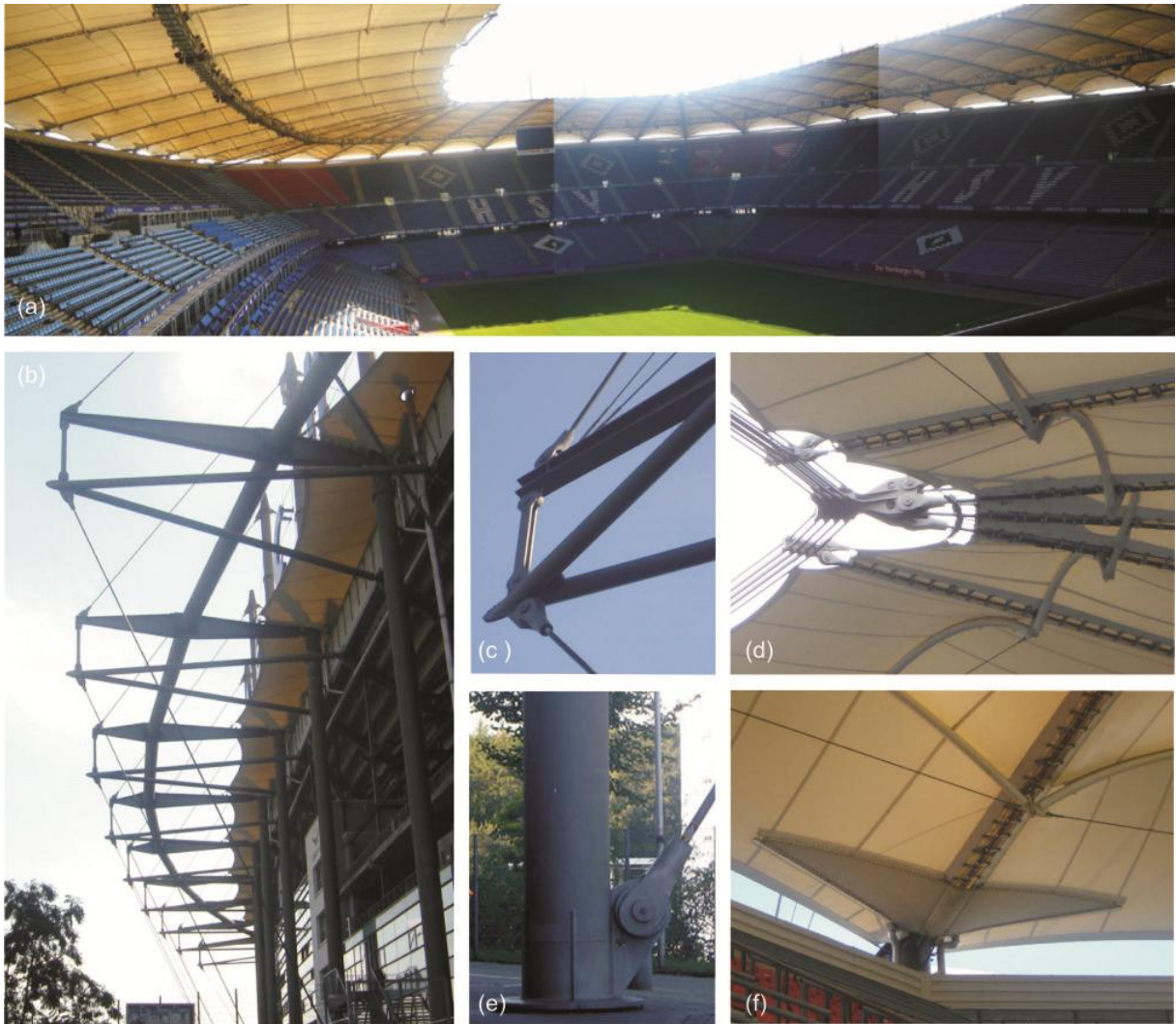
Figure 2.4-5 – Imtech Arena (Volksparkstadion), Hamburg



(a, b, c,d) 3D view, plant support system, vertical section and detail of the mast; (sketches by author).

<sup>3</sup> *Cable girders*: beam compounded by curved cables connected by vertical cables under pre-tension. In this arrangement, all components are under pre-tensioning (OTTO; TROSTEL, 1969).

Figure 2.4-6 – Imtech Arena (Volksparkstadion), Hamburg



(a) internal view; (b) external view (c) bars mast detail, (e) mast base; (d, h) union between surfaces and arcs with pre-stressed cables; (photos by author).

### *Retractable roof, Castle Kufstein, 2006 (2000m<sup>2</sup>)*

*Architects: N. Kugel; Engineers: A. Rein*

The retractable surface membrane roof (PTFE/PTFE<sup>4</sup>) located in the courtyard of the medieval castle of Kufstein is supported by steel tubular masts and a spatial supporting system. It presents polygonal shape, slightly circular, made up of 15 equal segments (Figure 2.4-7 and Figure 2.4-8).

The roof spatial supporting system is compound of cable girders associated to steel rings, internal tensile ring and external compression ring, presenting similar behaviour to a spoked wheel. The upper cables (of the cable girders) are tied to the

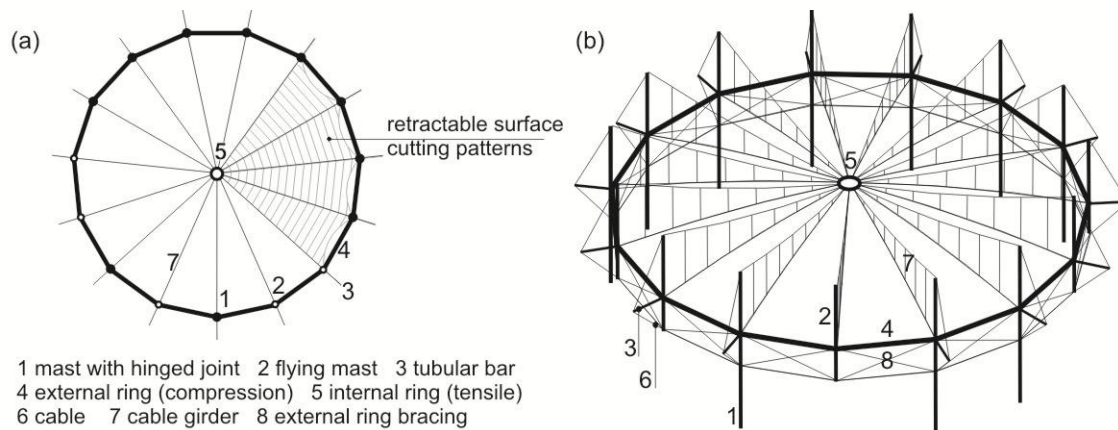
<sup>4</sup> PTFE/PTFE: membrane material compounded by PTFE fabric coated by PTFE, section 2.5.2.

top of the masts, and the lower ones to the connection between external compression ring and masts.

This system is supported by ten hinged masts and five flying masts. The flying masts resulted from anchor restrictions, since this roof is located in an area of historic preservation. Thus, to ensure overall stability and stiffness of the structure, the polygonal modules are braced and also count on the tensile ring (external) formed by cables. The masts have lateral tubular bars connected to them, reducing its buckling length and increasing its stability.

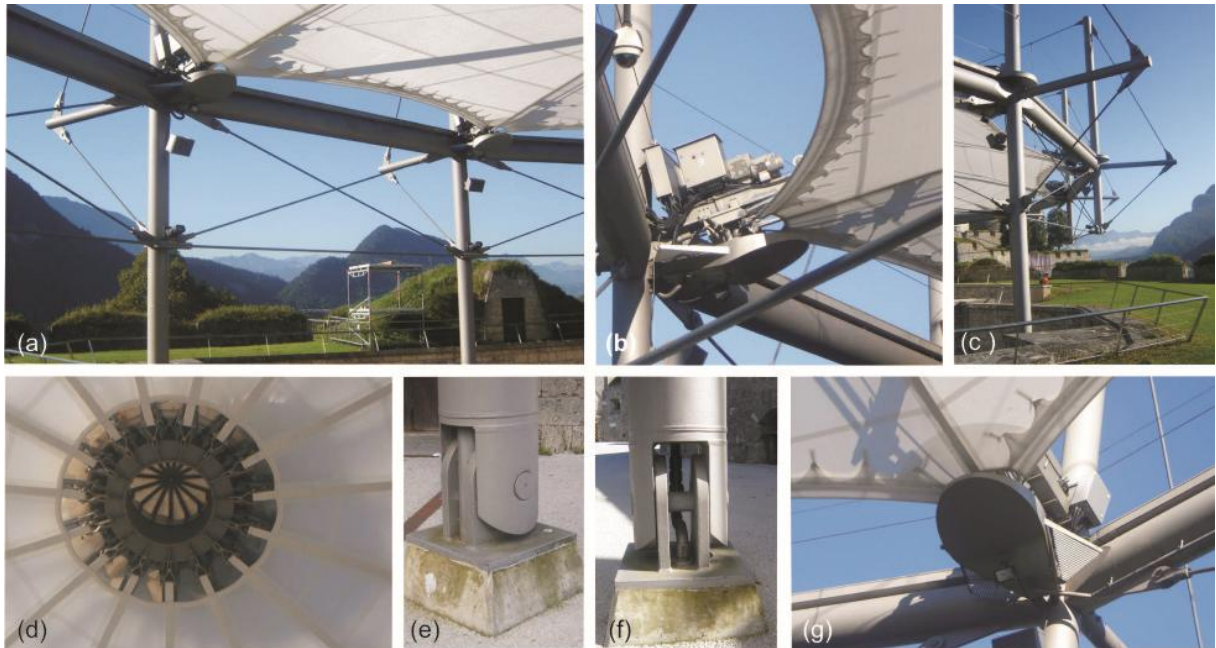
The roof is formed by radial saddle shape modules with smooth curvature. The retractable roof inner movement (opening and closing) is carried out by power tractors sliding in the lower cables of the cable girders.

Figure 2.4-7 – Retractable roof, Castle Kufstein



(a, b) 3D view and supporting system layout (sketches); (c) external view; (images by author).

Figure 2.4-8 – Retractable roof, Castle Kufstein



(a) compression ring with bracing; (b, d) Retractable membrane anchor; (c) masts with rigid bars hold by cables; (e, f) detail of hinged mast with internal piping for rainwater collecting; (g) tensile ring; (images by author).

### *New Waldstadion, Frankfurt/ Main, 2005*

*Architects: von Gerkan, Marg & Partner; Engineers: Schlaich Bergermann & Partner, Stuttgart.*

This stadium in Frankfurt/Main have polygonal base, compound of 44 segments, and two independent surface membrane roofs (internal and external) whose supporting system rests on concrete bleachers (Figure 2.4-9, Figure 2.4-10) . The internal roof (PVC / Polyester) is retractable and the external roof (PTFE/glass fiber<sup>5</sup>) is fixed being composed of saddle shape modules, totalising 264 modules. The transition between roofs is covered with translucent flat plates. In this transition are lain the gutter to collect rainwater/snow and the equipments (hydraulic pressure) for opening and closing the inner roof.

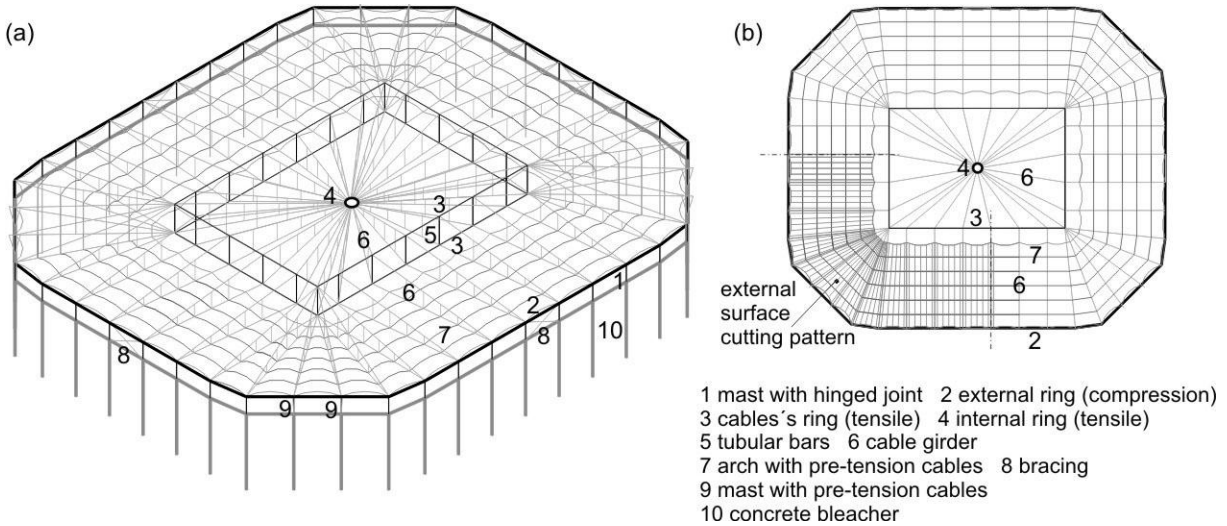
The roof supporting system is compound of masts and a spatial supporting system, This is formed of slender discontinuous tubular bars (in compression) inserted in a continuous cable net (under pre-stress), following the principle of *Tensegrity*. These cables are linked to internal (under tensile) and external (under compression) rings. The external ring is connected to articulated tubular masts, which rested on the concrete structure (bleachers). These masts are stabilized by bracings in the vertical plane, at the polygon corner and central part of the polygon face.

<sup>5</sup> PTFE/ glass fibre: material compounded by glass fibre fabric coated by PTFE (product brand-named Teflon), section 2.5.2

To increase the system stiffness, the inner corners of the rectangular polygon (defined by slender tubular bars or flying masts) are tensile connected to the bleacher concrete structure by tubular profiles. In parallel to these tubular profiles run pipes that carry water from rain and snow, collected by gutters located between the external and internal roofs.

The continuous cables (upper and lower) have internal vertical supports, i.e., they also work as cable girders. The lower internal cables are double allowing slippage of power tractors for opening and closing the inner roof. The lower external cables support tubular arches (with pre-stressed cables). The tubular arches and lower cables support saddle-shaped modules of the external roof.

Figure 2.4-9 – New Waldstadion, Frankfurt/ Main



(a, b) 3D view, plan; (c, d) internal and external views; (sketches by author).

Figure 2.4-10 – *New Waldstadion*, Frankfurt/ Main

(a) views: internal, external; (b) corner of the polygon connected to the bleacher concrete structure by tubular profiles (c) masts and pre-tension cables; (d, g, h) mast details; (e) aches with pre-tension cables; (f) joint between saddle shape modules; (images by author).

*Rothenbaum Tennis Stadion, Hamburg, 1997 (total 8500m<sup>2</sup>; interna3200m<sup>2</sup>)*

*Architects: ASP Architects Schweger & Partner, Hamburg; Engineers: Sobek & Rieger, Stuttgart.*

This arena in Hamburg presents polygonal base composed of 18 segments, resembling a circle. The surface membrane roof (PVC / Polyester) is composed of internal and external independent surfaces. The external roof is fixed and made up of triangular cone shape modules; the internal roof is retractable, a dome with smooth curvature (Figure 2.4-11, Figure 2.4-12).

The roof supporting system is independent of the concrete bleachers structure, and is comprised by masts and spatial support system. This presents discontinuous slender tubular profiles (under compression) inserted in a continuous cable net (Tensegrity principle) joined to the internal (tensile) and external (compression) rings. The external ring is also linked to the masts.

The external ring (compression) and the intermediate ring (defined by slender tubular profiles or flying masts) have the same modulation, but the masts and the profiles are not aligned radially. Thus, on top of each mast two cables are anchored. These cables are linked to two profiles (flying masts), creating a triangular mesh cables, that comprises the basis of each cone shape module. The top of cone shape module is supported by three cables which are anchored at the top of one slender tubular profile (flying mast) and at the top of two masts.

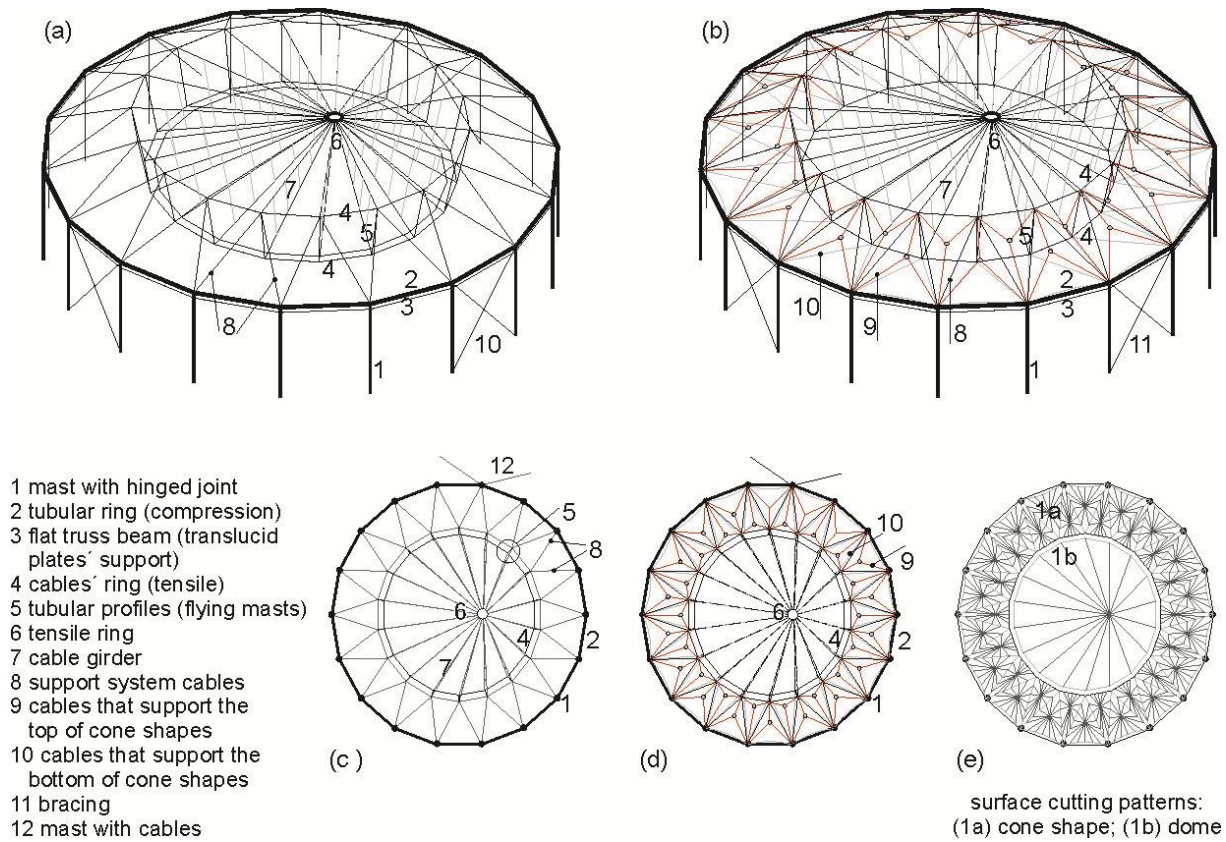
The continuous inner cables (upper and lower) are connected by vertical cables, which means, they work as cable girders. In the lower cables slid power tractors to permit opening and closing the internal roof.

Tubular masts are hinged and stabilized by the outer compression ring and bracing on the vertical plane.

As the concrete bleachers stands beyond the limits of roof membrane, the outer edges are covered by translucent plates (polycarbonate plates), which are supported by flat truss beams connected to the masts.

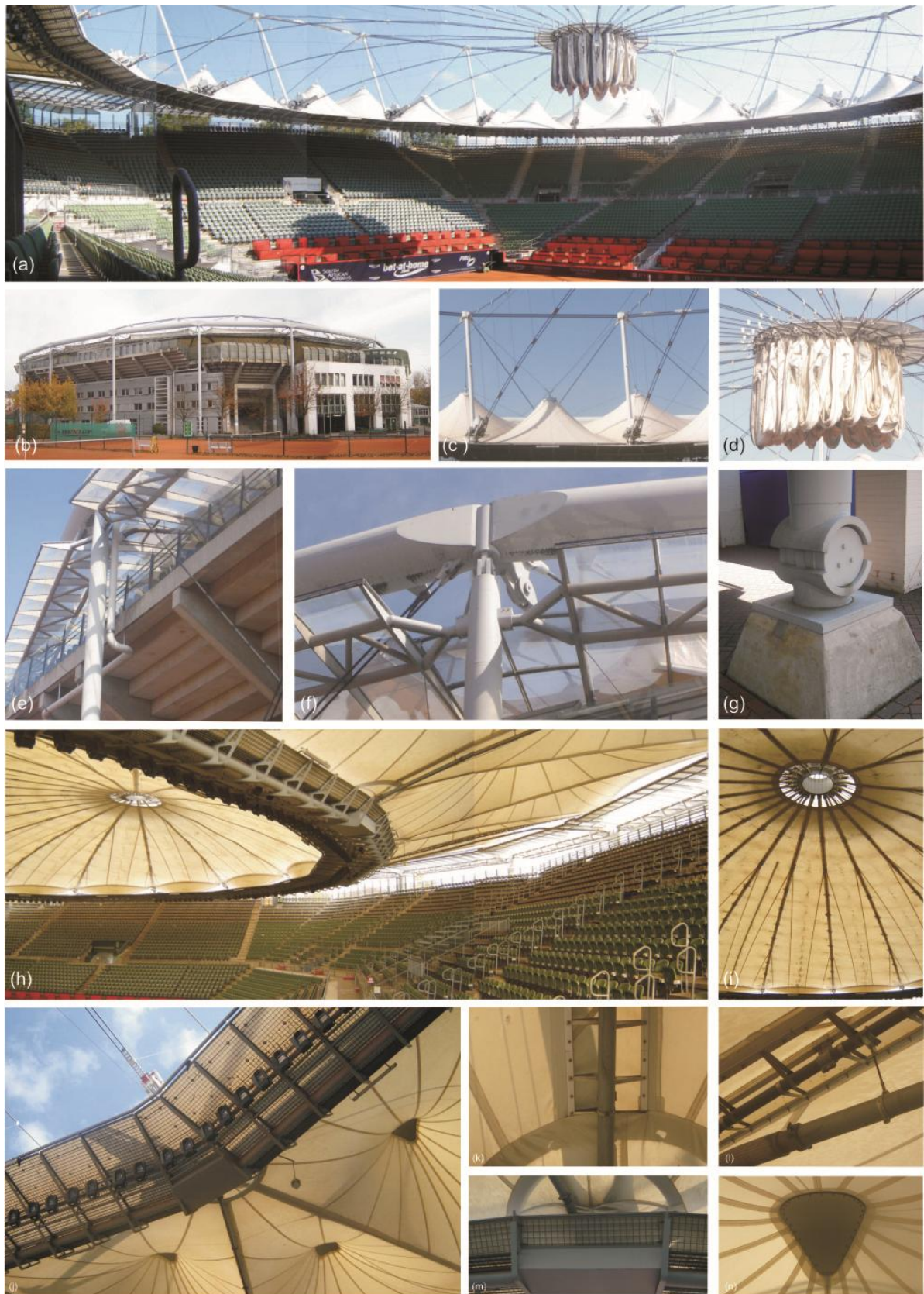
In the transition between the external and internal roofs (covered by translucent plane plates) there are the gutter for collecting rain water / snow, and equipment (hydraulic pressure) for opening and closing the inner roof. This water is sucked mechanically and transported by tubes which run parallel to the cables that support the base of cone shape modules.

Figure 2.4-11 – Rothenbaum Tennis Stadium, Hamburg



(a, b, c, d, e) 3D views; plans: support system, support system with cables that support the top of cone-shapes and surfaces' cutting patterns (sketches by author).

Figure 2.4-12 – Rothenbaum Tennis Stadium, Hamburg



(a) inside view; (b) external view (c, d) views: cone shape modules and inner roof closed; (e, f, g) mast details (top and bottom); (f) compression ring and flat truss beam; (h, i) Internal views of the inner roof open; (j, m) cone shapes and transition between roofs; (n) cone shape (top); (k, l) joint between cone shapes; (e) tube that transports rain water; (images by author).

*Ice rink (Wolfgang Meyer Sports Arena), Hamburg, 1997, (7000m<sup>2</sup>)*

Architects.: ASW Silcher, Werner + Redante, Hamburg; Eng.: Schlaich Bergermann und Partner, Stuttgart

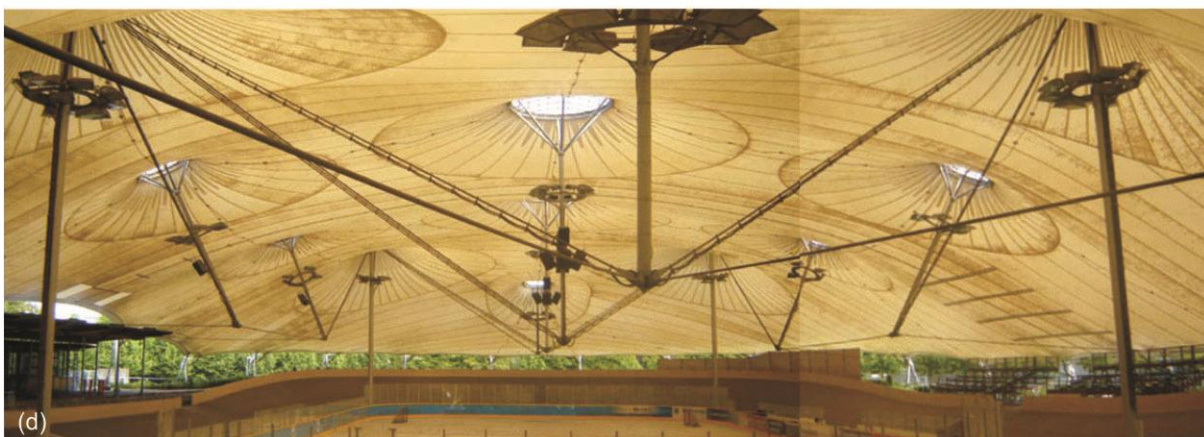
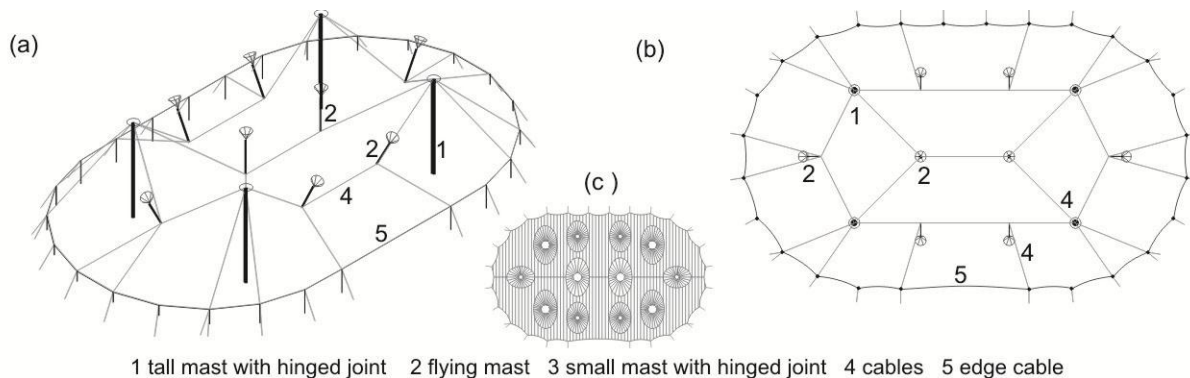
The roof of this ice rink is tensile surface membrane (PVC / polyester), with symmetry in the transverse axis, is supported by four tall masts and eight flying masts. This roof is pre-tensioned by edge cables that anchored in 26 small masts, (Figure 2.4-13, Figure 2.4-14).

The tall and small masts are hinged and held by cables to the basis. The top of the flying masts and tall masts have radial bars that connect to a ring. This fitting enables the support and better stress distribution on top of the membrane, as well as, the overhead illumination. The base of the flying masts rests against the three or four cables.

The spatial arrangement of the system has great simplicity and favours the complete integration between the membrane and the support system on the distribution of forces, ensuring the stiffness and stability of the structure.

The double curvature of the surface is achieved with the arrangement of various cone shapes (surface support at the top of masts). The cone shape is emphasized by the radial cutting patterns inserted in the mesh composed by parallel strips.

Figure 2.4-13 – Ice rink (*Eisbahn Stellingen*), Hamburg



(a, b) 3D view, plan of support system; (c) roof modules; (d) internal view; (sketches and photo by author)

Figure 2.4-14 – Ice rink (*Eisbahn Stellingen*), Hamburg

(a, b) external and internal views; (c, d, e) top and bottom of small masts (f) cable anchors, (g,h) top and bottom of flying mast; (photos by author).

### *Olympic stadium, Munich, 1967*

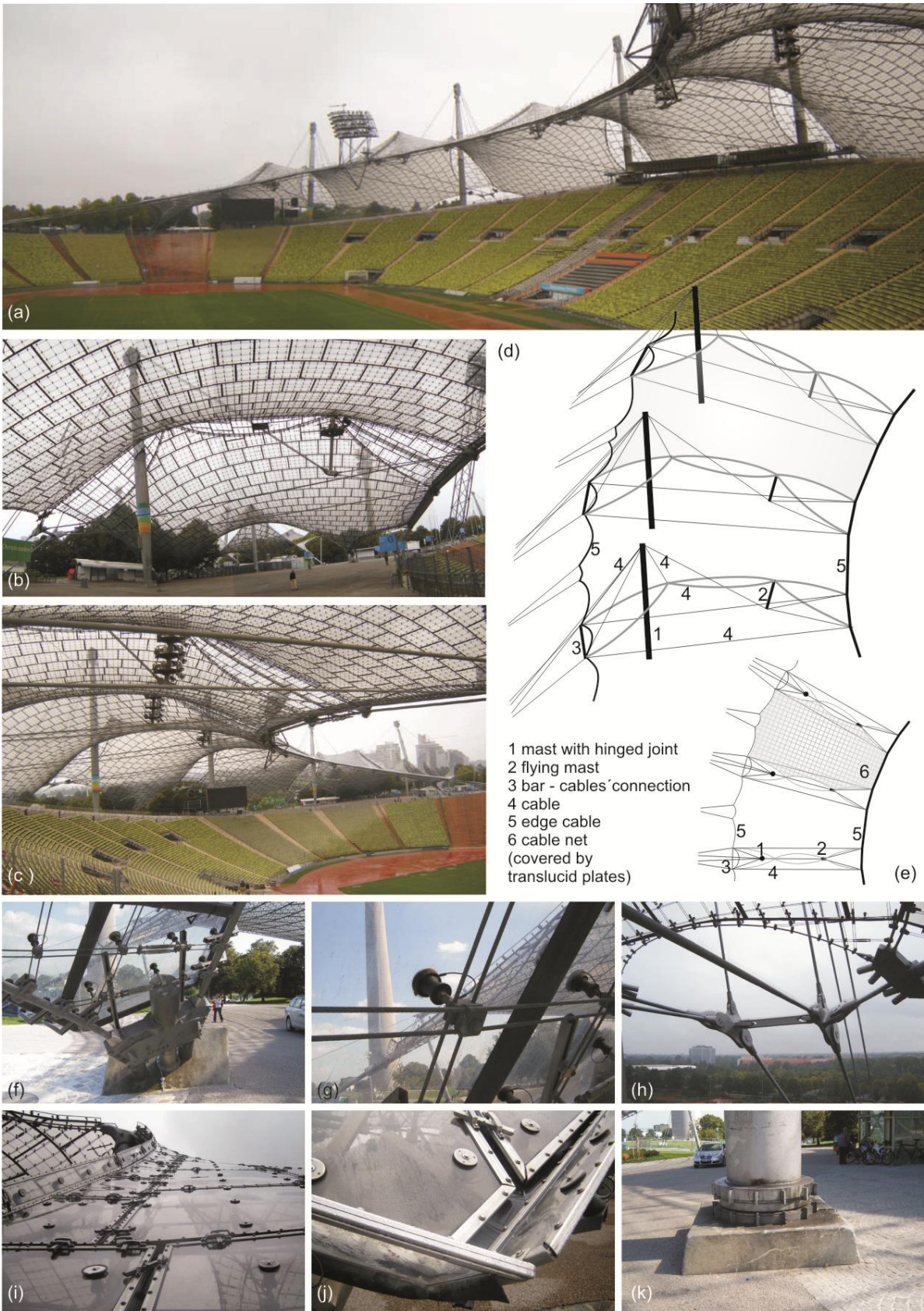
*Arquitetos: Behnisch + Partner, Stuttgart; Frei Otto, Warmbronn; Eng.: J. Schlaich und R. Bergermann and Leonhardt und Andrä.*

This Olympic stadium has a cable net roof (pair of cables) covered by translucent plates of polycarbonate, Figure 2.4-15. These plates rely on suction cups that are connect to the cable net at junctions between cables. The joint of the plates is made by black plastic profiles and permits the drainage of water.

The cable net roof is compound of radial modules that are joined by edge cables. These modules are supported by cables, flying masts and tall masts. The tall masts are hinged and have pre-tensioned cables. The roof is also pre-stressed by internal tensile arch (composed by cables) and the external tensile edge cable.

The spatial configuration of the cables ensures stiffness and provides complete integration between the cable net and support system.

Figure 2.4-15 – Olympic stadium, Munich



(a, b, c) internal views (sketches); (d, e) views: 3D plant; (f, g, i, h) internal and external views of the cable net covered with translucent polycarbonate plates; (h) bar connection between cables; (k) anchoring of hinged mast; (sketches and images by author).

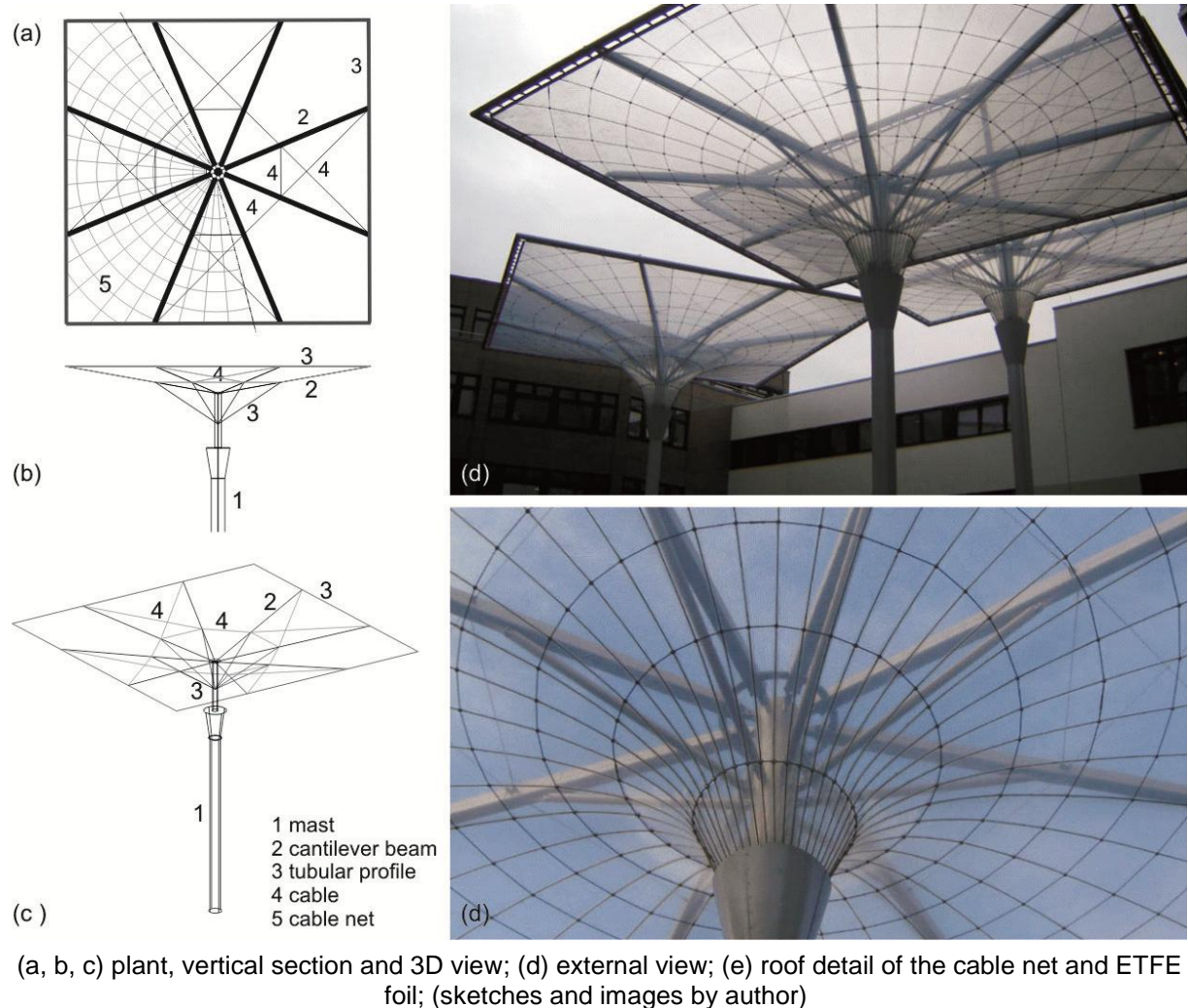
*Umbrellas - courtyard of the company IHK, Würzburg, 2003 (aprox. 475m<sup>2</sup>)*

*Architects: Franz Gröger, Georg Redelbach; Eng.: SMP Schöne/ Maatz + Partner (IPZ, Berlin).*

The roofs (umbrellas) located in the courtyard of IHK company have a square base and inverted cone shape (Figure 2.4-16, Figure 2.4-17). They are compound of ETFE<sup>6</sup> foil and cable net (working together) that are stabilized under pre-tension. In this case, the cable net and the foil have the same pattern. The foil is printed with small dots to minimize the incidence of light.

This foil presents the elongation trends requiring the pre-stress adjustment during the life of the structure. Thus, when this foil is used in pneumatic structures (synclastic surfaces), this behaviour is compensated by increasing inner pressure. However, when used in anticlastic surfaces, this behaviour can be reduced by the restriction imposed by the cable net, made of small linear elements, as in this case.

Figure 2.4-16 – Roof - courtyard of the company IHK, Würzburg



<sup>6</sup> ETFE - translucent foil, section 2.5.2.4.

This roof is supported by eight cantilever beams, arranged radially, joint in the square tubular base and supported by a single mast, which is rigidly supported to the itsbasis. These cantilever beams (square profiles) have lateral bracing by tubular profiles and are also connected by pre-stressed cables.

Figure 2.4-17 – Roof - courtyard of the company IHK, Würzburg



(a, b, c) details of the roof support system; (images by author).

## 2.4.2 STRATEGIES OR RULES IDENTIFIED

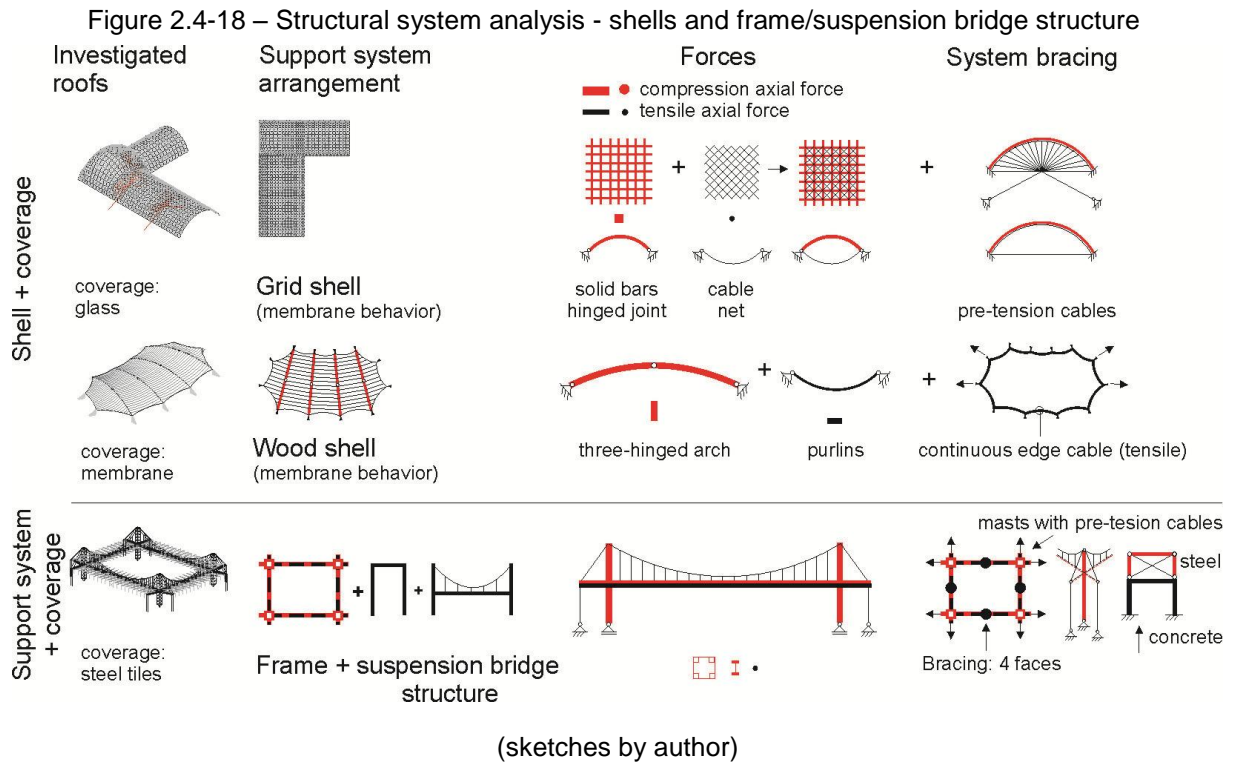
Different roofs were investigated: wooden shell, grid shell, frame/suspension bridge structure covered by tiles, as well as structural membrane and cable net roofs. This investigation allowed an overview of how these systems are organized and what components are used in pursuit of optimal performance.

### 2.4.2.1 Organization and performance of investigated systems

In the wooden shell and grid shell, of small thickness, the optimum performance is associated to the surface geometry (curvature), consisting of slender articulated components that support external loads by tensile and compression forces, working together and under pre-tension, defining the membrane behaviour of the surface, according to the analysis of the structural system (Figure 2.4-18). These shells are covered by membrane and glass, respectively.

In the support system compounded by frame/suspension bridge structure covered with tiles, the optimum performance is associated to the three dimensional organization and the cooperation among hinged components (beams and masts) stabilized by cables under pre-tension in the vertical and horizontal planes; and the use of components with lower density (truss components and or components with

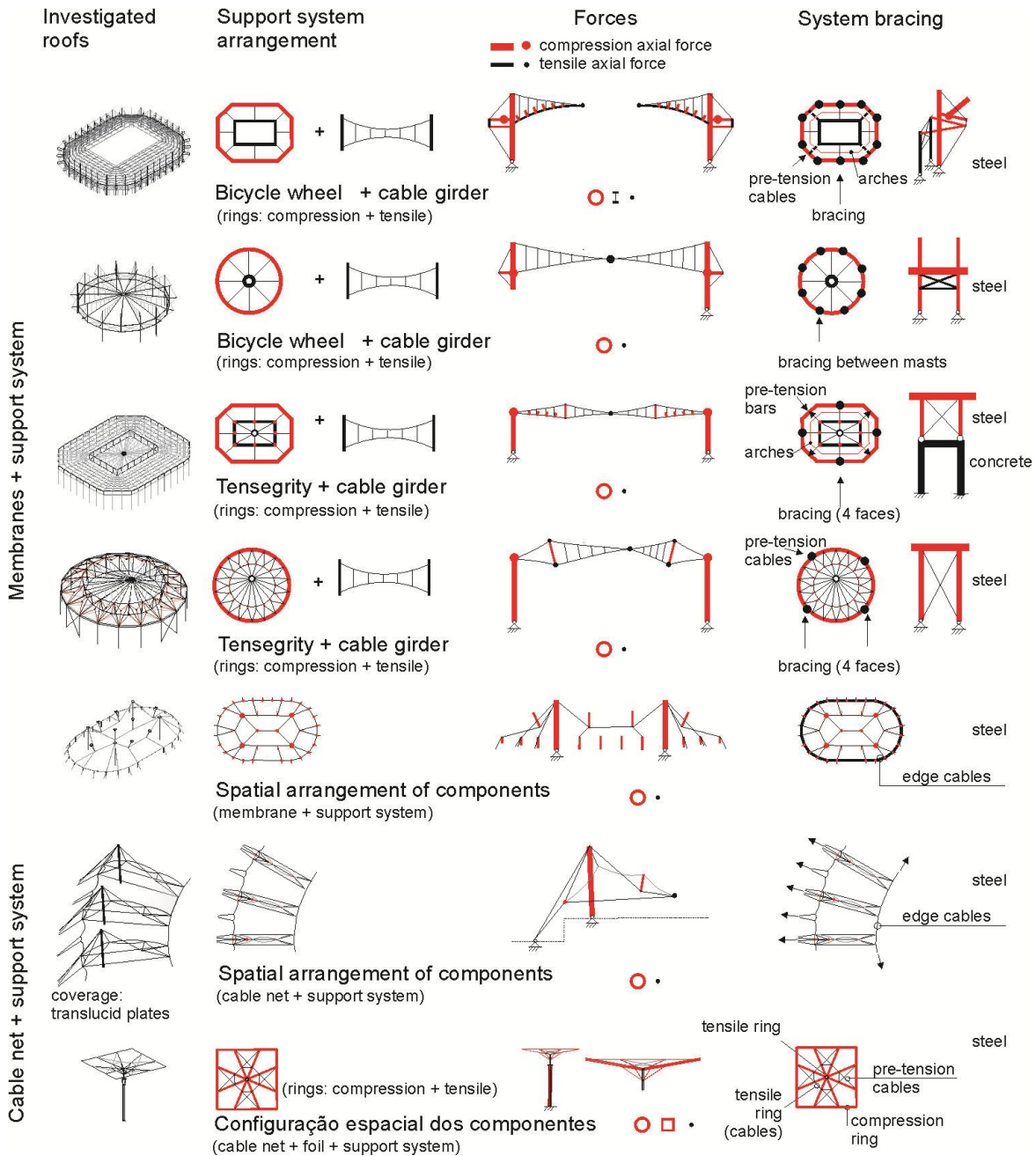
hollow cross section) and under compression and tensile axial forces (mainly), according to the analysis of the structural system (Figure 2.4-18).



In the surface membrane roof for large spans, the optimum performance is associated to the geometry and pre-stress state of its surfaces, working together with the supporting system. The supporting system consists of masts (hinged and braced in the vertical plane) and the spatial supporting system (consisting of cable girders or *Tensegrity* system) associated to internal ring (under traction) and external ring (under compression), featuring great stiffness, lightweight and overall stability, according to the analysis of the structural system (Figure 2.4-19).

In the surface membrane roof for medium and small spans, the optimum performance is related to the least amount of support elements (e.g., hinged masts with cables, flying masts and cables), the geometry and pre-tension of the membrane (and or cable net) stabilized by edge cables, and the cooperation and integrated work of the components, according to the analysis of the structural system (Figure 2.4-19).

Figure 2.4-19 – Structural system analysis - surface membrane roof and cable net roof



(sketches by author)

2.4.2.2 Surface membrane roof – geometry and arrangement of components

Among the investigated structures, the surface membrane roofs stand out. They are both structure and roof, working together with the supporting system as a whole, helping to withstand loads under pre-tension. In other roofs, tiles, glass, membrane and polycarbonate sheets have only a function of top covering.

### *Arrangement of membrane surface*

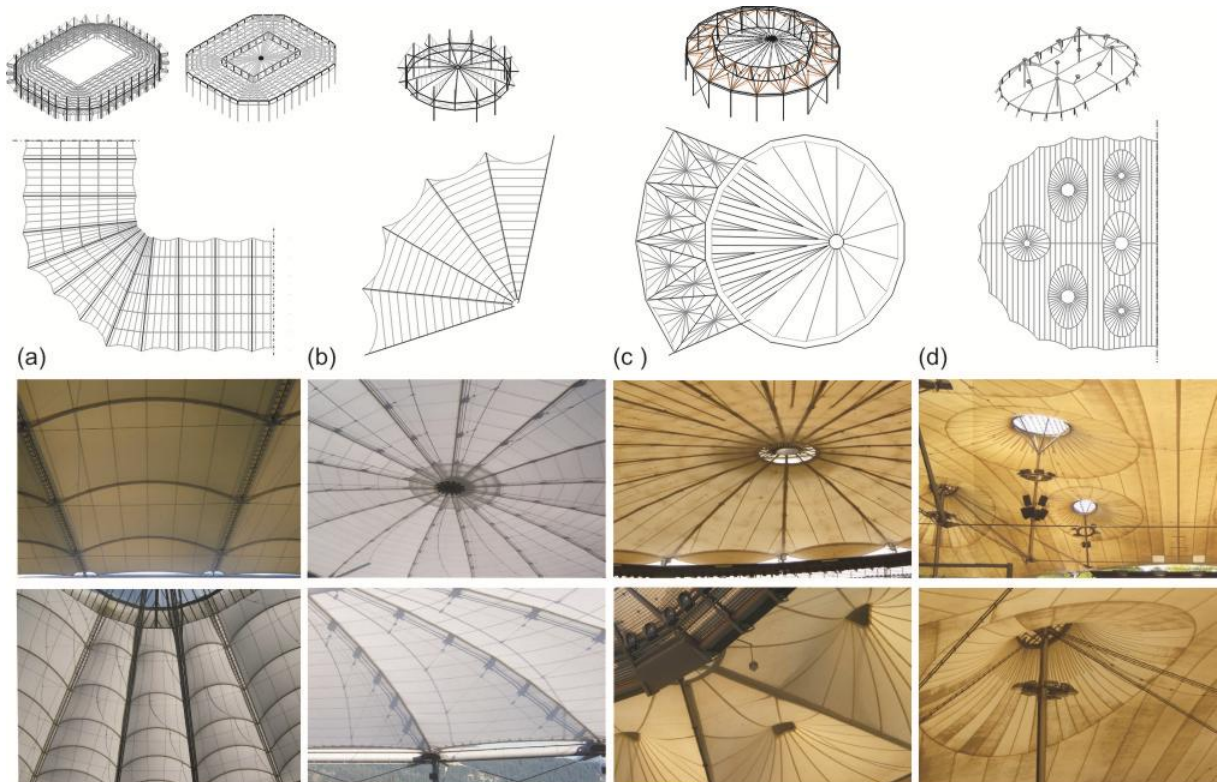
It was observed that the three-dimensional arrangement of the supporting system (arches, masts, cables, edge cables, etc.) is linked to the surface membrane arrangement and geometry.

Among membrane roofs for large spans, the large surface area is comprised of cone shape or saddle shape modules (supported by arches and high points) arranged in parallel or radially (Figure 2.4-20a-b-c).

Among membrane roofs for small and medium spans, there was also the adjustment and organization of the surface form in pursuit of symmetry and repeated patterns. However, the formal expressiveness of the system is more explored (Figure 2.4-20-d).

The surface membrane modules (cones, saddles, etc.) are generally divided into strips (cutting patterns) radial or parallel which align to the flow of forces and principal curvatures of the surface. In the surface membrane areas subjected of high stress (near the anchor points) the removal of membrane material was observed, and around these areas the use of double layer membrane was also verified.

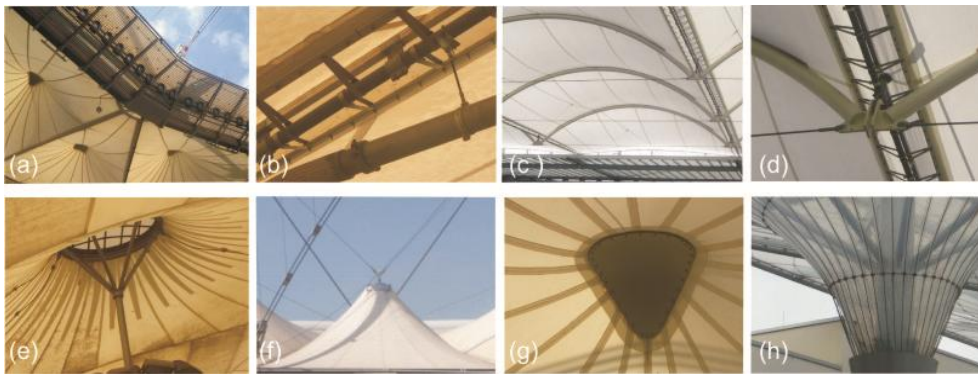
Figure 2.4-20 – Membrane arrangement (investigated roofs)



(a) parallel saddle shape modules and material threads parallel to seam; (b) saddle shape modules organized radially, material threads predominantly parallel to seam; (c) dome with radial cutting patterns and cone shapes (triangular base) arranged radially and with radial cutting patterns; (d) combination of parallel and radial cutting patterns; (sketches and images by author).

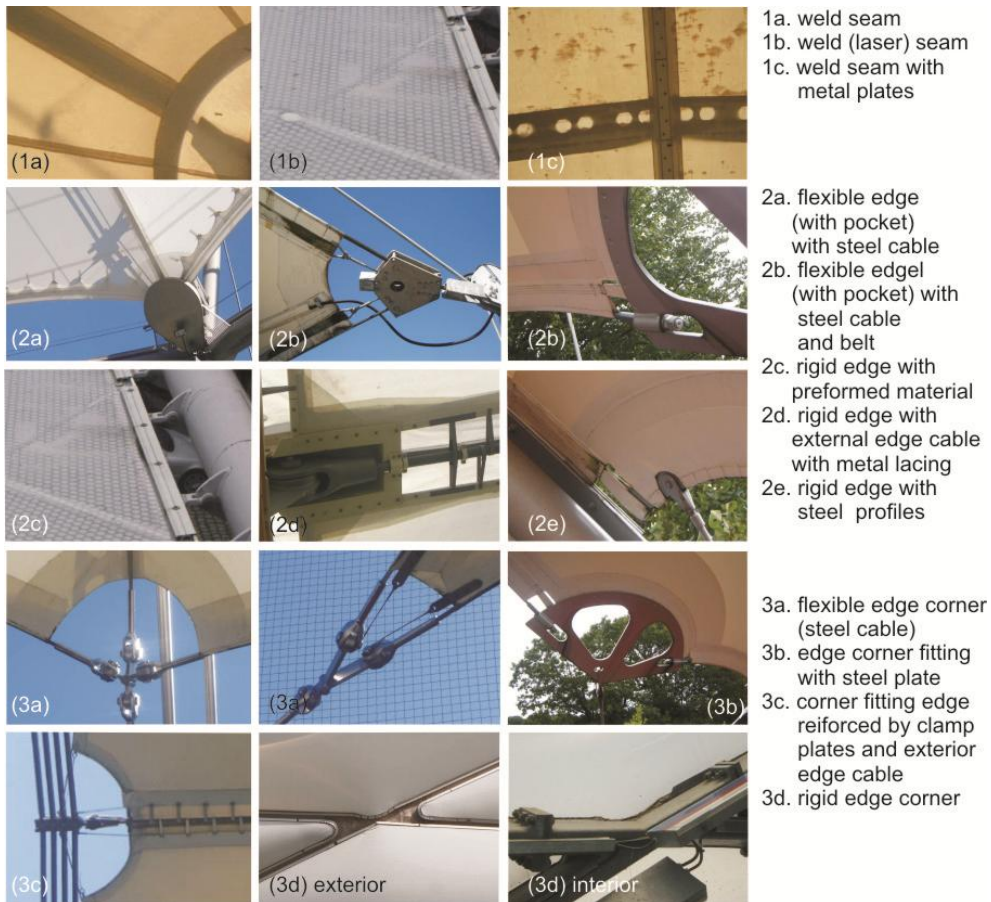
Regarding the system characteristics and surface anchor points (Figure 2.4-21), ridges and valleys, highs and low points were observed as organized by Bubner (2005). Regarding the seam between panels, welded joints were observed in membrane surfaces (Figure 2.4-22-1a, 1c) and in translucent foils (Figure 2.4-22-1b). Regarding the edges and corners of the surfaces, flexible and rigid edges fittings were noticed, as shown in Figure 2.4-22 (2a-2e, 3a-3d).

Figure 2.4-21 – (a-d) Ridges and valleys; (e-h) Highs and low points



(images by author).

Figure 2.4-22 – Seam and fittings

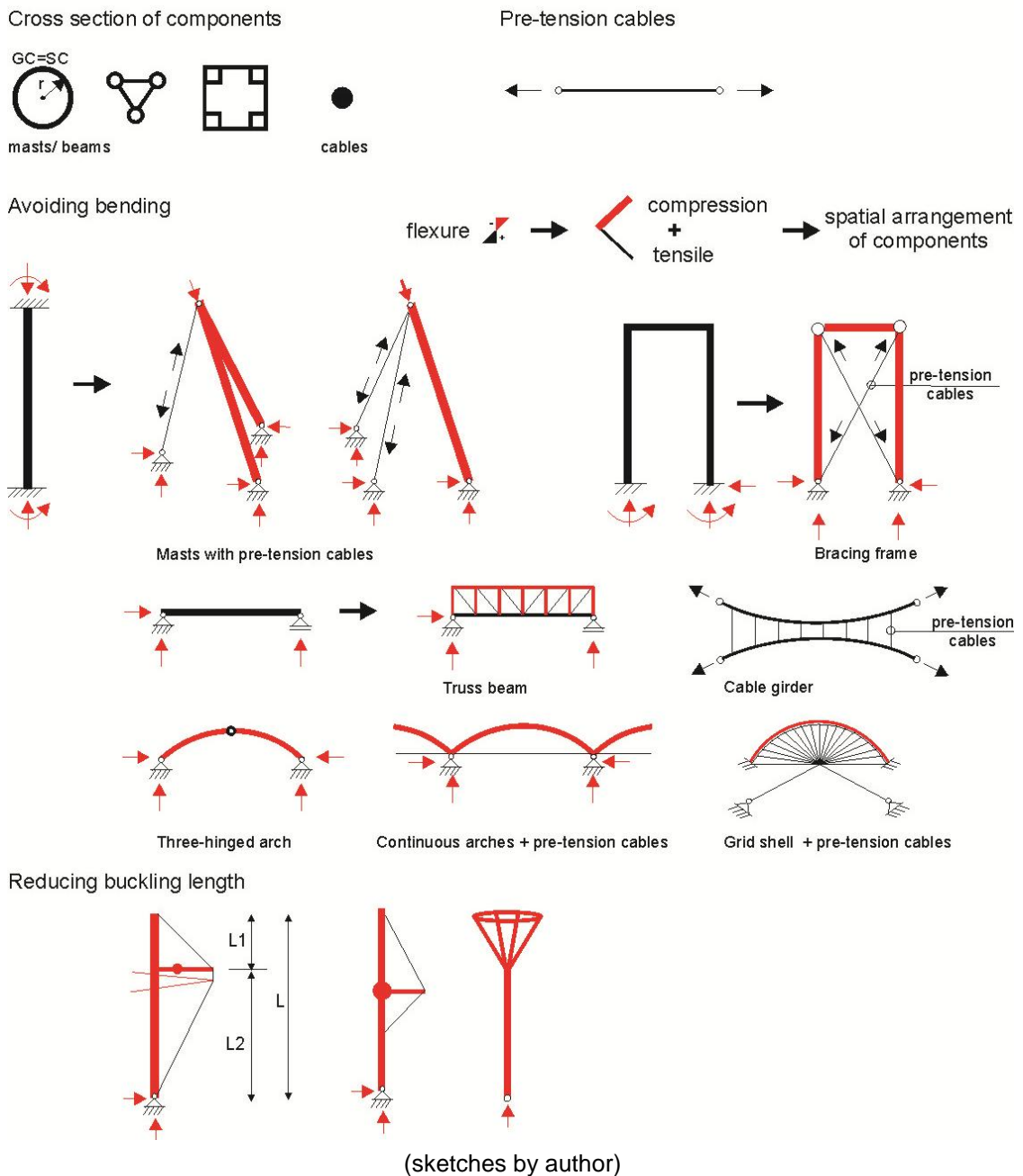


(1a-1c) membranes and foils seam; (2a- 2c) flexible edges (3a-3d) surface rigid corners; (images by author).

*Arrangement of the supporting system component*

Arrangement of jointed components under pre-tension (e.g. masts with cables, cable girders), masts and cables with hinged anchor points, as well as components with hollow transversal sections are predominant in the supporting system (Figure 2.4-23, Figure 2.4-24a-l). In other words, it is sought to understand the global system behavior, to combine and to organize three-dimensionally linear components (ex. cables, masts), mainly under axial forces (tensile and compression), choosing the transversal section of the components appropriated to the acting forces. These make possible to reduce the system mass to the same volume, i.e., the system density.

Figure 2.4-23 – Geometry and arrangement of the supporting system components



Components and arrangements that stand out:

- Cables under pre-tension: the cable is a flexible and lightweight element with unlimited length and concentrated mass near the gravity centre; it has no bending and compression stiffness. Its rupture occurs when the material resistance reaches its limit, i.e., it is associated with the amount of material and not the way that it is distributed in the cross section. Thus, the tensile cable offers more stability and uses more efficiently all its section.
- Circular cross section of masts and beams under compression: in the circular cross section, the material is symmetrically distributed and with the same distance to the gravity centre of the section, furthermore, the gravity centre of the cross section matches the shear centre regarding the perfect symmetry of the section. Thus, it is more difficult for the mast to rotate or lose its stability.
- Hollow cross section to masts and beams under compression (comprising of tubular profiles arrangement): prevents the use of robust components enabling material savings and better stability.
- Spatial components (masts, beams and frames) arrangement to prevent bending:
  - . Masts with cables: have hinged base (e.g. ball joint cast in concrete) and are stabilized by cables under pre-tension. This three dimensional configuration with hinged anchor points decomposes the bending moment in tensile and compressive forces, enabling to reduce the mass of components and to increase structural efficiency.
  - . Truss beams and truss masts: a system that allows the use of slender elements, bearing loads without developing bending stresses, working only under compression and tensile axial forces (combined effect of cable and arch).
  - . Lateral bracing of the mast with rigid bars and cables: in components subjected to compression forces, lateral displacement can occur (buckling). As the critical buckling load given by Euler's formula<sup>7</sup> is inversely proportional to the square of the length of the mast, the mast lateral bracing enables to reduce the mast length and to increase the buckling stability.
  - . Bracing frame: the diagonals under pre-tension divide the loading and enables to transform (by pre-tension) compressive stress into tensile stress.

---

<sup>7</sup> Critical buckling load given by Euler's formula:  $P_c = \frac{\pi^2 EI}{(kL)^2}$ , where: k – buckling coefficient, E – modulus of elasticity, I – moment of inertia, L – length of member.

. Beams comprised by hinged tubular arches with pre-tension cables: enables to eliminate horizontal reaction.

. Truss girder comprised of external curved cables with opposite curvatures, connected by vertical internal cables (OTTO; TROSTEL, 1969): all components work under tension. The internal cables ensure the pre-tensioning of external cables.

Figure 2.4-24 – Anchor points of components



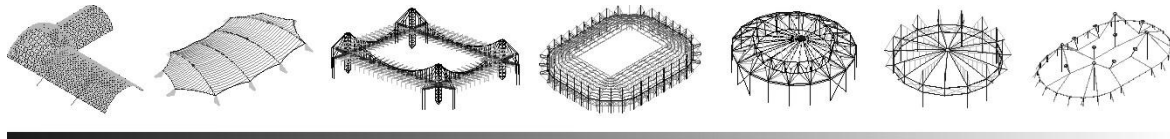
(a, b, c, d, e, f, g) base (with ball joint) of hinged masts; (h) base of flying mast; (i, j, k, l) base of cables; (m, n, o, p) components anchor points on the top of the masts. Image (a): mast ball joint later cast in concrete) by SCHLAICH (2003), p.109; images (b-p) and sketch (a) by author.

It's important to highlight that the observed connections between the membranes and supporting system components enable the load transmission and are also means of applying pre-tension to components. They also enable rotations and displacements, since the membrane structures are subjected to large movements under load, have low shear strength and do not support bending and compression. These connections are usually exposed in the structure and reveal great precision of detailing and manufacturing, shown in Figure 2.4-22(2a-2e; 3a-3d) and Figure 2.4-24 (m-n).

### 2.4.2.3 Strategies to the optimal performance of this system

It was observed that the progressive capacity of these lightweight structures presenting optimum performance – supporting and transmitting large forces with smaller mass – is associated to the spatial stability of the structural system (whole structure), the high strength of materials (e.g. steel and synthetic fibres), as well as the low density<sup>8</sup> of the structural system (Figure 2.4-25).

Figure 2.4-25 – Progressive capacity of lightweight structures support large forces with smaller mass



This performance derives from three-dimensional geometry of the membrane surface in a state of pre-tension, the arrangement of supporting system components, as well as the spatial organization of structural system components (membrane and supporting system) working together (as a whole) and continuously under pre-tension.

The membrane surfaces are organized in modules and or subdivided in strips which align to the flow of forces and to the principal curvatures of the surface.

The supporting system is characterized by the combination of systems and/or by the use of slender components three dimensionally arranged and hinged joint. In this spatial arrangement predominates: increased number of components and arrangements that allow bearing external loads by axial tensile and compression forces, up to material resistance (tensile) and stability of the component (compression); the subdivision or modular organization of components, in order to reduce the spans and avoid robust components, making the manufacture and assembly of components more feasible; greater use of flexible fittings.

So, it can be said that the strategies used by architects and engineers to achieve optimal performance of this system are related to:

- the structural system arrangement: three-dimensional configuration whose overall stability derives from the cooperative work done by components, and reveals the shortest force path;
- the geometry and arrangement of all components: form that reveals the best use of material and the shortest force path.

<sup>8</sup> The low density of the structural system results of the use of fabric compounded of synthetic fibres that supported large tensile forces with small density, and of the arrangement/geometry of supporting system components (e.g. components with hollow transversal sections, truss components, masts with pre-tension cables).

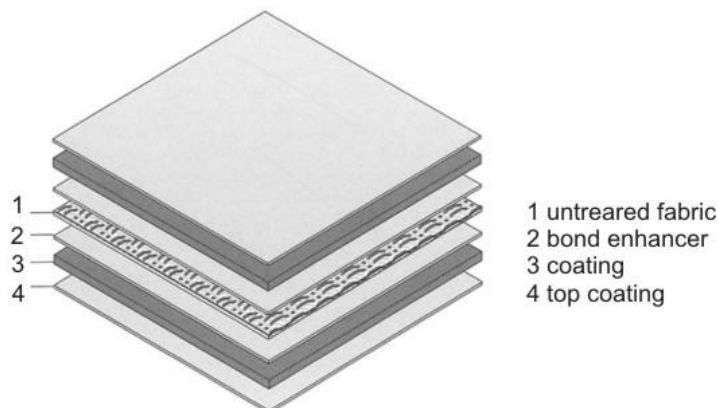
## 2.5 MEMBRANE MATERIAL

### 2.5.1 MEMBRANE MATERIAL CHARACTERISTICS

The material used for membrane structures, known as technical membrane and named here as structural fabric, is usually a composite material. According to the Material Engineering, composite material is defined as a material, made artificially, consisting of several phases or materials which are chemically different and separated by a different interface. The mixture of these materials is carried on a macroscopic scale, forming a unit to obtain a better combination of properties (CALLISTER, 2009).

This structural fabric is compounded of two parts: a matrix (protective layer) which is continuous and covers the dispersed part (fibres). The matrix and the fibers work together, but perform different structural tasks (Figure 2.5-1).

Figure 2.5-1 – Material structure (fabric + PVC coating)

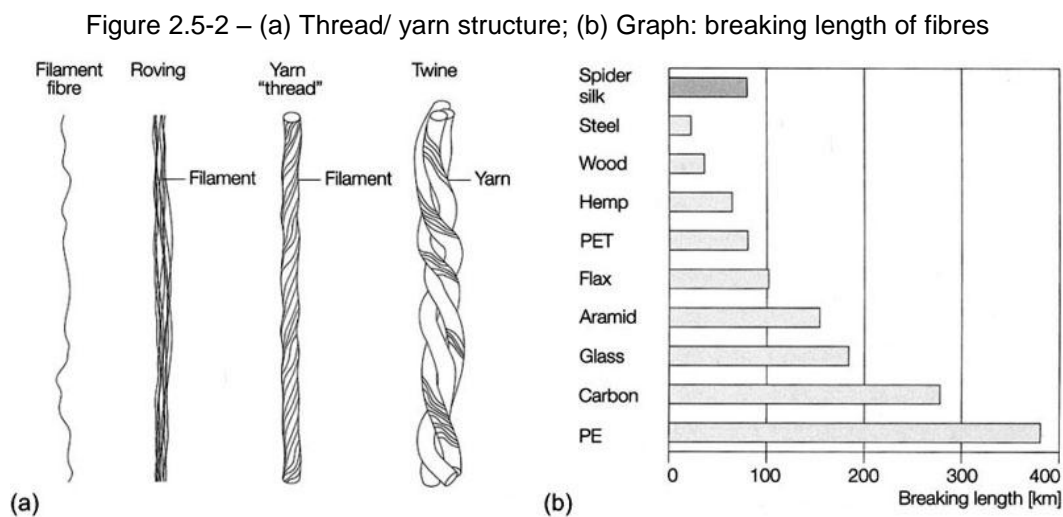


Source: KINIPPERS *et al.*, 2011, p.101.

The fibers are responsible for the great tensile strength and load bearing capacity of the material. They are filaments of infinite length resulted from melt spinning materials (polyester, glass) or solution (aramid), (BÖGNER-BALZ; BLUM, 2008). The individual fibres or filaments, positioned parallel, gathering in bundles (known as roving) which are twisted to form a yarn (or thread), as shown in Figure 2.5-2a. In this procedure the individual filaments are loaded uniformly, increasing the twisted filaments (thread) strength (KNIPPERS *et al.*, 2011).

Then, the yarns are interlaced in the weaving process, forming the uniform and thin mesh of the fabric. In structural fabric, the most used fibres are: polyester fibre, glass fibre, and currently the PTFE (polytetrafluoroethylene) fibre.

According Knippers *et al.* (2011), the relationship between strength and self-weight of the fibres is an interesting parameter in lightweight structures design. In this case, the breaking length of the fibre is an indicator to select the material. This value corresponds to the length that a fibre, hanging on its own weight, could reach before rupture. According to Roland (1973), this length is not related to the size and cross section form of the material. The most efficient fibres are the ones that could support great stress with less density. In Figure 2.5-2b, it is possible to observe the breaking length and excellent performance of glass fibres and polyester fibres (PET), used on structural fabric, when compared to steel.



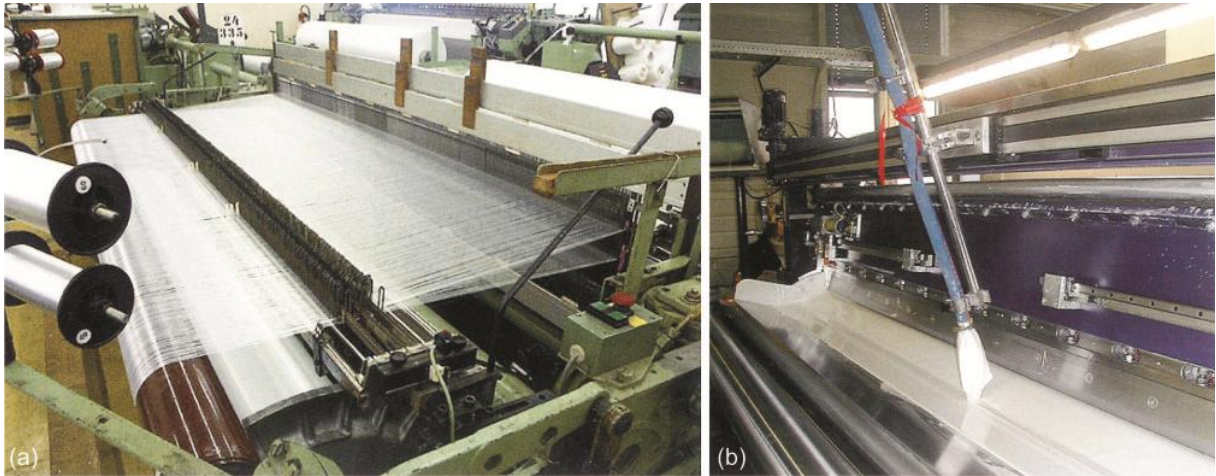
Source: KNIPPERS *et al.*, 2011, p.49.

The continuous matrix is compounded by different layers of polymeric substances that embed predominantly on both sides of the fabric (Figure 2.5-1). It provides protection to chemical attacks and also protects the surface against ultraviolet radiation (UV), abrasion, atmospheric effects and fungi. According to Bögner-Balz; Blum (2008), the coating also protects the threads to external influences and helps stabilizing the fabric geometry, assuring its durability. Among the coverings, the most used are PVC - Poly (vinyl chloride) and PTFE (polytetrafluoroethylene).

The manufacturing procedure of the structural coated fabric, used on textile construction, is industrial and has high quality. This includes the yarn production, the

weaving and coating process (Figure 2.5-3). It is important to emphasize that the first layer of the covering provides the compatibility (physical and chemical) and the adhesion resistance between the fabric and coating. This adhesion (between fabric and coating) contributes to increase the material tear strength and, according to Seidel (2009), it also increases the seam strength.

Figure 2.5-3 – (a-b) Polyester fabric weaving and PVC coating process



Source: SEIDEL, 2009, p.29 e 31.

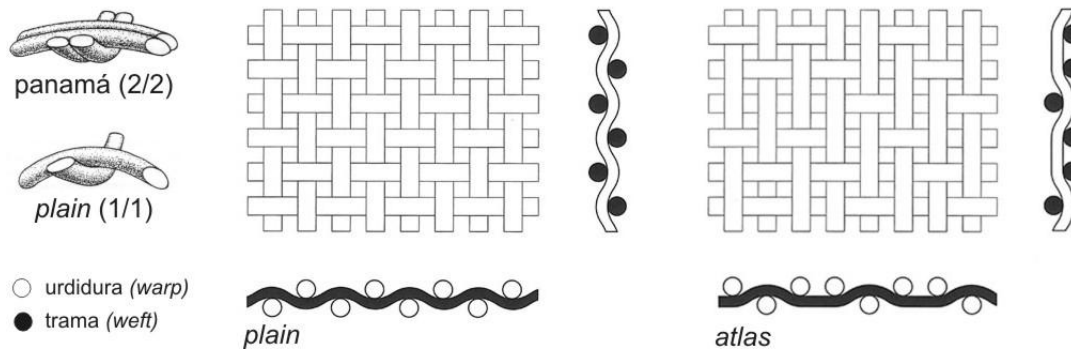
The most used materials in membrane construction are the woven coated fabrics. However, woven fabric without coating and material without fibres (foils) are also used. According to Milwich (2010), the woven fabrics are categorized, mostly by the weight per square meter ( $\text{g/m}^2$ ). The heaviest fabrics generally offer great strength, as they have more fibres.

The woven fabrics are systems formed by two types of threads, warp and weft. The longitudinal straight direction of the threads, is the warp direction, and on the perpendicular direction is inserted the weft threads, enabling the interwoven. The warp direction is stretched in the length of the material, and generally has more stiffness (Figure 2.5-4). The most important types of weave are *plain* (or *canvas*, *tabby*, *linen* or *taffeta*) and *atlas* (or *satin* or *twill*). However, the majority of fabric in the textile building use plain or panama (*basket*) weave (BAIER, 2010).

The weaving process results from different arrangement of the warp thread during the weft insertion, and has influence on the mechanical properties of materials. The plain weave results from alternate movement of the weft which passes above and below the warp direction. The panama weave is a special form of plain, in which two or three warp and weft threads are interwoven together. The twill (atlas)

weave is the result of an irregular rhythm, in which the weft threads pass once above and then below at least two warp threads, producing diagonal ribs (KNIPPERS *et al.*, 2011), as shown in Figure 2.5-4.

Figure 2.5-4 – Woven fabrics (*plain e atlas*): thread direction and arrangement



Source: MOLLAERT; HEBBELINK; HAASE, 2002, p.70; Adapted from KNIPPERS *et al.*, 2011, p.70.

## 2.5.2 MOST USED MATERIALS

The most used materials in membrane construction are PVC coated polyester fibre, PTFE coated glass fibre and, currently, PTFE fibre coated or uncoated.

### 2.5.2.1 Fabric without coating

#### *Polyester fabric*

The Polyester is a synthetic polymer<sup>9</sup> which contains the Ester functional group in the main chain. The polyester type used as fabric base refers to Polyethylene terephthalate or PET, and is also referenced in textile terminology as PES. So, the filaments, formed by PET granules are converted into yarn for the fabric production. The polyester fabrics have high tenacity and elasticity module, as well as low water absorption and low shrinkage comparing to the other fibres (BAIER, 2010). This behavior results from the crystallization and organized orientation of the molecular chain (FOSTER; MOLLAERT, 2004). They also have low resistance to UV radiation, and are also flammable at high temperatures, but self extinguishing after ignition. These disadvantages are reduced with PVC covering. It is also necessary the

<sup>9</sup> Polymer is a compound of high molecular weight (macromolecule), which structure (long main chain) is compounded of simple chemical units repeated. It comes from mineral (ex.: oil, coal, natural gas), vegetal (ex.: latex of tropical trees) or animal (ex.: casein) source, which can be natural or synthetic. Some polymers can be used in engineering applications, being able to replace traditional materials; according to some authors they are called engineering plastics (MANO; MENDES, 1991).

treatment of the polyester fibres (sensitive to hydrolysis) with a substance that does not absorb water or moisture preventing its capillarity.

#### *Glass-fibre fabric*

According to Milwich (2010), the glass-fibre fabric has been manufactured since 1930. The glass fibre is produced out of an inorganic<sup>10</sup> material mixture melted at 1600° that is forced through spinning nozzles and then cooled (BAIER, 2010). They have high strength, low stretching, low creep and they do not burn. However, they are sensitive to moisture and are brittle, being not suitable for retractable structures. The glass fibers are isotropic because of their amorphous structure. They have uniform cross section (approximately circular) and they exhibit linear elastic behavior up to its brittle failure (KNIPPERS *et al.*, 2010). According to Baier (2010), the most used yarns are made of *E-glass* (electrical). The glass fiber fabric has no resistance to UV radiation and dirt. This disadvantage is reduced with the PTFE or silicone covering.

#### *PTFE fabric*

The Polytetrafluoroethylene or PTFE is a polymer whose molecular structure contains fluorine<sup>11</sup> atoms tightly linked to carbon atoms. This fluorine-polymer, also known as Teflon, was discovered in 1938, by the engineer Roy J. Plunkett, but it has been used as fabric glass covering from the 70s (KOCH, 2004). The fabric, made of 100% high strength expanded PTFE fibres, is completely immune to UV radiation, chemical products, pollution, and is easy to clean. It endures extreme temperatures and has inflammable properties. The light transmission is approximately of 30% and the colors are genuine (i.e., white is white). This fabric is flexible and can be used in retractable membranes and high quality permanent structures that do not require waterproof qualities, in other words, the PTFE fabric can be used without covering. It is recyclable, but it is not ecofriendly. It has an expected life time more than 25 years (BAIER, 2010). This fabric tends to creep, but on the other hand, it has high tear propagation resistance (KNIPPERS *et al.*, 2011).

---

10 Sand/ Quartz (SiO<sub>2</sub>), limestone (CaO<sub>3</sub> and MgO), alumina (AL<sub>2</sub>O<sub>3</sub>), soda, boron (BAIER, 2010).

11 Fluorine has a mineral (fluorite) source (Sefar Architecture, 2011).

### 2.5.2.2 Coating

#### *PVC coating*

The Poli (vinyl chloride) or PVC is a synthetic polymer that has high strength and elastic module. However, it is brittle requiring plasticizers to increase its flexibility (KNIPPERS *et al.*, 2011). In order to be applied as a covering, ensuring impermeability to the material, it needs to be dissolved into a paste which is spread in both sides of the fabric. It is a chemical compound that includes additives to optimize its properties such as: flame retarding agents, plasticizers, pigments (to control translucence, transparency, UV range, visible light and colors), softeners (to prevent the coating from going brittle), stabilizers (thermals, oxidative and UV radiation).

Despite the qualities and impermeability properties of PVC layer, the plasticizer used in its compound has the tendency to migrate to the surface. Thus, it allows the accumulation of dirt and it is susceptible to the growth of bacteria and fungi on its surface. It contributes to the loss of the material ductility and it may lead to the appearance of cracks in the covering and to the exposure of polyester fibers. So, top layers of protections (lacquers) are used. Among the materials used as top coat, the PVDF (polyvinylidene fluoride) is highlighted. This lacquer has similar characteristics to PTFE, endures the cleanliness and provides a more effective barrier to the plasticizer migration and climate influences, increasing the covering quality.

#### *PTFE coating*

As stated before, the PTFE – Polytetrafluoroethyelene is a polymer with exceptional chemical qualities. It is generally applied to fibre glass material by dip coating. Then the material is dried and sintered at temperatures around 350° to 380°C. So, PTFE coating has an approximated behavior of a ceramic substance (BÖGNER-BALZ; BLUM, 2008). Therefore, it is not possible to be used with polyester substrates. It is available in beige color, but turns white after the exposure to UV radiation (MILWICH, 2010). It is inflammable under normal conditions, has resistance to UV (ultraviolet) and IR (infrared) radiation and to corrosive substances, and it is inert to environment pollutants. Exhibits self-cleaning properties and it is water repellent (FOSTER; MOLLAERT, 2004).

### 2.5.2.3 Coated fabric

The coating fabrics and films are classified in Europe, according to tensile strength and weight per square meter ( $\text{g/m}^2$ ), in approximately five types. In Table 2.5-1, it is possible to observe the weight, strength and elongation of the materials.

Table 2.5-1 – Technical characteristics of materials

<i>Fabric/ coating foils</i> Tecido/ cobertura	<i>Quality type</i> <i>thickness</i> Tipo de qualidade espessura	<i>Weight</i> Peso ( $\text{g/m}^2$ )	<i>Tensile strength</i> <i>warp/weft</i> Resistência a tração urdidura/ trama (N/50mm)	<i>Elongation at</i> <i>rupture - warp/weft</i> Alongamento na ruptura urdidura/ trama (%)
<i>Polyester/PVC-coating</i> Tecido em Poliéster revestido por PVC	Type I	600- 800	3000/3000	15/20
	Type II	900	4400/4000	15/20
	Type III	1100	5750/5200	15/25
	Type IV	1300	7400/ 6400	15/25
	Type V	1450	9800/ 8300	15/25
<i>Fibreglass/PTFE-coating</i> Tecido em fibra de vidro revestido por PTFE	Type I	800	3500/3000	3-12
	Type II	1050	5000/4400	3-12
	Type III	1250	6900/5900	3-12
	Type IV	1500	7300/ 6500	3-12
<i>PTFE- fabric non-coated</i> Tecido de PTFE não revestido		300- 800	3880/3500	30/40
<i>ETFE foils</i> Filme de ETFE	50 $\mu\text{m}$	87.5	64/56	450-500
	80 $\mu\text{m}$	140	58/54	500-600
	100 $\mu\text{m}$	175	58/57	550-600
	150 $\mu\text{m}$	262.5	58/57	600-650
	200 $\mu\text{m}$	350	52/52	600

Source: BAIER, 2004 *apud* BAIER, 2010, p.60.

It is important to highlight that the synthetic polymers used on the production of fabric, coatings and films here mentioned (polyester, PVC, PTFE, PTFE, PDVF, ETFE) are classified as thermoplastics, in other words, they are plastics that have the fusibility property. So, they can be melted and solidified several times without changing significantly their basic properties. Therefore, they are solids at environment temperature (final state) and fluid at some stage of processing. Thus, these materials can be recycled or reused as raw material for other products, since disposal is one of the major problems of plastic considering that they need approximately 400 to 500 years to degrade.

In Brazil, the PVC/polyester materials are reused as raw materials of others products like hoses, switches, etc. In Europe, according to Baier (2010), the Leading European manufactures of PVC/PES membranes have united efforts to recycle post-consumer waste (material and PVC membranes), in the majority of modern factories that rely on thermo physical procedures. In this procedure, the preparation and classification of materials are very important.

#### *PVC coated Polyester fabric*

The Polyester fabric coated with PVC (Figure 2.5-5a) has been the most widely used material in membrane structures since '50s, because of its performance and cost. It has light transmittance about 5 to 15% (Figure 2.5-5a), according to Knippers *et al.*, 2011. It is classified as building material class B1, related to fire behavior (flammable with difficult), in accordance to DIN 4102 (Germany Industrial Standard). It has an expected life span of approximately 25 years. It also has flexibility, is easy to handle and can be used in permanent and retractable roofs (BAIER, 2010).

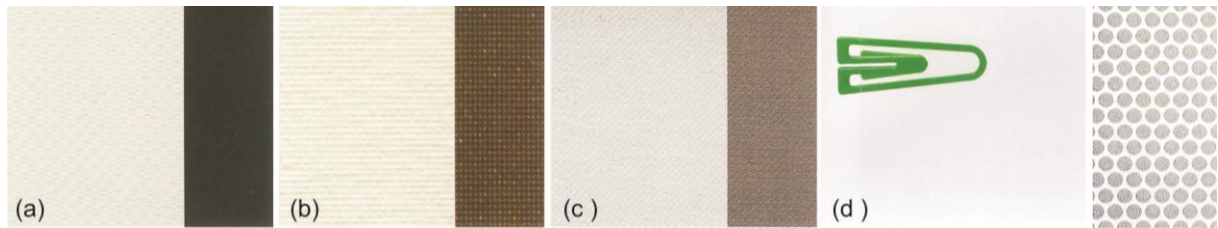
#### *PTFE coated fiber glass fabric*

The fiber glass fabric coated by PTFE (Figure 2.5-5b) has high durability, being auto-cleaning and moisture stable. It has light transmittance about 8 to 20% (Figure 2.5-5b). It is classified as building material class A2 (not combustible) to materials type I and type II, class B1 (flammable with difficult) for types III and IV, in accordance to DIN 4102 (KNIPPERS *et al.*, 2011). It is usually available in white. It has an expected life span of approximately 40 years (BAIER, 2010).

#### *PTFE fabric with PTFE coating*

The PTFE fabric with thermoplastic fluoropolymer coatings (Figure 2.5-5c) applied by extrusion method can be welded and are fully watertight. The coated PTFE has light transmittance about 20 to 40% (Figure 2.5-5c). It is classified as building material class B1 (DIN 4102) and S1-d0 (no smoke, no burning droplets/ particles) in accordance to EN13501 (European Standard to fire resistance), and has an expected life span of more than 25 years (KNIPPERS *et al.*, 2011).

Figure 2.5-5 – Light transmittance of coated fabric (a, b, c) and foil (d)



The coated fabrics (a, b, c) were photographed by direct light to permit the qualitative comparison of the light transmittance: (a) Polyester/ PVC; (b) Glass fibre/ PTFE; (c) PTFE/ PTFE; (d) ETFE foil: translucent and printed. Source: adapted from KNIPPERS *et al.*, 2011, p.97, p.103.

#### 2.5.2.4 ETFE foils

The translucent ETFE (Ethylene tetrafluoroethylene) foil<sup>12</sup> was introduced to the market in 1970, but began to be used significantly in pneumatic building facades in the beginning of the 80s. The ETFE is a synthetic copolymer<sup>13</sup> which has a semi crystalline molecular structure. It is classified as building material class B1 (flammable with difficult) in accordance to DIN 4102 - *Germany Industrial Standard*, (SCHIEMANN; MORITZ, 2010). It is a stable material and is suitable for being used in environments with aggressive actions (acids, alkalis, and UV radiation). It has high resistance to dirt and heat. It hardly absorbs UV radiation, so it never turns yellow or goes brittle. It can be produced in several colors and be printed. As it has high light transmittance and UV radiation permeability (Figure 2.5-5d), it is mainly used to cover swimming pools, zoological gardens and greenhouses, enabling plant growth and limiting the growth of bacteria (KNIPPERS *et al.*, 2011).

It has low strength when compared to the polyester and glass fibers, and it also presents elongation tendency, but high tear propagation resistance. Thus, it is mainly used in inflated pneumatic coverings and facades, in which the elongation does not have a significant influence to the applied pre-tension. It is also used with cable nets or individual cables, which enhances the ETFE foil load bearing capacity. It has an expected life span of approximately 25 years (SCHIEMANN; MORITZ, 2010).

<sup>12</sup> The term film, commonly used to describe thin steel sheet, is also used in building industry to describe homogeneous polymeric materials that has minimal thickness relative to its surface area. (KNIPPERS *et al.*, 2011).

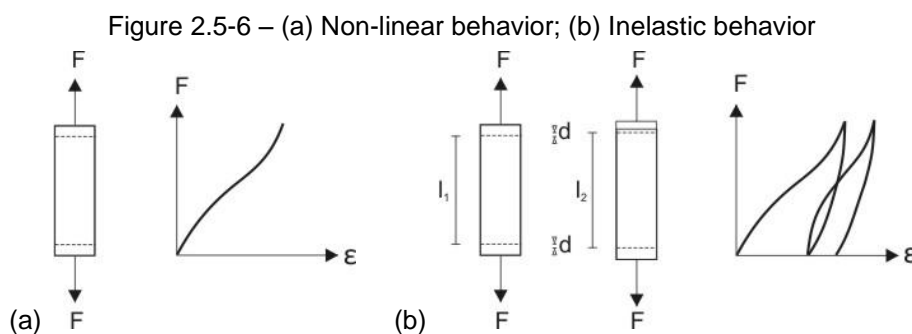
<sup>13</sup> Copolymer is a compound of high molecular weight (macromolecule), which structure (long main chain), has different chemical units (mers) repeated, organized in alternately, arranged randomly or in block (MANO; MENDES, 1991).

### 2.5.3 MATERIAL BEHAVIOR

The membrane material when stretched shows non-linear and inelastic behavior and, in most cases, anisotropic properties. These mechanical properties vary with the material composition, number and diameter of the yarns, coating type, woven type and total thickness of the fabric (ALVIM; PAULETTI, 2004).

It is possible to observe the non-linear behavior (Figure 2.5-6a) when the material is loaded in a uniaxial test. The stresses are not proportional to strains, i.e., the material stress-strain relationship cannot be determined by a linear equation (SEIDEL, 2009). Considering polymers such as polyester, this behavior is related to the sliding of long chains (linear or branched) interlaced (non rigid connections) under the action of forces (WAGNER, 2008).

The inelastic behavior can be observed when the material is subjected to several cycles of loading and unloading (Figure 2.5-6b). When the load tends to zero, residual strains remain on the material. It is also possible to observe in Figure 2.5-6b that the loading curves are different to the unloading curves (SEIDEL, 2009).

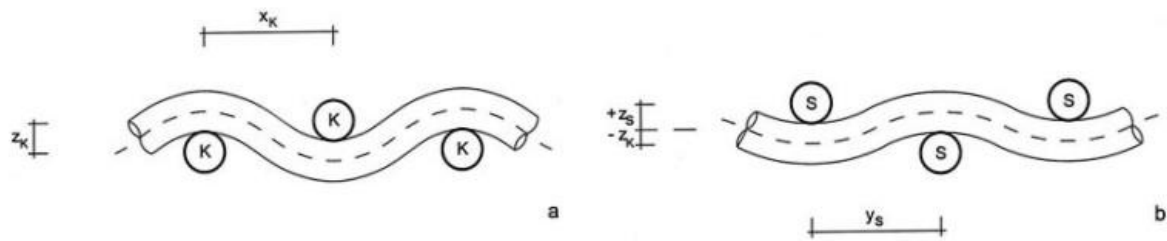


Source: adapted from SEIDEL (2009), p, 40.

The elastic material that shows the same mechanical properties in all directions is called isotropic. However, the woven membranes have two orthogonal symmetric axis and generally different mechanical behavior in their directions. In this case, the behavior is described as orthogonal anisotropic (SEIDEL, 2009).

The anisotropic behavior is a result of the weaving procedure, in which the yarn geometry is defined. According to Figure 2.5-7, the warp thread has less curvature and deformation than the weft thread. The difference in the thread curvature causes distinct mechanical behavior in the material directions. Thus, the greater curvature of the weft thread is the reason for the low stiffness in this direction (SEIDEL, 2009).

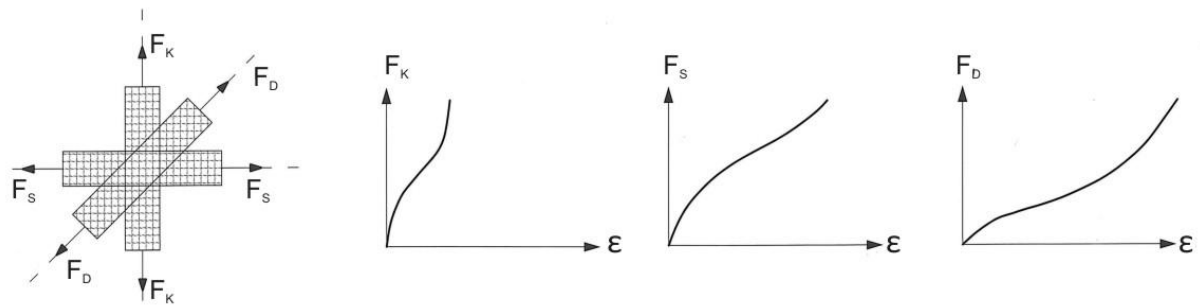
Figure 2.5-7 – Thread curves: (a) weft; (b) warp



Source: adapted from SEIDEL, 2009. p.42

This behavior can be observed in the material uniaxial test of the fabric, whose directions (0° warp, 90° weft e 45°) were subjected to the same force. It was observed higher stiffness at warp direction (90°), and large strain at weft direction (0°), and the maximum strain at 45° (Figure 2.5-8).

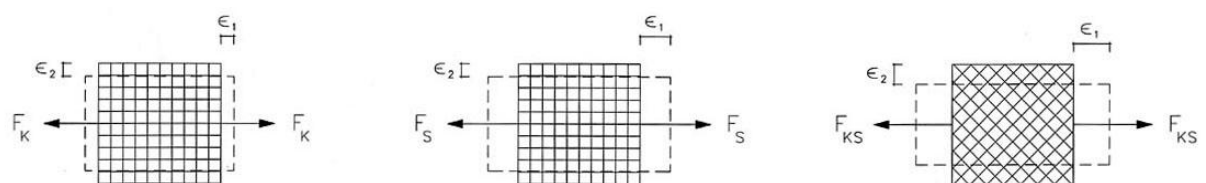
Figure 2.5-8 – Fabric behavior – thread directions: 90°, 0° e 45°



Source: SEIDEL, 2009. p.41

In this anisotropic fabric, when the material is stretched over the warp direction, warp elongation and warp curvature changes are observed (Figure 2.5-9). However, the weft curvature will also change, as a result of the interaction of threads. Consequently, there are different strains in these directions (e.g. elongation in the load direction and contraction in the transversal direction), whose relationship is described by the Poisson ratio and depends on the level of force applied in these directions (SEIDEL, 2009).

Figure 2.5-9 – Different strains in the fabric directions



Source: SEIDEL, 2009, p.42

The stiffness or non linear stress-strain behavior of the membrane material also depends on the ratio of forces (magnitude, duration and ratio of loads) applied on each material direction. This behavior also varies according to the type, manufacture and batch of the selected material. Because of these characteristics, it is usual to evaluate experimentally the biaxial behavior of each membrane structure (UHLEMANN *et al.*, 2011).

The fabrics and foils also exhibit behavior that combines solid<sup>14</sup> and liquid<sup>15</sup> (viscous fluid) characteristics, in other words, a visco-elastic behavior, which depends on time and temperature (BÖGNER-BALZ, 2008).

To understand this behavior it is important to observe how these materials deform<sup>16</sup>. The fluid under pressure deforms continuously, but the solid, in the elastic behavior do not. Therefore, the viscous-elastic behavior combines viscous irreversible deformations (which is caused by the sliding of the polymer chains) and reversible elastic deformation (which depends on the time and chain entanglements that hinder the macromolecular movement), (KROSCWITZ, 1990).

So, with soft solids as fabric and films, the stress-strain relationship does not follow the Hooke's law. The deformation is not only related to stress magnitude, but it is also related to time. It means that the material strain under constant stress (e.g. long-term loading) increases with time (creep), according to Figure 2.5-10a. As a result, the stress required to keep the material under constant strain gradually decreases with time (relaxation) according to Figure 2.5-10b. This deformation is also influenced by temperature. Under low temperatures the material becomes brittle and by increasing the temperature, the material stiffness decreases (SEIDEL, 2009).

According to Lewis (2004), to optimize the creep and material fatigue, the same state of stress in the warp and weft direction is desirable. So, loads tend to appear equally in the set of fibres and there are comparable ageing effects in both directions.

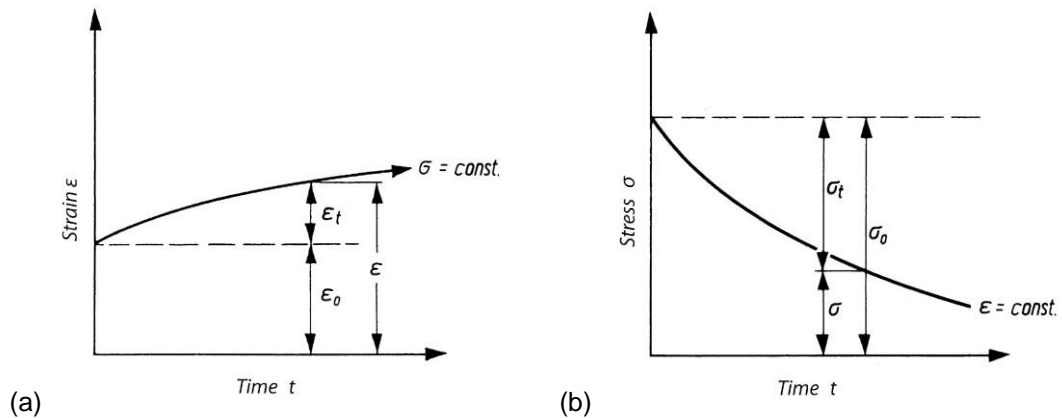
---

14 The stress in the solid is directly proportional to strain for small deformations, as the classical theory of elasticity (Hooke's law), (KROSCWITZ, 1990).

15 The stress in the viscous liquids is always directly proportional to the time rate of strain, but is independent of strain, according to the classical second theory of hydrodynamics (Newton's law), (KROSCWITZ, 1990).

16 The science that studies the strain (reversible) and the flow (irreversible) is the Rheology, and this behavior is interpreted as the response of the material to the applied force (KROSCWITZ, 1990).

Figure 2.5-10 – (a) Creep (fluência); (b) Relaxation



Source: SEIDEL, 2009, p.48.

## 2.6 DESIGNING PROCESS

In membrane structures and cable nets, characterized by lightweight and flexibility, the form of equilibrium occurs in a deformed position and in a state of pre-tension (Figure 2.2-1).

These structures balance external loads by large displacements that change the surface geometry, even though the working loads are within the elastic limit, producing geometrically non-linear behavior (LEWIS, 2003). These movements allow the stress distribution on the surface and a more efficient use of material. This behavior can be understood by analogy, when observing the movement of trees under wind action; the movement itself enables them to withstand loads, reducing the internal stress. However, they have to be controlled to avoid unexpected stiffness or failures (WAGNER, 2005).

It is noted that the membrane surfaces and cable nets are not free form; they follow the forces acting on them, i.e., they are forms of equilibrium (LINKWITZ, 1999), defined by differential equations.

Moreover, the membrane material has a complex behavior and anisotropic properties.

Due to these particularities, they are hardly analyzed by traditional methods. The designing process includes form finding, static analysis and patterning procedure.

The initial designing stage, that comprises the form finding procedure, distinguishes tensile structures from rigid-type structures in concrete, steel or wood, in which the shape can be previously determined (LEWIS, 2003). The form finding is

the search for three-dimensional equilibrium of the membrane surface (double curvature) for certain stress distribution (only tension) and boundary conditions (high points, flexible edge cables, rigid edges, etc), not considering the material behavior (WAGNER, 2005).

Later, it is carried out the static analysis of the structural system (form of equilibrium of the membrane surface and the support system) under certain load action. According to Lewis (2003), if the initial surface configuration does not satisfy the conditions of static equilibrium, the form finding stage is repeated after changing the surface geometry (boundaries configuration and or pre-stress level).

Usually, the design calculation of a membrane structure is performed using modern software packages which are based on finite elements and which are able to handle global geometric non linearity as well as non-linearity, although the latter only in terms of the membrane's inability to carry in-plane compression. For simplicity, the load-deformation-behaviour of the membrane in tension is usually treated linear-elastically, which means that the non-linear load-deformation-behaviour is not considered in the design process. There seems to exist a great lack of knowledge how to simulate and herewith how to include the non-linearity of the membrane material in the design process (UHLEMANN *et al.*, 2011, p.2).

In the stages described previously it can be observed the initial pre-stress imposed to the form of equilibrium during form finding stage and the pre-stress induced during analysis to reduce the amount of deformations under loads (SAITOH, 1997).

According to Wagner (2005), the patterning is a geometrical procedure of flattening the double curved surface (form of equilibrium), enabling the surface manufacture. In most cases, the stress distribution and material behavior are not considered in this procedure. However, recent designing procedures aim to simulate the membrane structure behavior more realistically. Thus, the evaluation of structural behavior, under load action, also considers the cutting patterns (width of strips), orientation of the fabric, and the pre-tensioning process, due to the great influence of these parameters and procedures in the stress distribution over the surface. This simulation aims to approximate the geometry and the stress distribution of the form of equilibrium to the real structure, contributing to minimize wrinkles and stress peaks on the surface.

Due to these characteristics, it is important the development of a designing process by an interdisciplinary team, involving architects, engineers and builders, right from the initial stage enabling the integration and quality of design and building procedures.

It is important to highlight that the initial procedures of form finding can also use flexible physical models (e.g. using fabric or soap film). The building procedure, observation and qualitative analysis of the flexible models enable the global view of the system and an immediate understanding of structural behavior. They also allow the spontaneous development of the structure design in site, enhancing the development of feasible configurations to be studied (NUNES, 2008).

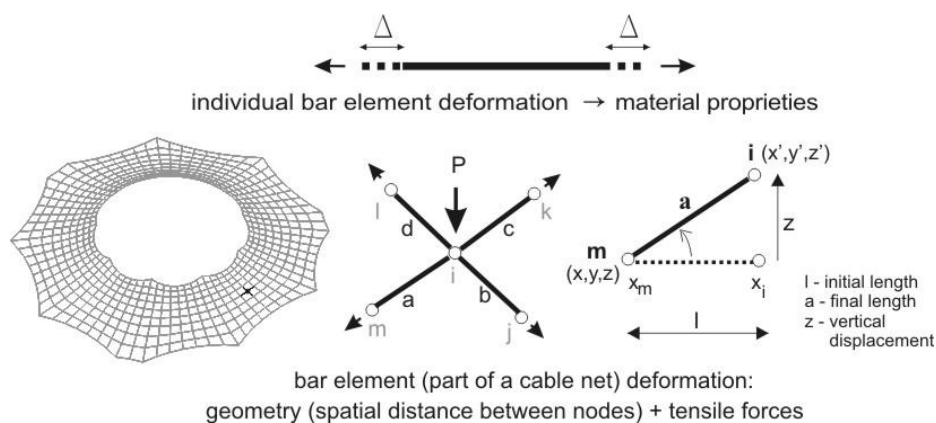
The Force Density Method (FDM), Dynamic Relaxation Method and Finite Element Method (FEM) are used for modeling and simulation of these structures. The FDM and FEM are mentioned in this investigation.

### 2.6.1 FORMFINDING – FORCE DENSITY METHOD

This method was developed by Klaus Linkwitz and his team for modelling the structures of Munich Olympic complex, in the 60s (LEWIS, 2003).

This mathematical approach does not present parameters which refer to the cable net material. It only allows defining the surface configuration in static equilibrium, represented as a cable net. According to Linkwitz (1999), this principle can be demonstrated by observing the behavior of elastic bar element independently and as a part of a cable net. The cable net is compounded by individual elements with flexible joints fixed in its anchor points and under pre-stress, considering that Hooke's Law is valid, (Figure 2.6-1).

Figure 2.6-1 – Elastic behavior of the bar element: individually and as a part of a cable net.



Source: adapted from GRÜNDIG *et al.*, 2000, p.4.

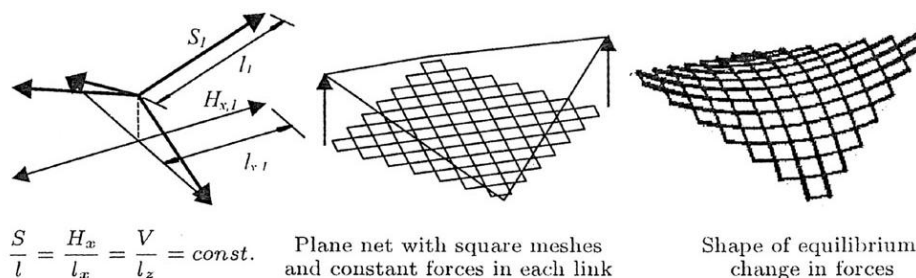
When tensile forces are applied to the individual bar element, it deforms longitudinally, and the difference between the initial length and the elastically deformed length, is determined by the bar properties. When the element is part of a

cable net under pre-tension, all elements work together. There are curvatures in opposite directions in each node of the anticlastic cable net. So, each node is a fixed point in space. Thus, the cable net geometry is a result of the equilibrium of tensile forces acting simultaneously in each node. As a result, the length of each bar element elastically elongated is equal to the spatial distance between nodes.

In this method, the tensile forces that act in each node are represented by a system of linear equations. This approach considers, as a principle, that the vertical component of the tensile force acting on each bar element (defined by initial and final nodes) depends on the angle and the horizontal component of this tensile force. Thus, the horizontal component of this tensile force acting in each bar element, at any angle, is assumed as a constant parameter. This parameter is named force density and is described as a ratio of force by the length of each element. So, only vertical displacements are calculated and the equilibrium configuration results from geometry and pre-stress applied (Figure 2.6-2, Figure 2.6-3, Appendix H), (KOENEN, 2012). Thus, according to Wagner (2005), the force and length of each bar element are free parameters in the search of three-dimensional equilibrium.

It is interesting to compare this approach with the behavior of the soap film (surfaces of minimum area). While the horizontal component of the tensile force acting in each bar element for any angle is considered constant in the Density Force Method, variable components (xyz) of the tensile force acting in each node defines the equilibrium and the constant stress in the soap film, according to Figure 2.6-3 (verbal information)<sup>17</sup>.

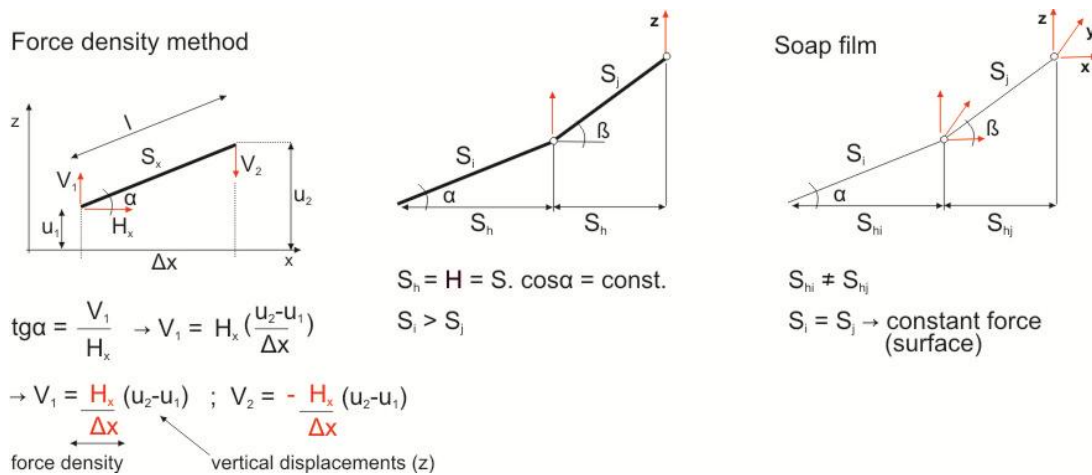
Figure 2.6-2 – Form of equilibrium fulfilling vertical equilibrium



Source: WAGNER (2005), p.4.

<sup>17</sup> KOENEN, Reinhold. Institut für Metall-und Leichtbau. Universität Duisburg Essen. Design of lightweight shell structures – Master course, elective module, 2011. [explanation and sketches of the author]

Figure 2.6-3 – Density force method and soap film behavior



## 2.6.2 NUMERICAL ANALYSIS – FINITE ELEMENTS METHOD

The Finite Elements Method is a numerical method that provides resources to simulate the membrane surface (form of equilibrium) and supporting system, considering the material properties and load actions.

According to Azevedo (2003), FEM is based on the structure discretization, i.e., the subdivision of the structure in substructures (parts, elements) in which each element exhibits known or assumed behavior. Thus, the approximately behavior of the whole structure is estimated as the sum of the behavior of the elements.

In the non linear case, the solution is generally obtained by an iterative method, in other words, it is necessary several calculation steps in which the solution is continuously approximated until it gets 'right' within a given tolerance.

## 2.6.3 PATTERNING PROCESS

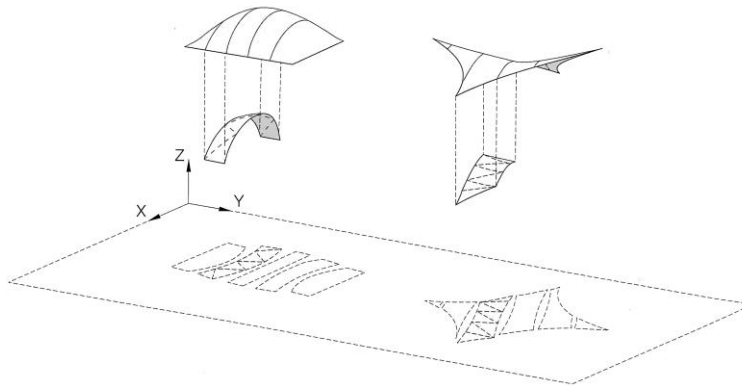
The membrane material is produced by an industrial process, in which the width of material ranges from two to five meters. So, the continuous three-dimensional membrane surface (form of equilibrium) needs to be flattened to be manufactured.

In this procedure, the double curved surface is firstly divided in three-dimensional patterns (double curved strips). To define these patterns it is necessary to find geodesic lines across the surface. This process uses, in most cases, geodesic<sup>18</sup> trajectories (WAGNER, 2005). Then, these three-dimensional patterns

<sup>18</sup> The geodesic trajectory can be described as the smallest distance between two points in a surface. In the two-dimensional surface, they are straight lines and in the spherical surface, they are arcs of large circles formed

are translated to two-dimensional panels (flat panels), being the cutting patterns of the material (Figure 2.6-4). Later, these flat panels will be joined by seams to compound the final shape of the surface (SEIDEL, 2009).

Figure 2.6-4 – Patterning process



Source: KNIPPERS *et al.*, 2011, p.146.

However, the flattening process of the anticlastic surface causes dimensional distortions (LEWIS, 2003), because it is a non-developable<sup>19</sup> surface. In other words, the anticlastic surface cannot be open and projected in such a way that the entire surface is contained on the plane, such as cones and cylinders. According to Otto *et al.* (1983), the magnitude of these dimensional distortions depends on surface curvature degree, the limits of the projected surface segment and projection method selected. In general, these distortions increase with the size of the projected segment.

As noted (section 2.6.1), the form of equilibrium is the base of patterning process. However, this form resulted from the form finding stage which does not consider the material behavior. According to Wagner (2008) the form of equilibrium behavior resembles the soap film behavior, in other words, does not have shear strength.

However, the real form of membrane structures is influenced by the material behavior and the dimensional distortions of the patterning process. Consequently, the geometry and stress distribution of the real form are different from the ones

---

by the intersection of the sphere and plane (which cross two points and the center of the sphere), for example the Ecuador line. Moreover, it can be “defined as the orthogonal projection of the curvature radii over the normal plane of the surface, in the consider point” (ZHANG E LUO, 2002 *apud* DIAS JUNIOR, 2006, p.18).

<sup>19</sup> Considering the surface represented by a cable net with triangle mesh, “the develop surface is characterized by this mathematical condition: the sum of the angles of the triangles meeting in one point equals 360°. In surfaces of the same curvature, (sphere), the sum of the angles is smaller than 360°, whereas for surfaces with opposite curvature (hyperbolic paraboloid) the sum of the angles is greater than 360°” (OTTO, *et al.*, 1983, 246-247p.).

predicted by the form of equilibrium. These differences can be seen in wrinkles and surfaces distortions and have influence of width of panels, seam, orientation of the fabric and pre-tensioning process (WAGNER, 2005).

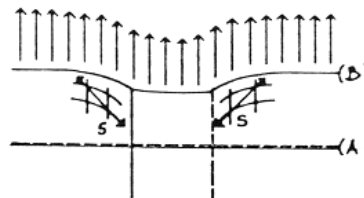
Thus, to define adequately the cutting patterns of the material, it is important to know the strains in the material directions. This information is obtained by material tests and guides the procedure known as compensation. In this procedure, the size of the flat panels is adjusted or compensated. This means that at the relaxed state, the flat panel will be smaller than the same amount that it will deform under pre-tension, and the membrane surface will take the specified form throughout its life time (BLUM, 1982).

### *Panels seam*

The seam allows applying or transporting forces between panels. However, the seam “represents a geometrical discontinuity in the flow of forces in the curved membrane surface” (SEIDEL, 2009, p.45), and disturb the membrane behavior.

In addition, the seam area has more material and more stiffness than the flat panel. Therefore, the seam has less deformation. So, in adjacent region to the seam, it is possible to observe wrinkles as it presents less deformation of the seam (OTTO *et al.*, 1983), according to Figure 2.6-5.

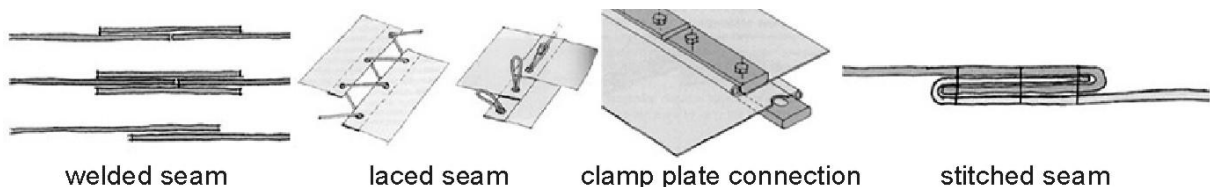
Figure 2.6-5 – Seam detail - areas with less deformation



Source: OTTO *et al.*, 1983, p.78.

The seam of the panel can be carried out by welding, glued seam (with double-side adhesives), stitching, lacing or clamped (Figure 2.6-6). The welding is the most used seam due to water tightness and its facility to control the production process during surface manufacture (FOSTER; MOLLAERT, 2004).

Figure 2.6-6 – Types of seam



Source: FOSTER; MOLLAERT, 2004, p.152, p.154, p.153, p.151.

During welding process, the ends of the panels are overlapped, and the hot with pressure applied merge the coatings of both panels. So, there is no mechanical connection between the fabric threads. The seam adhesion is responsible of transporting the fabric stress from one panel to the other panel.

According to Seidel (2009), the strength and quality of the seam depends on coating adhesion to the fabric, to the seam width and production conditions. However, by increasing temperature the coating tends to soften and the adhesion and efficiency of the seam is reduced.

## **2.7 CHALLENGES OF DESIGNING AND CONSTRUCTION PROCESS IN BRAZIL**

During the initial stage of this research the building procedures of two membrane roofs were observed closely. These studies aimed to understand the interfaces and procedures of designing and constructive work of these structures in Brazil, and to investigate the factors that affect the geometry and structural behavior of membrane structures.

This investigation was based on interviews with designing and constructive teams, including enterprise managers, as well as on observations over manufacture and building procedures in site, together with photographs. The final step included the analysis of procedures and challenges.

The first study includes the analysis of the membrane roof of the Convention center/Cenpes II, Petrobras, RJ, Petrobras/CNC enterprise. The design was done by the architects Siegbert Zanettini and José Wagner Garcia and developed by Zanettini Architecture; the membrane roof was built by Fiedler-Tensoestrutura, from August 2009 to January 2010.

The second study involves the membrane roof of Boulevard Cidade Nova Courtyard, RJ, Synthesis Group/Confidere enterprise. The design and development was done by Ruy Rezende Architecture; the membrane roof was built by Tensitex, from September to October 2009.

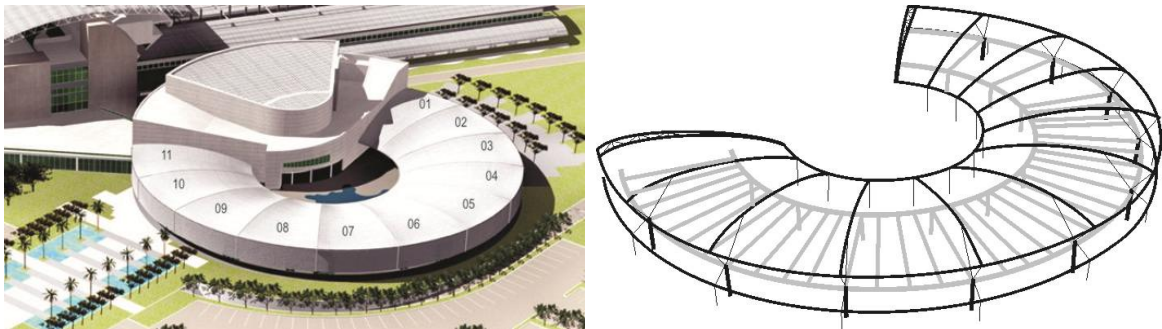
The structural analyses of the membrane surface and supporting system for both membrane roofs were carried out by the engineers Prof Ruy Marcelo Pauletti e Prof<sup>a</sup> Heloísa Maringoni respectively.

### 2.7.1 MEMBRANE ROOFS DESCRIPTION

The membrane roof of the Convention center/Cenpes II exhibits a circular ring form, divided into 11 saddle shape modules with smooth curvature (total area: 3741m<sup>2</sup>). These modules are independent and are rigidly connected to the supporting system. The building structure is also surrounded by a membrane surface, produced as a single module, called lateral membrane (Figure 2.7-1).

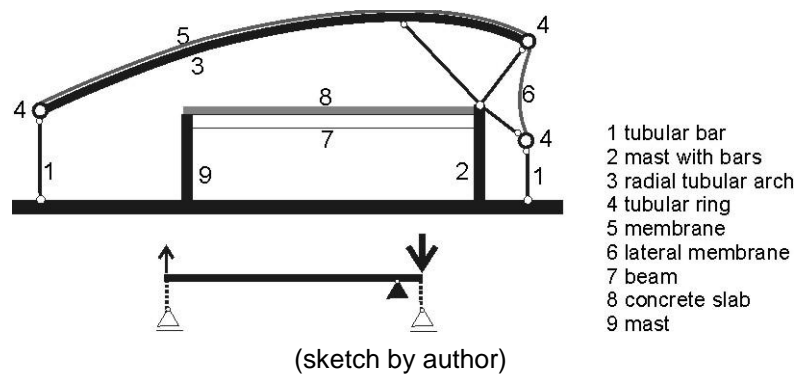
The supporting system is compounded by radial arcs supported by masts with projecting bars and pre-tension tubular bars. They are surrounded by concentric rings (internal and external) whose ends are joined to the auditorium structure (Figure 2.7-2).

Figure 2.7-1– Membrane roof of the Convention center: aerial view; support system



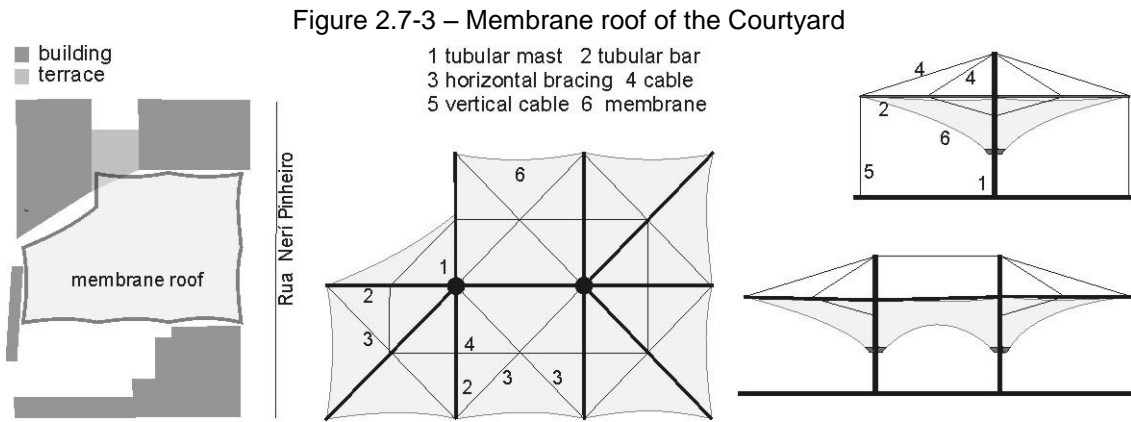
Source aerial view: ZANETTINI; GARCIA, 2006; support system: sketch by author.

Figure 2.7-2 – Support system of the Convention center (vertical section)



The membrane roof of the Courtyard of Boulevard Cidade Nova is a double inverted cone shape (area 524m<sup>2</sup>). It is supported by tubular profiles hinged joined to the masts rigidly connected to the base plate. These profiles are held by pre-tension cables placed vertically (and it was initially proposed bracing in horizontal plane). The top of membrane roof is connected to the supporting system by flexible edge cables

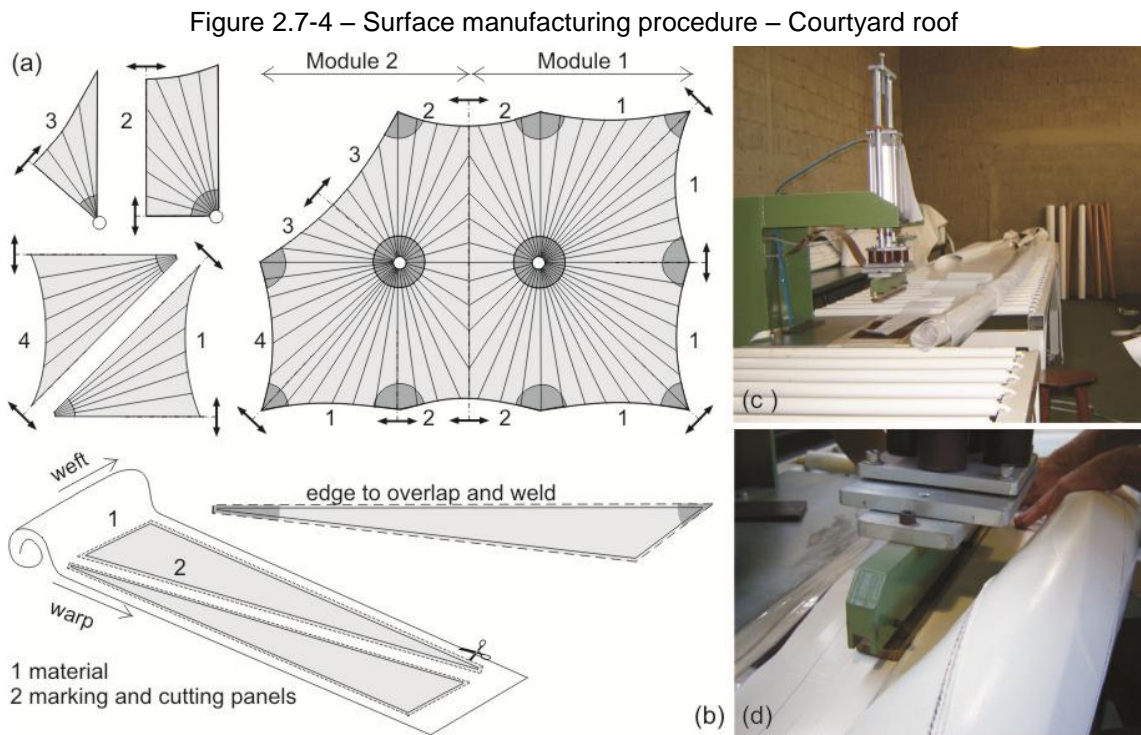
that anchored at the profile ends. The base of membrane roof is rigidly joined to cone rings connected to the masts (Figure 2.7-3).



Plants: site, roof; transversal and longitudinal sections; (sketch by author).

### 2.7.2 MANUFACTURING AND ASSEMBLY PROCEDURES

The manufacturing procedure of these membrane surfaces was similar. They were carried out in factory and comprise the panel dimensions marking for fabric cutting and flat panels joining by welding seam (hot welding with pressure, 180° to 220°C, by radio frequency), according to Figure 2.7-4. Subsequently, the surface finishing was carried out. Later, the flattened surfaces were folded (as zigzag to avoid damaging of the fabric and to facilitate its opening) and packaged for transport.



(a, b) surface cutting patterns; fabric marking and cutting; (c, d) overlapping of surface edge for welded seam procedure; (sketches and images by author).

Both membrane roofs used PVC coated polyester fabric. However, the specified material of the Convention center roof had a PVDF top coat. In this case it was necessary to do an abrasion of the edges of each panel to remove this top layer before the welding process. Moreover, the panel edges were overlapped and pre-tensioned during welding process.

As the membrane roof of the Courtyard was carried out as a single module, it has being positioned at the work place prior to the supporting system assembly. On the membrane roof of the Convention center, the saddle shape modules were assembled independently, and the lateral membrane was assembled as a single module.

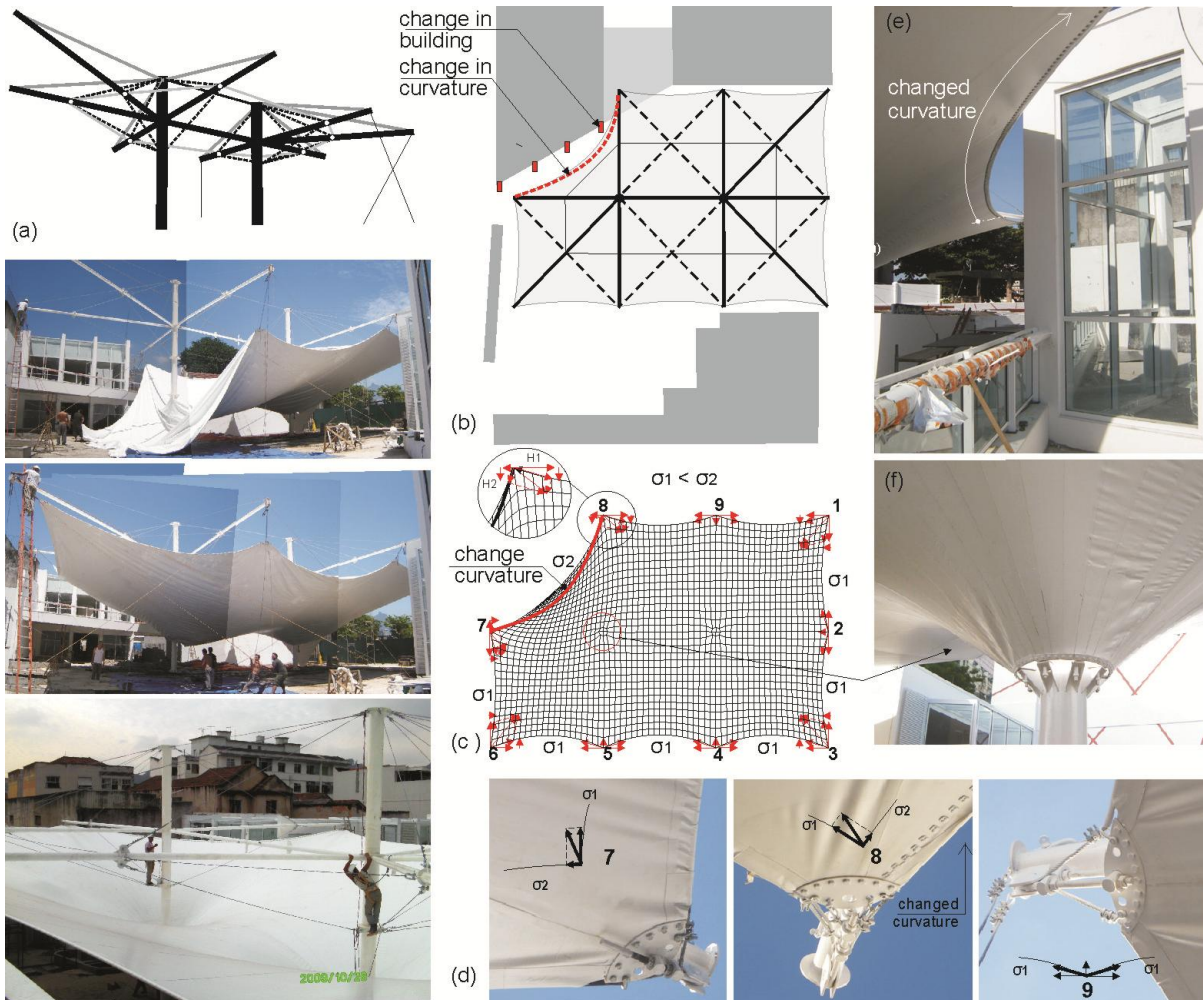
The assembly procedure of membrane roofs was also similar and comprised the following steps: opening the surface on site, lifting and connecting the membrane surface to the supporting system, and pre-tension of the surface. The lifting and the initial connection of the surface to the supporting system were carried out manually using ropes. They facilitated the handling of this flexible material and are easy to be removed of the structure. The adjustment of the surface to the supporting system was made in sequential steps of pre-tension and pause, aiming the material accommodation and stretching, as it can be seen in Figure 2.7-5 and Figure 2.7-6.

The adjustment of connections on membrane roof that has flexible edge (Courtyard roof) was challenging. The aerial work involves setting the correct position of membrane ends at the connections placed on the supporting system. The adjustment of each hinged connection allowed also the pre-tension of the continuous cable and the whole surface.

The assembling of connections of the membrane roof that has rigid edge (Convention center roof), involved the sequential positioning and adjustment of individual screws. This adjustment was done in small patches and carefully.

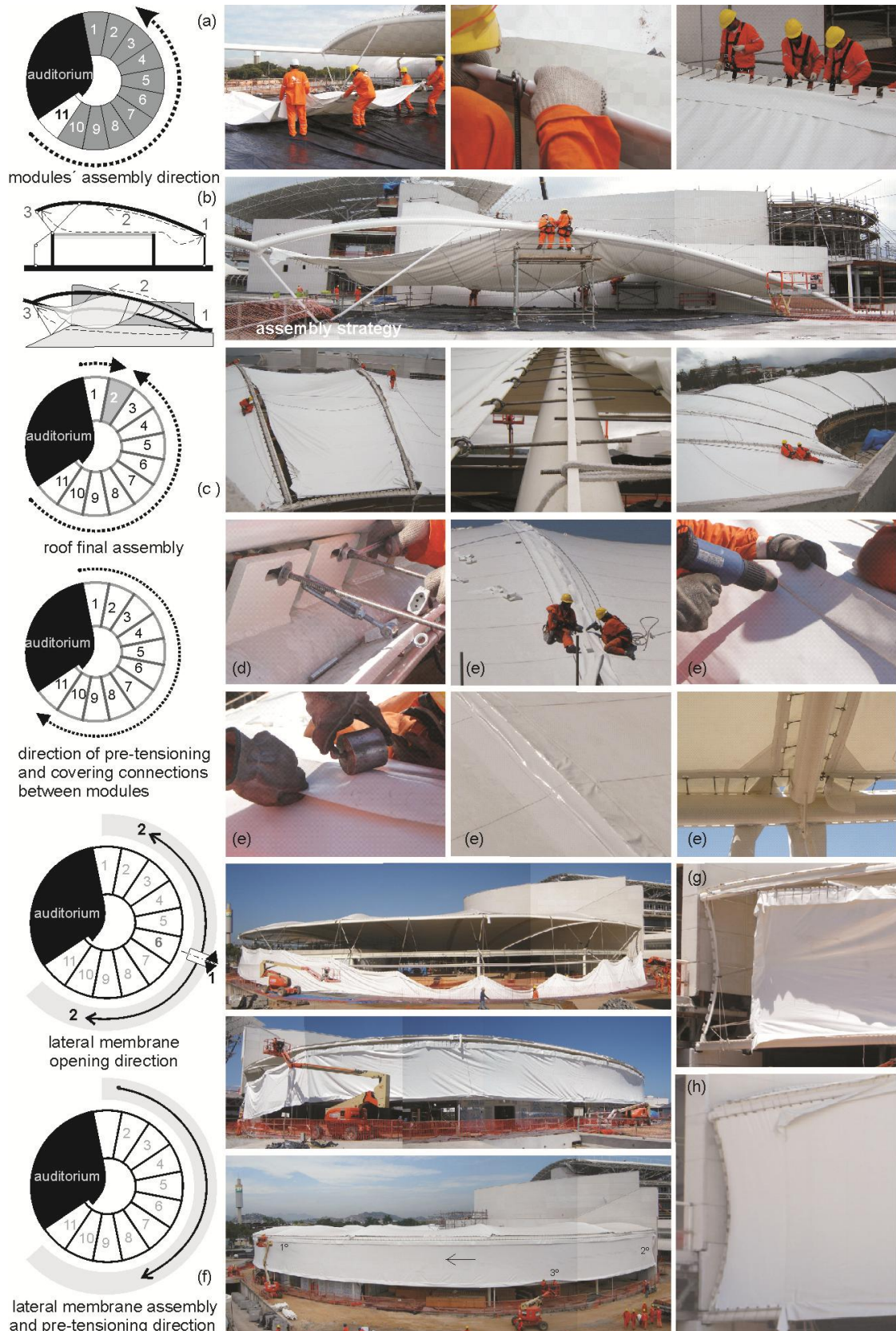
It was also observed that the early stages of initial lifting and pre-tensioning cannot be done in certain weather conditions (rain and wind), because the surface is not yet in equilibrium and can be damaged.

Figure 2.7-5 – Surface assembly procedure – Courtyard roof



(a) surface lifting; (b) changes on the building shape (masts placed on the external plane of the building) caused changes on the surface edge in the building site; (c) directions of the forces that act on the edge cables; (d, f) connections and cone shape base after changing boundary curvature (e) changed boundary curvature; (sketches and images by author, except roof superior view, image by Ozana Vieira, and roof mesh done by builder - Tensitex)

Figure 2.7-6 – Surface assembly procedure - Convention center roof



(a,b) direction and assembly strategy of the roof modules; (c) covering between roof modules; (d) pre-tensioning and covering between roof modules; (e) lateral membrane assembly; (f) assembly of lateral membrane; (g, h) added panel to the lateral membrane by hot welding during assembly; (sketches and images by author).

### 2.7.3 WORK PROCEDURES AND ITS CHALLENGES

#### *Challenges in designing stage*

Independent contracts for designing and construction jobs were settled, by enterprise responsables, making dialogue difficult between both working teams.

It was also noted that in Brazil, material and wind test data is not commonly used to guide the design process of small and medium structures. Due to the uncertain of the evaluated data (material and wind load), it is usual to adopt simplifications in numerical simulations.

#### *Challenges in constructive stage*

It was also observed that the uncertainties regarding material behavior have influence in the surface patterning and assembly procedure, hindering the work of engineers and especially the builders (responsible by membrane manufacture and assembly).

These uncertainties reduce the accuracy of the designing process and hinder the correct adjustment of the flat panels shape. Consequently, excessive cutting of the material can hinder the assembly and minimal adjustments may require further steps to pre-tension of the surface during its life time.

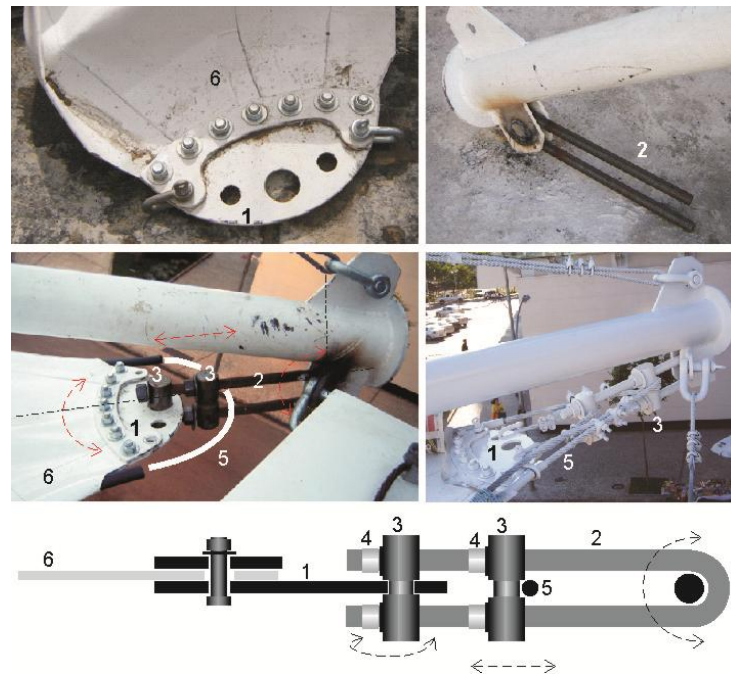
So, to deal with material deformations and possible building inaccuracies, some strategies were observed: the development of connections with large adjustment capacity (Figure 2.7-7, Figure 2.7-8). These are characterized by the arrangement of modular components of easy fabrication, transport and assembly.

Figure 2.7-7 – Connections of saddle shape modules (rigid edge) proposed by engineer Prof Ruy Pauletti



components: individual screw with eyes and nuts, and bars; (images by author).

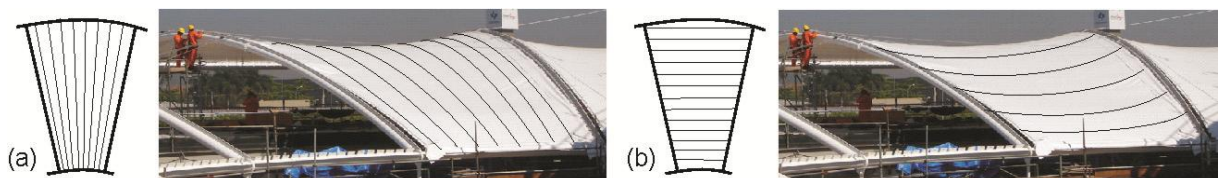
Figure 2.7-8 – Connections of double inverted cone shape (flexible edge) proposed by Tensitex



components: (1) terminal plate; (2) threaded bar (3) steel cylinder; (4) nut; (5) cable; (6) membrane;  
(sketch and images by author)

Some of these strategies proposed by builders also result in changes in the geometry of the flattened membrane (cutting patterns) and supporting system. So, some stages of the designing process had to be redone. The new cutting pattern proposed to the membrane roof of the Convention center can be mentioned as an example. In this case, the material threads were oriented parallel to the panels seam, seeking to minimize the material distortion (Figure 2.7-9).

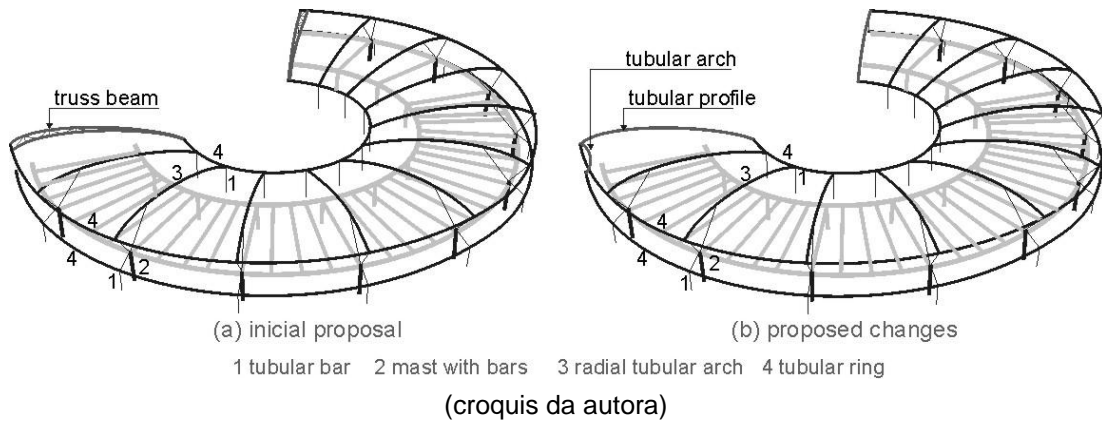
Figure 2.7-9 – Cutting patterns of the membrane roof of the Convention center



(a) initial design: radial patterns, (b) proposed changes and realized design: circumferential pattern;  
(drawings over image done by author).

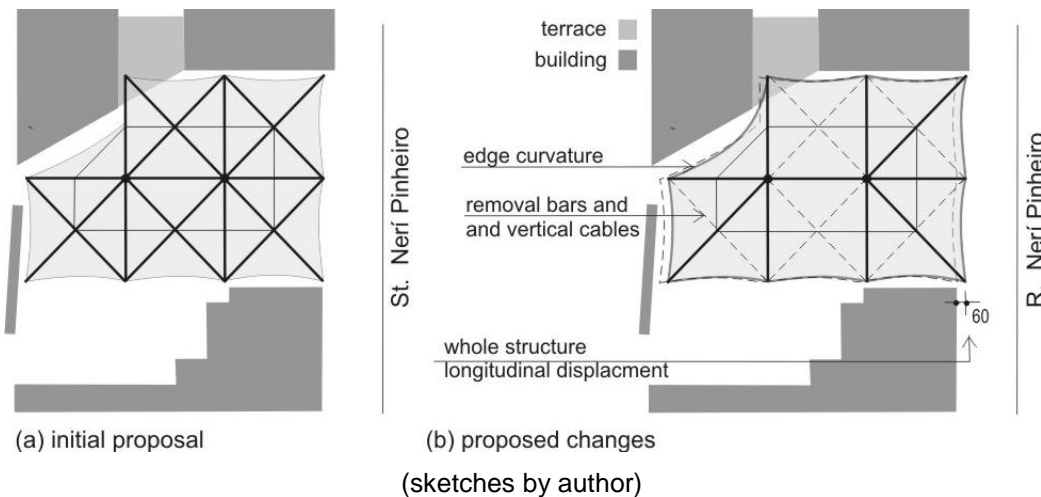
In the membrane roof of the Convention center it was also added tubular arches at the end of the circumferential ring to the lateral membrane anchoring; tubular profiles instead of the truss beams at the ends of the roof were also proposed (Figure 2.7-10).

Figure 2.7-10– Support system of the membrane roof of the Convention center – proposed changes



On the membrane roof of the Courtyard, there were also adjustments on the edge curvature of the surface and on the supporting system configuration (the horizontal bracing and vertical cables of the tubular profiles were removed; this make difficult the adjustment of the support system), according to Figure 2.7-11. The material specification was also changed due to the period required to import the membrane material specified.

Figure 2.7-11 – Adjustments of the membrane roof of the Courtyard



Manufacture inaccuracies of the supporting system components were observed on both structures.

On the supporting system of the Convention center it was necessary to include and weld a new row of plates at internal ring (Figure 2.7-12). There was also the absence of small holes in these plates (to connect membrane covering between saddle shape modules). So, this membrane covering was welded (Figure 2.7-6-d-e). It was also observed differences between the lateral membrane dimensions and the

perimeter of the building. So, a new panel was welded during assembly (Figure 2.7-6- g-h).

Figure 2.7-12 – Supporting system inaccuracy – roof of the Convention center



(a, b, c) welding of new row of plates at internal ring

On the supporting system of the Courtyard roof, it was noted the mast manufacture inaccuracy; the profiles connections were in different levels hindering its assembly between masts (Figure 2.7-13).

Figure 2.7-13 – Supporting system inaccuracy – roof of the Courtyard



Mast inaccuracy: profile connections in different levels

There was also a small change in the building shape located near the membrane roof of the Courtyard (masts placed on the external plane of the building). So, it was required to move the surface away from this building. This caused a new adjustment in the surface edge curvature during assembly procedure. This change occurred in a region that has high stress on membrane surface and edge cable. So, the geometry adjustment altered significantly the membrane surface stress, hindering the adjustment of the surface to its anchor points and causing visible deformations (Figure 2.7-5- b,c,d,e,f).

These studies confirmed that errors or changes in the membrane geometry disturb the flow of forces, causing distortions or deformations that can be observed and cannot be disguised. Moreover, membrane surface behavior is also influenced by organization, shape and dimensions of flat panels, as well as the membrane material behavior.

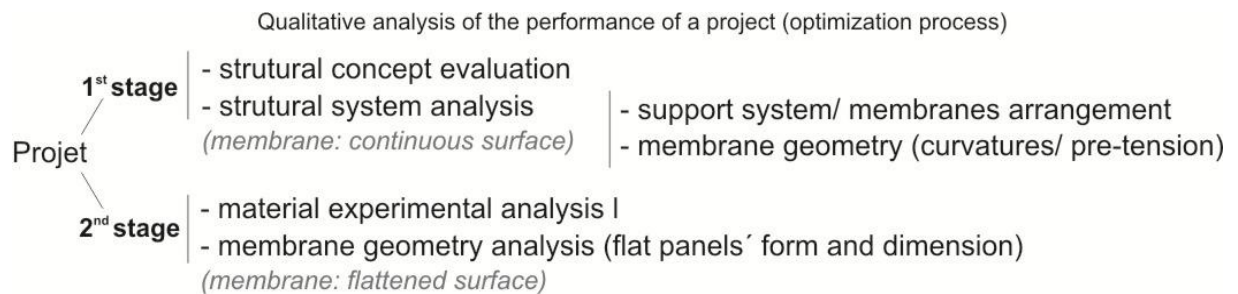
The inaccuracies observed showed that the strategies proposed by engineers and builders cannot preview all uncertainties. They also confirmed the importance of detailing components with more accuracy, as well as monitoring the manufacture of components, avoiding membrane changes during the assembly procedure.

So, it was verified that it is very important to know the membrane material behavior and the system construction particularities (manufacture and assembly), as well as to motivate the cooperative work between architects, engineers and builders, sharing knowledge and responsibilities that contribute to optimize the proposed configuration, and favor the building performance.

### 3 CASE STUDY

According to strategies identified in the qualitative analysis of lightweight structures buildings (section 2.4.2.3), the optimum performance of membrane structures and cable nets is related to system structural arrangement, as well as geometry and arrangement of all components. It was also observed in constructive work process of membrane roof (section 2.7), that uncertainties regarding material behavior decreases the accuracy of the theoretical model and hinder the proper adjustment of the panels geometry, i.e., contribute to reduce constructive efficiency and surface performance throughout its useful life.

Therefore, in this part of the work the qualitative analysis of the performance of a structural membrane roof project was carried out, i.e., a particular situation, as example. This case study aimed to evaluate the influence of the membrane geometry and system arrangement, as well as, membrane material behavior on system performance. It was also investigated the procedures that can contribute to minimize the methodological flaws of the design preliminary stage. This case study was conducted in two stages.



The first stage involved the structural concept of the project (here called original model or A1) evaluation, the pursuit of its optimal performance. To analyze the structural system as a set of variables that produced changes in the system arrangement (support system and membrane) and in the membrane geometry (continuous three-dimensional surface) of the original model was investigated. This set of variables originated models with different geometries. After that, the behavior and performance of these models under load action were investigated. This research or optimization process of the original model involved the preliminary structural analysis and comparison among these models in order to identify which one showed the best results and which variables contributed to the optimal performance of this project.

The second stage involved the analysis of the geometry of the flattened surface. This analysis was guided by the experimental investigation of the membrane material and the preliminary analysis performed in the first stage. It was sought to broaden the material particularities understanding, as well as, to verify the influence of material behavior and surface stresses distribution in the final surface geometry, consisting of flat panels. It was also investigated the parameters and procedures that can help to minimize the differences between the real model and theoretical model (form of equilibrium) and surround the methodological flaws of this preliminary stage of work.

### 3.1 1<sup>ST</sup> STAGE OF QUALITATIVE ANALYSIS

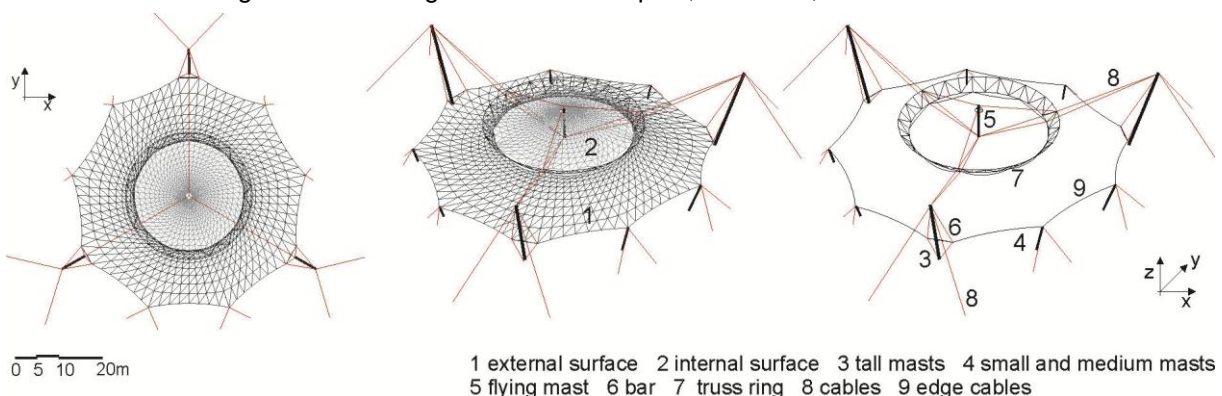
#### 3.1.1 STRUCTURAL CONCEPT OF THE PROJECT THAT GUIDES ANALYSIS

The project that guides this research is the roof model for the amphitheater at Federal University of Ouro Preto (UFOP) developed during the author's master research, here named as A1 or original model, having an approximate area of 2000m<sup>2</sup>, (Figure 3.1-1, Appendix A).

##### *Original model - structural concept and identified strategies*

The system arrangement of A1 model is characterized by combination and cooperation between membranes and supporting system in a pre-tension state, enabling a large span.

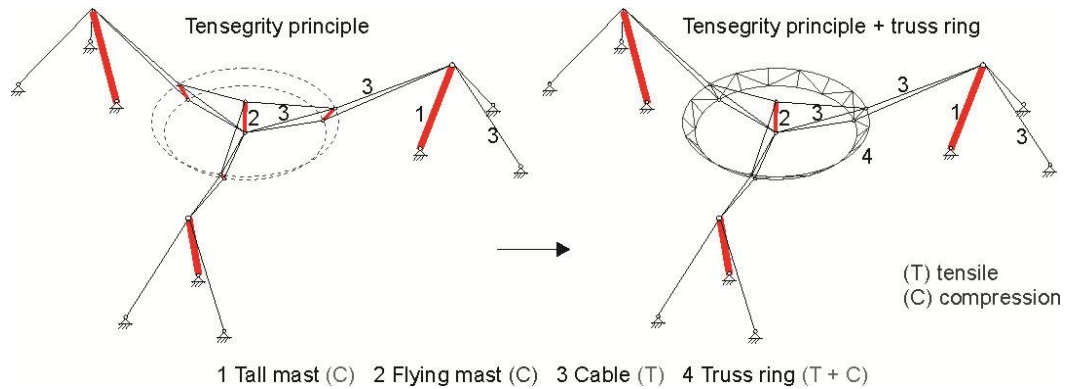
Figure 3.1-1 – Original model – A1: plan, 3D views, lateral section.



The supporting system comprises three tall masts that hold the spatial support system, as well as small and medium masts. The spatial support system is guided by

Tensegrity principle, comprising of the spatial arrangement of the flying mast and truss ring, within a continuous net of cables forming a stable volume in space (Figure 3.1-2).

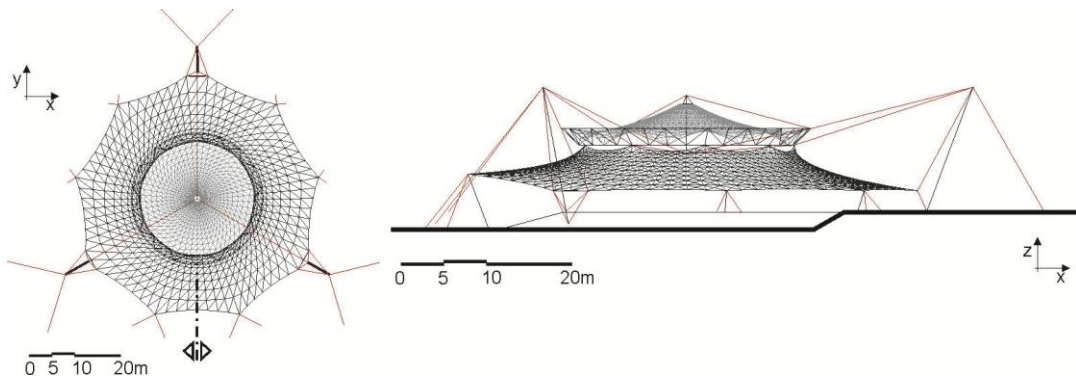
Figure 3.1-2 – Original model – A1: support system (masts + spatial support system)



This model has two anticlastic membrane surfaces, with smooth curvature, different shapes and behavior. The internal surface is retractable and comprises the radial arrangement of nine saddle shape modules; and the external surface is fixed, having a cone shape form. The external surface is anchored in the truss ring and in small and medium masts, as well as in the flying bars (that are hung by cables connected to the base and top of tall masts). The top of the internal surface rests on the top of flying mast and its base on the truss ring.

This structure has radial form with symmetry at Y axis, due to different levels of the external surface anchor points, as well as to different levels of the anchor points of masts and cables (Figure 3.1-3).

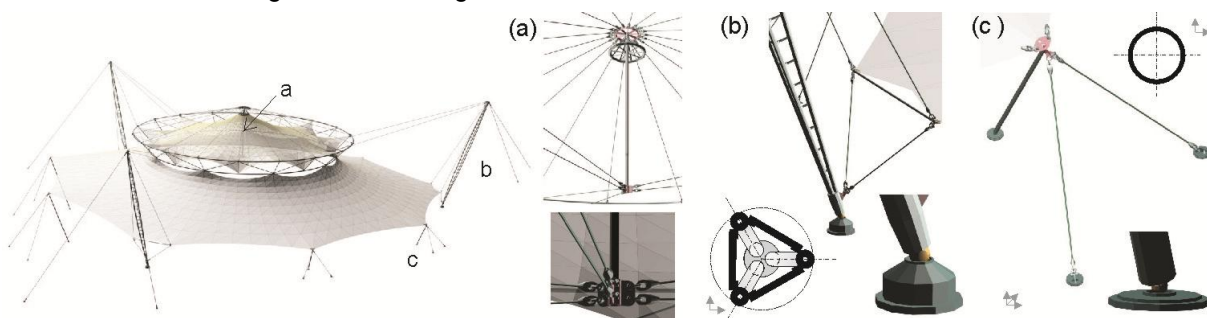
Figure 3.1-3 – Original model – A1: plant and vertical section.



The structural system arrangement is similar to membrane roof configuration for large spans (in which the support system comprises masts and the spatial support system), according to identified strategies (section 2.4.2.1, Figure 2.4-19).

Components with circular cross section and hollow section (comprising tubular profiles), and the arrangement of components to avoid bending (e.g. hinged masts with pre-tensioning cables; truss ring) are also predominant in the support system, according to identified strategies (section 2.4.2.2) and Figure 3.1-4. However, it was considered in the preliminary analysis that all masts have circular cross section.

Figure 3.1-4 – Original model – 3D view and details of masts



(a) flying mast; (b) tall mast with hollow section and flying bar hung by cables; (c) small and medium mast; Source: adapted from NUNES, 2008 p.115, 116, 118, 121.

### 3.1.2 VARIABLES THAT GUIDE THE PROJECT PERFORMANCE ANALYSIS

The qualitative analysis of the optimal performance of this membrane roof project was based on identified strategies, i.e., in pursuit of the structural system arrangement whose global stability result of joint work and cooperation among components, and whose geometry and arrangement of the components reveals the best use of the material and the shortest force path (section 2.4.2.3).

This research or optimization process of the A1 model (under load action) aimed to maximize the stiffness and global stability of the system, as well as, the ability of the membranes to withstand loads having a more homogeneous stress distribution, with lower system weight.

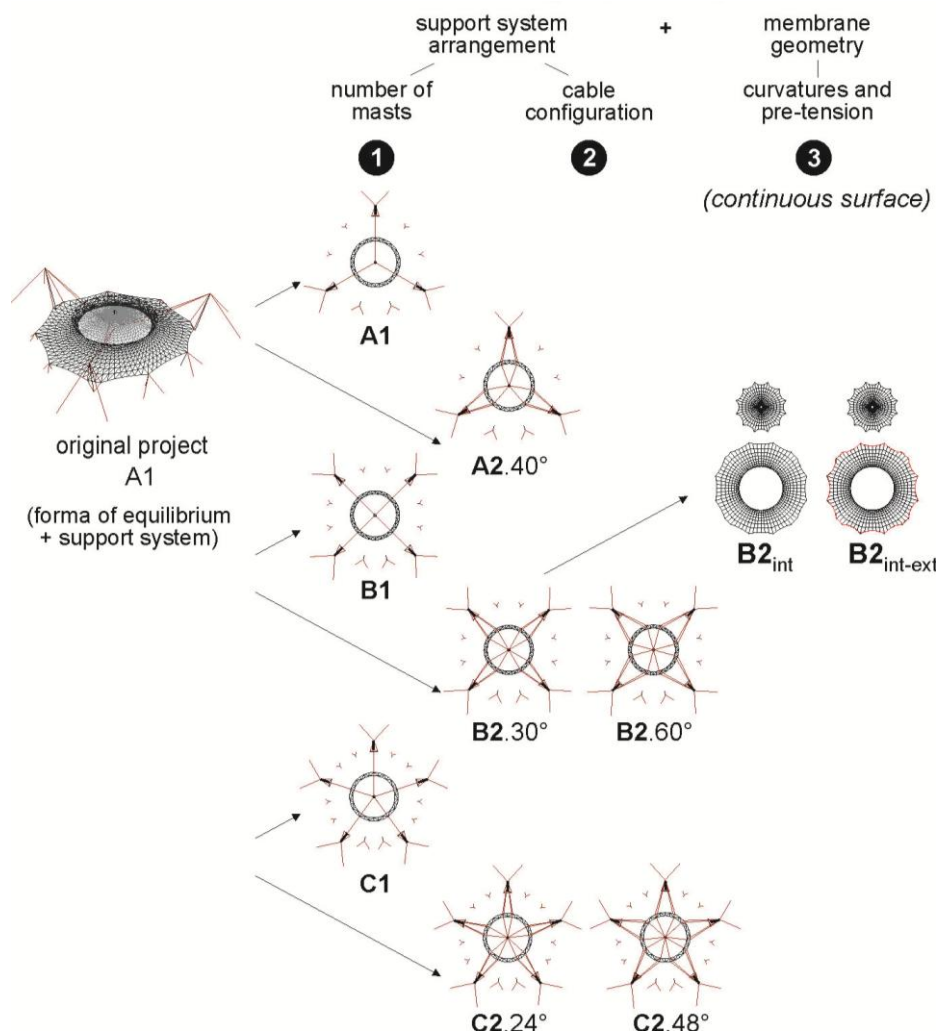
So, a set of variables that generated changes in the structural system arrangement and membrane surface geometry of the A1 model were investigated. These variables are: number of masts, cable configuration, surface pre-stress and surface curvature, as shown in Figure 3.1-5.

Each variable was added gradually to the original model, making it possible to observe the influence of each variable and of the set of variables in each case of analysis. Thus, these variables generated adjustments in the arrangement of surfaces (internal and external surfaces) and system support (truss ring, masts and cables), and consequently models with different geometries. However, the surfaces of these models retain proportionality with respect to the applied stress field, defined during form finding procedure (section 3.1.4.1).

### 3.1.3 INVESTIGATED CASES (VARIABLES) AND EVALUATED MODELS

Models that resulted from adjustments of surfaces and support system were assembled in cases of analysis, according to variable (s) that was (were) investigated for analysis and comparison (Figure 3.1-5).

Figure 3.1-5 – 1<sup>st</sup> stage of the qualitative analysis of the performance of the project

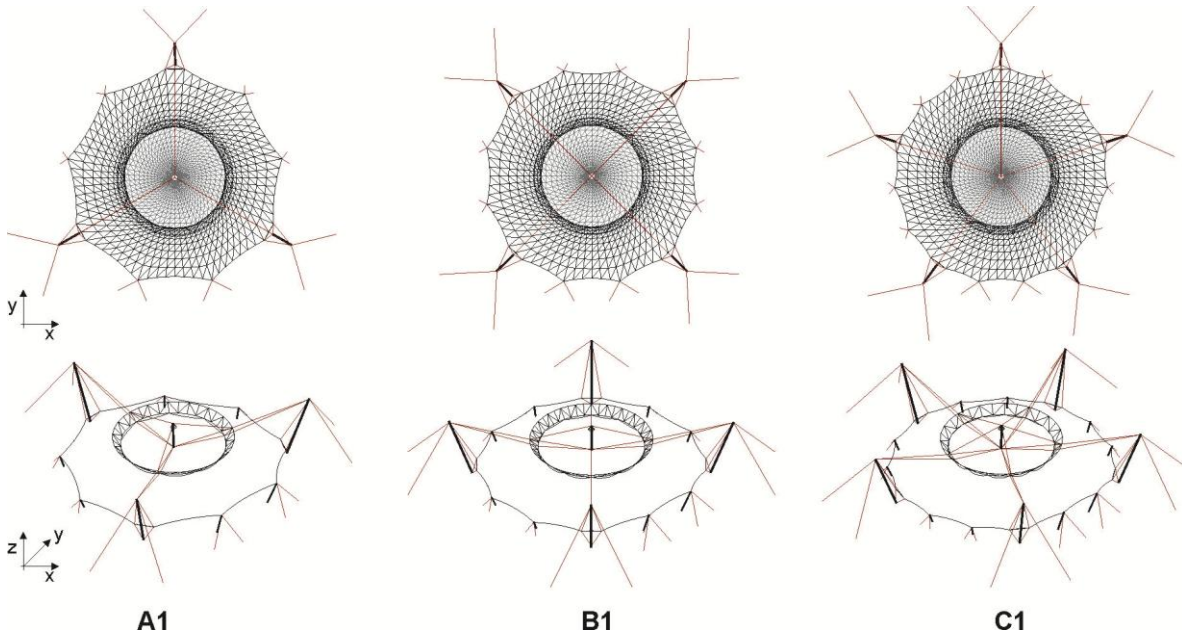


number of masts (1<sup>st</sup> case); cable configuration (2<sup>nd</sup> case); membrane geometry (3<sup>rd</sup> case)

*1<sup>st</sup> Case: Number of masts - models: A1, B1, C1*

The influence of the number of masts which hold the spatial support system was evaluated. Configurations were proposed with three, four and five tall masts. In each tall mast anchors a pair of cables positioned perpendicularly to the truss ring (Figure 3.1-6).

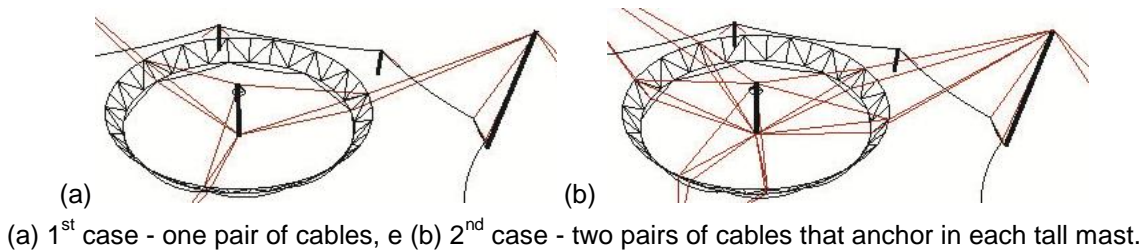
Figure 3.1-6 – 1<sup>st</sup> Case: number of masts (investigated variable) - A1, B1, C1 models



*2<sup>nd</sup> Case: Number of mast + cable configuration - models A2-40°, B2-30°, C2-24°, 60°, B2, C2-48°*

It was evaluated the influence of the cable configuration that holds the truss ring and flying mast, i.e., the arrangement of cables of spatial support system. In this case, two pairs of cables anchored in three, four and five tall masts (Figure 3.1-7b). Models whose angle between the pair of cable is defined by one and two modules of the inner surface were verified (Figure 3.1-8, Figure 3.1-9, Figure 3.1-10, Figure 3.1-11).

Figure 3.1-7 – Cable configuration that holds the spatial support system (e.g. A1model)



(a) 1<sup>st</sup> case - one pair of cables, e (b) 2<sup>nd</sup> case - two pairs of cables that anchor in each tall mast.

Figure 3.1-8 – 2<sup>nd</sup> Case: cable configuration (investigated variables) - A2.40°, B2.30°, C2.24° models

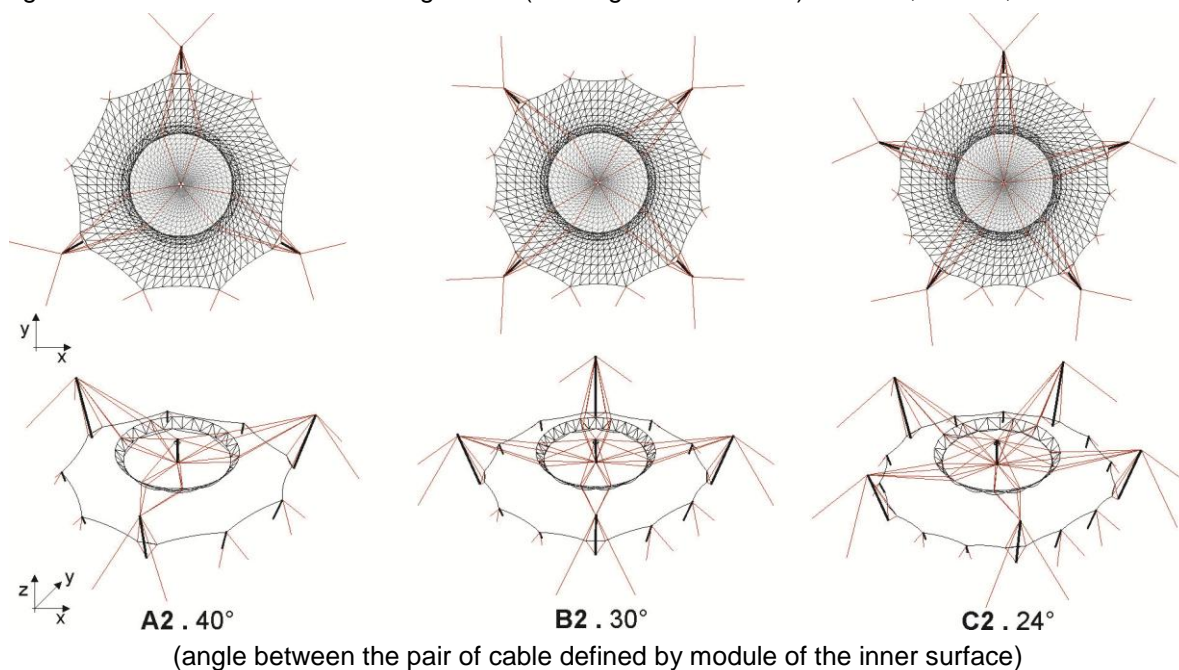


Figure 3.1-9 – 2<sup>nd</sup> Case: cable configuration (investigated variable) - B2.60° and C2.48° models

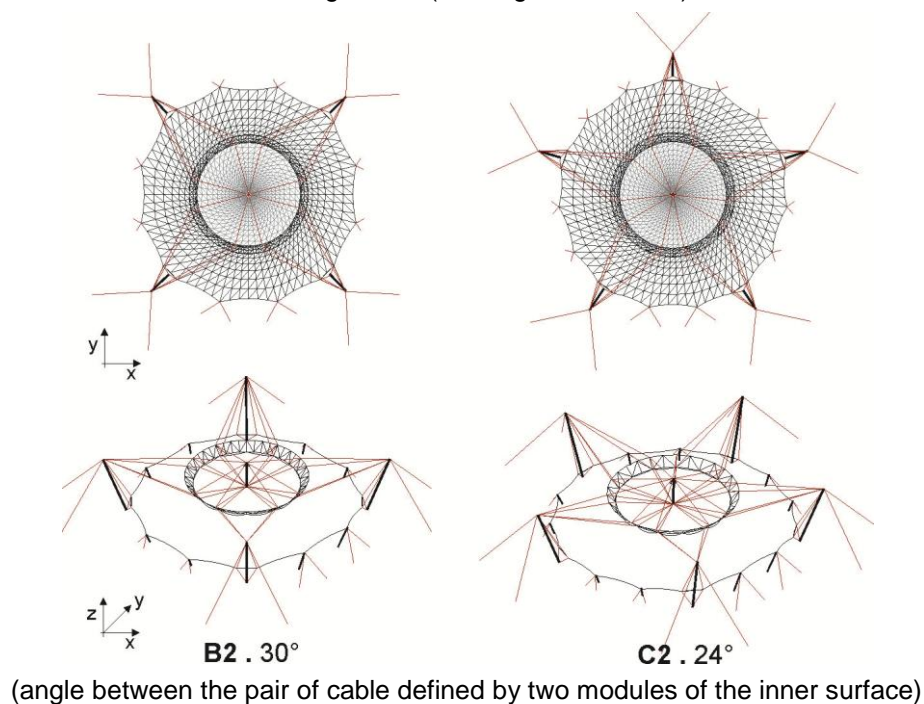
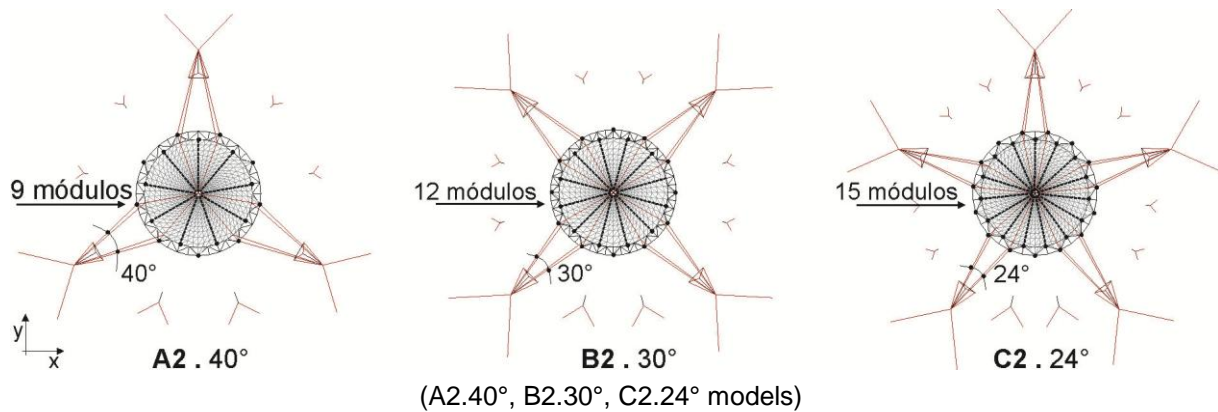
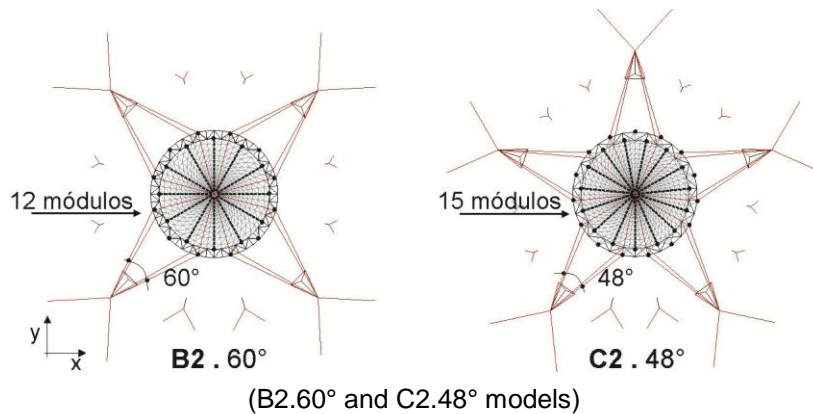


Figure 3.1-10 – 2<sup>nd</sup> Case: angle between the pair of cable defined by one module of internal membraneFigure 3.1-11 – 2<sup>nd</sup> Case: angle between the pair of cable defined by two modules of internal membrane

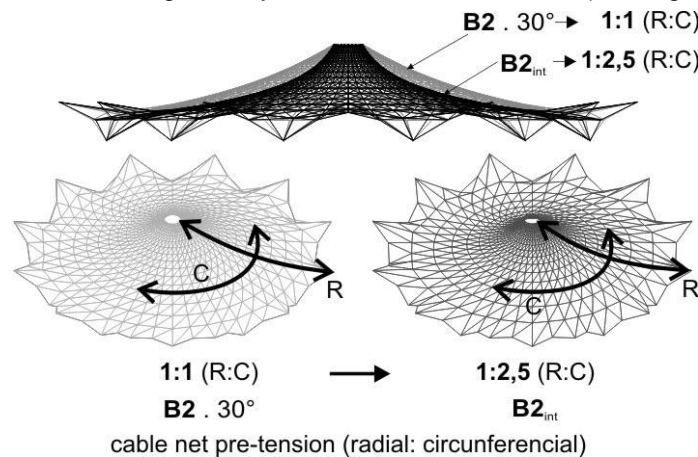
3<sup>rd</sup> Case: Number of masts + cable configuration + membrane geometry -  
models:  $B2_{int}$ ,  $B2_{int-ext}$

For this investigation it was selected the model whose spatial support system is supported by two pairs of cables which are anchored into four tall masts, i.e., the model: B2-30° (Figure 3.1-8). Thus, it was evaluated the influence of changes in membrane surface geometry (pre-tensioning and curvature).

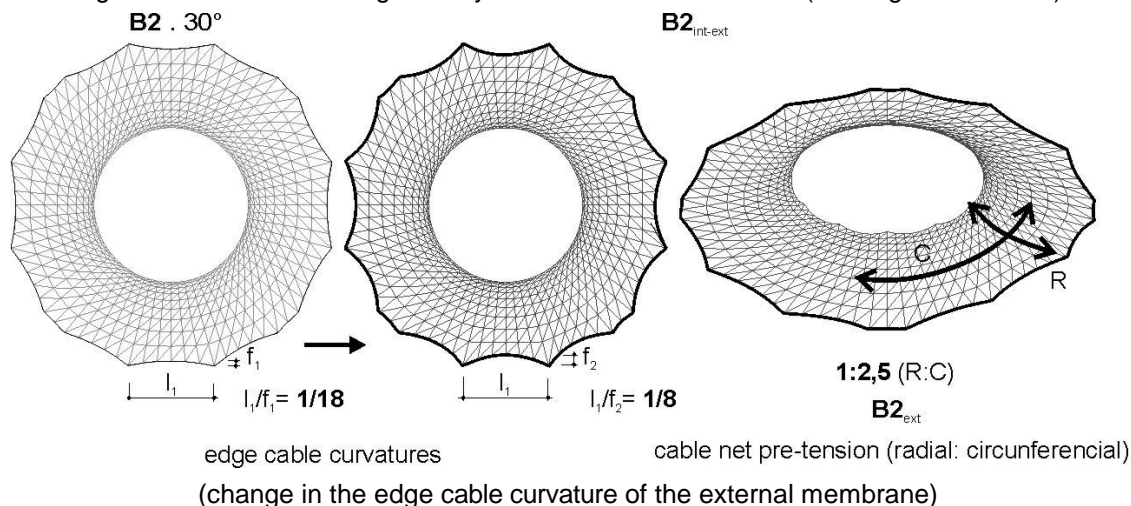
Initially, the pre-tensioning ratio applied in the radial (R) and circumferential (C) directions of the internal surface was changed, originating the  $B2_{int}$  model (Figure 3.1-12).

Then, it was also changed the ratio ( $f/l$ ) between the rise of the curvature ( $f$ ) and the length between anchor points ( $l$ ) of the external surface, generating the model  $B2_{int-ext}$  (Figure 3.1-13). This has as reference the rise/ length ratio used in the Olympic Stadium roofs in Munich (1/8 to 1/10), (verbal information)<sup>20</sup>.

<sup>20</sup> Information about the ratio rise/ length of the Olympic Stadium roofs was given by Prof Dr. Baier.

Figure 3.1-12– 3<sup>rd</sup> Case: geometry of the internal membrane (investigated variable)

(change in the pre-tension applied in the radial and circumferential directions of the internal membrane)

Figure 3.1-13 – 3<sup>rd</sup> Case: geometry of the external membrane (investigated variable)

edge cable curvatures

cable net pre-tension (radial: circumferential)

(change in the edge cable curvature of the external membrane)

The original model optimization process involved initially, the following definitions:

- the methods used in form finding and preliminary analysis;
- the procedures adopted for form finding and preliminary analysis;
- the membrane material and loads applied;
- restraints and performance evaluations proposed for membrane and support system.

Then, it was evaluated the response of each model: membrane stress distribution (ability of the membrane to withstand loads, investigating the existence of compression areas), system stiffness (membrane and support system displacements) and the mass/ area of each model. Subsequently, it was carried out the comparison of the models in order to identify which one had better results.

### 3.1.4 FORM FINDING AND ANALYSIS PROCEDURES OF THE MODELS

In this study, the form finding stage was carried out using Force Density Method (FDM) and the software DENSALFA<sup>21</sup>, and the preliminary analysis of the models was performed using the Finite Element Method and STRAUS7<sup>22</sup> software.

The form finding and analysis procedures of each model were developed in three stages: surface form finding, system three-dimensional modeling and system preliminary analysis. These were followed by the evaluation of each model and comparison among them.

#### 3.1.4.1 1<sup>st</sup> stage – Form finding

The first stage encompasses the definition of the form of equilibrium of the membrane surfaces of the studied models, having as reference the original model (A1) geometry.

This procedure used initially physical models (Figure 3.1-14). Then, the form of equilibrium of the internal and external surfaces was defined using FDM. These surfaces were represented as cable net, i.e., divided into small and hinged bar elements (connectivity between nodes).

The first step involved the initial setting definition: number of nodes and bar elements of the cable net, as well as definition of its anchor points (spatial coordinates XYZ of the restraint nodes). The internal nodes of the cable net are free to move (Figure 3.1-15, Table 3.1-1).

Subsequently, it was carried out the adjustment of the pre-tension applied to the bar elements that comprise the cable net, seeking to approximate curvatures of cable nets to the ones of the physical model. This procedure was checked by means of superposing cable nets and physical model image (Figure 3.1-16). It had as result cable nets (internal and external) with different geometries due to mesh, number of anchor points and pre-tension applied.

The same procedure was adopted for the other models. The stress field (density force) applied on the surfaces of these models also maintained a proportionality to A1 model surfaces (Table 3.1-1).

---

21 DENSALFA was developed by the engineer Vinícius Maia Barreto de Oliveira in his doctoral thesis dissertation COPPE/ UFRJ (OLIVEIRA, 2003) and kindly lend for the author's master and doctoral thesis.

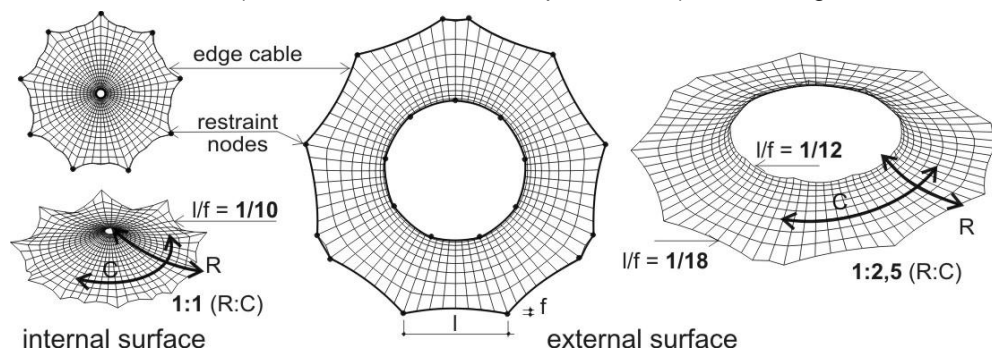
22 STRAUS7 is market outside Europa as STRAND 7- <http://www.straus7.com/>. This software provides a friendly and intuitive interface, favoring the study of structural membranes integrated to support system.

Figure 3.1-14 – Physical models (scales 1/1500, 1/200, 1/100) of A1 model



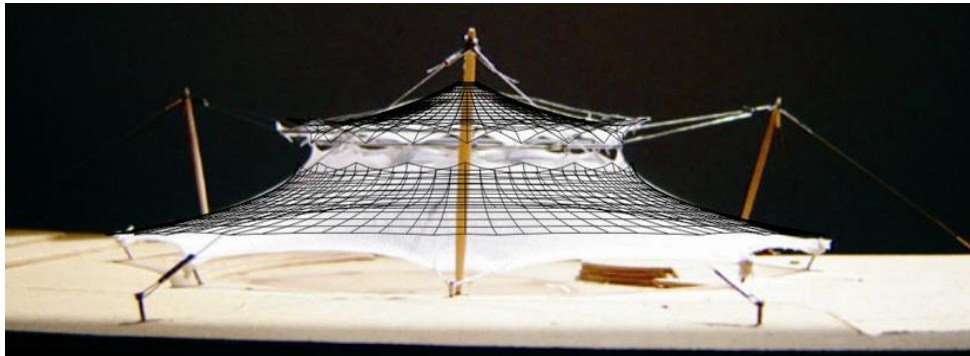
Source: NUNES, 2008, p.73, 79,111.

Figure 3.1-15 – Information (nodes, net elements and pre-tension) for defining the form of equilibrium



form of equilibrium of internal and external membranes - applied pre-tension

Figure 3.1-16 – Superposing cable nets (computational models) and physical model



Source: NUNES, 2008, p.87.

### Proportionality of surfaces

The surface stress field (external and internal surfaces of models investigated) was defined by the pre-tension applied to the net elements and net edge curvatures (Table 3.1-1). This stress field had as reference curvatures of the physical model (Figure 3.1-16) and coordinates of the anchor points of the surfaces of each model.

Table 3.1-1 – Characteristics and pre-tension applied to the surfaces in form finding

Information		External surface				Internal surface					
		A	B	B2-ext modif.	C	A	B	B2-int modif.	C		
<b>Characteristics</b>	anchor points on the top of surface	9	12	12	15	18	24	24	30		
	anchor points on the bottom of surface	12	16	16	20	18	24	24	30		
	radial elements	72	72	72	75	54	48	48	60		
	circumferential elements	10	10	10	10	15	15	15	15		
	nodes	720	720	720	750	818	720	720	900		
	total number of elements	1368	1368	1368	1425	1566	1392	1392	1740		
	restraint nodes/ imposed displacements	21	28	28	35	36	48	48	60		
<b>Stress field</b> force density (DF) applied	internal net	DF radial elements (R)	10	10	10	10	10	10	10		
		DF circumferential elements (C)	25	25	25	25	10	10	25	10	
		cable net stress field R:C	1,0: 2,5	1,0: 2,5	1,0: 2,5	1,0: 2,5	1,0: 1,0	1,0: 1,0	1,0: 2,5	1,0: 1,0	
	edge cable	top	DF edge cable	45	34	34	27.5	60	41	41	39
			edge cable curvature ratio (f/l)*	1/12	1/12	1/12	1/12	1/3	1/3	1/3	1/3
		bottom	DF cabo de borda	200	151	59	121	20	16	16	14
			edge cable curvature ratio (f/l)*	1/18	1/18	1/8	1/18	1/10	1/10	1/10	1/10
				0,06	0,06	0,12	0,06	0,10	0,10	0,10	0,10

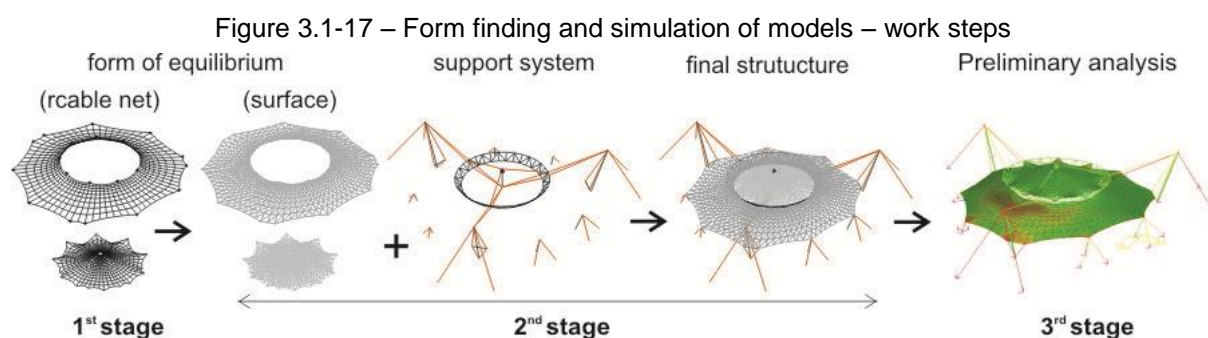
\* f/l: ratio of edge cables curvature rise of (f) and anchor points length (l)

The stress field of the surfaces was defined as follow:

- the ratios of pre-tension applied to cable nets of the models in radial/ circumferential directions were: 1,0 / 2,5 (external surface) and 1,0 / 1,0 (internal surface), except for the model B2<sub>int</sub> (3<sup>rd</sup> Case), whose pre-tension applied in the internal surface was 1,0 / 2,5;
- the pre-tension applied to top and bottom edge cables of the external and internal surfaces of the models evaluated was changed aiming to maintain the similarity of the edge curvatures of the surfaces among physical model, i.e., the same ratio: curvature rise and length between supports (f / l); however, in the B2<sub>int-ext</sub> (3<sup>rd</sup> Case) the pre-tension applied in the bottom edge cables of external surface was changed.

### 3.1.4.2 2<sup>nd</sup> stage – Three-dimensional modeling of the structural system

At this stage, the forms of equilibrium, represented by the cable nets were converted into surfaces (with triangular faces), and connected to the support system component (defined by axis of elements), procedure that allowed the three-dimensional modeling of each study model (Figure 3.1-17). This procedure was carried out using the AutoCAD ® graphical platform, and was the basis for subsequent preliminary analysis.



### 3.1.4.3 3<sup>rd</sup> stage – Preliminary analysis of the structural system

The third stage involved the preliminary analysis (non linear static) of each model studied under load action; it was carried out considering previous definition:

- three-dimensional geometry of the structural system of each model (2<sup>nd</sup> stage);
- materials of membrane (initial choice) and support system;
- applied loads (rain and wind).

In addition, were proposed:

- membrane and system support performance evaluations;
- parameters for analysis and comparison of the models.

Therefore, based on these data and parameters, the data modeling of the structure was performed, i.e., the properties of the structure components, the imposed restraints on the anchor points and load steps were defined.

In the initial analyses, the performance of membrane material was evaluated.

Subsequently, it was carried out the preliminary analysis of each model for comparison between them. In this procedure, the behavior of membrane and the support system (stresses and displacements), mass/area ratio and overall stability of each model were evaluated.

This preliminary analysis was also the basis of membrane material experimental tests.

It is suggested that the final analysis may have information obtained directly from experimental tests (material and wind), membrane surface refined mesh and cutting pattern definition. So, it will be possible to increase the quality of the structure simulation and to minimize the differences between the numerical model and real model.

### 3.1.5 DATA/ PARAMETERS THAT GUIDES THE SIMULATION OF THE MODELS

#### 3.1.5.1 Membrane material initial data

For the choice of the membrane material, preliminary analyses were performed having as reference the A2 model, and the characteristics of the materials type III and type IV (material class according to tensile strength and weight per square meter, Table 3.1-2). These analyses aimed to identify which of these materials had better performance, in relation to membrane stress field provided by the numerical model, according to the applied loads (pre-tension, gravity, wind and rain). The material type IV was the most appropriate being considered for further analysis.

Table 3.1-2 – Material (type 3 and type 4) data

Membrane material (ref. Mehler Technologies)		FR 1000 - type III	FR 1400 - type IV
coating material: PVC (finish: PVDF + UV-protected, low-wick)			
fabric material: PES (woven type: panama)			
mass	g/m <sup>2</sup>	1050	1350
tensile strength (warp/ weft)	N/50mm	6000/5500	7500/6500
	N/m	120/110	150/130
tear strength	N	900/800	1200/1200
coating adhesion strength	N/cm	26	26

Source: MEHLER (2008)

The elastic modulus of the materials considered in these analyses had as reference values presented in the dissertation of Meeß-Olsohn (2004), (Table 3.1-3).

However, in these preliminary analyses the membrane material behavior was considered isotropic and linear. So, the following values for the elastic modulus were assumed:

- . Material type III:  $E=1100\text{kN/m}$  ( $E_{\text{urdidura}}=1200\text{kN/m}$ ;  $E_{\text{trama}}=800\text{kN/m}$ , table 3.1.3);
- . Material type IV:  $E=1300\text{kN/m}$  ( $E_{\text{urdidura}}=1500\text{kN/m}$ ;  $E_{\text{trama}}=1100\text{kN/m}$ , table 3.1.3).

The material elastic constants of the external surface were evaluated with the experimental biaxial test (section 3.2.1.1), i.e., after the previous simulation of the model, verifying the surface stresses during its life time.

Table 3.1-3 – Table with the tangential stiffness of technical membranes

<i>Gewebematerial/ Beschichtung</i> Material do tecido/ revestimento		<i>Faden-Richtung/ Direção</i> do fio		<i>Bruchdehnung/</i> Alongamento a ruptura
	<i>Typ/</i> Tipo	<i>Kette/</i> urdidura [kN/m]	<i>Schuß/</i> trama [kN/m]	in %
Polyester/ PVC	1	<b>60</b> (800)	<b>58</b> (500)	15-20
	2	<b>84</b> (1000)	<b>80</b> (600)	15-20
	3	<b>114</b> (1200)	<b>104</b> (800)	15-25
	4	<b>146</b> (1500)	<b>126</b> (1100)	15-25
	5	<b>196</b> (1800)	<b>166</b> (1200)	15-25
<i>Glasfaser/PTFE</i> Fibra de vidro (2400 ,2400) ( <i>Handelsname/</i> nome comercial: Teflon, Hostaflon)	1	<b>70</b>	<b>60</b>	3-12
	2	<b>100</b>	<b>88</b>	3-12
	3	<b>138</b>	<b>118</b>	3-12
	4	<b>146</b>	<b>130</b>	3-12

Source: MEEß-OLSOHN (2004), Tabelle 6, p.34.

### 3.1.5.2 Wind load

The wind is generally considered the critical load in these lightweight structures, requiring a carefully analysis of its action. However, to know and evaluate precisely how wind is distributed and its intensity on membrane structures is complex. Firstly, because of the geometry (double curvature) and geometrically non-linear behavior of these structures; secondly, due to the particularities of the wind, “a random load, whose characteristics are only known in a statistical mode, with a large degree of uncertainty” (PAULETTI, 2003, 186p.). Furthermore, the wind standards, described for buildings with standardized shape and behavior, are not applied to these structures.

The wind load simulation on these structures considering the fluid structure interaction (computational fluid dynamics: CFD) has great developed recently, but so far not all results showed accuracy (FOSTER; MOLLAERT, 2004). Thus, the usual method of obtaining information about the dynamic effects of wind in these structures results of wind tunnel experimental tests. In these tests using scale models, the pressure coefficients used in the static forces calculation for analysis (approximate) and dimensioning of the structures are obtained. Besides the reliability of the results, the cost of tests is less than the cost wasted on the overestimated structure, also contributing towards a better structure safety (VILELA, 2011).

To understand the relevance of the analysis considering the pressure coefficients is important to understand the wind action on buildings. According to Gonçalves *et al.* (2004), the wind action on buildings is associated with meteorological and aerodynamic aspects. The meteorological aspects result from wind speed. It depends on the building location, topography of the site, height of building, roughness of the terrain (type and height of obstacles to the wind flow) and function/ occupancy of the building. The aerodynamic aspects define wind behavior and trajectory in relation to building shape (size, slope and relative height, openings). Therefore, it makes possible identifying pressures (external and internal), described by wind pressure coefficients, which act on the building surface geometry, from wind directions.

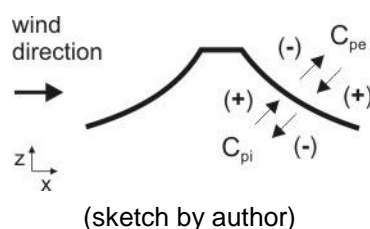
According Vilela (2011), the wind is generally considered a static load, defined by a dynamic pressure of reference ( $q$ ) multiplied by the pressure coefficient ( $C_p$ ). This is dimensionless factor and results of the ratio between the effective pressure caused by the wind on a small area of the body surface and the wind dynamic pressure of reference:

$$C_{pe} = \frac{\Delta p_e}{q} \quad C_{pi} = \frac{\Delta p_i}{q} \quad C_p = C_{pe} + C_{pi} \quad q = \frac{1}{2} \rho V^2$$

$C_{pe}$  - external pressure coefficient (on upper face of the roof);  $C_{pi}$  - internal pressure coefficient (on the underside of the roof);  $C_p$  - pressure coefficient (total or resultant);  $\Delta p_e$  - effective static pressure coefficient (average at the point under consideration on the upper surface of the roof);  $\Delta p_i$  effective static pressure coefficient (average at the point under consideration on roof underside);  $q$  - dynamic pressure of reference.

The modeling and analysis of wind load on membrane structures, has as principle that wind action is applied on both sides of the single layer element simultaneously (Figure 3.1-18). So, the effects of internal and external pressure coefficients on the surface model are considered (Vilela, 2011).

Figure 3.1-18 – Wind pressures acting on the surface geometry



Positive values of  $C_p$  indicate an effective pressure meaning external pressure, and negative values indicate an effective pressure meaning external suction (ABNT, 1988, *apud* VILELA, 2011).

In this preliminary investigation there was no planned wind tunnel testing. So, wind load simulation had as reference the procedure laid down by Brazilian standard NBR 6123:1988, and pressure coefficients (internal and external) resulting from wind tunnel tests of membrane structure models (cone shape - open high point) performed by Cristina Vilela in her doctoral thesis (VILELA, 2011).

#### *Wind loads – reference parameters*

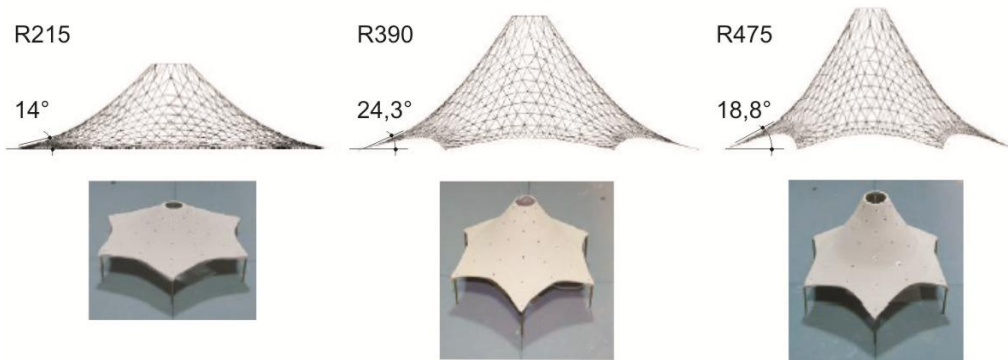
The tests on models of membrane structures (cone shapes of one, two and three peaks) conducted by Cristina Vilela (VILELA, 2011) were carried out in the wind tunnel Pr. Joaquim Blessmann, Aerodynamics Laboratory of Construction, University of Rio Grande do Sul - LAC / UFRGS, Brazil.

The measuring method of instantaneous pressure was used, that is, a traditional measuring method of floating pressure on the outer and inner surface of rigid models. Tests were performed with scale models in 1/75 (cone shapes with open high point, with different ratios height / diameter; and cone shapes with one, two and three close high points) in flow of low turbulence with subcritical Reynolds number and roof model with smooth surface.

The cone shapes with one high point (named according to the ratio height/diameter) have hexagonal base (diameter: 9m) and top circular ring (diameter: 1,5m). In geometric scale 1/75, the diameter of the base is 20cm.

It was selected the tested models R215, R390 and R475 (Figure 3.1-19 and Table 3.1-4), whose angles of inclination of the surfaces (slope) bring close to angles of the curvatures of the study models (Figure 3.1-21).

Figure 3.1-19 – Models (R215, R30, R475) used as a reference to the case study.



Source: VILELA, 2011, p.77.

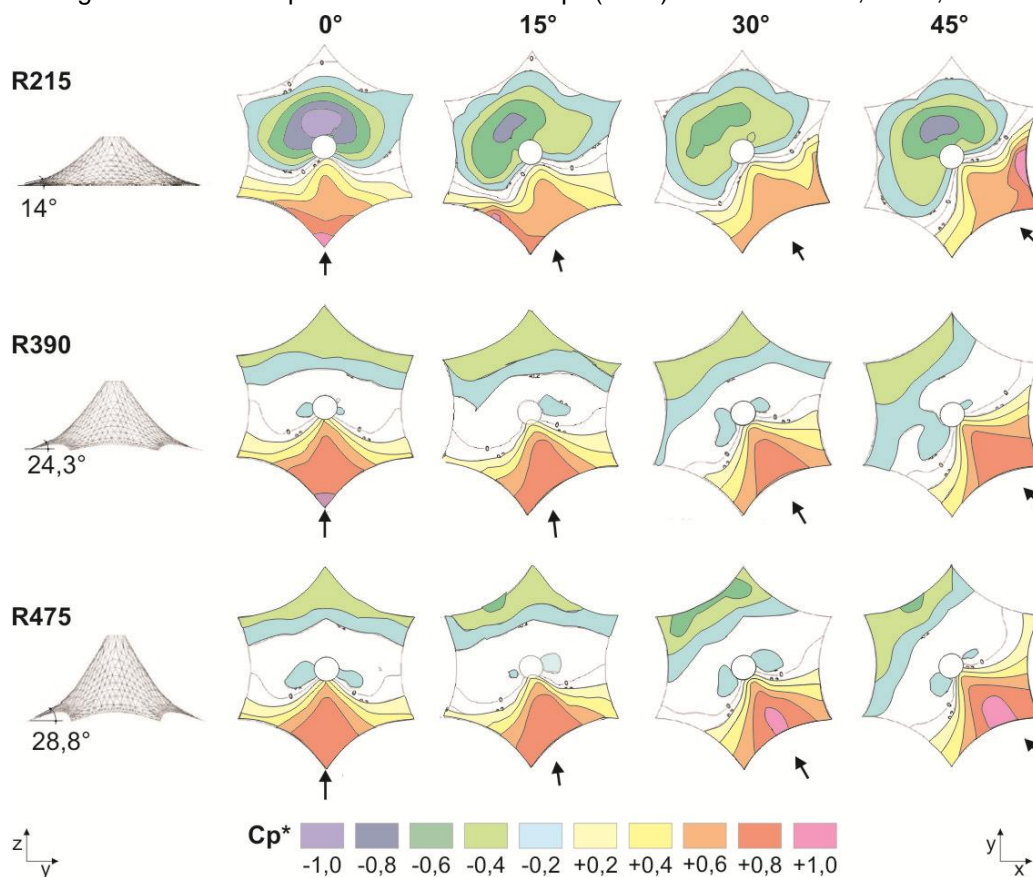
Table 3.1-4 – Characteristics of the models R215, R390 and R475 and wind direction

Model	Ø bottom = 9m			Ø bottom (1/75) = 20cm	
	height/ diameter (h/d)	membrane surface angle	ring vertical displacement (m)	membrane height (cm) (escala 1/75)	
R0215	0,215	14,0°	6,25	4,3	y ↑ x → 180° 120° 60° 45° 30° 15° 0° Direção do vento 1/4 1/2
R0390	0,390	24,3°	8,85	7,8	
R0475	0,475	28,8°	10,15	9,5	

Tests were performed varying the angle of the wind direction, between 0° and 180°, checking internal and external pressures at each 15°. As the models tested R215, R390 and R475 have symmetrical basis (pattern that repeats every 60°), the resulting average pressure coefficient values were calculated ( $C_p^*$ ) for 0°, 15°, 30° and 45°.

Therefore, it was verified how the wind is distributed and which is its intensity on the geometry of the models (with different surface angles) according to the following wind directions: perpendicular to the anchor point (0°); the half the length between two anchoring points of the surface (30°); the fourth portion of the length between two anchoring points of the surface (15° and 45°).

The results were presented as graphs of isobar lines of  $C_p^*$  (resulting average values), according to Appendix I; Table 3.1-5. To facilitate the analysis and application of pressure coefficients in case study models, the graphs of isobar lines of  $C_p^*$  of tested models R215, R390 and R475 were represented with colors as shown in Figure 3.1-20.

Figure 3.1-20 – Graphs of Isobar lines of  $C_p^*$  (color) - models: R215, R390, R47

Source: adapted from VILELA, 2011, p.77, 91, 94, 95, 96

Table 3.1-5 – Limit values of  $C_p^*$  (mean values resulted) – tested models

model	wind direction							
	0°		15°		30°		45°	
	(+)	(-)	(+)	(-)	(+)	(-)	(+)	(-)
R0215	1,08	-1,13	1,06	-0,87	0,74	-0,70	1,35	-0,91
R0390	1,03	-0,67	0,94	-0,65	1,00	-0,68	0,94	-0,68
R0475	0,99	-0,71	0,95	-0,69	1,05	-0,73	0,99	0,68

Fonte: adapted from VILELA (2011), p.89.

- In the graphs of isobar lines (Figure 3.1-20) and Table 3.1-5 were observed:
- the wind direction of 0°, 15°; and 45° are the most unfavorable because wind action occurs directly or near the anchor points of the structure;
  - the wind direction of 30°, is the most favorable because the wind action occurs between two anchor points of the structure, which divides the wind pressure;
  - surfaces with smaller angles of inclination (slope) showed the highest suction and pressure values at wind direction of 0°, 15° and 45°.

### Wind loads – adopted parameters

The wind loads used in simulation of the models, were based on wind pressure calculation NBR 6123 (ABNT1988) and mapping of wind pressure coefficients on the surfaces of the study models, according to parameters defined by Vilela (2011).

The wind speed calculation initially involved the definition of the characteristic velocity ( $V_k$ ), considering the following aspects of the site (amphitheater of the UFOP campus) and building function:

- wind speed ( $V_o$ ) is 35m/s, according Isopleth curves (wind speed map -NBR 6123);
- topographic factor ( $S_1 = 1$ ): flat ground with few undulations;
- factor of roughness/ obstacles of terrain ( $S_2 = 0.96$ ): flat or wavy with obstacles (Category III); horizontal dimension of building larger than 50m (class C) and average height of 20m;
- Statistical factor ( $S_3 = 1$ ): buildings with high occupancy factor.

$$\text{Thus: } V_k = V_o \cdot S_1 \cdot S_2 \cdot S_3 = 33,6\text{m/s}$$

$$q_o = \frac{1}{2} \cdot C_p \cdot \rho \cdot V_k^2 = 0,69 C_p \text{ kN/m}^2 = 0,00069 C_p \text{ MPa}$$

Where:  $V_o$  (basic wind speed);  $S_1$  (roughness factor);  $S_2$  (statistical factor);  $S_3$  (statistical factor);  $V_k$  (characteristic wind velocity);  $q_o$  (dynamic pressure);  $\rho$  (air density:  $1,226\text{Ns}^2/\text{m}^4$ );  $C_p$  (pressure coefficient).

It had as result a dynamic pressure of 0.00069 MPa which was multiplied to wind pressure coefficients values (according tests performed by Vilela, 2011), and applied perpendicular to the surfaces of the models, as mapping of pressure coefficients (Table 3.1-6, Figure 3.1-23, Appendix C), to identify the pressures acting in surface geometry, according to wind directions.

Table 3.1-6 – Pressure coefficients and dynamic pressure applied to models

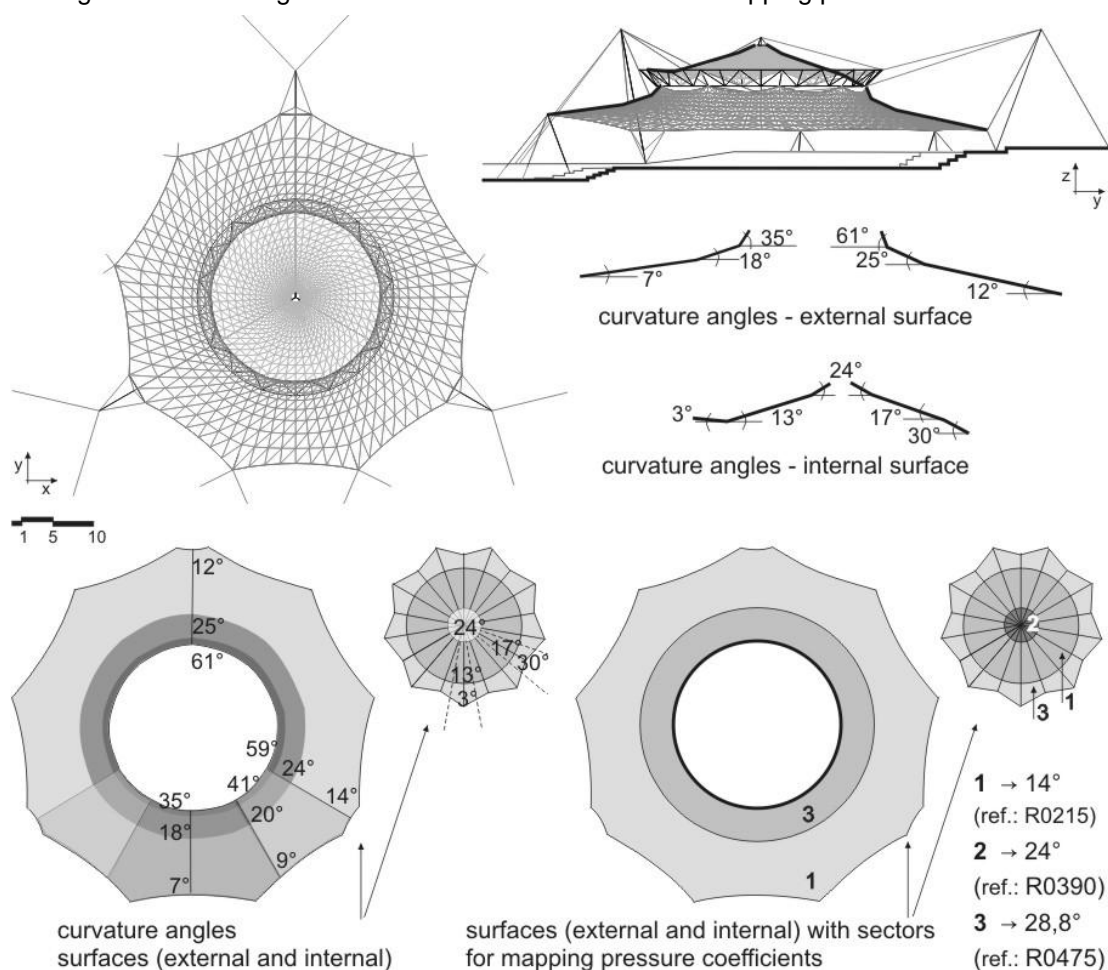
pressure coefficients	pressure (+)				
	1,00	0,80	0,60	0,40	0,20
dynamic pressure [MPa]	0,000690	0,000552	0,000414	0,000276	0,000138
pressure coefficients	suction (-)				
	-1,00	-0,80	-0,60	-0,40	-0,20
dynamic pressure [MPa]	-0,000690	-0,000552	-0,000414	-0,000276	-0,000138

The mapping of wind coefficients on surfaces (external and internal) of the different study models had as reference the following parameters defined by Vilela (2011): surface angles (slope) and wind direction at models.

This procedure was initially performed with original model (A1) and adopted for the other models, according to the following steps:

- 1<sup>st</sup> step: it was verified the angles (approx.) of the external and internal surfaces of the model A1 (Figure 3.1-21);
- 2<sup>nd</sup> step 2: the tested models (whose surface angles bring close to the surface model angles) were identified (VILELA, 2011), i.e., models R0215, R0390 and R475 (Figure 3.1-19);

Figure 3.1-21 – Angles and sectors of the Model A1 for mapping pressure coefficients



- 3<sup>rd</sup> step: the model surfaces (external/ internal) were sectorized (circumferentially), in accordance with the angles selected, for mapping pressure coefficients. Thus, the outer surface was divided in two rings (angles 14° and 28,8°), and the inner surface into three rings (angles 14°, 24° and 28,8°) as show in Figure 3.1-21 .

- 4<sup>th</sup> step: the wind direction was defined (Figure 3.1-22, Appendix B). As the model A1 (original) has symmetry only on the Y axis, it was selected the following directions: X-, Y, -Y and -Y2 (only for model B), which in this study were named

global directions. Moreover, it was verified the wind direction in relation to surface anchor points of each model: perpendicular to the anchor point, mid-span (between two anchoring points), and the fourth portion of the span, which in this study were named local direction.

Thus, the mapping of the pressure coefficients on the surfaces (external and internal) of each model (Figure 3.1-23, Appendix C) was defined by the angles of the surface rings, global and local wind directions.

Figure 3.1-22 – Wind directions (global and local) - external surface models A, B, C

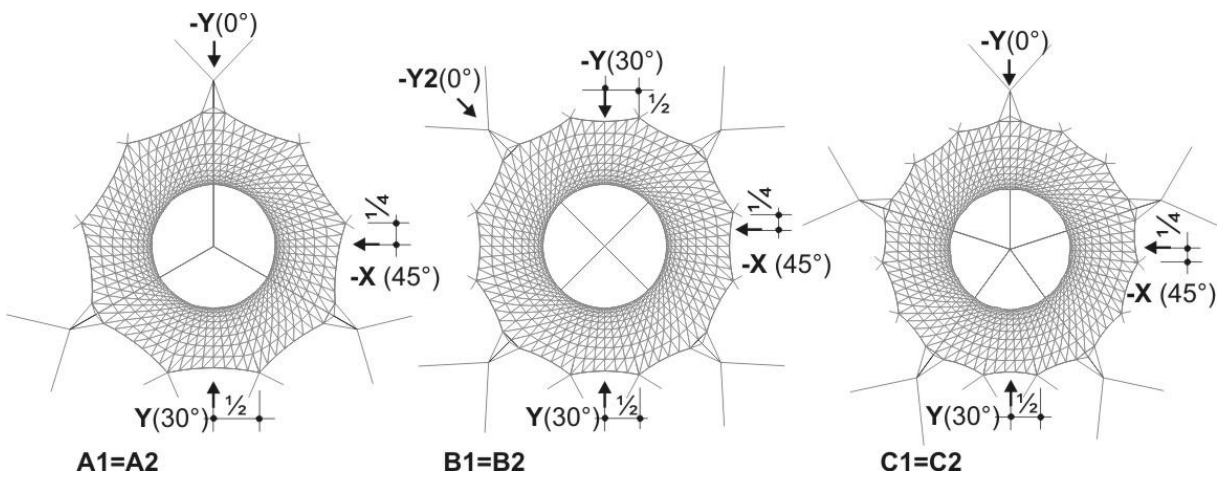
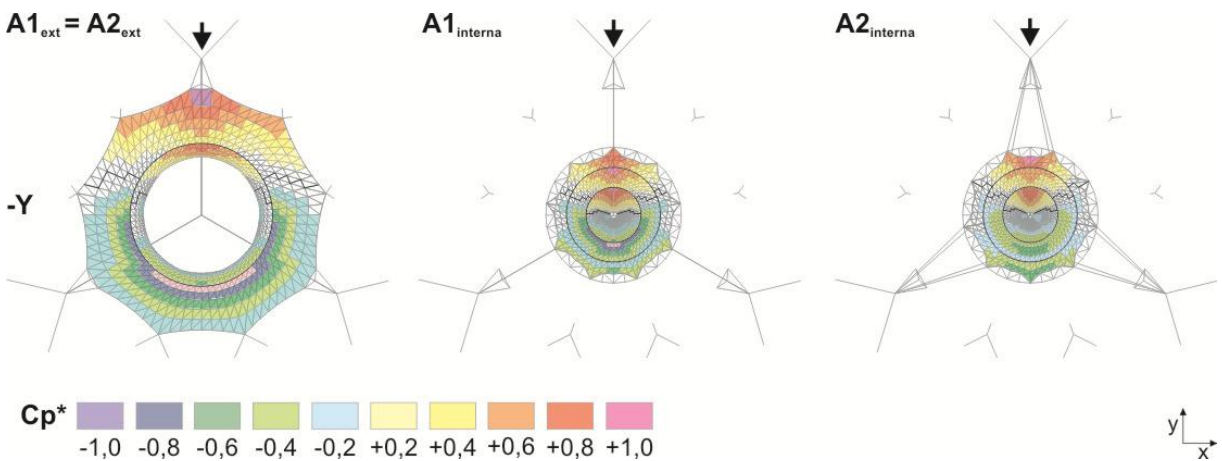


Figure 3.1-23 – Mapping of wind pressure coefficients (direction -Y)



external and internal surfaces of models: A1 e A2.

### 3.1.5.3 Load rain

It has been proposed the rain load evaluation. This was calculated considering the water pressure of 0,01m over surface.

Considering: - water specific weight ( $1\text{m}^3$ ) = 1000kgf/m<sup>3</sup>;

- water volume ( $h=0,01\text{m}$ ) = 0,01 m<sup>3</sup>

- strength (volume x specific weight) = 10kgf

It had as result a pressure (force / area) of 10kgf/m<sup>2</sup> (0,0001MPa), which was applied to the surface in -Z direction.

### 3.1.5.4 Proposed performance evaluation

According Knippers *et al.* (2011), membrane structural analysis methods generally consider the influence of the following factors or uncertainties: duration and magnitude of the loads, temperature and environmental conditions (e.g. moisture, pollution), the life time of the structure and material behavior (creep). However, how these factors affect the membrane strength depends on the material used, construction details realized, seam procedure, dimensions and life time of the structure.

As these uncertainties add to geometrically non-linear behavior of the system and material non-linear behavior, is complex to estimate the structural safety of the membranes (GOSLING; ZHANG, 2010). These uncertainties and system particularities make difficult to establish a single analysis method for all types of membranes and materials of construction. So engineers from various countries and institutions have adopted different safety factors, and these factors result of evaluated and combined uncertainties (KNIPPERS *et al.*, 2011).

In Germany so far, there are no regulations for membranes and foils design. There are only standards for temporary buildings (DIN4112: 1983-02) and for pneumatic buildings (DIN4131: 1983-02).

The DIN 4112 is based on allowable stresses and considers load 1:1 (no factored load), and pre-tension values recommended has as reference engineers experience. The DIN 4131 is based on the allowable deformations and adopts safety factors combination; these factors had as reference the dissertation of Jörg Minte (1981), (KOENEN, 2012).

In Brazil, until now there are not standards guiding safety and performance of membrane structures. Thus, in this preliminary analysis, two performance evaluations were proposed in order to guide preliminary structural simulation of the models:

- evaluation of membrane performance, based on allowable stress; real load 1:1 (not factored) was applied;
- evaluation of steel support system performance, considering combination of actions (factored loads), having as reference American standard AISC (2010; 2000).

#### *Evaluation of membrane performance*

This evaluation used as reference load values (pre-tension) recommended according to the experience of the engineers (KOENEN, 2012).

It was verified the influence of magnitude and duration of loads (permanent action: self-weight, pre-tension; variable action: rain load, wind/critical load) in the membrane material behavior of the evaluated structure. This evaluation considers that material deformation (viscoelastic) is not only related to stress magnitude but is also function of time (section 2.5.3). The influence of snow load was not considered in this analysis.

Regarding load duration, Knippers *et al.* (2011) highlights that wind load occurs relatively frequently and may have great intensity, but the wind gust lasts only a few seconds. Thus, during the life time of the structure, the wind has relatively shorter duration (short term) and therefore less influence on deformation of the material under constant stress with time (creep). However, self-weight and pre-tension, acting in constant state (long-term), have a significant influence on the deformation of the material.

Moreover, it was considered the range in which the membrane materials can behave reasonably linear, i.e., between the level of pre-tension and approximately 25% of the tensile stress of the material selected (KOCH, 2004). Thus, the material strength was reduced to an allowable value.

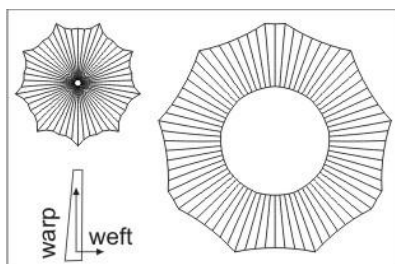
So, the maximum stress provided by the numerical model under the wind load action (short-term load) was 25% of the material tensile strength (or breaking strength) in the directions of the fabric (warp and weft), (Table 3.1-7).

It is also important to control pre-tension values (load permanent or long term load) for the durability of membrane material and to minimize surface displacements under the wind action. So, the maximum pre-tension provided by the numerical

model was limited to 5% of the selected material tensile strength, at fabric directions (warp and weft), i.e., 20% of the maximum stress provided by the numerical model under wind action, as shown in Table 3.1-7.

Therefore, to evaluate load action is required to define surface cutting patterns and material directions according to this patterns.

Table 3.1-7 – Maximum stress at membrane surface



Material Type 4 strength [kN/m]*		Membrane maximum load (load not factored)			
		initial pre-tension 5% [kN/m]*		critical load 25% [kN/m]*	
warp	weft	warp	weft	warp	weft
150	130	7,5	6,5	37,5	32,5

(\*) 1kN/m= 1MPa, considering material thickness: 1mm

### *Evaluation of steel support system*

The safety evaluation and steel support system performance were based on the most critical combination of actions to the study models, having as reference the American standard AISC (2010).

Initially, it was evaluated the following combination of actions:

$$1,2D + 1,6W + 0,5R + 1PT \quad (1)$$

$$1,2D + 0,8W + 1,6R + 1PT \quad (2)$$

where: D: self weight (dead load); W: wind; R: rain; PT: pre-tension.

The combination of actions (1) was selected, because it was the most unfavorable to the models.

The performance factor (load/ resistance) considered to the support system components was approximately 80%. However, the cables showed greater variation because of the dimensions and characteristics of the components used as reference in this analysis (Appendix E, F).

#### 3.1.5.5 Parameters adopted for analysis and comparison of models

To the analysis and comparison of study models, the same loads were considered.

Furthermore, the same pre-tension was applied on membrane surfaces and edge cables (in each load step) of all models.

However, the pre-tension applied to support system cables changed in each model, according to Table 3.1-8. Thus, it was possible to evaluate the level of pre-

tension of support system cables and dimensioning of the system components necessary to each model withstand load actions, considering membrane maximum stress around 25% of the selected material tensile strength.

Table 3.1-8 – Parameters for analysis and comparison of the study models - applied pre-tension

load cases		membrane analysis								support system analysis (factored loads)				
		membrane maximum stress												
		5%	25% material strength											
		1 ° step	wind (critical load)				wind + rain							
		pré + grav	-X	Y	-Y	-Y2	-X	Y	-Y	-Y2	-X	Y	-Y	-Y2
pre-tension	membrane*	x	x	x	x	x	x	x	x	x	x	x	x	x
	edge cables *	x	x	x	x	x	x	x	x	x	x	x	x	x
	support system cables	pre-tension can change												
gravity		1,0	1,0	1,0	1,0	—	1,0	1,0	1,0	1,0	1,2	1,2	1,2	1,2
external loads	chuva	—	—	—	—	—	1,0	1,0	1,0	1,0	0,5	0,5	0,5	0,5
	vento: -X	—	1,0	—	—	—	1,0	—	—	—	1,6	—	—	—
	vento: Y	—	—	1,0	—	—	—	1,0	—	—	—	1,6	—	—
	vento: -Y	—	—	—	1,0	—	—	—	1,0	—	—	—	1,6	—
	vento: -Y2	—	—	—	—	1,0	—	—	—	1,0	—	—	—	1,6

(\*) it was applied the same pre-tension (magnitude) on membrane surfaces and edge cables (in each load step) for all models

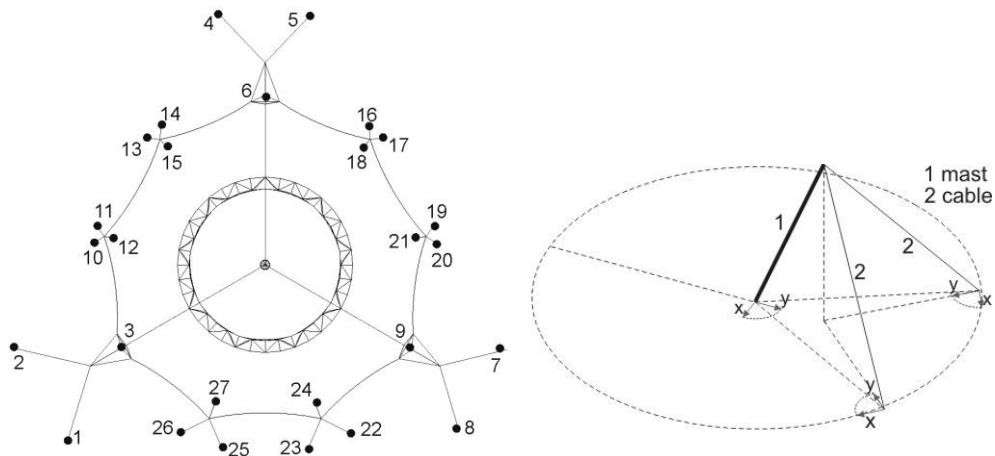
To identify the pre-tension adopted for the membrane and edge cables of all models, it was performed previously the preliminary analysis of models of the first and second cases. To the models of the first case be in equilibrium under wind load, the pre-tension was approximately 2.8 times the initial pre-tension (step 1); in the models of the second case, it was 3.5 times the initial pre-tension. Therefore, it was considered the pre-tension checked in second case, allowing its use in all models, and therefore the comparison among them.

### 3.1.5.6 General data for preliminary analysis of the structural system

#### *Anchoring restraints*

In the structure anchor points (basis of the masts and cables) the translation movement is restraint in XYZ directions (local) and rotation is allowed in XYZ directions (local). That means for fixing these restraints, the local coordinates of these components for each model were initially defined, as shown in Figure 3.1-24, Appendix D.

Figure 3.1-24 – Structure anchor points; restraints considering local coordinates, e.g. A1model



### *Structural components specification*

The preliminary dimensioning and specification of the support system components (masts, cables and truss ring) of each model are not strictly accurate. They result of preliminary analysis procedure considering the combination of actions (Appendix E and F) and guide the comparison of the models.

### *Applied loads*

The initial pre-tension applied to membrane was 1.00 MPa (considering material thickness 1mm) and to cable edges and support system cables was 10.00 kN. The increments of pre-tension applied to membrane, cable edges and support system cables required for each model to withstand wind load (critical load) can be verified in Table 3.1 9.

### 3.1.6 INTERPRETATION AND ANALYSIS OF THE MODELS

The models were assembled in groups or analysis cases, according to variables that were investigated for proposed evaluation.

It was observed: the pre-tension applied to the components of the models (Table 3.1-9), the ratio mass/area of the models (Table 3.1-10), and the displacements of membrane and support system (Table 3.1-11) for comparison. It was evaluated the surface stress trajectories (maximum and minimum) and Von Mises stress.

The Von Mises stress calculation identifies whether the material is working in the elastic range. The analysis of membrane material behavior is carried in the elastic state, because the deformation of membrane material (fabric and foil) is permanent in the plastic state, i.e., it does not return to its original shape after removing the applied force. So, this calculation is based on principle according to which an elastic body subjected to loads in XYZ directions, presents a complex stress system. Thus, at any point in this body there are stress in different directions, and from one point to another point, the stress directions and magnitudes changes. This calculation, according to Lewis (2003) relates this three-dimensional stress field that acts on an elastic body to an equivalent uniaxial stress. Thus, a value above this stress indicates the ductile failure of the material.

The wind was responsible for the critical load observed in these structures, as can be observed in analyses of the models and Table 3.1-11. In the Y direction, the wind falls between two supporting points of the membrane, being supported more evenly. In -X, -Y, -Y2 directions, wind direction occurs directly or near anchor points of the membrane, being the most unfavorable directions (Figure 3.1-25). So, it was highlighted the critical directions (-Y; -Y2) in the model analysis, and at the end of each case it was shown all wind directions evaluated.

Figure 3.1-25 – Wind directions

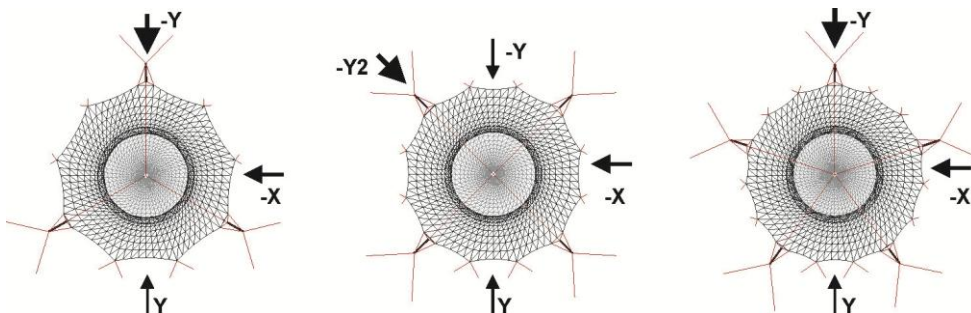


Table 3.1-9 – Load steps and pre-tensioning applied to components of the study models

load cases		membrane analysis									
		1° step	wind				wind + rain				
		pré + grav	-X	Y	-Y	-Y2	-X	Y	-Y	-Y2	
pre-tension	membrane	4,5	16,0	16,0	16,0	16,0	16,0	16,0	16,0	16,0	
	edge cables	4,5	16,0	16,0	16,0	16,0	16,0	16,0	16,0	16,0	
	support system cables	A1 	9,5	19,0	19,0	19,0	—	19,0	19,0	19,0	—
		B1 	7,0	10,0	10,0	10,0	10,0	10,0	10,0	10,0	10,0
		C1 	6,5	2,5	2,5	2,5	—	2,5	2,5	2,5	—
		A2.40° 	7,0	38,0	38,0	38,0	—	38,0	38,0	38,0	—
		B2.30° 	7,0	22,0	22,0	22,0	22,0	22,0	22,0	22,0	22,0
		C2.24° 	4,5	4,5	4,5	4,5	—	4,5	4,5	4,5	—
		B2.60° 	10,0	28,5	28,5	28,5	28,5	28,5	28,5	28,5	28,5
		C2.48° 	6,0	13,5	13,5	13,5	—	13,5	13,5	13,5	—
B2 <sub>int</sub> 	7,3	22,0	22,0	22,0	22,0	22,0	22,0	22,0	22,0		
B2 <sub>int-ext</sub> 	4,0	14,0	14,0	14,0	14,0	14,0	14,0	14,0	14,0		
gravity		1,0	1,0	1,0	1,0	1,0	1,0	1,0	1,0	1,0	
external loads	rain	—	—	—	—	—	1,0	1,0	1,0	1,0	
	wind: -X	—	1,0	—	—	—	1,0	—	—	—	
	wind: Y	—	—	1,0	—	—	—	1,0	—	—	
	wind: -Y	—	—	—	1,0	—	—	—	1,0	—	
	wind: -Y2	—	—	—	—	1,0	—	—	—	1,0	

Table 3.1-10 – Ratio mass / area of each study model

Models		support system		membrane			support system + membrane		
		mass (kg)	%	mass (kg)	area (m <sup>2</sup> )	%	mass (kg)	mass/ area	
								(kg/m <sup>2</sup> )	%
	A1	23.850,53	1,00	3.224,79	2.388,73	1,00	27.075,32	<b>11,33</b>	1,00
	B1	23.729,89	0,99	3.394,94	2.514,77	1,05	27.124,83	<b>10,79</b>	0,95
	C1	24.398,18	1,02	3.461,56	2.564,12	1,07	27.859,74	<b>10,87</b>	0,96
	A2 40°	49.089,02	2,06	3.224,79	2.388,73	1,00	52.313,81	<b>21,90</b>	1,93
	B2 30°	33.111,38	1,39	3.394,94	2.514,77	1,05	36.506,32	<b>14,52</b>	1,28
	B2 60°	43.628,78	0,89	3.394,94	2.514,77	1,05	47.023,72	<b>18,70</b>	1,65
	C2 24°	21.672,05	0,91	3.461,56	2.564,12	1,07	25.133,61	<b>9,80</b>	0,86
	C2 48°	28.935,63	1,21	3.461,56	2.564,12	1,07	32.397,19	<b>12,63</b>	1,11
	B2 int	33.047,46	1,39	3.378,64	2.502,70	1,05	36.426,10	<b>14,55</b>	1,28
	B2 int-ext	27.134,83	1,14	3.260,89	2.415,48	1,01	30.395,72	<b>12,58</b>	1,11

Table 3.1-11 – Displacements (system support/ membranes) of the study models (wind and rain actions)

			A1	B1	C1	A2 40°	B2 30°	C2 24°	B2 60°	C2 48°	B2 <sub>int</sub>	B2 <sub>int-ext</sub>		
														
displacements [m] resulted of wind action	support system	-X	(+)	0,98	0,87	0,86	0,26	0,35	0,62	0,23	0,36	0,35	0,46	
			(-)	-0,65	-0,55	-0,35	-0,40	-0,40	-0,27	-0,38	-0,26	-0,40	-0,30	
		Y	(+)	0,72	0,65	0,67	0,16	0,23	0,46	0,12	0,23	0,23	0,23	0,33
			(+)	-0,41	-0,42	-0,23	-0,36	-0,32	-0,20	-0,34	-0,20	-0,32	-0,32	-0,21
		-Y	(+)	0,72	0,84	0,82	0,15	0,29	0,56	0,16	0,34	0,29	0,29	0,40
			(-)	-0,80	-0,47	-0,40	-0,36	-0,35	-0,31	-0,36	-0,29	-0,34	-0,34	-0,24
	-Y2	(+)		0,73				0,25		0,22		0,25	0,38	
		(-)		-0,50				-0,43		-0,35		-0,43	-0,31	
	external surface	-X	(+)	1,06	1,06	1,09	0,61	0,63	0,87	0,53	0,62	0,63	0,73	
			(-)	-1,03	-0,94	-0,81	-0,88	-0,88	-0,78	-0,86	-0,76	-0,88	-0,79	
		Y	(+)	0,77	0,72	0,68	0,44	0,40	0,52	0,32	0,33	0,40	0,43	
			(+)	-0,83	-0,78	-0,69	-0,79	-0,76	-0,68	-0,75	-0,67	-0,76	-0,68	
		-Y	(+)	1,04	0,97	1,10	0,49	0,53	0,84	0,44	0,58	0,53	0,59	
			(-)	-1,12	-0,79	-0,86	-0,95	-0,73	-0,83	-0,70	-0,81	-0,73	-0,65	
	-Y2	(+)		0,99				0,57		0,47		0,57	0,70	
		(-)		-1,03				-0,99		-0,95		-0,99	-0,90	
	internal surface	-X	(+)	0,93	0,86	0,86	0,25	0,34	0,60	0,23	0,36	0,35	0,45	
			(-)	-0,65	-0,55	-0,35	-0,40	-0,40	-0,27	-0,36	-0,26	-0,40	-0,30	
		Y	(+)	0,63	0,62	0,65	0,16	0,23	0,46	0,12	0,45	0,23	0,33	
			(+)	-0,41	-0,41	-0,23	-0,33	-0,32	-0,20	-0,31	-0,19	-0,32	-0,21	
		-Y	(+)	0,71	0,79	0,82	0,14	0,29	0,55	0,15	0,34	0,29	0,40	
			(-)	-0,76	-0,47	-0,40	-0,36	-0,35	-0,31	-0,33	-0,28	-0,34	-0,24	
	-Y2	(+)		0,72				0,23		0,22		0,23	0,37	
		(-)		-0,50				-0,41		-0,35		-0,41	-0,31	
displacements [m] resulted of wind + rain	support system	-X	(+)	1,14	1,02	0,99	0,35	0,44	0,74	0,32	0,46	0,45	0,56	
			(-)	-0,55	-0,48	-0,31	-0,33	-0,33	-0,22	-0,31	-0,19	-0,33	-0,23	
		Y	(+)	0,86	0,77	0,78	0,25	0,32	0,56	0,19	0,32	0,32	0,43	
			(+)	-0,31	-0,35	-0,18	-0,28	-0,24	-0,13	-0,26	-0,12	-0,24	-0,14	
		-Y	(+)	0,85	0,97	0,95	0,24	0,39	0,68	0,24	0,43	0,39	0,51	
			(-)	-0,72	-0,42	-0,37	-0,29	-0,28	-0,26	-0,29	-0,23	-0,27	-0,18	
	-Y2	(+)		0,85				0,35		0,31		0,34	0,48	
		(-)		-0,42				-0,36		-0,28		-0,36	-0,25	
	external surface	-X	(+)	1,28	1,24	1,26	0,76	0,78	1,04	0,68	0,76	0,78	0,88	
			(-)	-0,84	-0,76	-0,65	-0,69	-0,70	-0,60	-0,68	-0,58	-0,70	-0,61	
		Y	(+)	0,96	0,89	0,90	0,58	0,53	0,73	0,45	0,51	0,53	0,56	
			(+)	-0,63	-0,60	-0,51	-0,61	-0,58	-0,49	-0,57	-0,49	-0,58	-0,50	
		-Y	(+)	1,25	1,17	1,28	0,65	0,69	1,01	0,59	0,73	0,69	0,75	
			(-)	-0,95	-0,63	-0,71	-0,76	-0,56	-0,65	-0,54	-0,64	-0,56	-0,49	
	-Y2	(+)		1,19				0,73		0,62		0,73	0,87	
		(-)		-0,86				-0,82		-0,77		-0,82	-0,72	
	internal surface	-X	(+)	1,09	1,00	1,05	0,34	0,44	0,71	0,31	0,45	0,44	0,56	
			(-)	-0,55	-0,47	-0,31	-0,32	0,33	-0,22	-0,29	-0,19	0,33	0,23	
		Y	(+)	0,77	0,74	0,76	0,25	0,32	0,56	0,19	0,31	0,32	0,42	
			(+)	-0,31	-0,34	-0,19	-0,26	-0,24	-0,13	-0,23	-0,12	-0,24	-0,14	
		-Y	(+)	0,95	0,91	0,94	0,24	0,39	0,67	0,23	0,43	0,39	0,51	
			(-)	-0,68	-0,42	-0,36	-0,29	-0,28	-0,26	-0,26	-0,21	-0,27	-0,18	
	-Y2	(+)		0,83				0,33		0,31		0,33	0,47	
		(-)		-0,42				-0,34		-0,28		-0,34	-0,24	

wind directions: -X, Y, -Y, -Y2; positive pressure (+), suction (-)

### 3.1.6.1 1<sup>st</sup> Case - Number of masts - A1, B1, C1 models

In the first case it was evaluated the influence of the number of masts which support the spatial support system (flying mast and truss ring supported by cables). Configurations were evaluated with three, four and five tall masts (Figure 3.1-6).

#### *System pre-tensioning*

According to Table 3.1-12 and Table 3.1-9 there was a progressive reduction of pre-tension magnitude applied to support system cables by increasing the number of masts, i.e., it was necessary the smallest pre-tension magnitude in the C1 model (with five tall masts).

Table 3.1-12 – Pre-tension applied to the support system cables – 1<sup>st</sup> case

load case			membrane analysis							
			wind				wind + rain			
			-X	Y	-Y	-Y2	-X	Y	-Y	-Y2
pre-tension support system cables		<b>A1</b>	19,0	19,0	19,0	—	19,0	19,0	19,0	—
		<b>B1</b>	10,0	10,0	10,0	10,0	10,0	10,0	10,0	10,0
		<b>C1</b>	2,5	2,5	2,5	—	2,5	2,5	2,5	—

#### *Mass / area of each model*

It was observed that all models have similar mass / total area, as Table 3.1-13 and Table 3.1-10. The most demanding components were masts and flying mast.

Table 3.1-13 – Ratio mass/area of models – 1<sup>st</sup> case

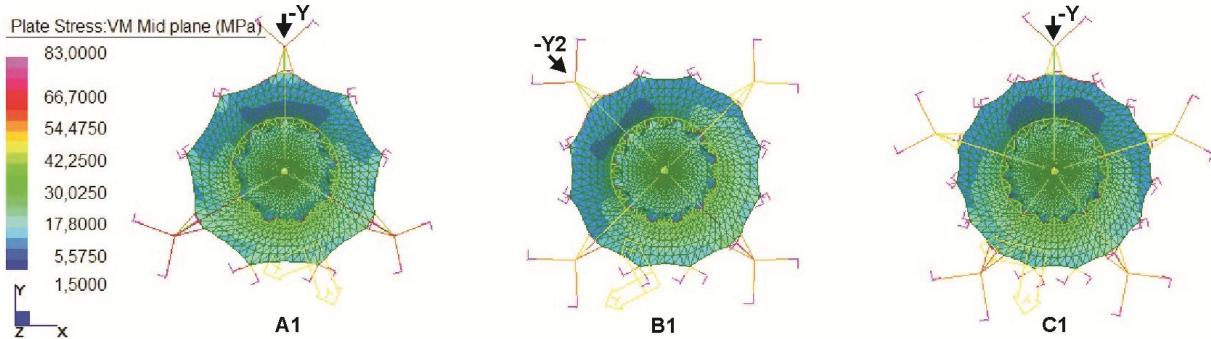
models		support system		membrane			support system + membrane		
		mass (kg)	%	mass (kg)	area (m <sup>2</sup> )	%	mass (kg)	mass/ area	
								(kg/m <sup>2</sup> )	%
	<b>A1</b>	23.850,53	1,00	3.224,79	2.388,73	1,00	27.075,32	<b>11,33</b>	1,00
	<b>B1</b>	23.729,89	0,99	3.394,94	2.514,77	1,05	27.124,83	<b>10,79</b>	0,95
	<b>C1</b>	24.398,18	1,02	3.461,56	2.564,12	1,07	27.859,74	<b>10,87</b>	0,96

#### *Stresses distribution in the external and external membrane surfaces*

It was observed that membrane surfaces (external and internal) of A1, B1, C1 models showed similar behavior, i.e., the stress concentration areas on the leeward side (derived to suction or negative pressure) and near the surfaces anchor points on windward side (resulted of positive pressure) were predominant. Increasing number of masts (support points of the membrane surface), the stress concentration areas near surface anchor points had a small reduction, and consequently a more

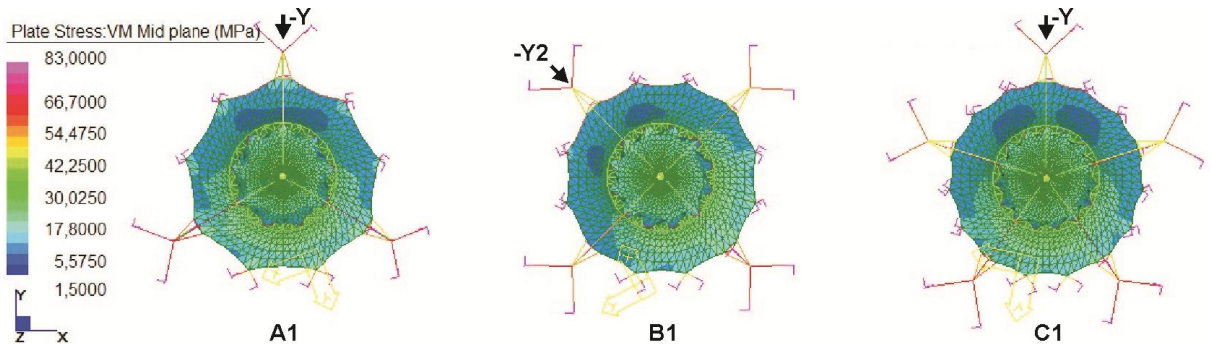
homogeneous stress distribution was observed on surfaces, according Figure 3.1-26, Figure 3.1-37.

Figure 3.1-26 – Von Mises stress – A1, B1, C1 (wind: -Y; -Y2)



With rain and wind load, the negative pressures decreased and consequently, stresses were reduced in the membrane surfaces (external and internal) and support system on the leeward side. However, stresses near the anchor points of the external surfaces increased on windward side (Figure 3.1-27, Figure 3.1-38).

Figure 3.1-27 – Von Mises stress – A1, B1, C1 (rain + wind: -Y; -Y2)

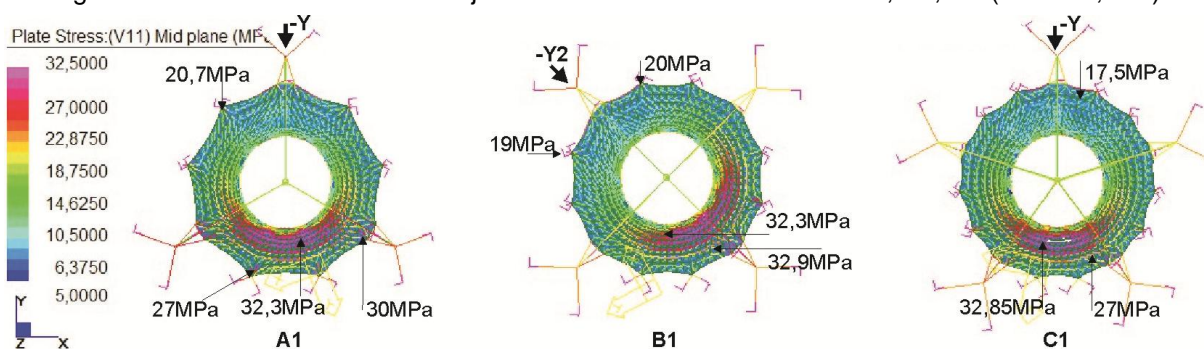


Higher stress concentration surrounding truss ring (areas with large displacements caused by wind suction) and near surface anchor points (masts) on the leeward and windward sides were observed on the external membrane surface (with smooth curvature) of these models (Figure 3.1-28, Figure 3.1-39).

On the external membrane surface, the trajectories of maximum stress occur in the circumferential direction (Figure 3.1-28, Figure 3.1-39). Consequently, the most requested direction of the material is the weft, considering radial cutting patterns.

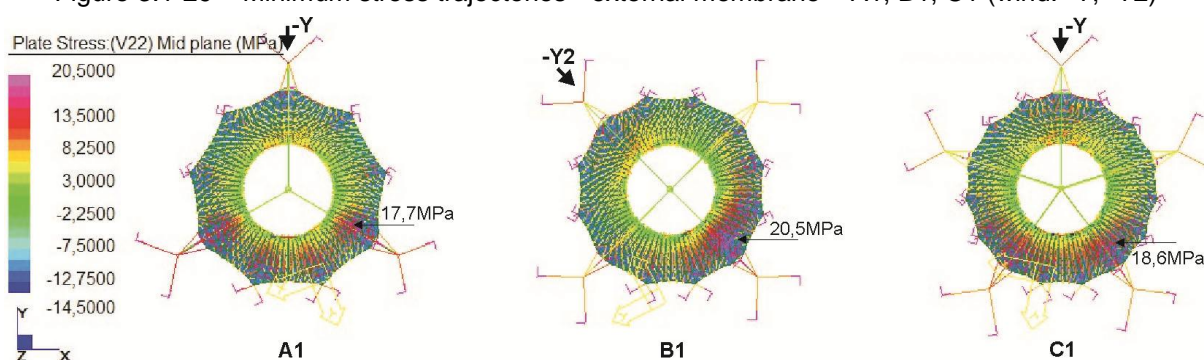
Despite the greater number of anchor points, the stress magnitude in the vicinity of the truss ring (-Y wind direction) became greater in the external membrane surface of C1 model on the leeward side (Figure 3.1-28).

Figure 3.1-28 – Maximum stress trajectories - external membrane – A1, B1, C1 (wind: -Y; -Y2)



Compression or ponding areas were not verified at the base of the external membrane surfaces of these models, according to trajectories of minimum stress (radial direction), as shown in Figure 3.1-29, Figure 3.1-40. However, the existence of small compression areas (wrinkles) was observed at the top of these surfaces (surface anchor points at truss ring), as shown in Figure 3.1-33a.

Figure 3.1-29 – Minimum stress trajectories - external membrane – A1, B1, C1 (wind: -Y; -Y2)



On internal membrane surface of these models, the highest concentration of stress was only observed at the top of the surface, surrounding the ring, mainly on windward side (Figure 3.1-30, Figure 3.1-41). Around this area predominates more homogeneous stress field with lower magnitude; areas of higher stress occurs near surface anchorage points at truss ring on the windward side due to wind positive pressure.

On internal membrane surface, the maximum stress trajectories occur in the surface radial direction (Figure 3.1-30, Figure 3.1-41). So, the most requested direction of the material is the warp, considering radial cutting patterns. On top of the surface the stress exceeds the material allowable stress and signals some procedures: removal of this area and or use of double layer of material (Figure 3.1-31, Figure 3.1-42).

Figure 3.1-30 – Maximum stress trajectories - internal membrane – A1, B1, C1 (wind: -Y; -Y2)

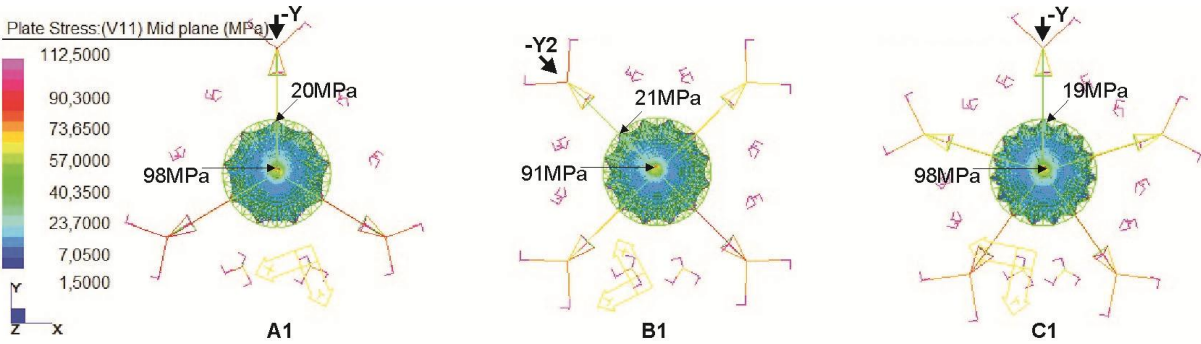
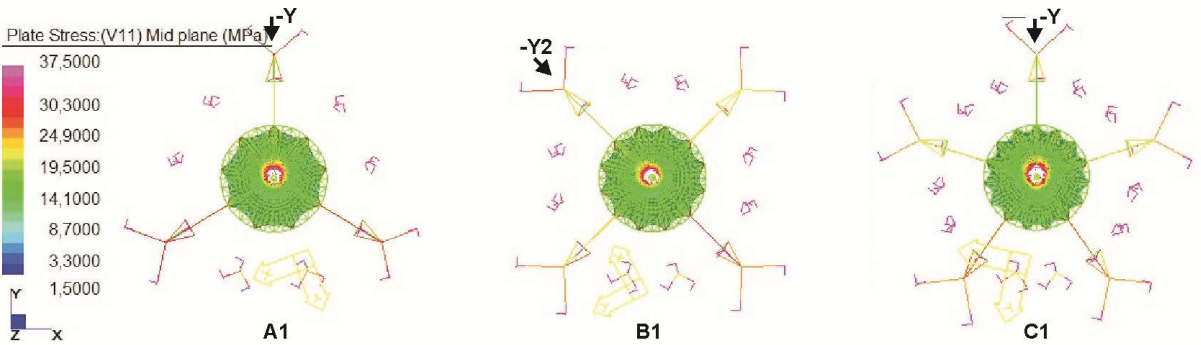


Figure 3.1-31 – Maximum stress trajectories - int. membrane – A1, B1, C1 (material allowable stress)



(removal of stress areas greater than material allowable stress - wind: -Y; -Y2)

It was not verified compression or ponding areas in the base of the internal membrane surfaces of these models, according to trajectories of minimum stress (circumferential direction) as shown in Figure 3.1-32 and Figure 3.1-43. Small compression areas (wrinkles) were observed at the top of surface, according to Figure 3.1-33b.

Figure 3.1-32 – Minimum stress trajectories - internal membrane – A1, B1, C1 (wind: -Y; -Y2)

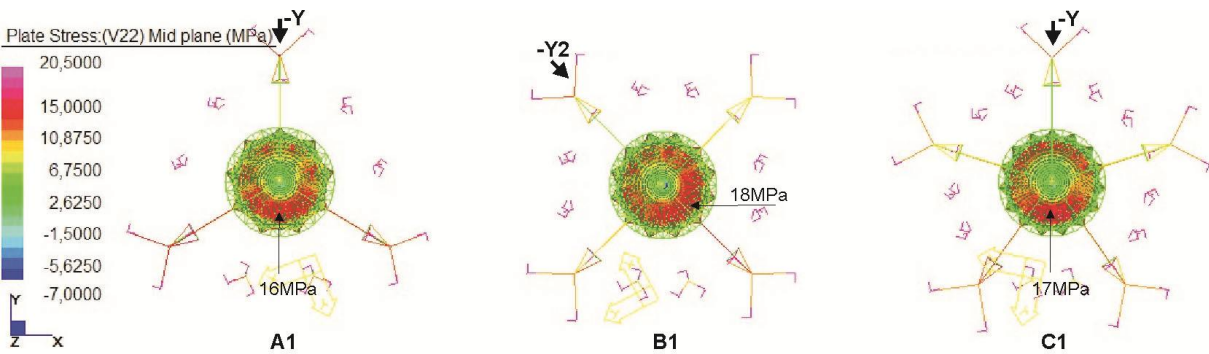
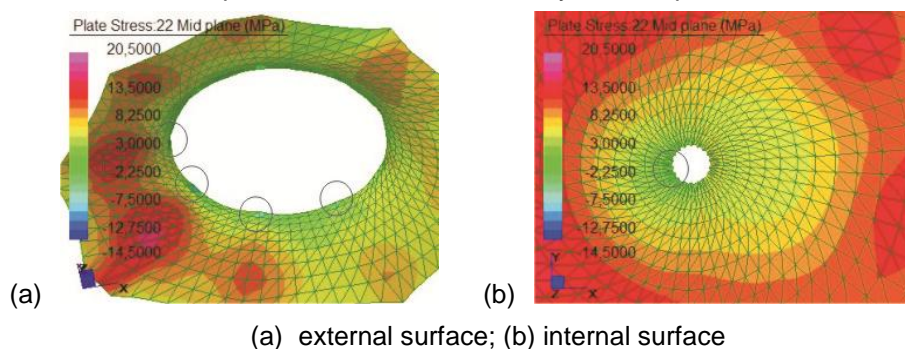


Figure 3.1-33 – Small compression areas observed only at the top of the surface – A1, B1, C1

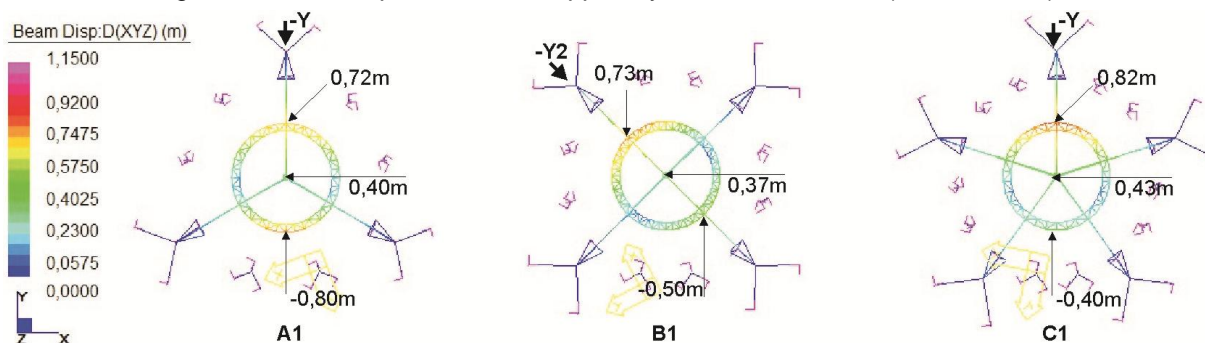


### Support system displacements

Large displacements on the support system were observed in these models, mainly of truss ring and flying mast. Pressure displacements of truss ring and flying mast were predominant on the windward side, in all directions. However, the A1 model in -Y direction had also large displacements of truss ring and flying mast on the leeward side (suction), according Figure 3.1-34, Figure 3.1-44 and Table 3.1-11.

Increasing number of tall masts, the reduction in the magnitude of support system displacements on the leeward side (suction) was verified; the maximum reduction was observed in C1 model (15% to 30%). However, with lower pre-tension of support system cables, a small increase in the support system displacements on the windward side (overpressure) was observed in C1 model in -Y direction, compared to A1 and B1 models.

Figure 3.1-34 – Displacements - support system – A1, B1, C1 (wind: -Y; -Y2)

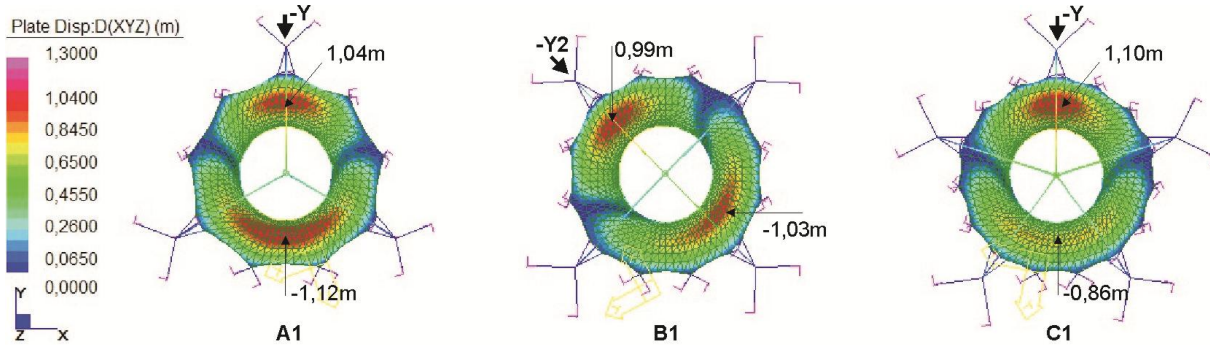


With the rain and wind loads, an increase (approx. 20%) in the support system displacements on the windward side (pressure) and a reduction (approx. 15%) in their displacements on the leeward side (suction) were observed, in all directions. This behavior was also verified on the external and internal surfaces (Table 3.1-11).

*Displacements of external membrane surface*

Large displacements of external membrane surface were observed on the windward (overpressure) and leeward sides (suction). Increasing the number of masts, a reduction in the magnitude of surface displacements on the leeward side was observed, and the maximum reduction (10%) was observed in C1 model (Figure 3.1-35, Figure 3.1-45, Table 3.1-11)

Figure 3.1-35 – Displacements – external membrane – A1, B1, C1 (wind: -Y; -Y2)

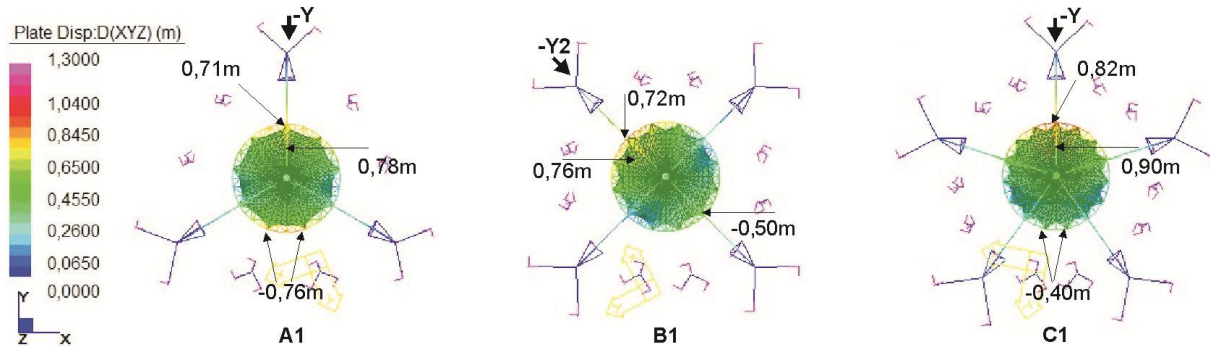


*Displacements of internal membrane surface*

The internal membrane surface of these models showed similar behavior to the support system. Large displacements on the windward side (overpressure) in all directions were predominant in the internal membrane surfaces, except to A1 model, in -Y direction, whose internal membrane had also large displacements in leeward side, (Figure 3.1-36, Figure 3.1-46, Table 3.1-11).

Increasing the number of masts, a reduction in the displacement magnitude on the leeward side (suction) was verified in internal membrane surface; the maximum reduction was observed in C1 model. However, with lower pre-tension applied in the support system cables, the increase in the internal membrane displacements on the windward side was observed in C1 model, compared to A1 and B1 models.

Figure 3.1-36 – Displacements - internal membrane – A1, B1, C1 (wind: -Y; -Y2)



### *Comparison of A1, B1, C1 models*

The first case configurations (A1, B1 and C1 models) are characterized by great flexibility, since these systems do not offer significant restraint to displacements of truss ring, flying mast (spatial support system) and membrane surfaces. In this case, masts were the most requested components.

However, increasing the number of masts (variable investigated in the first case) there was a reduction in the suction displacements of support system and surface on the leeward side. The reduction in the areas of stress concentration near surface anchor points (masts) was also verified and, thus surface ability to withstand loads increased.

By decreasing the pre-stress applied to support system cables, membrane stress magnitude increased, and, therefore greater movements were observed for membrane achieves equilibrium. There was also a small increase of membrane and support system displacements on windward side in C1 model.

Thus, increasing the number of masts helped reducing system flexibility and enabled more evenly stress distribution on membrane surfaces. Consequently, C1 model had better perform. This model also had the lowest pre-tensioning applied to support system cables and the same mass/area (system support and membrane) than other models.

Figure 3.1-37 – Von Mises stress – A1, B1, C1 (wind directions: -X, Y, -Y, -Y2)

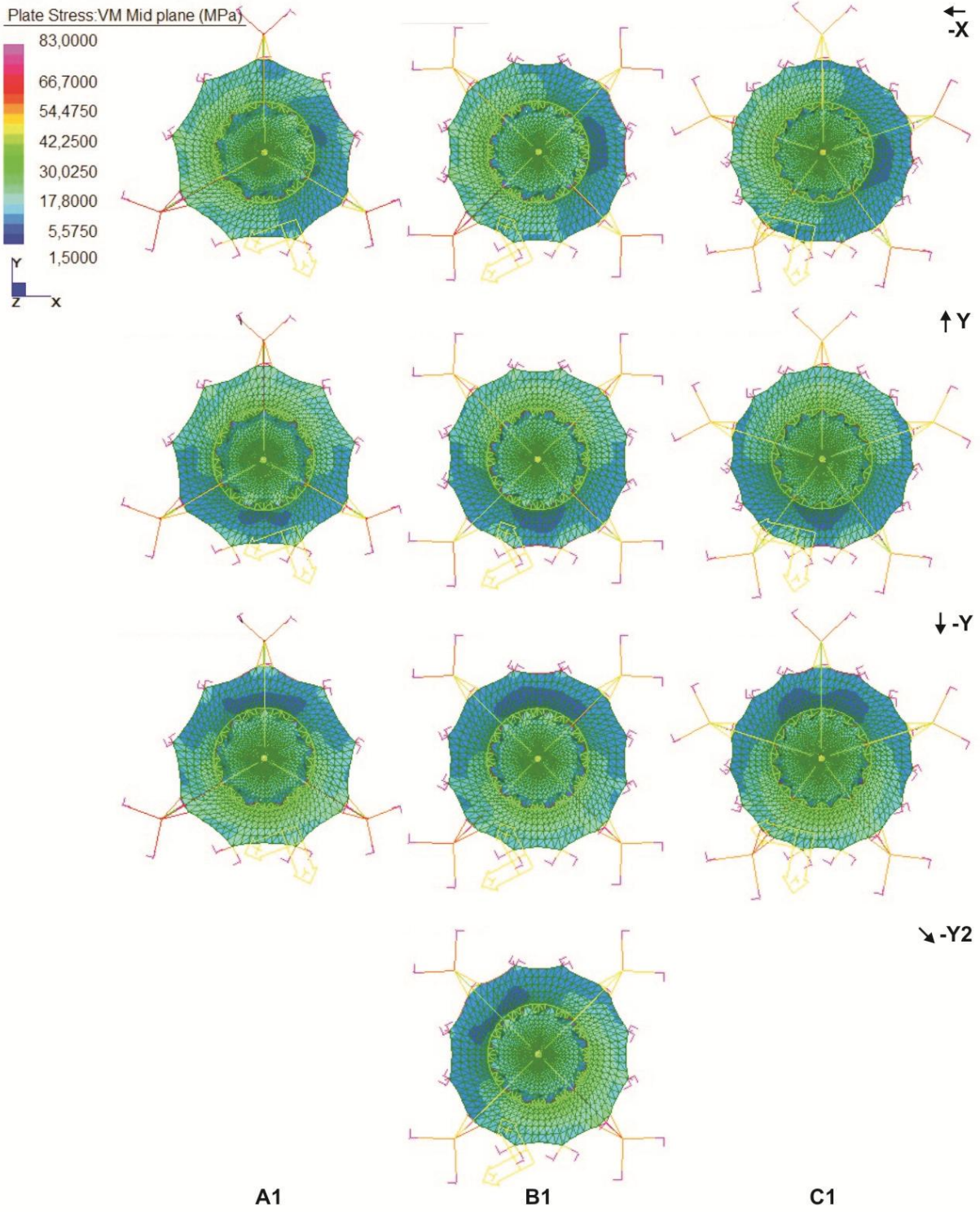


Figure 3.1-38 – Von Mises stress – A1, B1, C1 (rain + wind directions: -X, Y, -Y, -Y2)

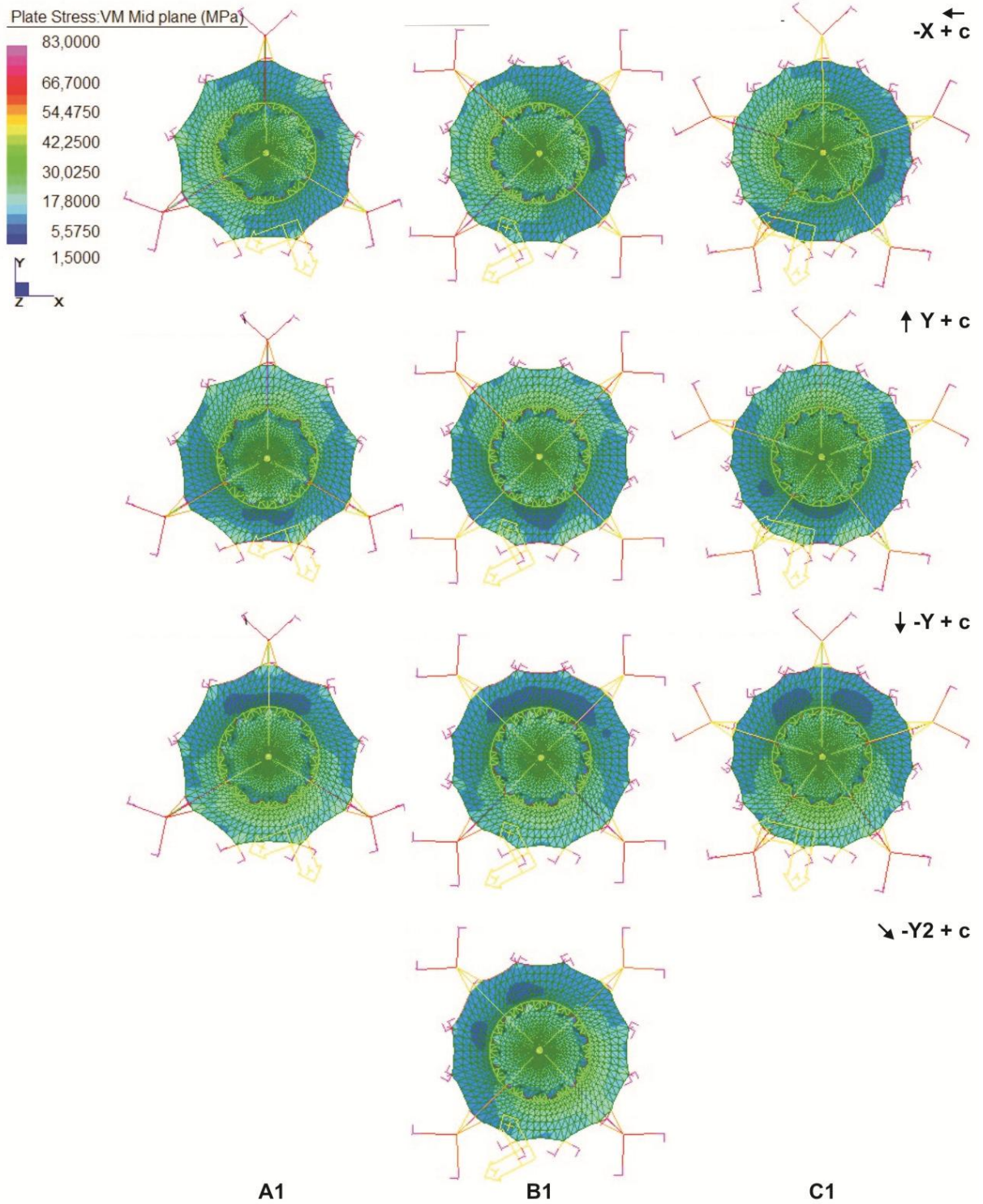


Figure 3.1-39 – Maximum stress trajectories - external membrane – A1, B1, C1 (wind: -X, Y, -Y, -Y2)

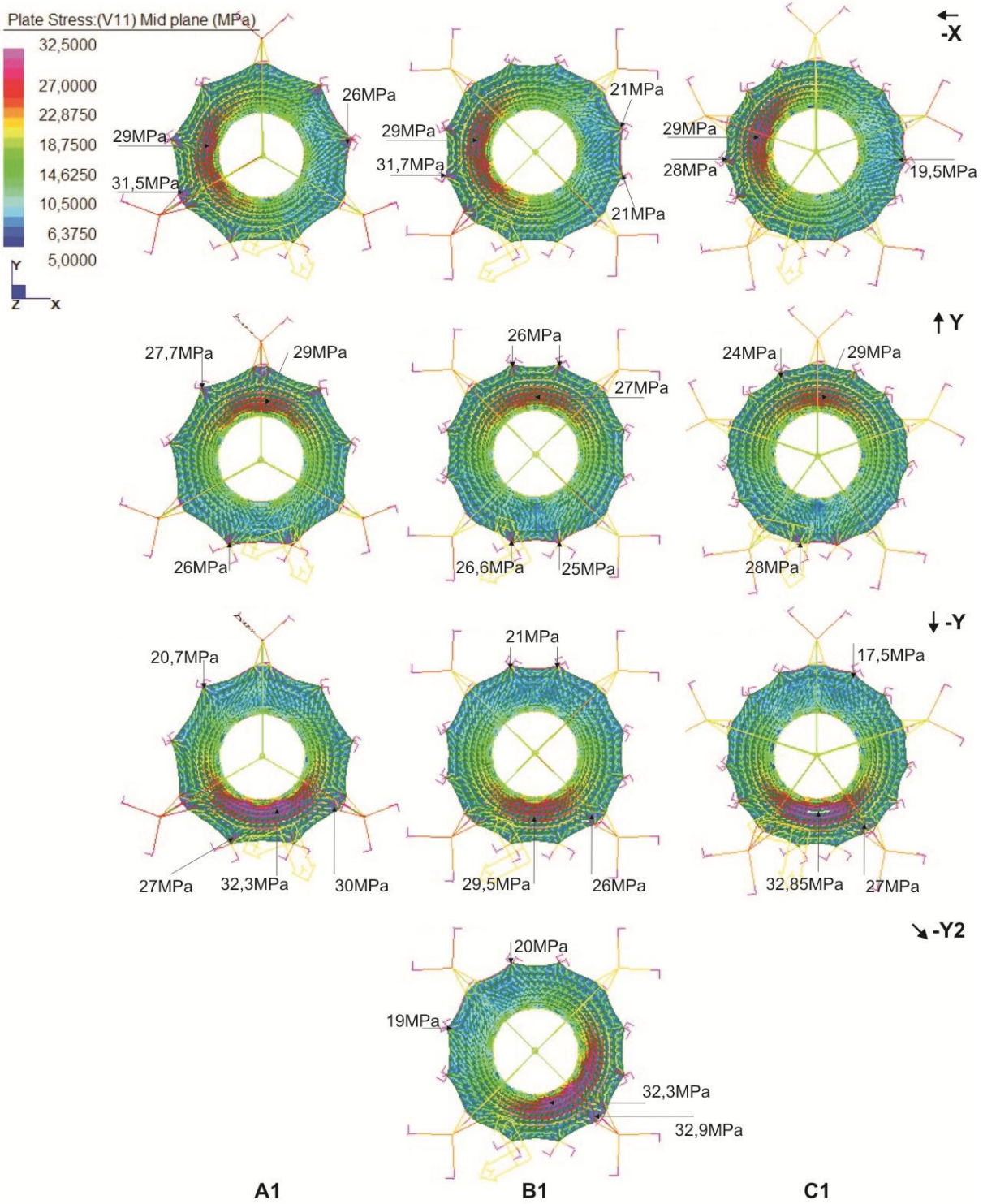


Figure 3.1-40 – Minimum stress trajectories - ext. membrane – A1, B1, C1 (wind: -X, Y, -Y, -Y2)

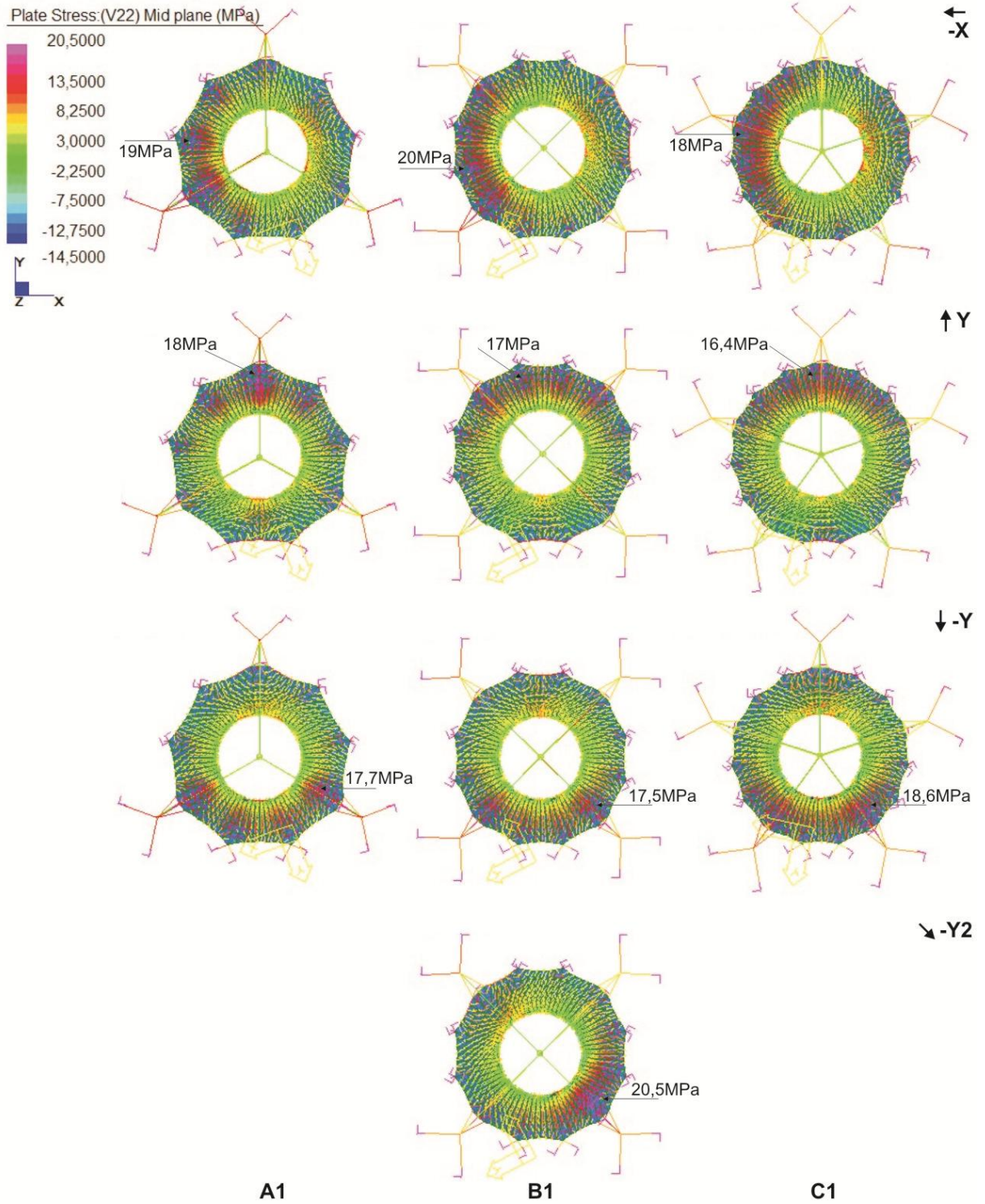


Figure 3.1-41 – Maximum stress trajectories - internal membrane – A1, B1, C1 (wind: -X, Y, -Y, -Y2)

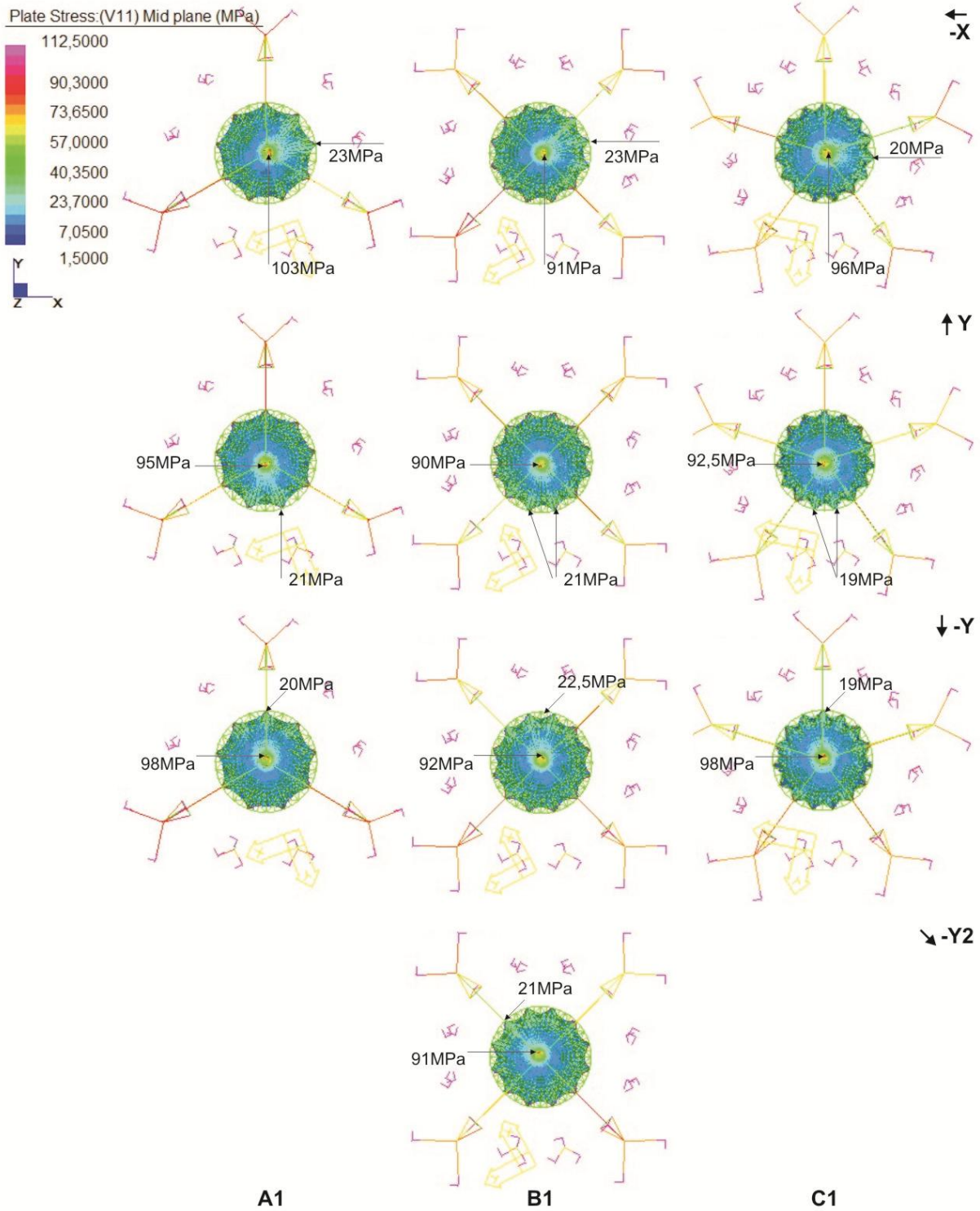
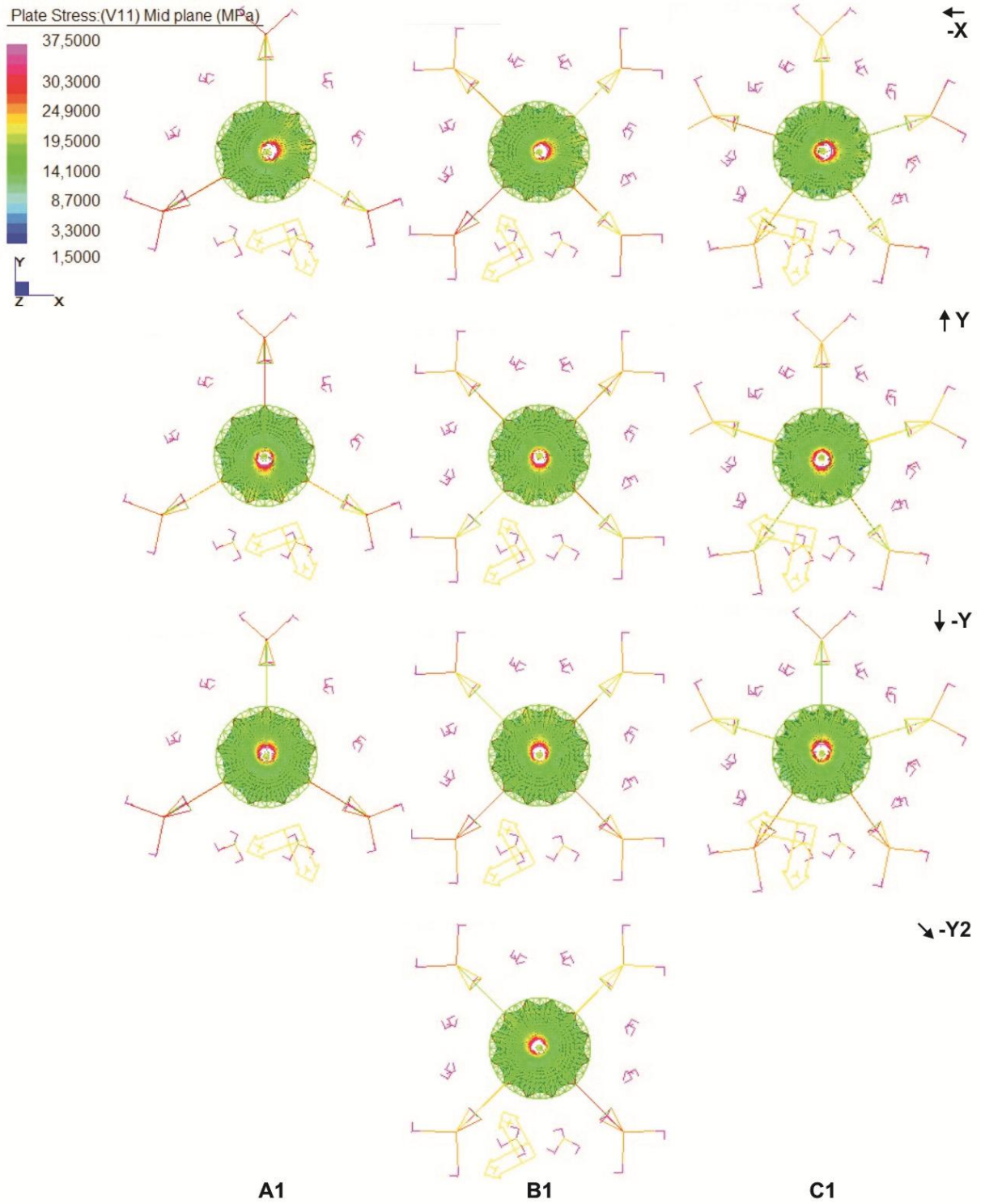


Figure 3.1-42– Maximum stress trajectories - A1, B1, C1 (material allowable stress)



considering maximum stress trajectories within material allowable stress (wind: -X, Y, -Y, -Y2)

Figure 3.1-43 – Minimum stress trajectories - int. membrane –A1, B1, C1 (wind: -X, Y, -Y, -Y2)

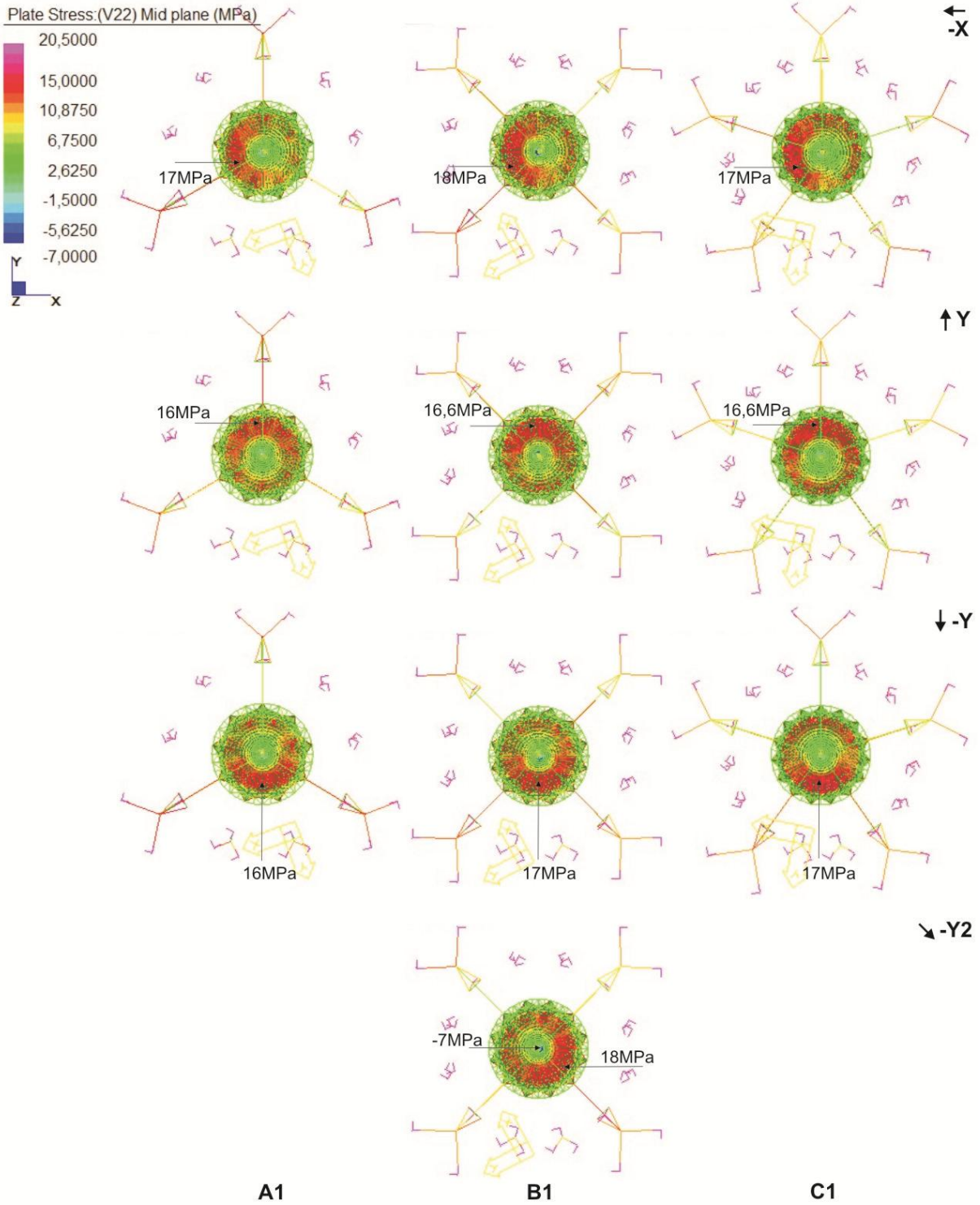


Figure 3.1-44 – Support system displacements – A1, B1, C1 (wind: -X, Y, -Y, -Y2)

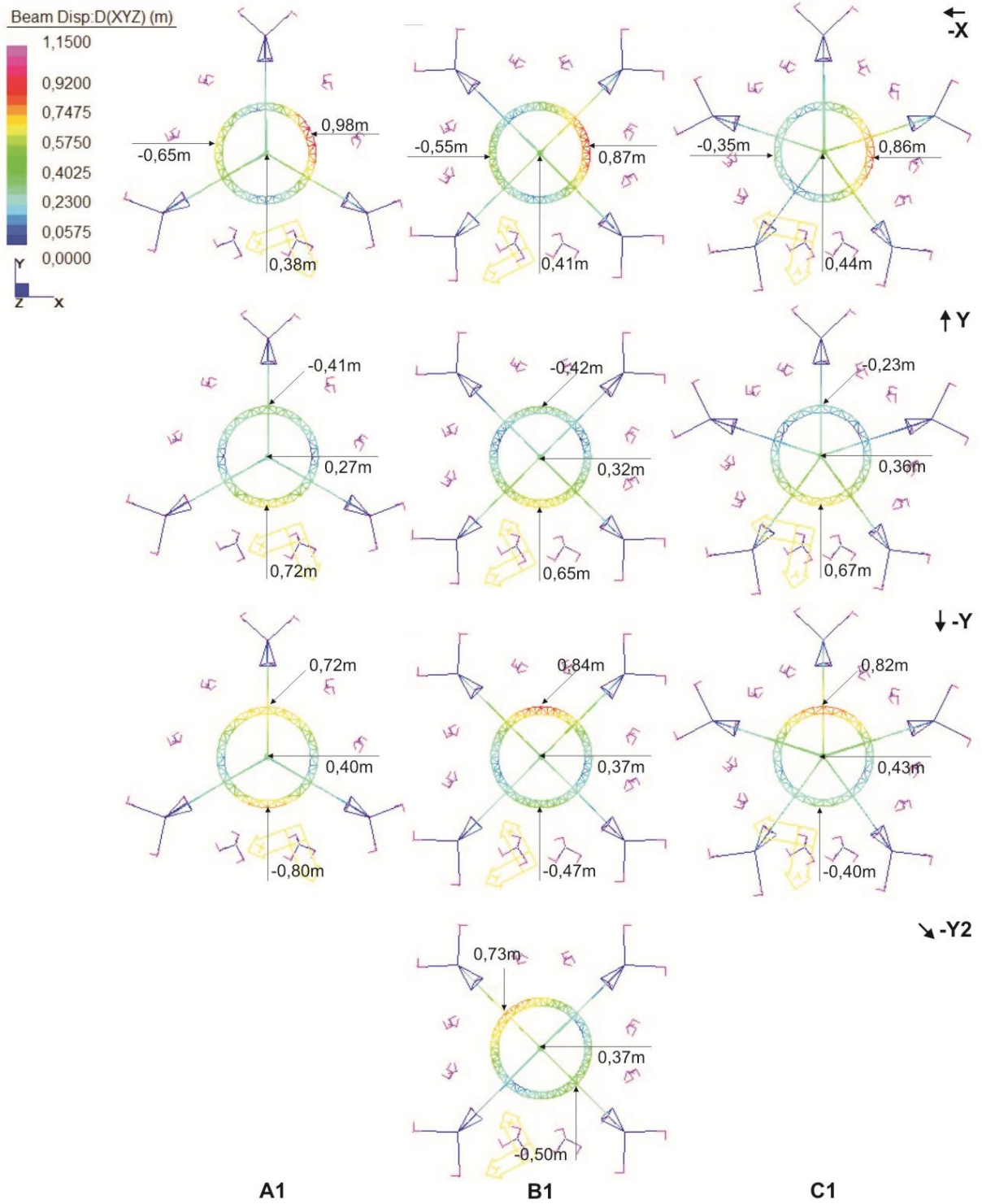


Figure 3.1-45 – External surface displacements – A1, B1, C1 (wind: -X, Y, -Y, -Y2)

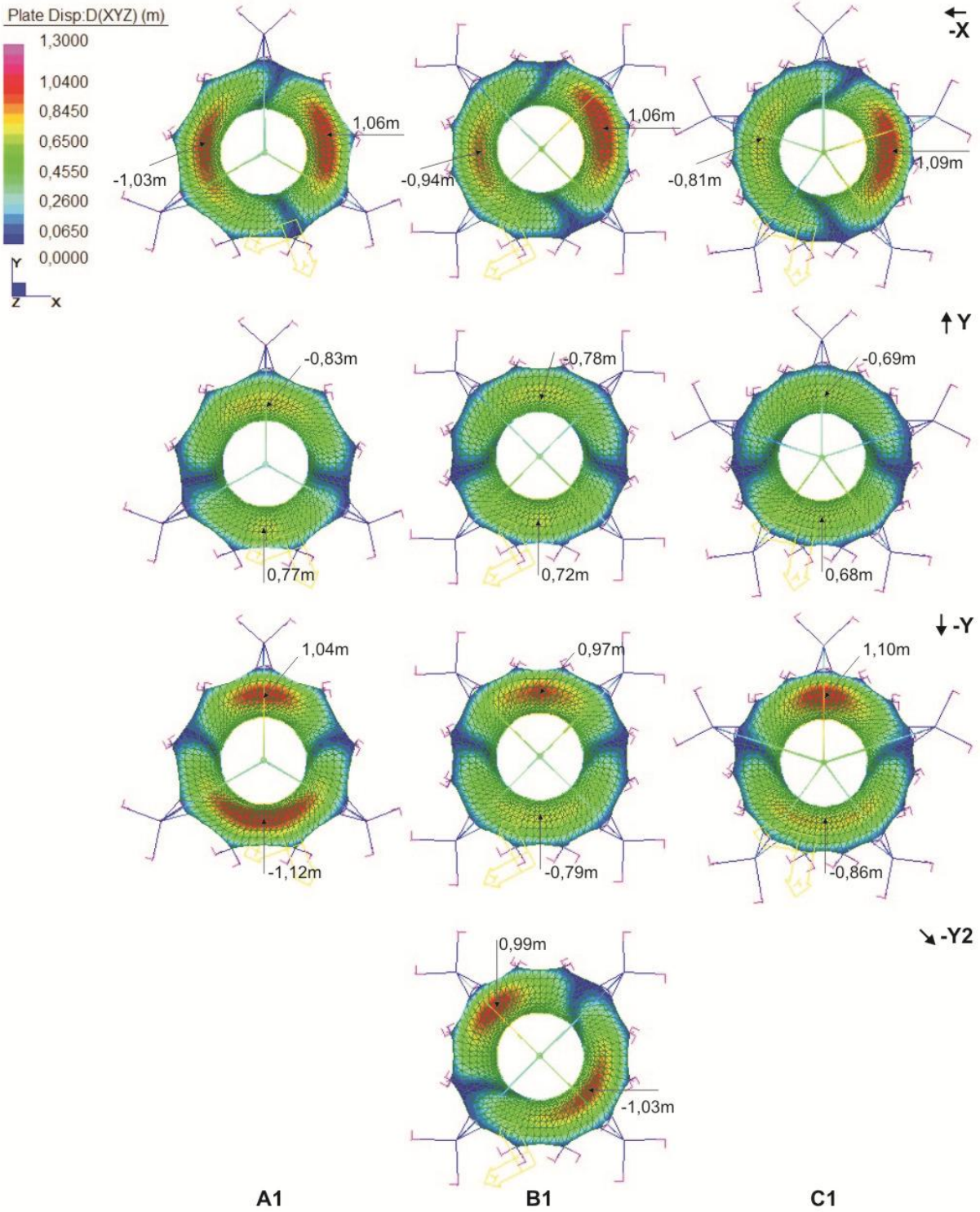
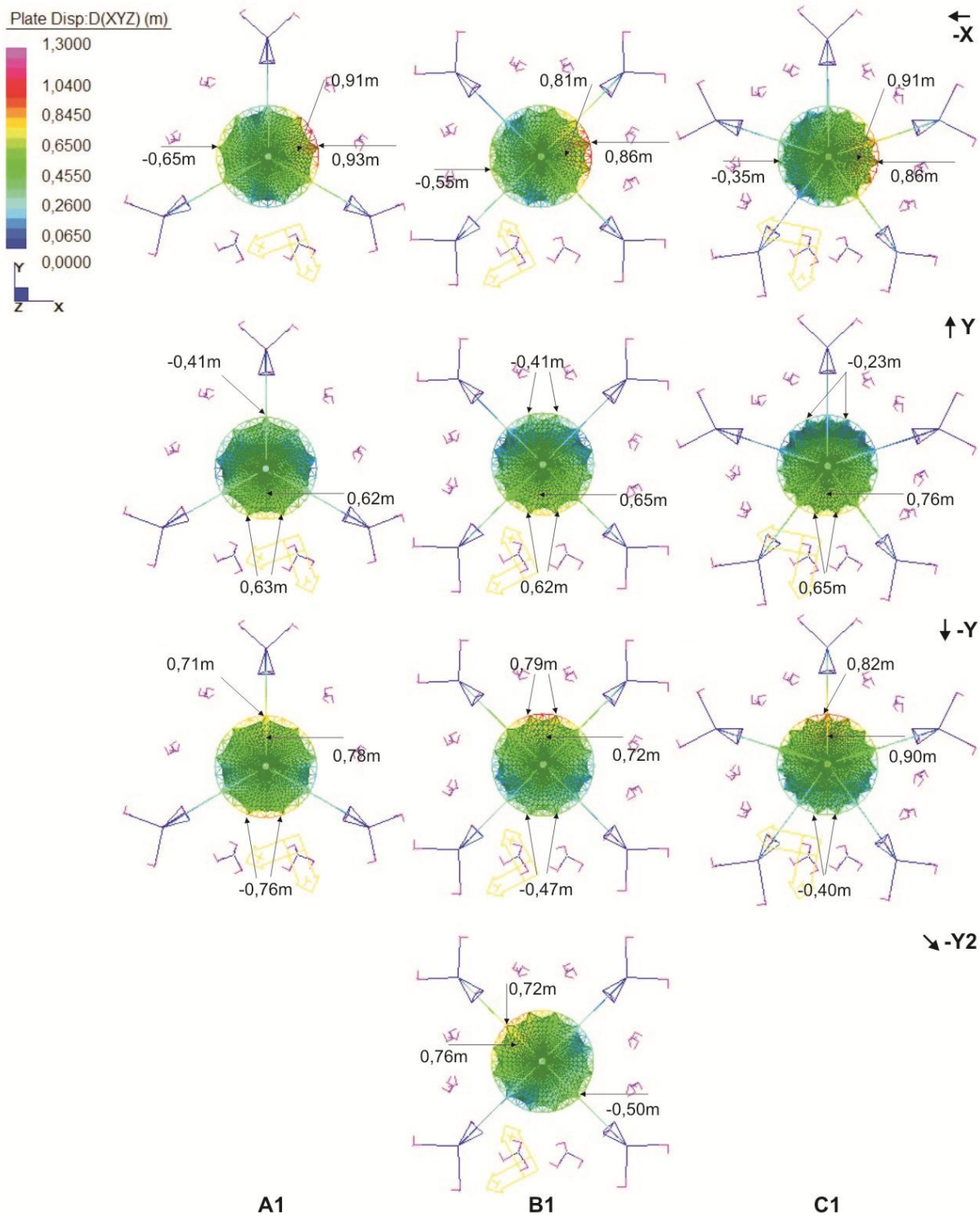


Figure 3.1-46 – Internal surface displacements – A1, B1, C1 (wind: -X, Y, -Y, -Y2)



### 3.1.6.2 2<sup>nd</sup> Case - Number of masts + cable configuration: A2-40°, B2-30°, C2-24°, B2-60°, C2-48° models

In the second case, it was evaluated the influence of the cable configuration of the spatial support system. In this case, two pairs of cables anchored in three, four and five tall masts. Models whose angle between pair of cables is defined by one module (A2-40°, B2-30°, C2-24°) and two modules (B2-60° C2-48°) of the internal surface, were verified, (Figure 3.1-8, Figure 3.1-9).

#### *System pre-tensioning*

The models A2-40°, B2-30°, C2-24° of the second case reveal the same behavior observed of first case models, i.e., a reduction of pre-tension applied to the support system cables, increasing number of masts (variable investigate in the first case). Furthermore, the pre-tension applied to support system cables of the models of the first case (A1, B1, C1) and second case (A2-40°, B2-30°, C2-24°) exhibited the same relationship, as shown in Table 3.1-9. However, pre-tension magnitude in second case increased 100%, with the new geometry of the cables (Table 3.1-14, Table 3.1-9).

Models with larger angle between cables (B2-60° and C2-48°) showed significant increase of pre-tension level applied to the support system cables when comparing them to B2-30° and C2-24° models (Table 3.1-14, Table 3.1-9).

Table 3.1-14 – Pre-tension applied to the support system cables – models of the 1<sup>st</sup> and 2<sup>nd</sup> cases

load case			membrane analysis							
			wind				wind + rain			
			-X	Y	-Y	-Y2	-X	Y	-Y	-Y2
pre-tension support system cables	 <b>A1</b>	19,0	19,0	19,0	—	19,0	19,0	19,0	—	
	 <b>B1</b>	10,0	10,0	10,0	10,0	10,0	10,0	10,0	10,0	
	 <b>C1</b>	2,5	2,5	2,5	—	2,5	2,5	2,5	—	
	 <b>A2.40°</b>	38,0	38,0	38,0	—	38,0	38,0	38,0	—	
	 <b>B2.30°</b>	22,0	22,0	22,0	22,0	22,0	22,0	22,0	22,0	
	 <b>C2.24°</b>	4,5	4,5	4,5	—	4,5	4,5	4,5	—	
	 <b>B2.60°</b>	28,5	28,5	28,5	28,5	28,5	28,5	28,5	28,5	
	 <b>C2.48°</b>	13,5	13,5	13,5	—	13,5	13,5	13,5	—	

### *Mass/ area of each model*

A significant increase of the ratio mass/ area of the system was observed in models A2-40°, B2-30°, B2-60°, C2-48°, compared to models A1, B1, C1 (first case), as a result of high stress in truss ring and tall masts (Table 3.1-15, Table 3.1-10).

Increasing the angle between cables that support the spatial support system, there was an increase in the mass/total area of models. This was evident when comparing B2-30° and B2-60°, C2-24° and C2-48° models.

However, increasing the number of masts and reducing the angle between cables that support the truss ring / flying mast, there was a significant decrease in mass/total area, according observed in C2-24° model (which have approximate mass/area to C1 model).

Table 3.1-15 – Ratio mass/area total – models of the 1<sup>st</sup> and 2<sup>nd</sup> cases

models		support system		membrane			support system + membrane		
		mass (kg)	%	mass (kg)	area (m <sup>2</sup> )	%	mass (kg)	mass/ area	
								(kg/m <sup>2</sup> )	%
	<b>A1</b>	23.850,53	1,00	3.224,79	2.388,73	1,00	27.075,32	<b>11,33</b>	1,00
	<b>B1</b>	23.729,89	0,99	3.394,94	2.514,77	1,05	27.124,83	<b>10,79</b>	0,95
	<b>C1</b>	24.398,18	1,02	3.461,56	2.564,12	1,07	27.859,74	<b>10,87</b>	0,96
	<b>A2 40°</b>	49.089,02	2,06	3.224,79	2.388,73	1,00	52.313,81	<b>21,90</b>	1,93
	<b>B2 30°</b>	33.111,38	1,39	3.394,94	2.514,77	1,05	36.506,32	<b>14,52</b>	1,28
	<b>C2 24°</b>	21.672,05	0,91	3.461,56	2.564,12	1,07	25.133,61	<b>9,80</b>	0,86
	<b>B2 60°</b>	43.628,78	0,89	3.394,94	2.514,77	1,05	47.023,72	<b>18,70</b>	1,65
	<b>C2 48°</b>	28.935,63	1,21	3.461,56	2.564,12	1,07	32.397,19	<b>12,63</b>	1,11

### *Stress distribution in the external and internal membrane surfaces*

The membrane surfaces of A2-40°, B2-30°, C2-24° models (Figure 3.1-48, Figure 3.1-64) showed similar behavior to the surfaces of A1, B1, C1 models (Figure 3.1-47, Figure 3.1-37), but with a small increase in the stress concentration areas on the windward side. On internal membranes, an increase in the stress concentration areas on the leeward side was also observed. However, increasing the number of masts, a reduction of these areas was verified, and thus, a more homogeneous stress distribution over the surface.

In C2-48° model and principally in B2-60° model (Figure 3.1-48, Figure 3.1-65) it an increase in areas of the stress concentration nearly anchor points of external and internal surfaces on the windward side was observed, compared to B2-30° and C2-24° models, respectively (Figure 3.1-48, Figure 3.1-64).

Figure 3.1-47 – Von Mises stress – A1, B1, C1 (wind: -Y; -Y2)

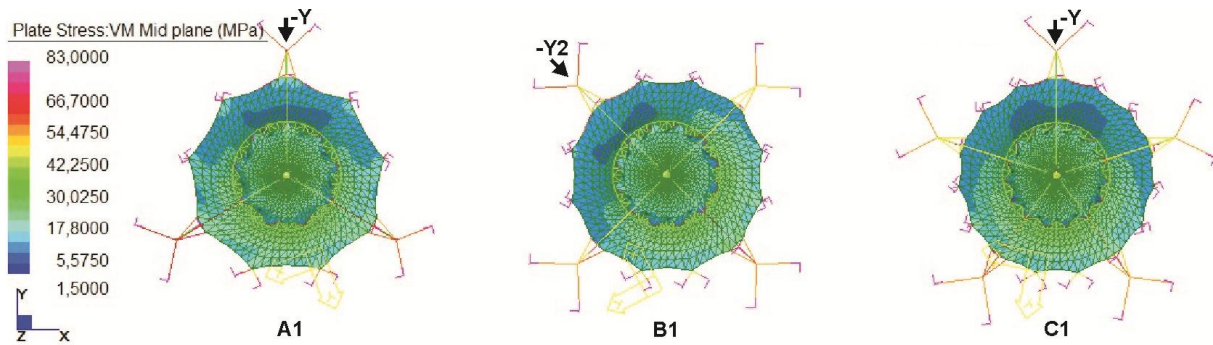
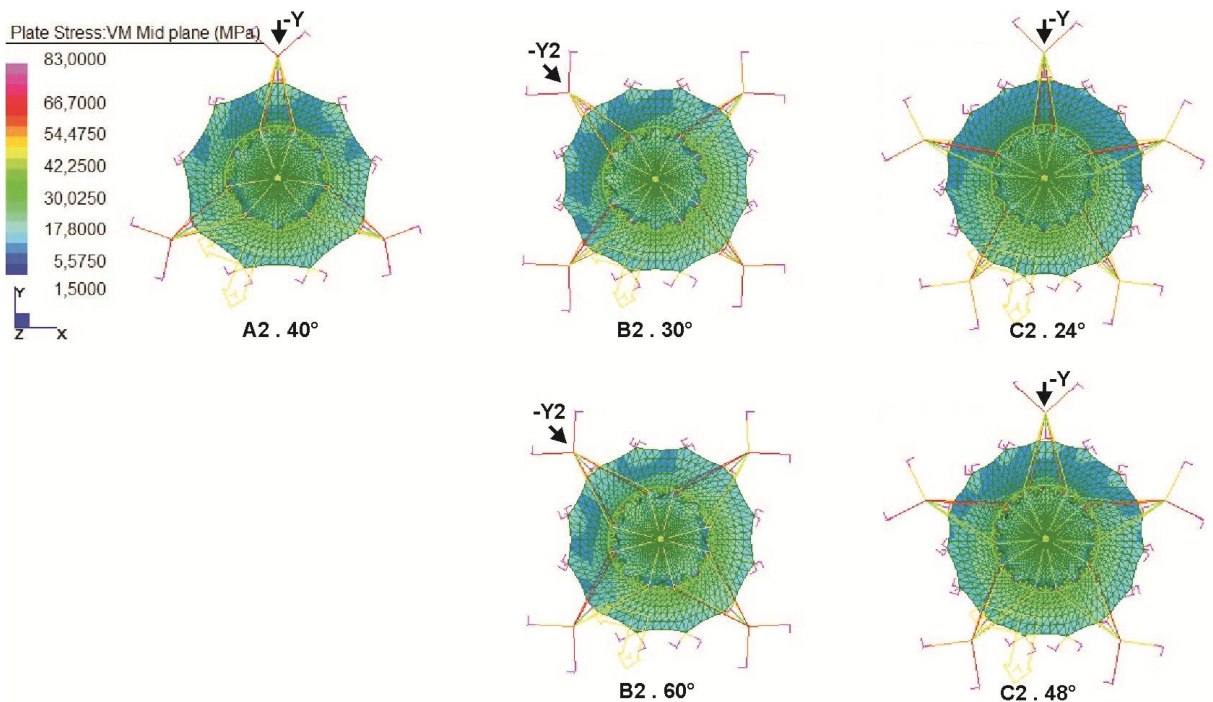


Figure 3.1-48 – Von Mises stress – A2-40°, B2-30°, C2-24°; B2-60°, C2-48° (wind -Y; -Y2)



On external membrane surfaces of A2-40°, B2-30°, C2-24° models (Figure 3.1-50, Figure 3.1-66), the highest stress concentration areas was observed in the vicinity of truss ring on leeward side (resulted of suction), and nearby surface anchor points (masts) on the leeward and windward sides, according maximum stress trajectories (circumferential direction). An increase of the stress magnitude nearby surface anchor points (masts) on the windward side was also observed, compared to A1, B1, C1 models (Figure 3.1-49, Figure 3.1-39). Increasing the number of masts a reduction of these stress concentration areas was verified.

On external membrane surfaces of B2-60° and C2-48° models (Figure 3.1-50, Figure 3.1-67), there was also an increase of stress magnitude nearby surface

anchor points (masts) on the windward side, when compared to B2-30° and C2-24° models, according maximum stress trajectories. Moreover, the stress magnitude near truss ring increased in C2-48° model on leeward side in Y direction.

Figure 3.1-49 – Maximum stress trajectories - external membrane – A1, B1, C1 (wind -Y; -Y2)

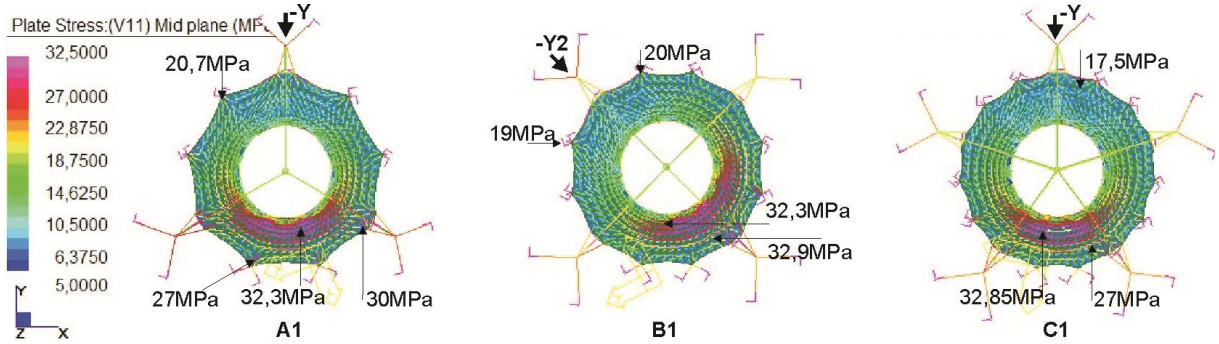
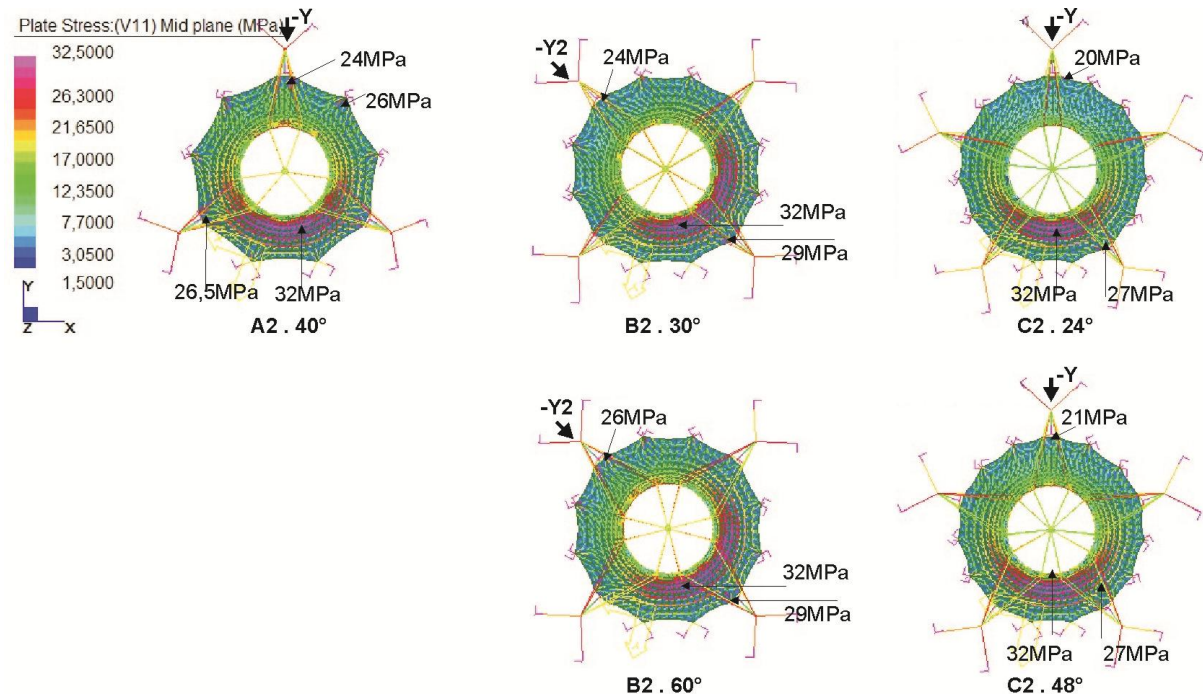


Figure 3.1-50 – Max. stress - ext. membrane – A2-40°, B2-30°, C2-24°; B2-60°, C2-48° (wind -Y; -Y2)



Compression or ponding areas were not verified at the base of the external membrane surfaces on the second case models (A2-40°, B2-30°, C2-24°; B2-60°, C2-48°), according to minimum stress trajectories (radial direction), as shown in Figure 3.1-52, Figure 3.1-68, Figure 3.1-69. On A1, B1, C1 models it predominates minimum stress areas and large displacements on windward side (Figure 3.1-51, Figure 3.1-40). However, on the second case models, the surfaces exhibited more stability on that side.

Figure 3.1-51– Minimum stress trajectories - external membrane – A1, B1, C1 (wind -Y; -Y2)

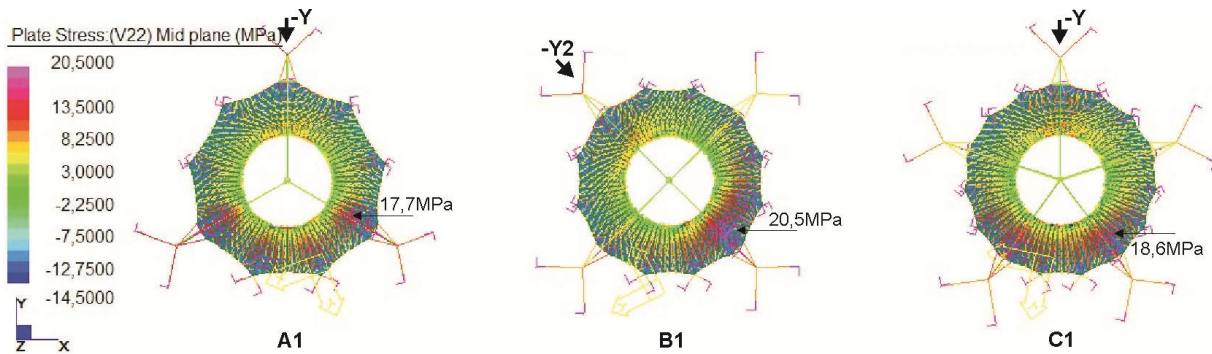
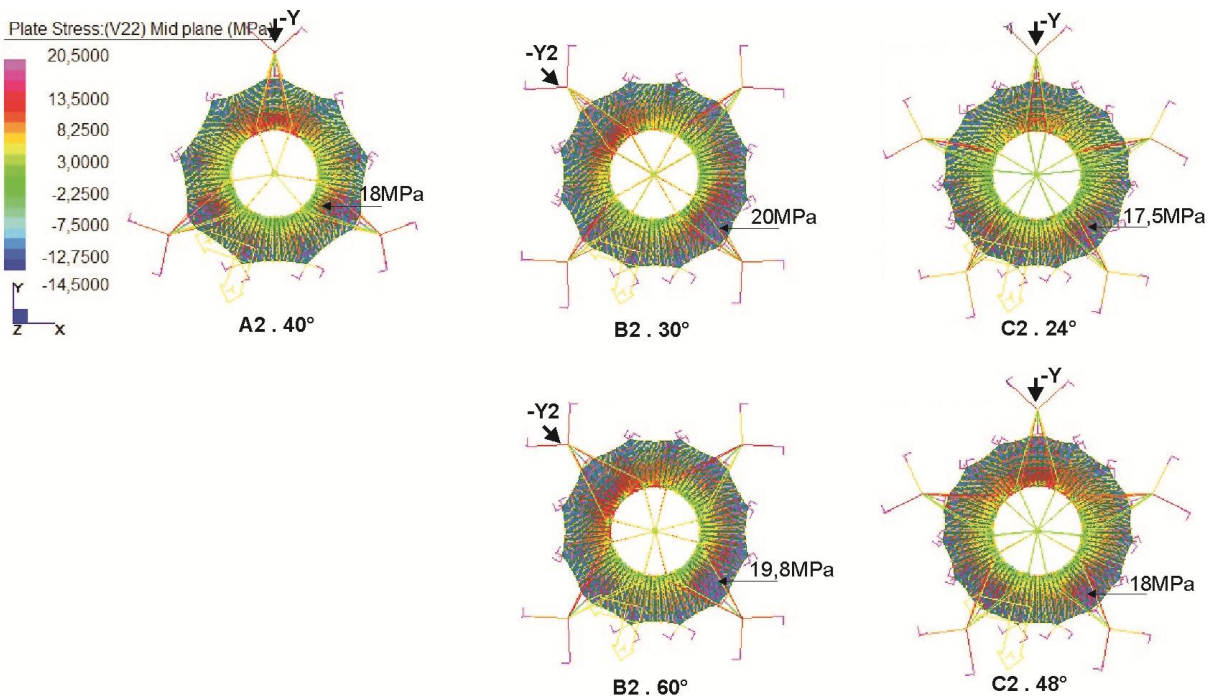


Figure 3.1-52 – Min. stress - ext. membrane – A2-40°, B2-30°, C2-24°; B2-60°, C2-48° (wind -Y; -Y2)



The internal membrane surfaces on A2-40°, B2-30°, C2-24° models (Figure 3.1-54, Figure 3.1-70) also exhibited the highest stress areas at the top of the surface on the windward side. Around this region it predominates a stress field of lower magnitude, but that showed a small increase of stress magnitude on windward and leeward sides, compared to A1, B1, C1 models (Figure 3.1-53, Figure 3.1-41). Areas of stress concentration were also verified near the anchorage points at truss ring, on the windward side. Lower stress is predominant at the base of the internal surfaces of C2-24° model on the windward side.

In the internal membrane surfaces of B2-C2-30° and C2-24° models (Figure 3.1-54, Figure 3.1-71) an increase of stress magnitude was observed nearly the surface anchor points at truss ring on the windward (mainly) and on leeward sides,

compared to B2-30° and C2-24° models, according to maximum stress trajectories (surface radial direction).

Figure 3.1-53 – Maximum stress trajectories - internal membrane – A1, B1, C1 (wind -Y; -Y2)

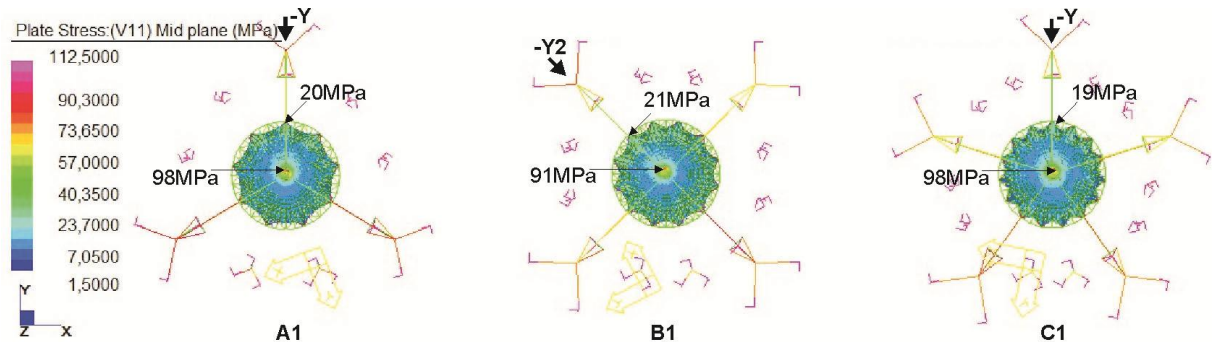
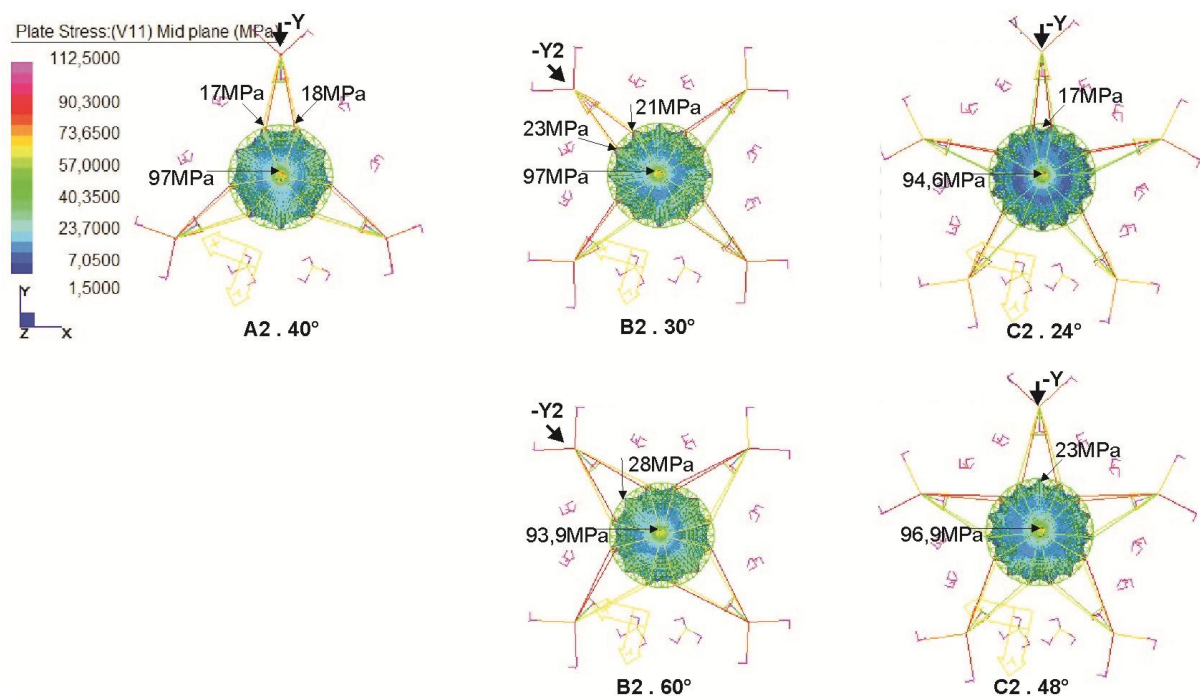


Figure 3.1-54 – Max. stress - int. membrane – A2-40°, B2-30°, C2-24°; B2-60°, C2-48° (wind -Y; -Y2)



Compression or ponding areas were not verified in the internal membrane surfaces of A2-40°, B2-30°, C2-24°; B2-60°, C2-48° models, according to minimum stress trajectories (circumferential direction), (Figure 3.1-56, Figure 3.1-72, Figure 3.1-73). The models' internal surfaces on the first (Figure 3.1-55, Figure 3.1-43) and second cases also exhibited similar stress distribution.

Figure 3.1-55 – Minimum stress trajectories - internal membrane – A1, B1, C1 (wind -Y; -Y2)

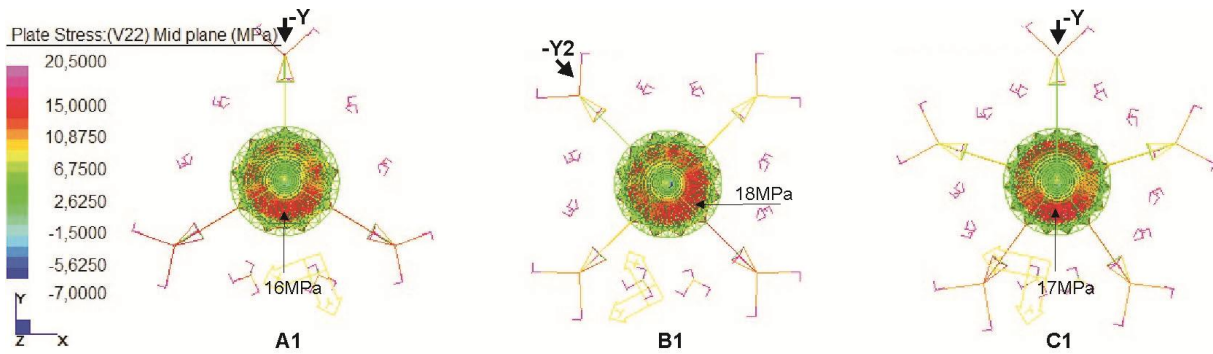
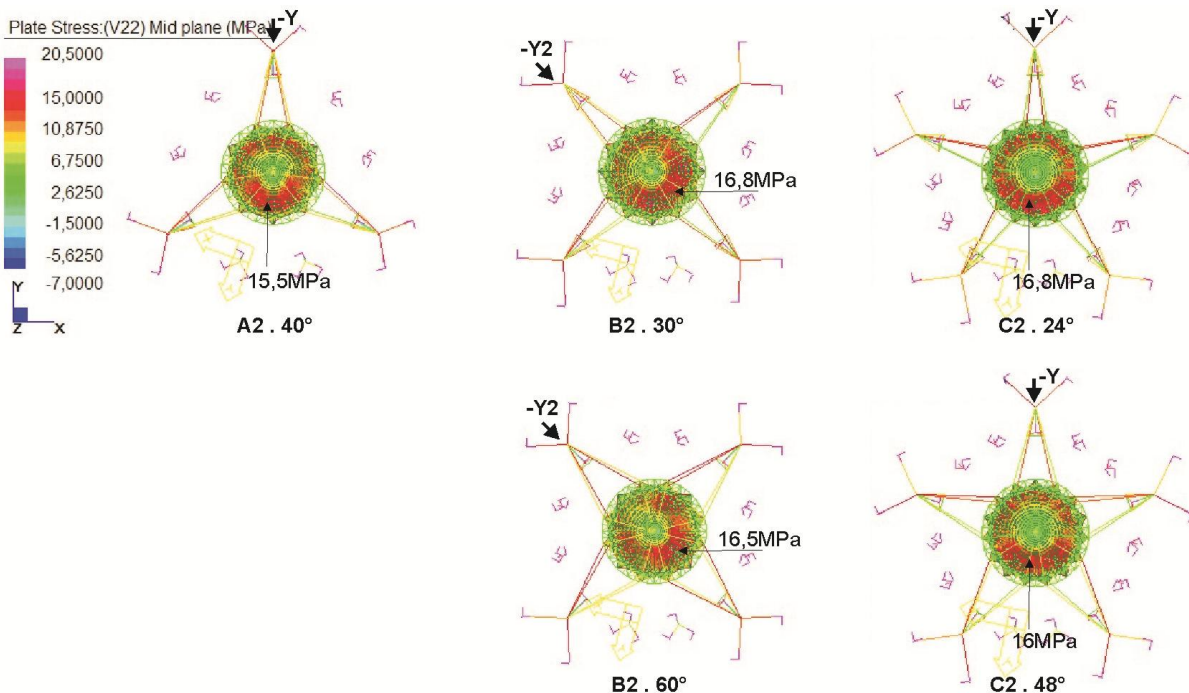


Figure 3.1-56 – Min. stress - int. membrane – A2-40°, B2-30°, C2-24°; B2-60°, C2-48° (wind -Y; -Y2)



### *Support system displacements*

A significant reduction in the support system displacements was observed in A2-40°, B2-30°, C2-24° models (Figure 3.1-58, Figure 3.1-74, Table 3.1-11), compared to A1, B1, C1 models (Figure 3.1-57, Figure 3.1-44), as it can be seen:

- A2-40°: reduction of approx. 75% on the windward side and 30% on the leeward side;
- B2-30°: reduction of approx. 65% on the windward side and 25% on the leeward side;
- C2-24°: reduction of approx. 30% on the windward side and 20% on the leeward side.

Displacements of truss ring on the leeward side were predominant in A2-40°, B2-30° models, in all wind directions. Pressure displacements were predominant in C2-24° model (with the smallest angle between cables and lower pre-tension applied

to cables) in all directions. Pressure displacements on windward side were predominant in the flying mast for all models.

Increasing the angle between cables, a reduction in the truss ring and flying mast displacements were observed in B2-60° model (approx. 20% on the leeward side) and C2-48° model (approx. 50% on the windward side), compared to B2-30° and C2-24° models, respectively (Figure 3.1-58, Figure 3.1-74, Figure 3.1-75).

Figure 3.1-57 – Support system displacements– A1, B1, C1 (wind -Y; -Y2)

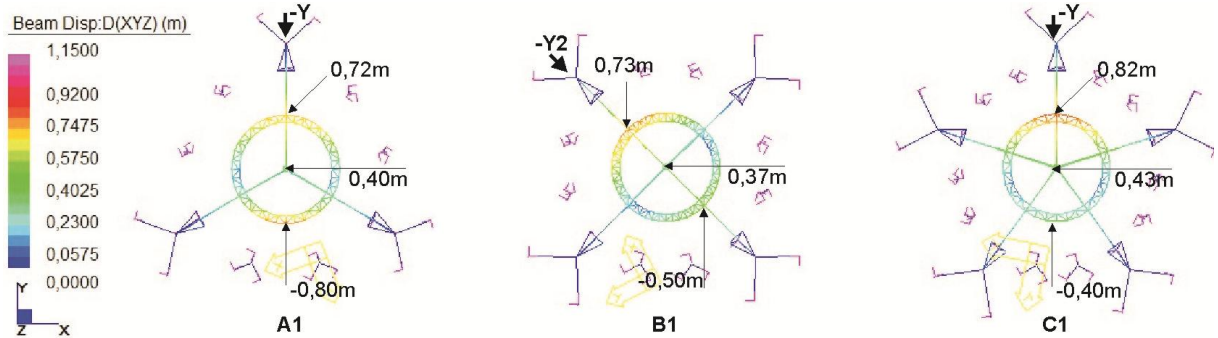
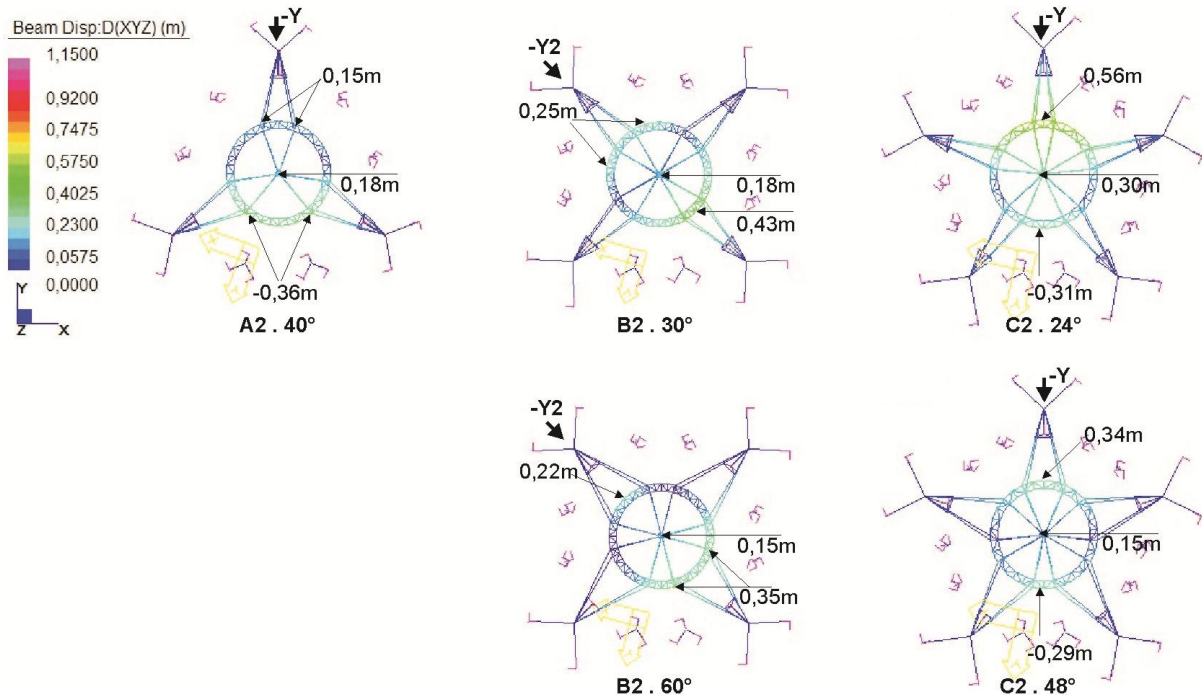


Figure 3.1-58 – Support system displacements – A2-40°, B2-30°, C2-24°; B2-60°, C2-48° (wind -Y; -Y2)



With rain and wind loads, a reduction in the support system displacements (approx. 20%) on the leeward side and an increasing in its displacements on the windward side were observed in A2-40°, B2-60°, C2-48° models (approx. 30% to 50%), and in B2-30° and C2-24° models (approx. 30% and 20%, respectively). This behavior was also observed on the external and internal surfaces (Table 3.1-11).

*Displacements of the external membrane surface*

A significant reduction in the external membrane displacements on the windward side was observed in A2-40°, B2-30°, C2-24° models (Figure 3.1-60, Figure 3.1-76, Table 3.1-11), compared to A1, B1, C1 models (Figure 3.1-59, Figure 3.1-45):

- A2-40°: reduction of approx. 45% on the windward side and 12% on the leeward side;
- B2-30°: reduction of approx. 45% on the windward side and 7% on the leeward side;
- C2-24°: reduction of approx. 25% on the windward side and 3% on the leeward side.

Figure 3.1-59 – External membrane displacements – A1, B1, C1 (wind -Y; -Y2)

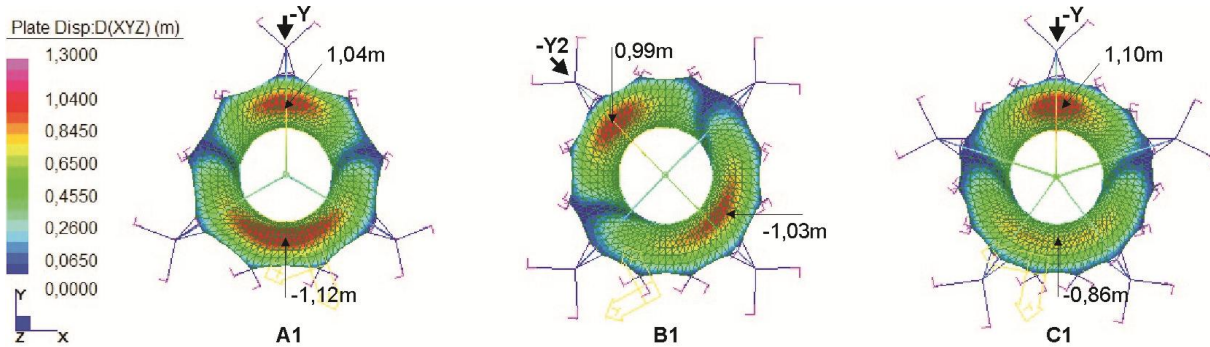
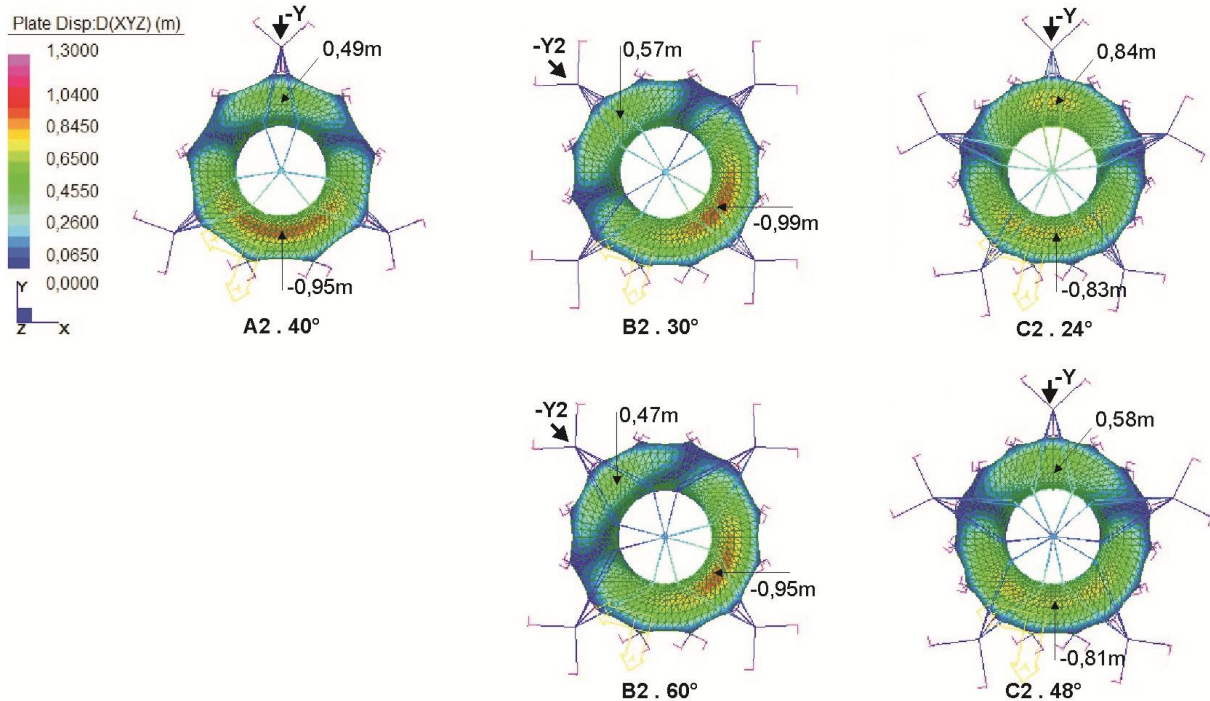


Figure 3.1-60 – Ext. membrane displacements – A2-40°, B2-30°, C2-24°; B2-60°, C2-48° (wind -Y; -Y2)



Increasing the angle between cables, there was a reduction in the external membrane displacements on the windward side in B2-60° model and principally in C2-48° model, compared to B2-30° and C2-24° models (Figure 3.1-60, Figure 3.1-77).

Large displacements of the external membrane surface were predominant on the leeward side in A2-40°, B2-30°, B2-C2-60°, C2-48° models, for all wind directions. Displacements on the leeward and windward sides are similar in C2-24° model.

#### *Displacements of the internal membrane surface*

A significant reduction in the internal membrane displacements was also verified in the A2-40°, B2-30°, C2-24° models (Figure 3.1-62, Figure 3.1-78), mostly on the windward side compared to A1, B1, C1 models (Figure 3.1-61, Figure 3.1-46).

Figure 3.1-61 – Internal membrane displacements - A1, B1, C1 (wind -Y; -Y2)

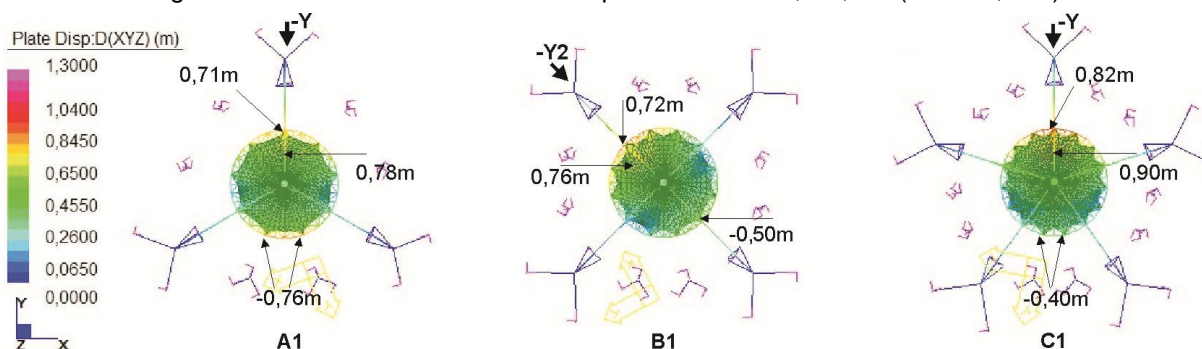
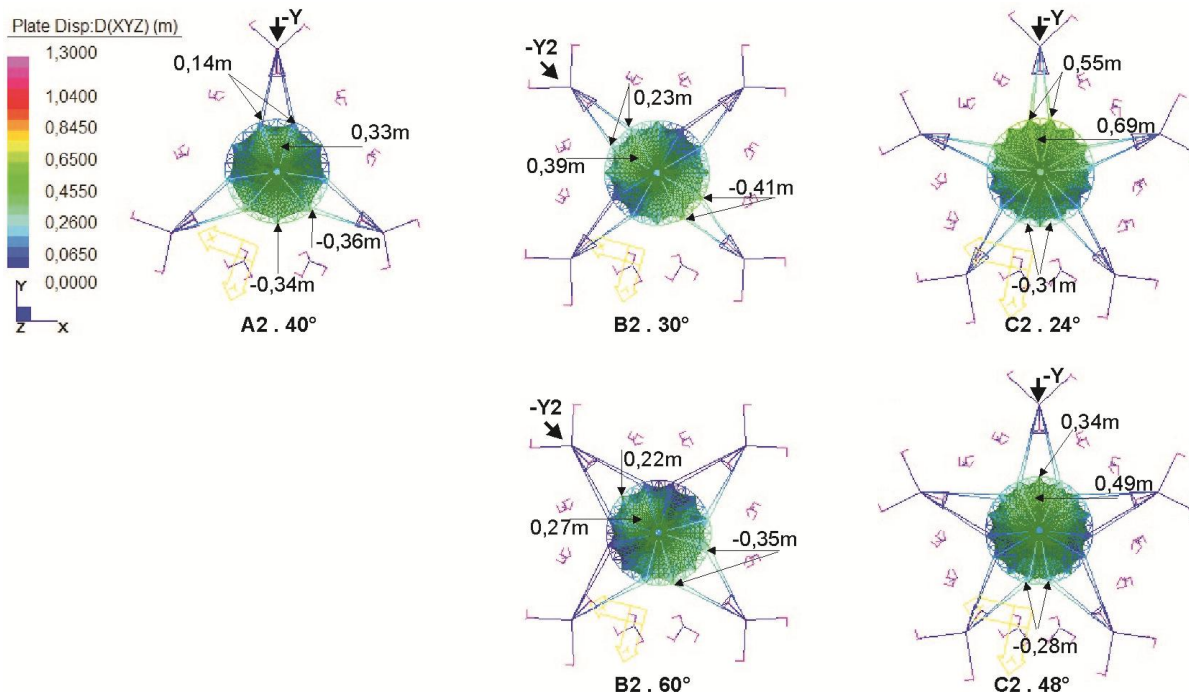


Figure 3.1-62 – Int. membrane displacements - A2-40°, B2-30°, C2-24°; B2-60°, C2-48° (wind -Y; -Y2)



The reduction in the internal membrane displacements was similar to the reduction observed in the support system displacements:

- A2-40°: reduction of approx. 75% on the windward side and 40% on the leeward side;
- B2-30°: reduction of approx. 60% on the windward side and 25% on the leeward side;

- C2-24°: reduction of approx. 30% on the windward side and 20% on the leeward side.

Increasing the angle between cables, a reduction in the internal membrane displacements on the windward side was also observed on B2-60° model (approx. 25%) and C2-48° model (approx. 50%), compared to B2-30° and C2-24° models (Figure 3.1-62, Figure 3.1-79).

Displacements on the leeward side were predominant in A2-40° model; displacements on the leeward and windward sides were similar in B2-30° and B2-60° models; displacements on the windward side were dominant on C2-24° and C2-48° models. The largest displacements were registered in C-24° model, and the smallest ones in A2-40° model.

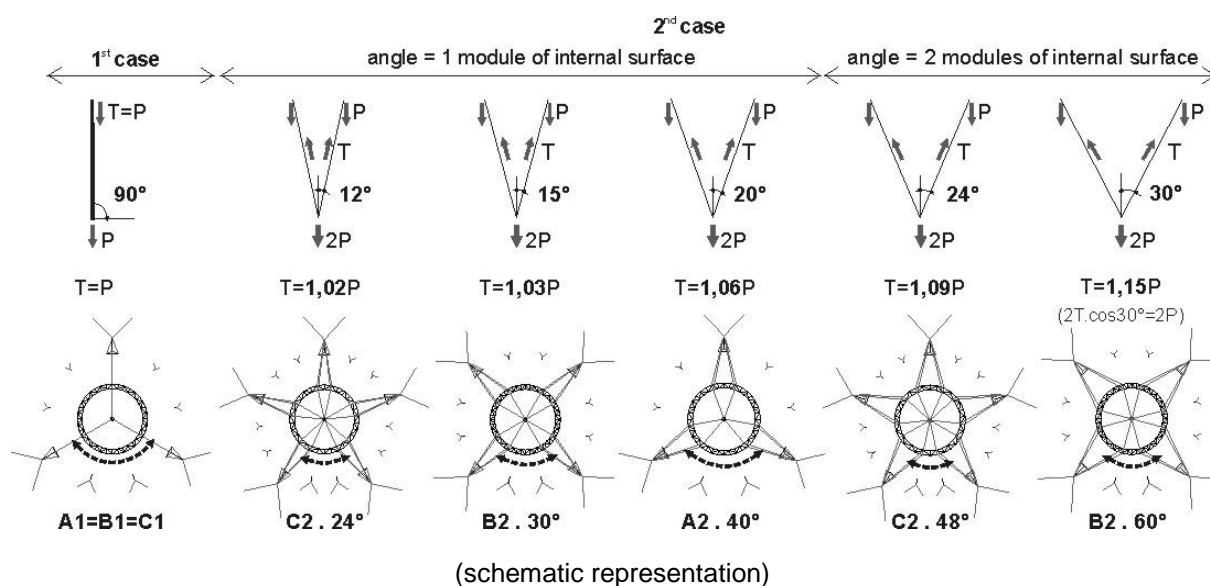
*Comparison of models: A2-40°, B2-30° and B2-60°, C2-24° and C2-48°*

The pre-tension applied to the support system cables of models of the second case (A2-40°, B2-30°, C2-24°) and first case models (A1, B1, C1) exhibited similar relationship. However, with new cable configuration the magnitude of pre-tension increased 100% (Table 3.1-14).

An increase in the system stiffness and greater integration between spatial support system and tall masts were observed in A2-40°, B2-30°, C2-24° models (with the new cable configuration and increased pre-tension applied to the support system cables), when compared to A1, B1, C1 models. Consequently, higher restrictions in the spatial support system and membrane displacements were verified, especially on windward side. An increase in the stress magnitude and areas of stress concentration nearly membrane anchor points were also observed.

The increase in the angle between pair of cables that hold special support system (B2-60°, C2-48° models) contributed to maximize support system stiffness and to reduce load path (Figure 3.1-63). However, this change caused a significant increase of pre-tension magnitude applied to support system cables and the mass/area of models, and thus, greater stress of truss ring and tall masts was observed. This behavior was evident when comparing models B2-30° and B2-60°, C2-24° and C2-48° (Figure 3.1-63, Table 3.1-14, Table 3.1-15).

Figure 3.1-63 – Angles between cables, applied pre-tension; load path



In models whose angle of spatial system cables is defined by one module of the internal surface (A2-40°, B2-30°, C2-24°), the smallest displacements of support system and the membranes were observed in A2-40° model on the windward side; and the lower mass and pre-tension, as well as, surfaces with more uniform stress field were observed in C2-24° model. However, the B2-30° model exhibited a good performance, displacements on the windward side with less intensity than C2-24° model; and lower mass and pre-tension than A2-40° model.

In models whose angle of spatial system cables is defined by two modules of the internal surface (B2-60°, C2-48°), the smallest displacements of support system and membranes was observed on windward side in B2-60° model, and on leeward side in C2-48° model. However, the lower mass and pre-tension, significant reduction of displacements, and surfaces with uniform stress field were verified in C2-48° model.

It was also observed that B2-30° and C2-48° models, showed comparable performance. So, to continue the analysis, checking the influence of membrane surface geometry on system performance, B2-30° model was chosen, i.e., the model which has lower number of masts and whose angle of spatial system cables is defined by one module of the internal surface.

Figure 3.1-64 – Von Mises stress – A2-40°, B2-30°, C2-24°

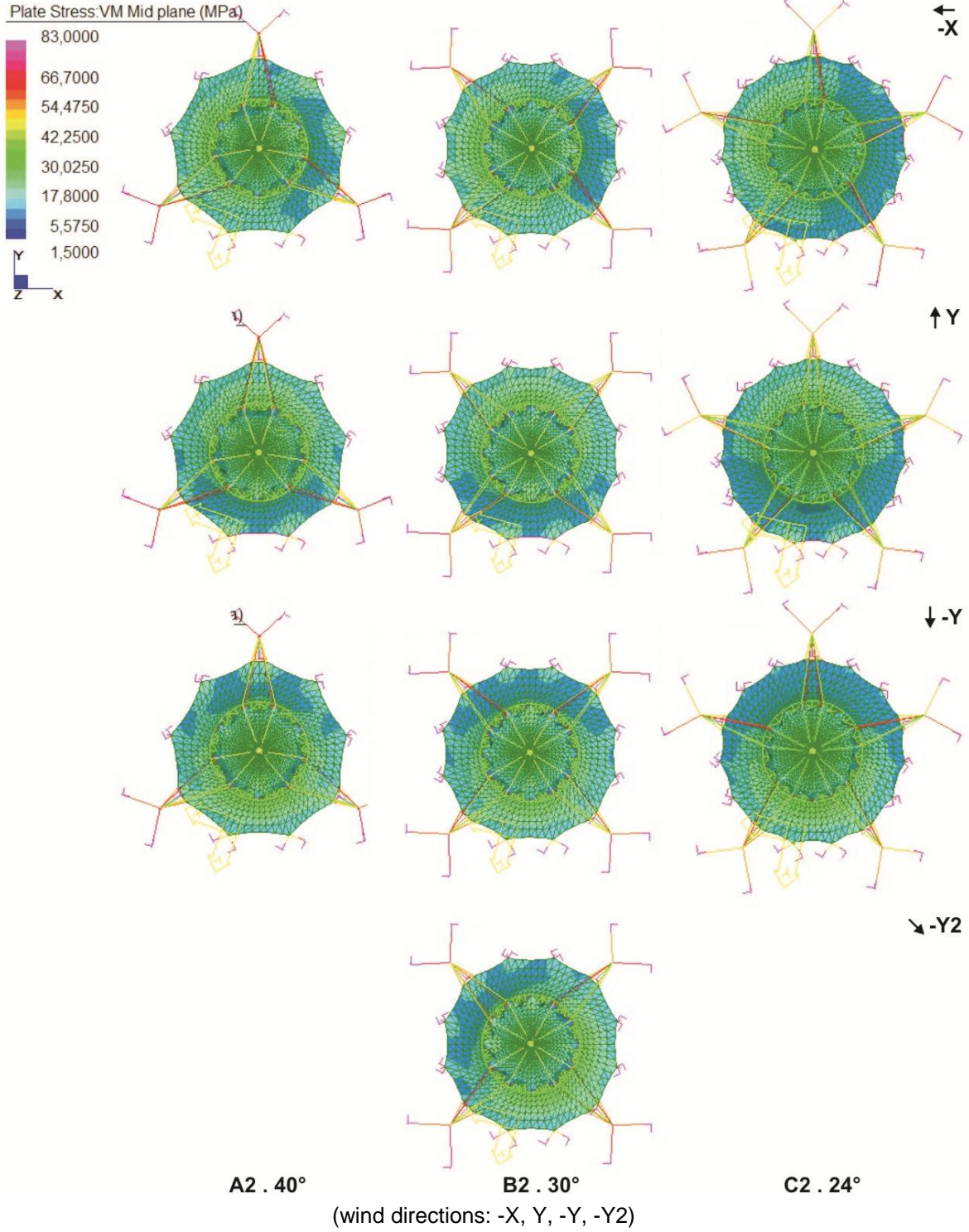


Figure 3.1-65 – Von Mises stress – B2-60°, C2-48°

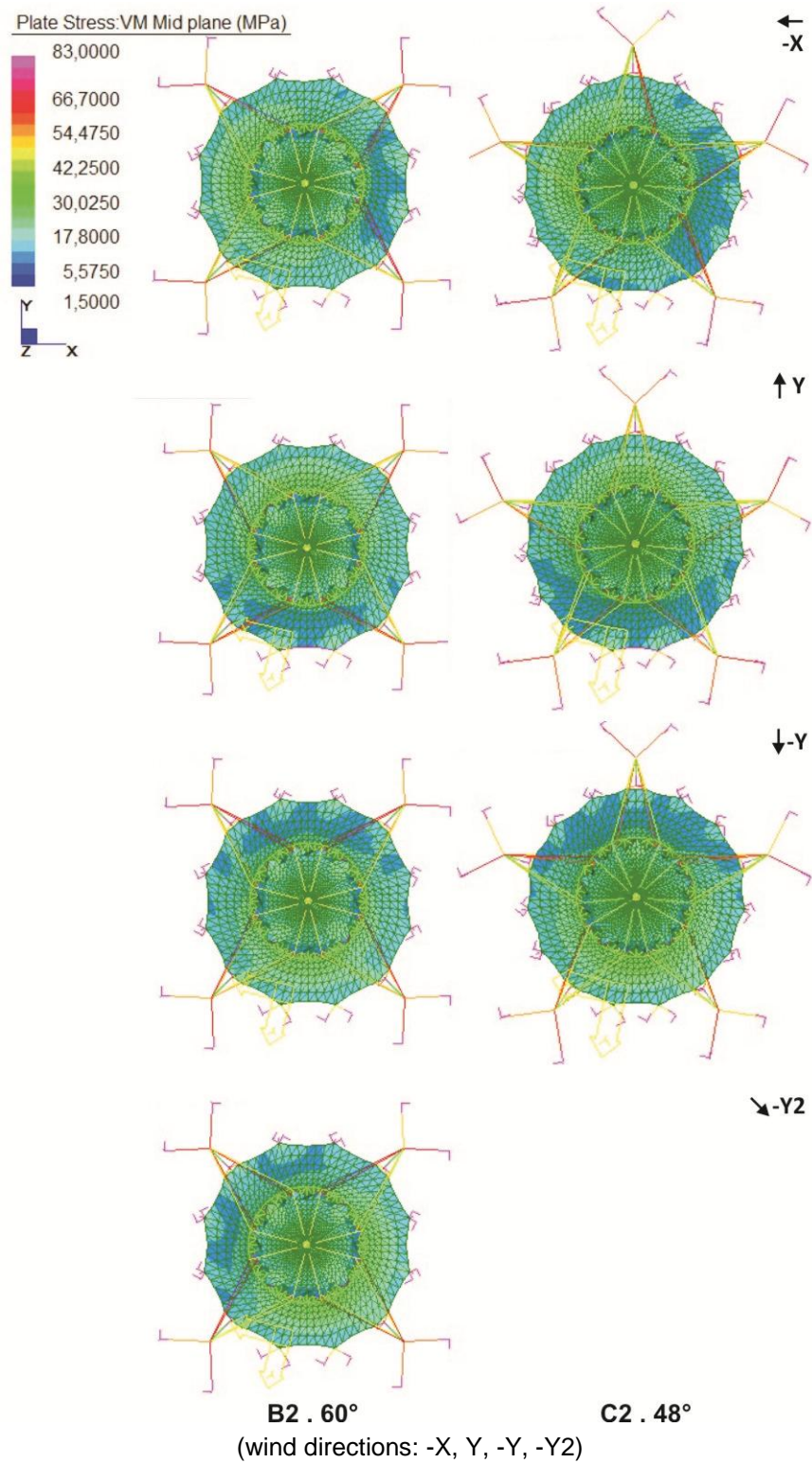


Figure 3.1-66 – Maximum stress trajectories – external membrane – A2-40°, B2-30°, C2-24°

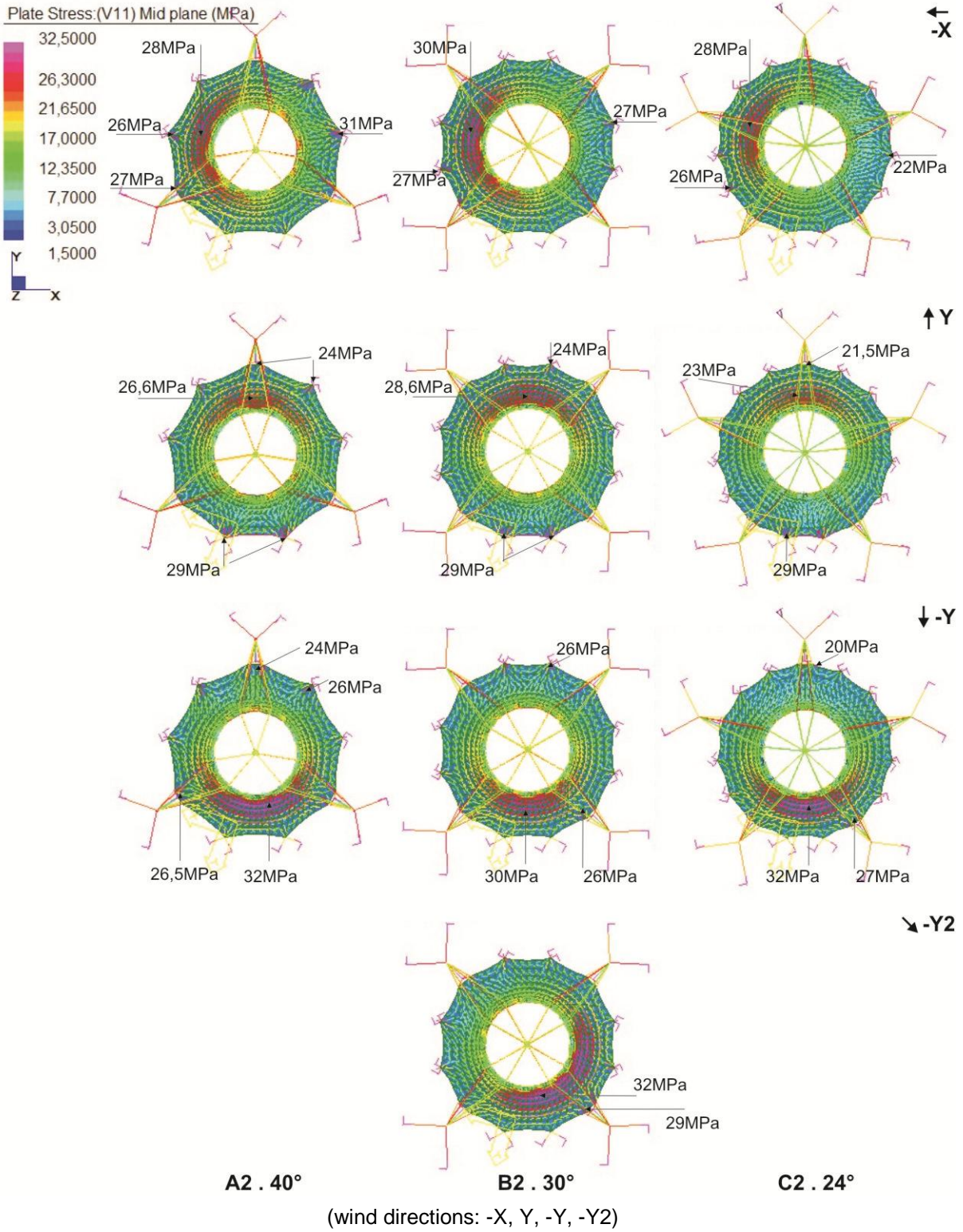


Figure 3.1-67 – Maximum stress trajectories - external membrane – B2-60°, C2-48°

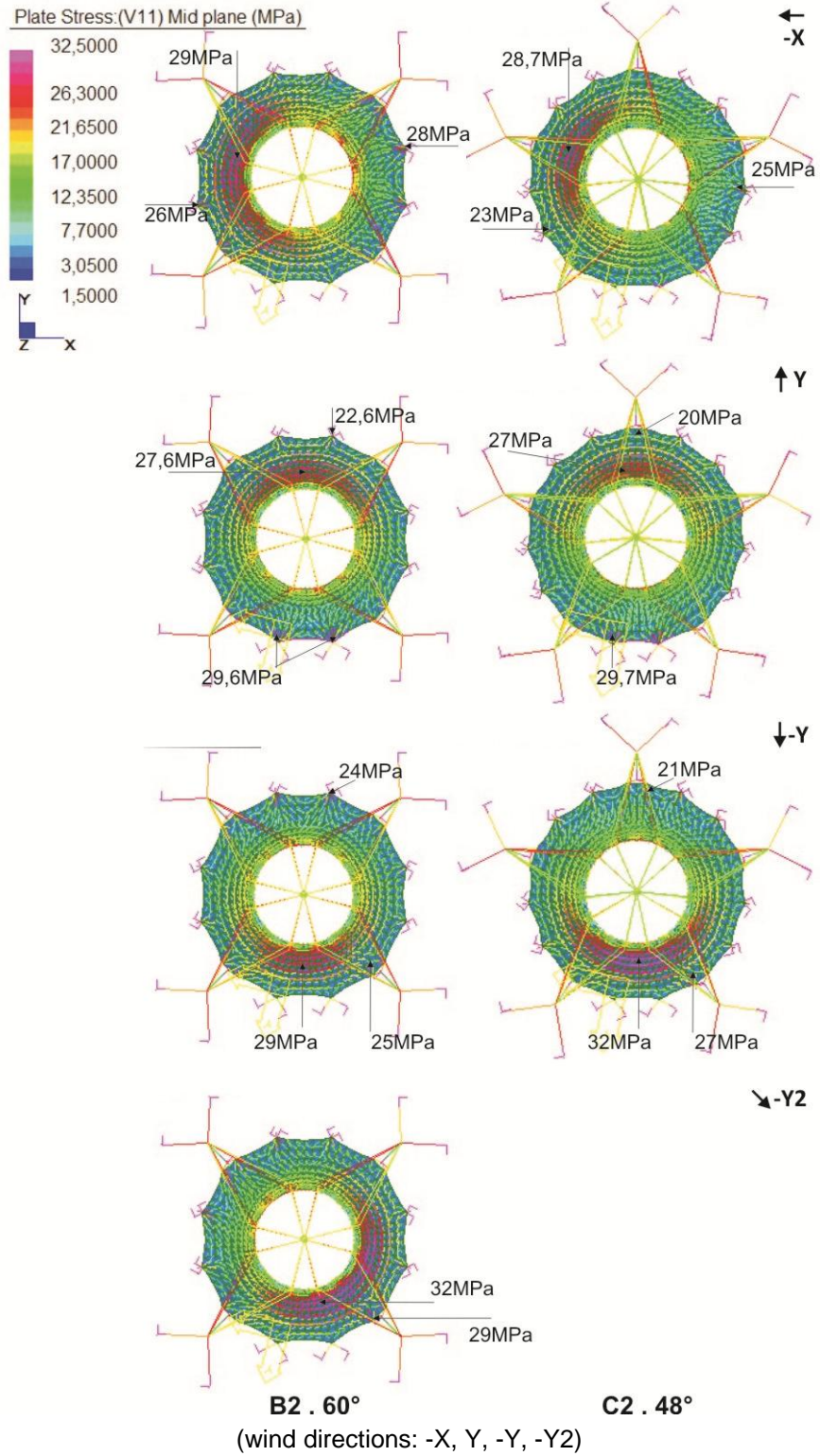


Figure 3.1-68 – Minimum stress trajectories - external membrane – A2-40°, B2-30°, C2-24°

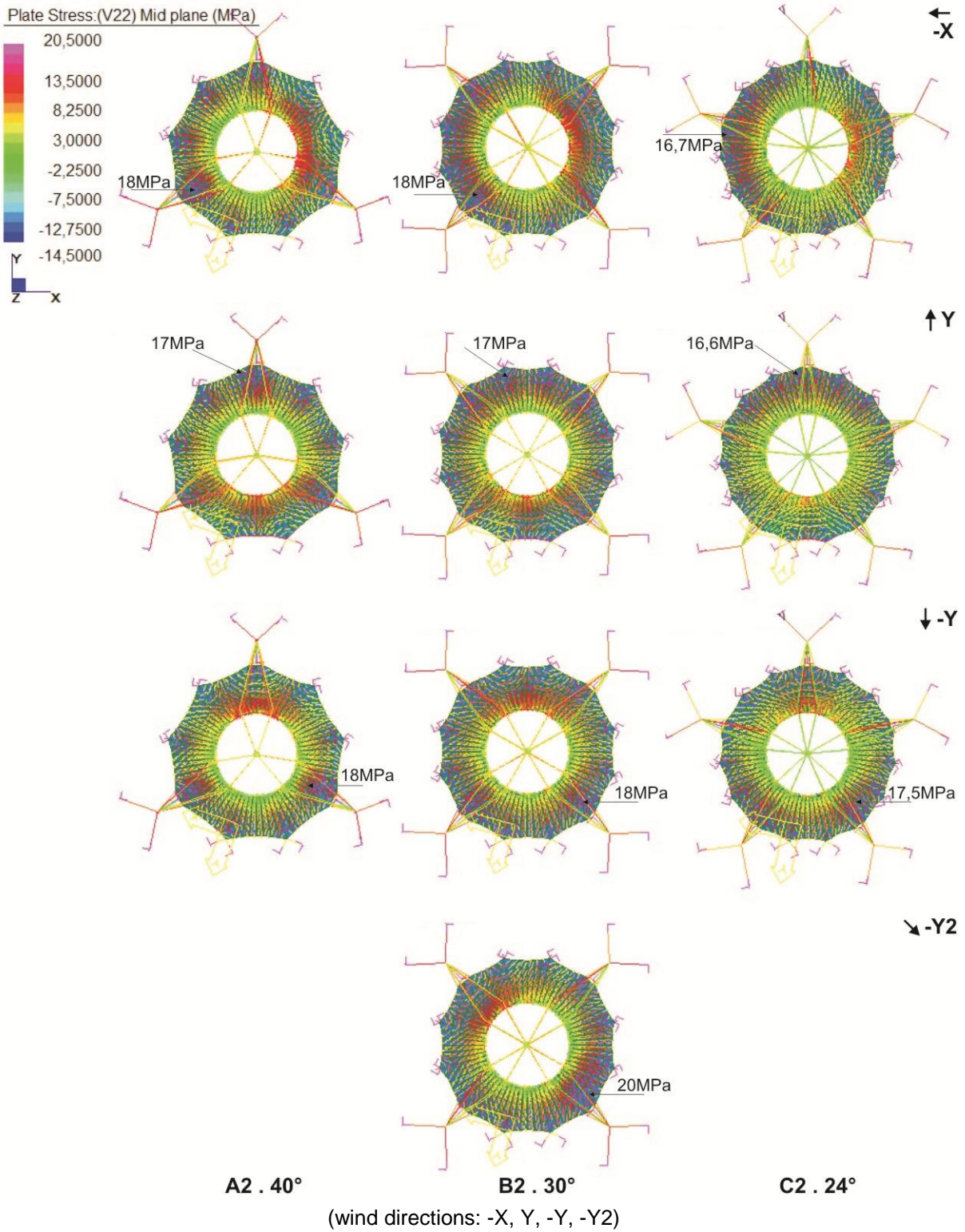


Figure 3.1-69 – Minimum stress trajectories - external surface – B2-60°, C2-48°

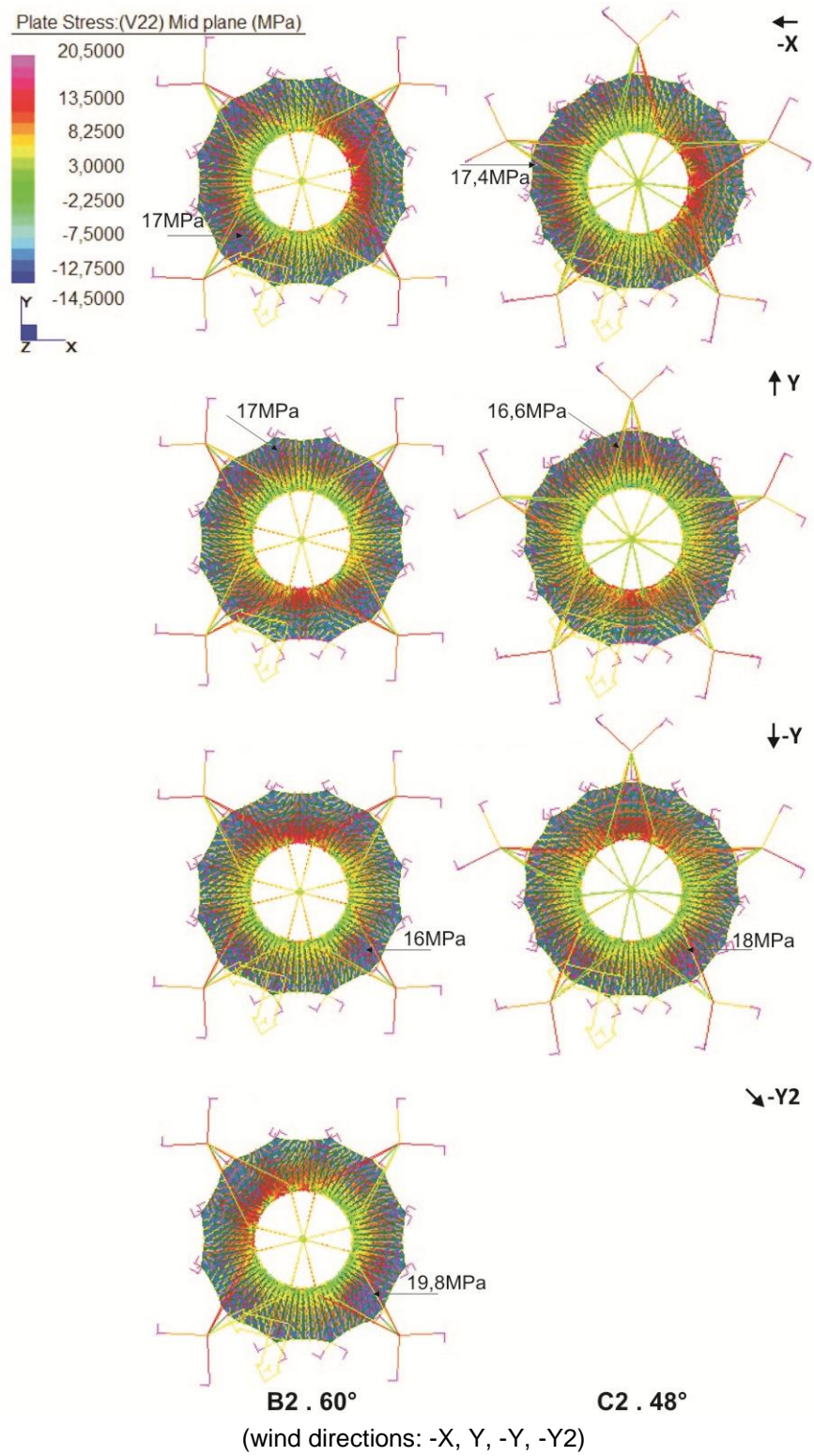


Figure 3.1-70 – Maximum stress trajectories - internal surface – A2-40°, B2-30°, C2-24°

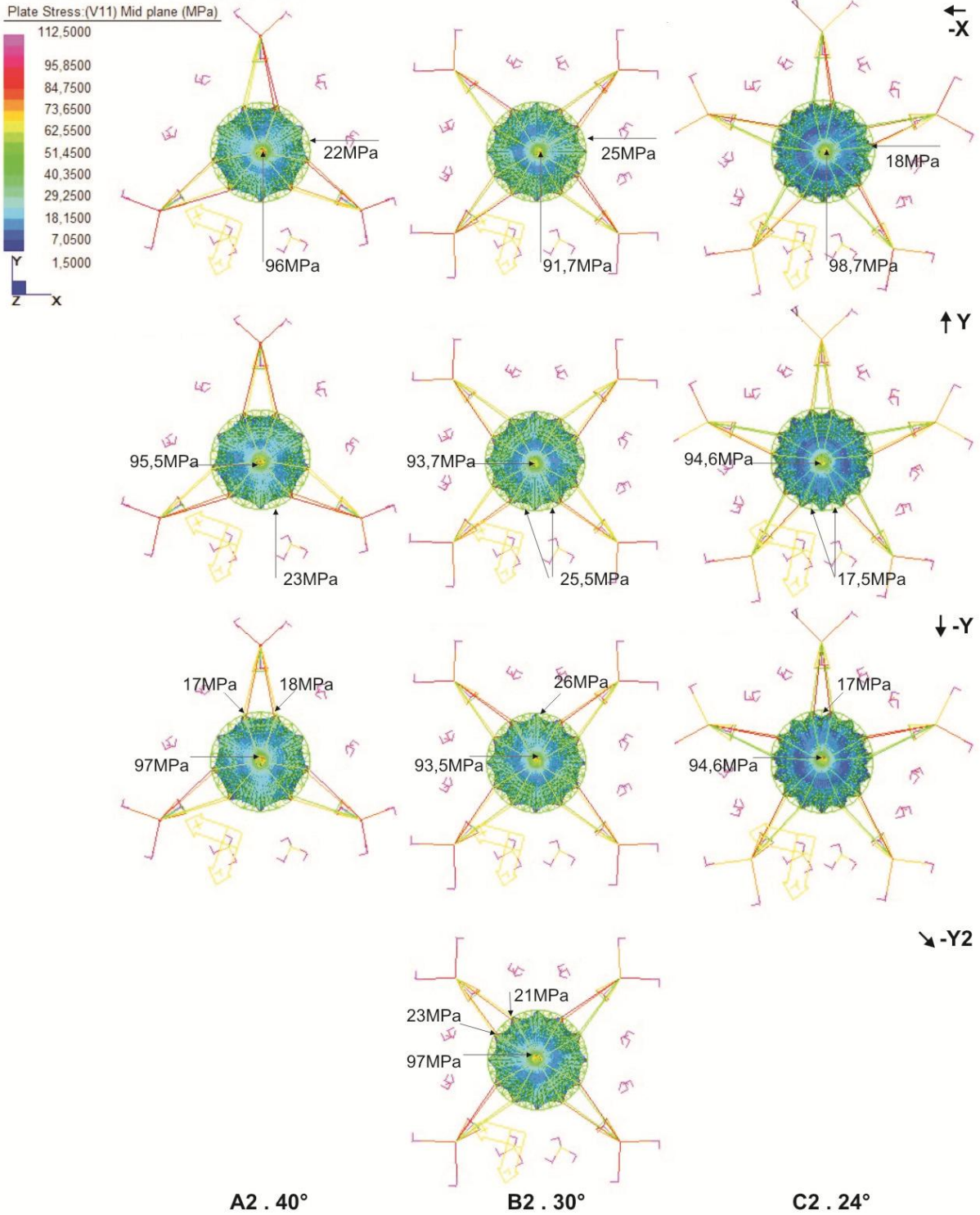


Figure 3.1-71 – Maximum stress trajectories - internal surface – B2-60°, C2-48°

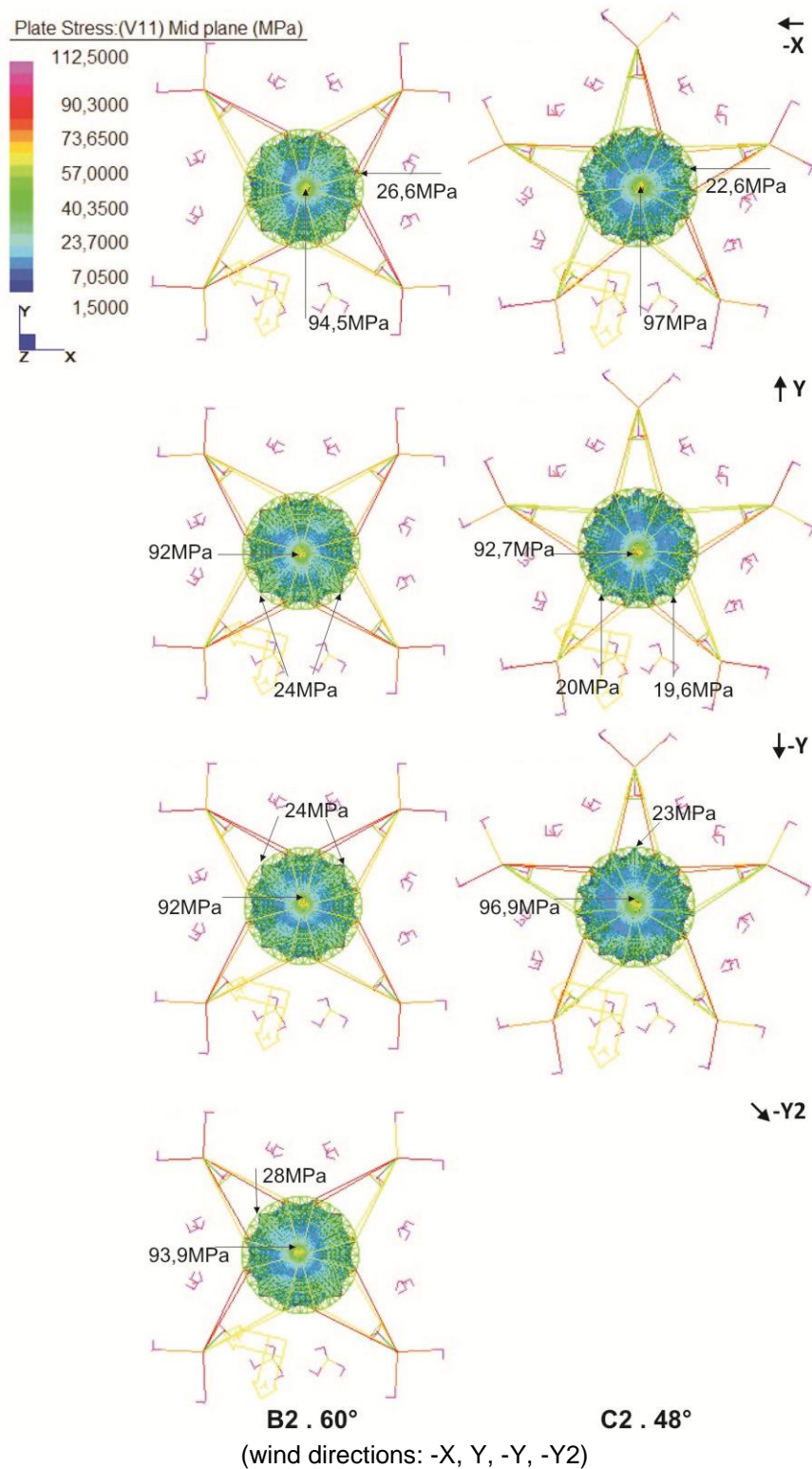


Figure 3.1-72 – Minimum stress trajectories - internal surface – A2-40°, B2-30°, C2-24°

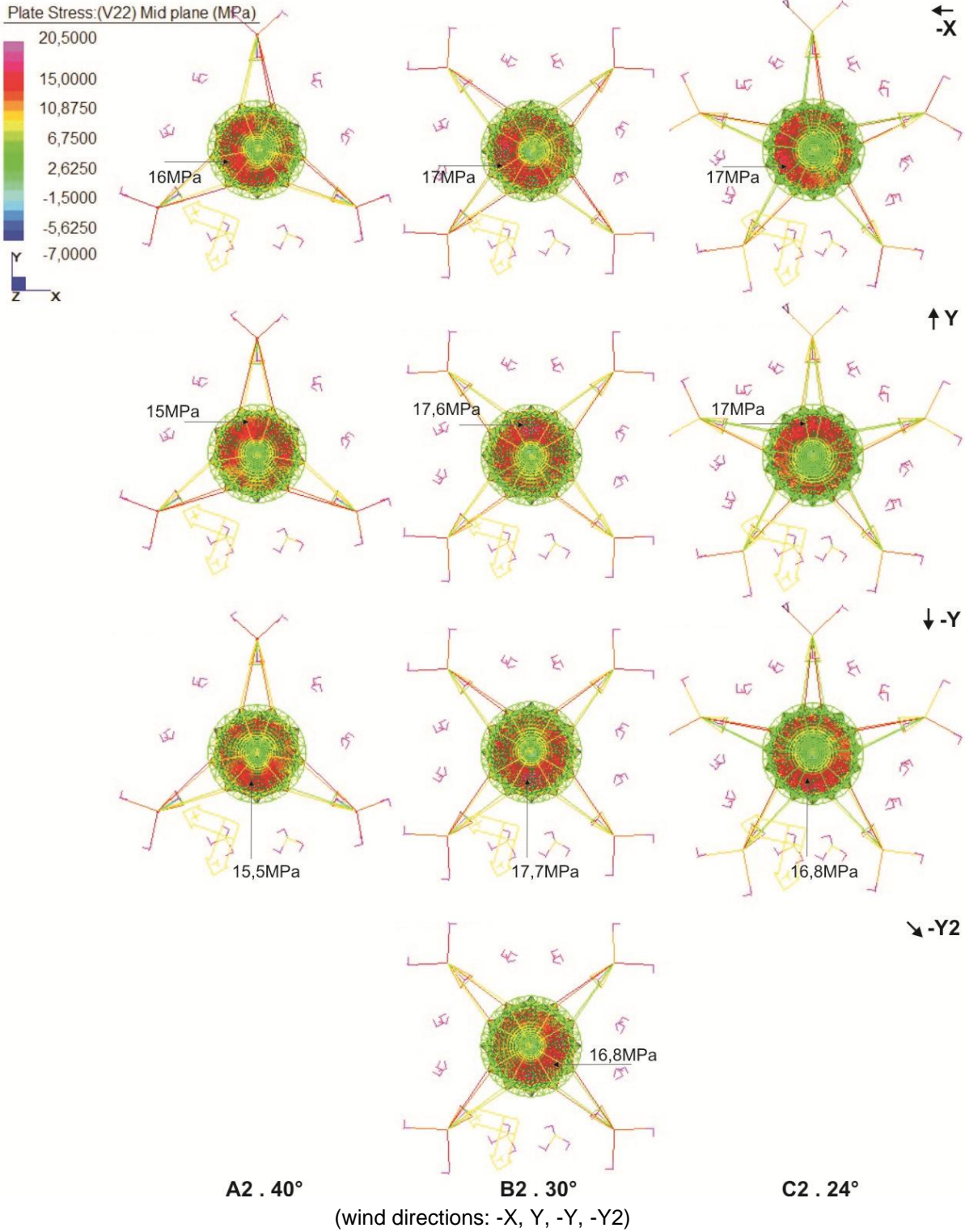


Figure 3.1-73 – Minimum stress trajectories - internal surface - B2-60°, C2-48° models

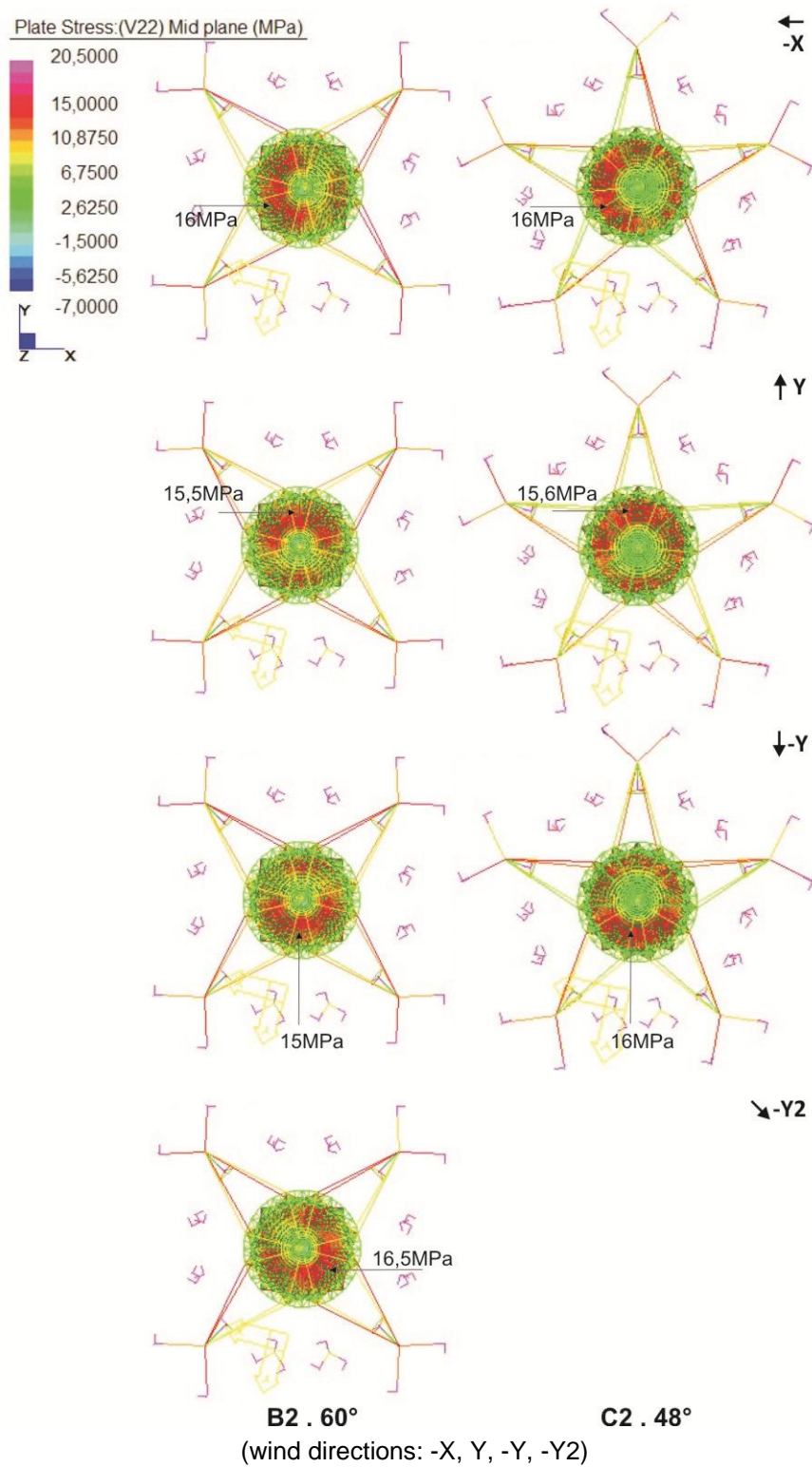


Figure 3.1-74 – Support system displacements – A2-40°, B2-30°, C2-24°

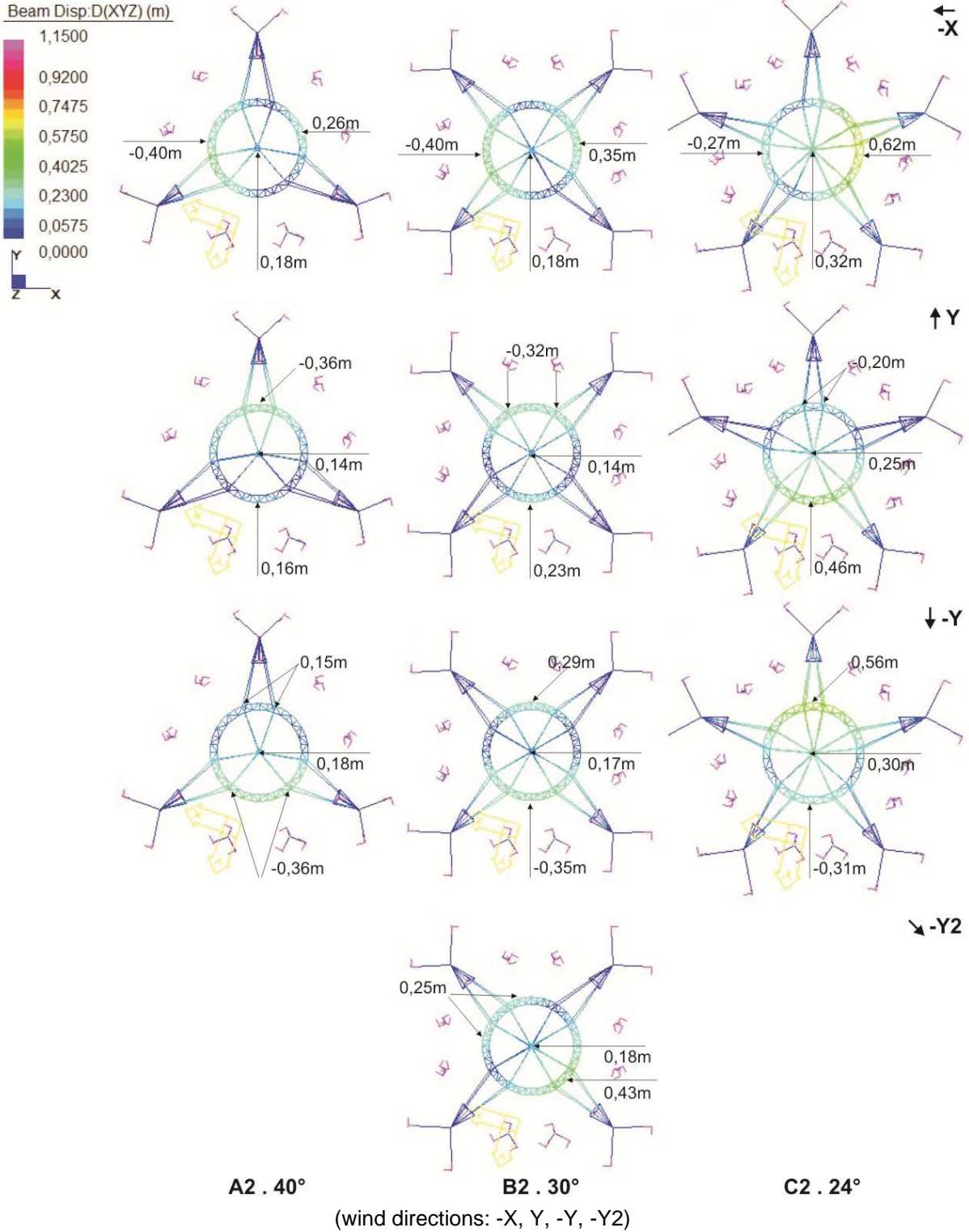


Figure 3.1-75 – Support system displacements – B2-60°, C2-48°

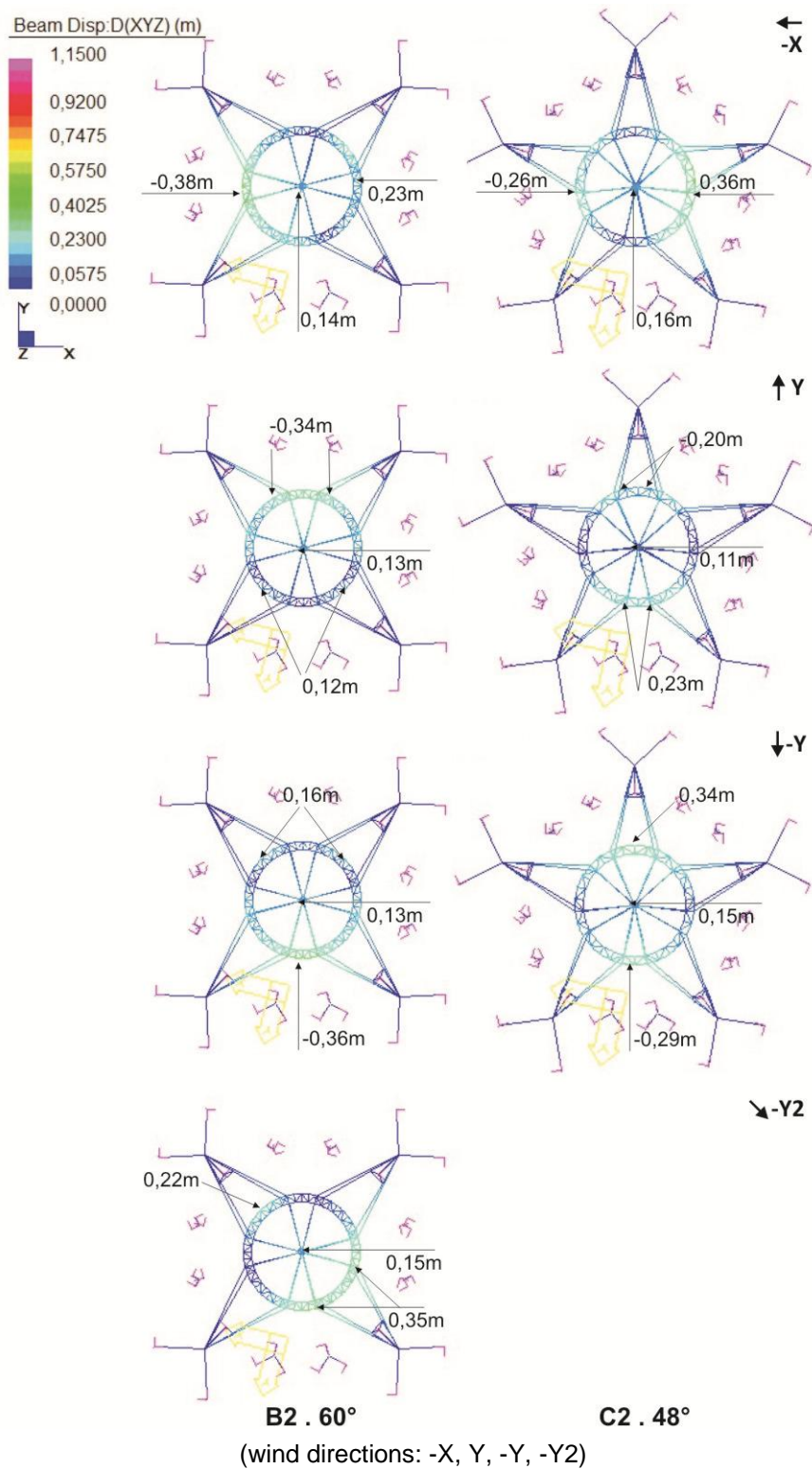
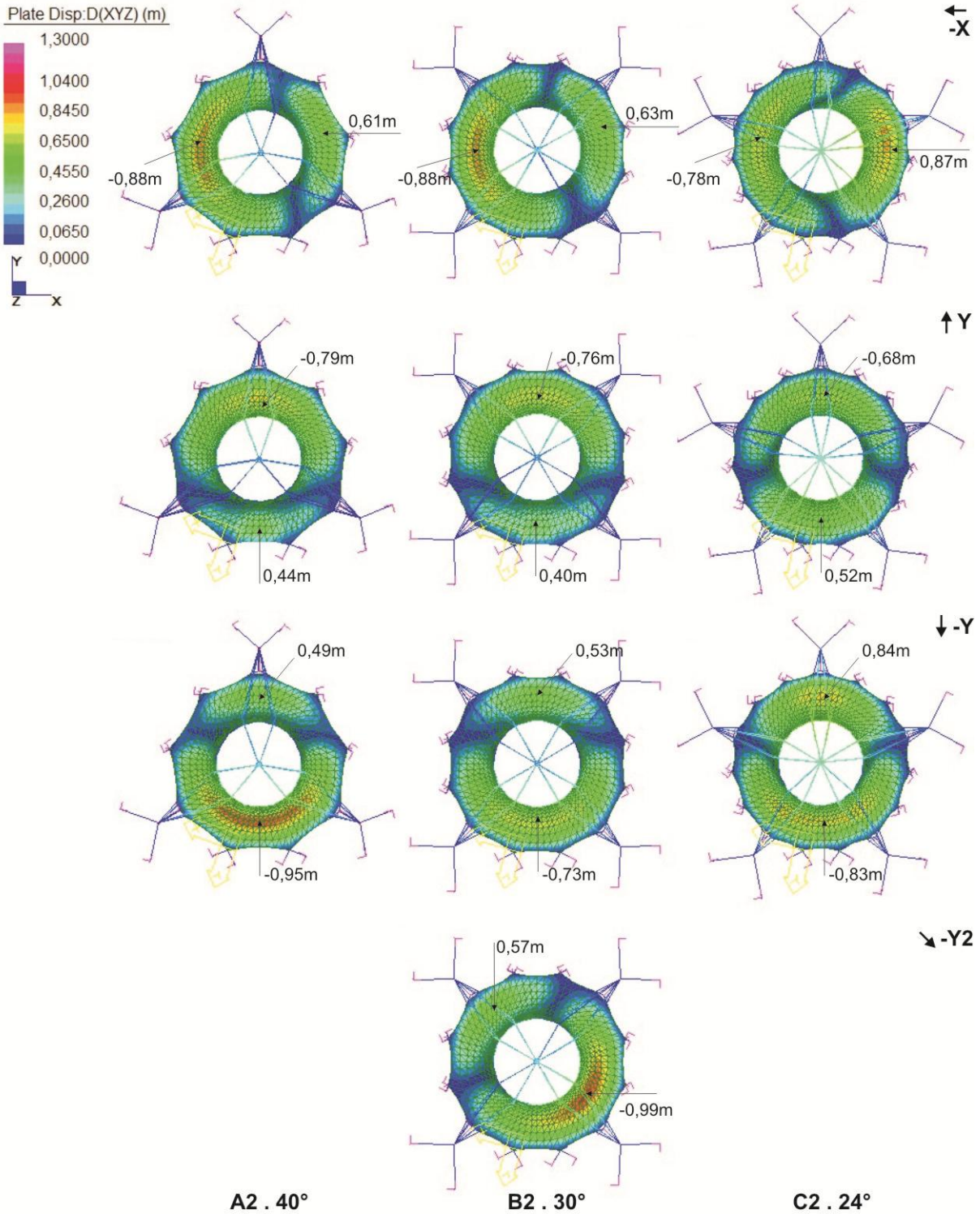


Figure 3.1-76 – External surface displacements – A2-40°, B2-30°, C2-24°



(wind directions: -X, Y, -Y, -Y2)

Figure 3.1-77 – External surface displacements - B2-60°, C2-48°

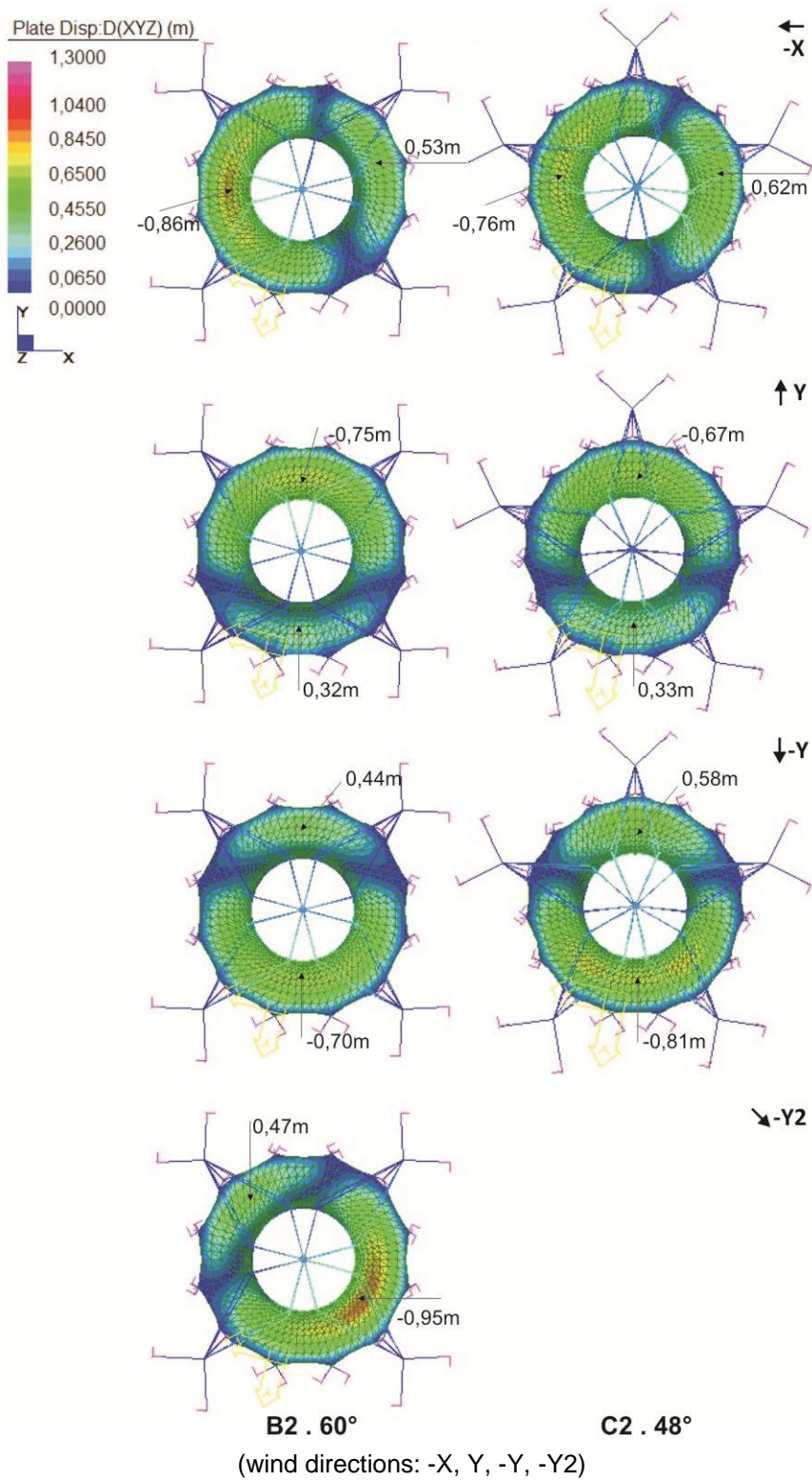
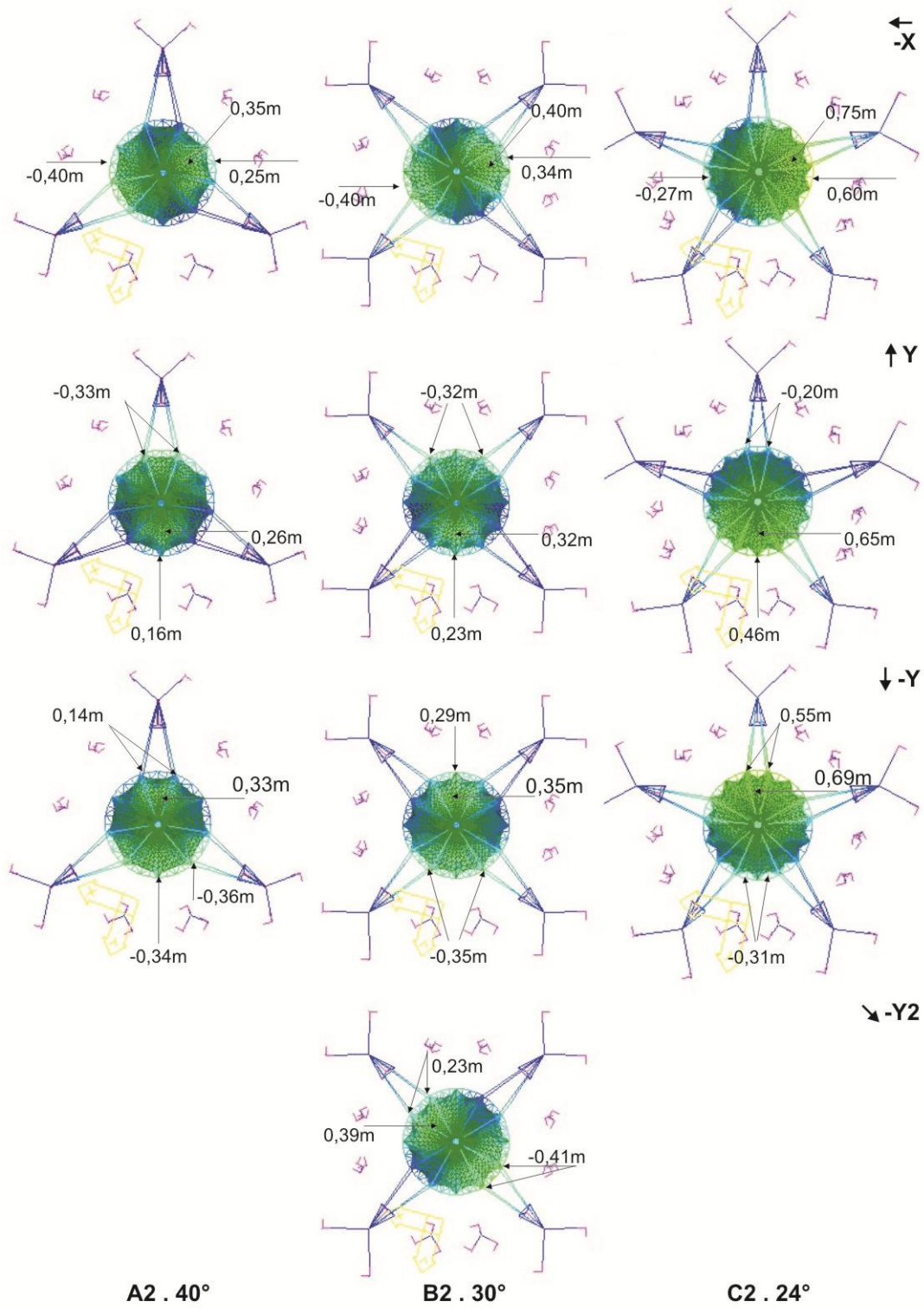


Figure 3.1-78 – Internal surface displacements – A2-40°, B2-30°, C2-24°



(wind directions: -X, Y, -Y, -Y2)

Figure 3.1-79 – Internal surface displacements - B2-60°, C2-48° models

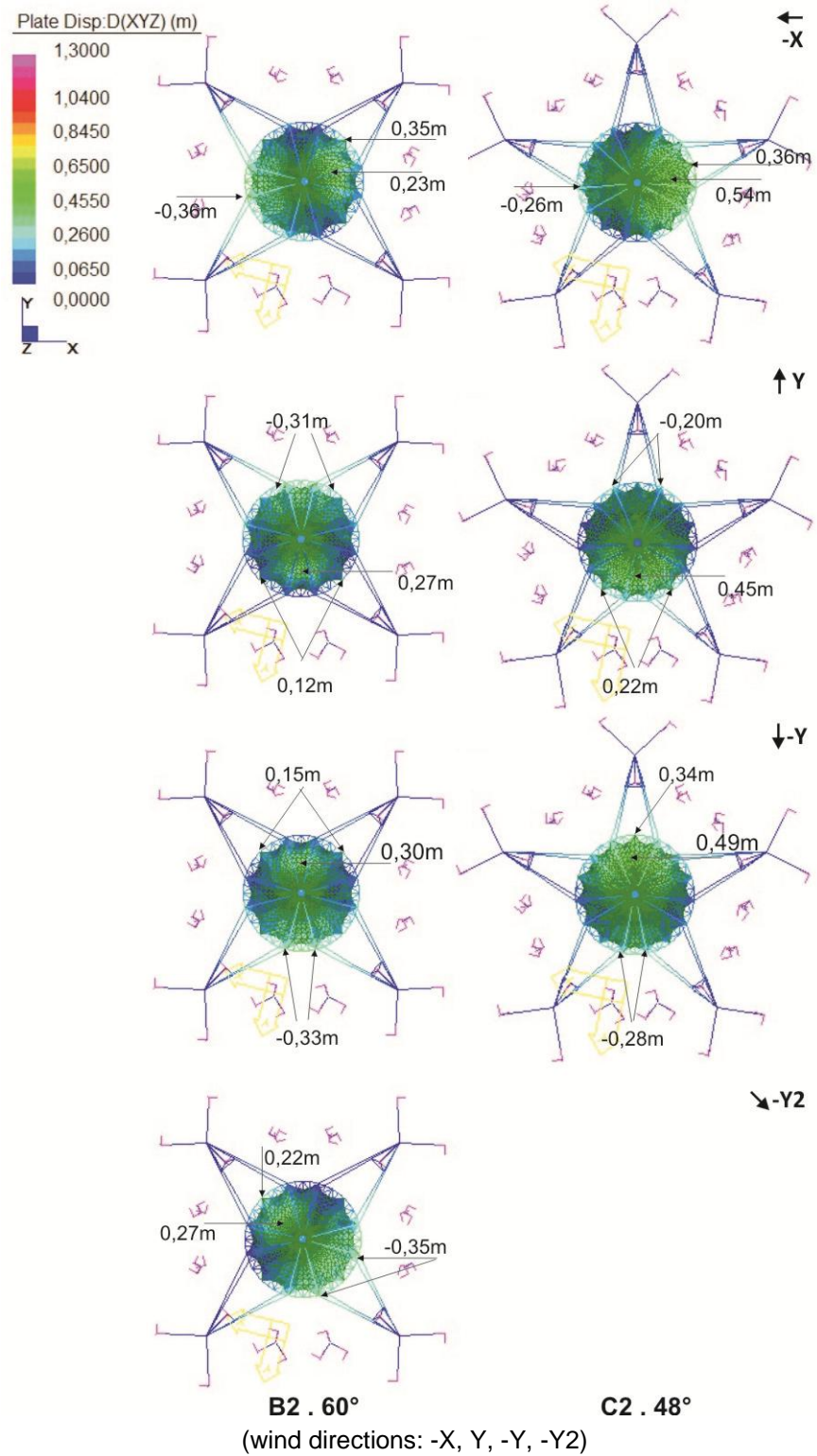
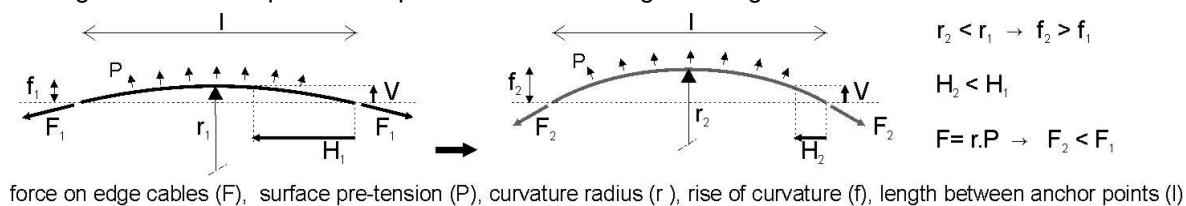




Figure 3.1-80 – Schematic representation of changes in edge cable curvature of the surface



Source: adapted from KNIPPERS *et al.*, 2011, p.145.

### Mass / area of each model

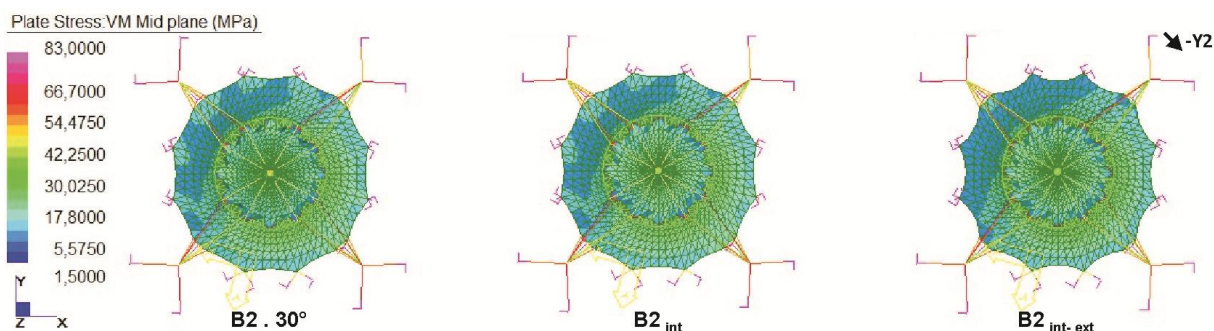
B2<sub>int</sub> model exhibited system mass/ area similar to B2-30° model. However, in B2<sub>int-ext</sub> model it was observed a reduction of system mass/ area (approx. 14%) according to Table 3.1-17, Table 3.1-10.

Table 3.1-17 – Ratio mass/ area – A1, B2-30°, B2<sub>int</sub> e B2<sub>int-ext</sub> models

models	support system		membrane			support system + membrane			
	mass (kg)	%	mass (kg)	area (m <sup>2</sup> )	%	mass (kg)	mass/ area		
							(kg/m <sup>2</sup> )	%	
A1	23.850,53	1,00	3.224,79	2.388,73	1,00	27.075,32	11,33	1,00	
B2 30°	33.111,38	1,39	3.394,94	2.514,77	1,05	36.506,32	14,52	1,28	
B2 <sub>int</sub>	33.047,46	1,39	3.378,64	2.502,70	1,05	36.426,10	14,55	1,28	
B2 <sub>int-ext</sub>	27.134,83	1,14	3.260,89	2.415,48	1,01	30.395,72	12,58	1,11	

### Stress distribution in the external and internal membrane surfaces

Membrane surfaces of B2<sub>int</sub> model (Figure 3.1-81, Figure 3.1-89) exhibited similar behavior to the surfaces of B2-30° model, but with reduction of stress magnitude of internal surface. A significant reduction in the areas of stress concentration on internal and external membrane surfaces were observed on B2<sub>int-ext</sub> model, and consequently a more homogeneous stress distribution on these surfaces.

Figure 3.1-81 – Von Mises stress – B2-30°, B2<sub>int</sub> and B2<sub>int-ext</sub> (wind -Y2)

The external membrane surfaces of  $B2_{int}$  and  $B2-30^\circ$  models (Figure 3.1-82, Figure 3.1-90) showed similar behavior, i.e., higher stress concentration in the vicinity of truss ring on the leeward side and nearby bottom anchor points of the surface on the windward and leeward sides.

The external membrane surface of  $B2_{int-ext}$  model (Figure 3.1-82, Figure 3.1-90) showed a significant reduction (approx. 70%) in the stress magnitude of surface anchor points (near masts) on the windward and leeward sides. This behavior resulted from an increase in the edge cable curvature, allowing to decrease pre-tension magnitude (applied to the support system cables) required to the system equilibrium.

There was also a small reduction in the minimum stress magnitude in radial direction of the membrane surface on  $B2_{int-ext}$  model compared to  $B2-30^\circ$  and  $B2_{int}$  models (Figure 3.1-83, Figure 3.1-91).

Figure 3.1-82 – Maximum stress trajectories - external membrane –  $B2-30^\circ$ ,  $B2_{int}$  and  $B2_{int-ext}$  (wind -Y2)

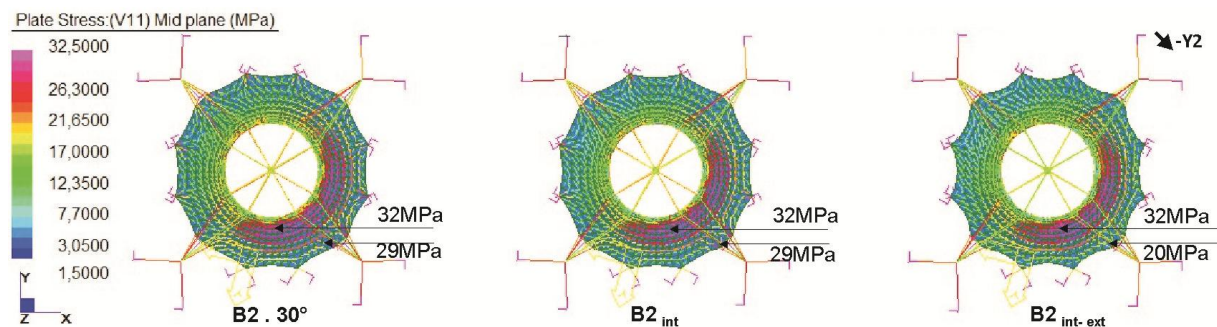
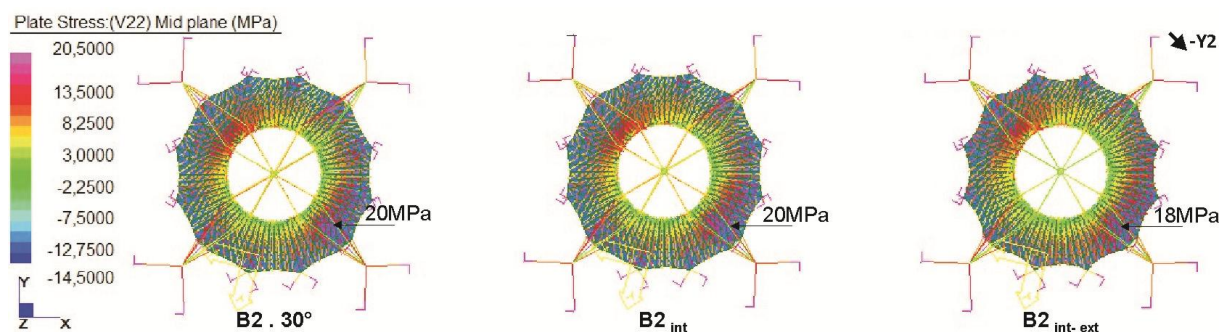


Figure 3.1-83 – Minimum stress trajectories - external membrane –  $B2-30^\circ$ ,  $B2_{int}$  and  $B2_{int-ext}$  (wind -Y2)



On the internal membrane surface of  $B2_{int}$  model (Figure 3.1-84, Figure 3.1-92), there was a reduction (approx. 8%) in the stress magnitude at the top of the surface (in the vicinity of the ring) compared to  $B2-30^\circ$  model, according to maximum

stress trajectories (radial direction). A small increase in the minimum stress magnitude (circumferential direction) was also observed.

The internal membrane surface of  $B2_{int-ext}$  model (Figure 3.1-84, Figure 3.1-92) showed little reduction in the stress magnitude in the bottom of the surface and near surface anchoring points at truss ring, compared to  $B2-30^\circ$  model.

Compression or ponding areas at the base of internal and external surfaces were not verified in these models, according to minimum stress trajectories (Figure 3.1-83, Figure 3.1-91, Figure 3.1-85, Figure 3.1-93).

Figure 3.1-84 – Maximum stress trajectories - internal membrane –  $B2-30^\circ$ ,  $B2_{int}$  and  $B2_{int-ext}$  (wind -Y2)

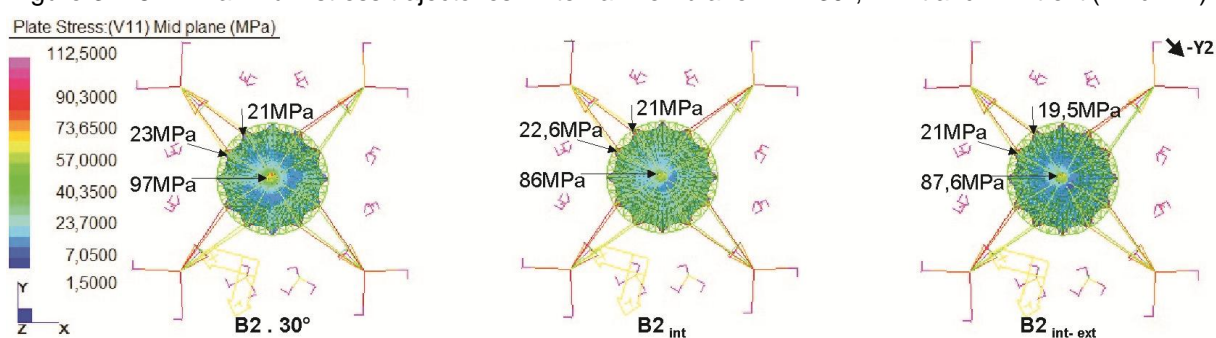
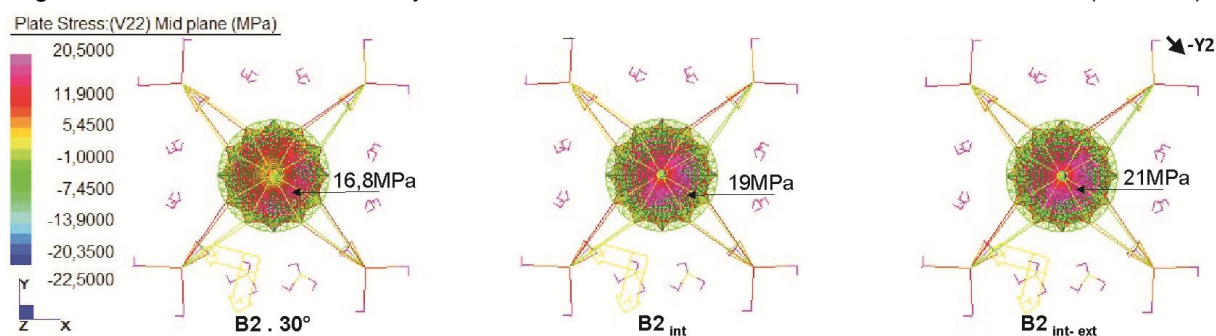


Figure 3.1-85 – Minimum stress trajectories - internal membrane –  $B2-30^\circ$ ,  $B2_{int}$  and  $B2_{int-ext}$  (wind -Y2)

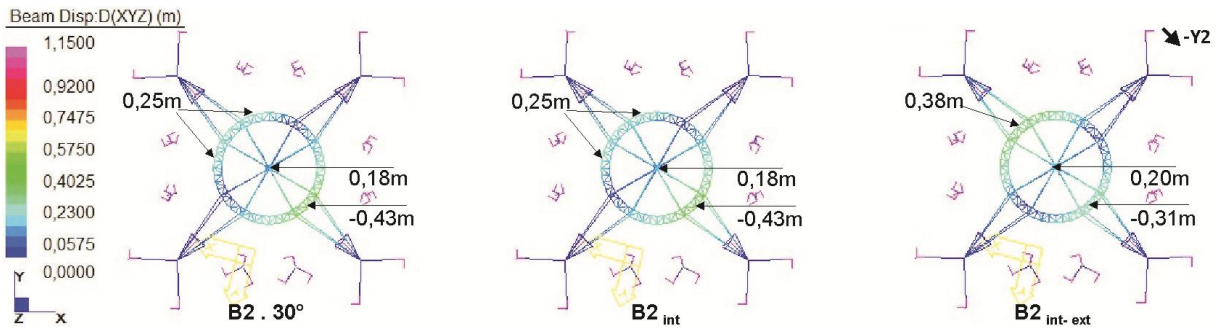


### *Support system displacements*

The support system of  $B2_{int}$  and  $B2-30^\circ$  models (Figure 3.1-86, Figure 3.1-94) showed similar behavior, i.e., displacements of truss ring on the leeward side (suction) were predominant in all wind directions.

In the support system of  $B2_{int-ext}$  model (Figure 3.1-86, Figure 3.1-94, Table 3.1-11) there was a reduction (approx. 30%) in the displacements of truss ring on leeward side (suction) and an increase (approx. 30%) in the displacements of truss ring on the windward side (pressure) in all directions; a result of a decrease in the magnitude of pre-tension applied to support system cables.

Figure 3.1-86 – Support system displacements – B2-30°, B2int and B2int-ext (wind -Y2)

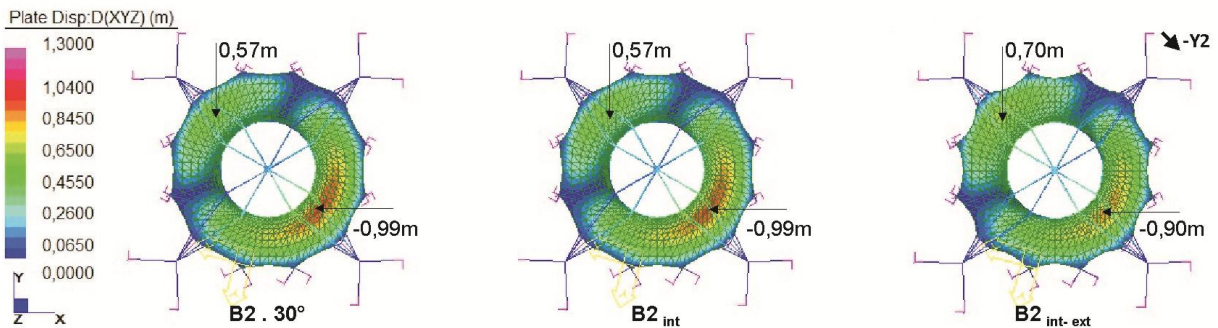


With rain and wind loads, an increasing (approx. 30%) in the displacements of truss ring on the windward side, and a reduction (approx. 20%) in the displacements of truss ring on the leeward side in all directions were observed in B2<sub>int</sub> model. Displacements of truss ring on the windward and leeward sides are similar (approx. 25%) in the B2<sub>int-ext</sub> model. This behavior was also observed on membrane surfaces (internal and external) of the B2<sub>int-ext</sub> model, showing that they exhibit better ability to withstand loads with curvature changes (Table 3.1-11).

*Displacements of external membrane surface*

Large displacements were predominant on the leeward side (suction) in the external membrane surfaces of B2<sub>int</sub>, B2-30°, B2<sub>int-ext</sub> models (Figure 3.1-87, Figure 3.1-95, Table 3.1-11), for all wind directions. However, in the external membrane surface of B2<sub>int-ext</sub> model there was a reduction (approx. 10%) in the displacements on the leeward side (suction) and an increase (approx. 10%) in displacements on the windward side (pressure) in all directions, compared to B2-30° and B2<sub>int</sub> model.

Figure 3.1-87 – External membrane displacements – B2-30°, B2int and B2int-ext (wind -Y2)

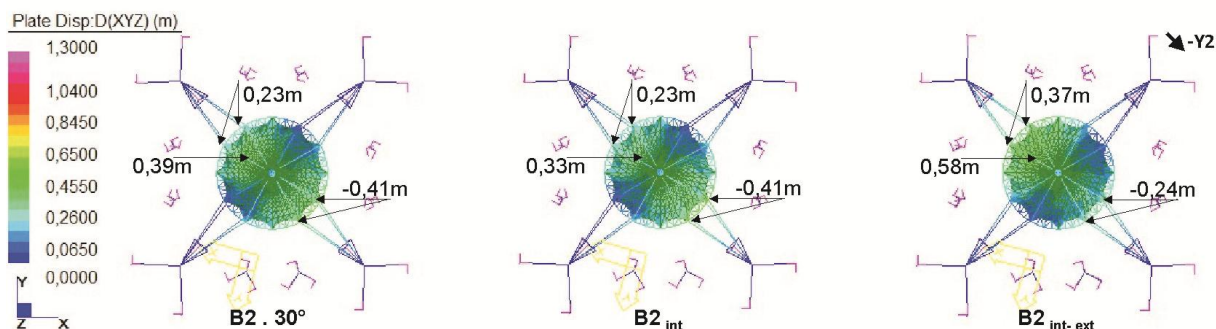


*Displacements of internal membrane surface*

The internal membrane surfaces of B2<sub>int</sub> and B2-30° models exhibited similar behavior (Figure 3.1-88, Figure 3.1-96).

In the internal membrane surface of  $B2_{int-ext}$  model (Figure 3.1-88, Figure 3.1-96, Table 3.1-11) there was a reduction in the suction displacements (approx. 30%) on the leeward side and an increase in the pressure displacements (approx. 35%) on the windward side (overpressure).

Figure 3.1-88 – Internal membrane displacements —  $B2-30^\circ$ ,  $B2_{int}$  and  $B2_{int-ext}$  (wind -Y2)



#### Comparison of models: $B2_{int-ext}$ , $B2_{int}$ and $C2-48^\circ$

A significant reduction in the magnitude of pre-tension applied to the support system cables, as well as a decrease of the mass/area total was observed in  $B2_{int-ext}$  model (with changes of the edge cable curvature in the external membrane and pre-tension ratio of internal surface) compared to  $B2_{int}$  and  $B2-30^\circ$  models. In addition, a reduction in the displacements of membranes and support system on leeward side (derived of suction), and a decrease in the magnitude and areas of stress concentration at the surface anchor points were observed in  $B2_{int-ext}$  model. Thus,  $B2_{int-ext}$  model exhibited a better performance than  $B2_{int}$  and  $B2-30^\circ$  models.

The proposed changes in surface geometry contributed significantly to increase the membrane surface stiffness, especially of the external membrane surface. That is, increasing surface curvatures (smaller radio), it was required lower forces to the membrane surface be in equilibrium and withstand loads (Figure 3.1-80). Consequently, the new geometry of the membrane contributed to increase the stability of the structural system and helped to reduce its mass.

It was observed that  $B2_{int-ext}$  and  $C2-48^\circ$  models showed similar mass/ area and the same pre-tension magnitude applied to the support system cables. However,  $B2_{int-ext}$  model – with less number of masts – showed a significant reduction in the magnitude and areas of stress concentration on external surface and exhibit more homogeneous stress distribution on surfaces (external and internal), and thus, better performance than  $C2-48^\circ$  model.

Figure 3.1-89 – Von Mises stress - B2<sub>int</sub> e B2<sub>int-ext</sub> models

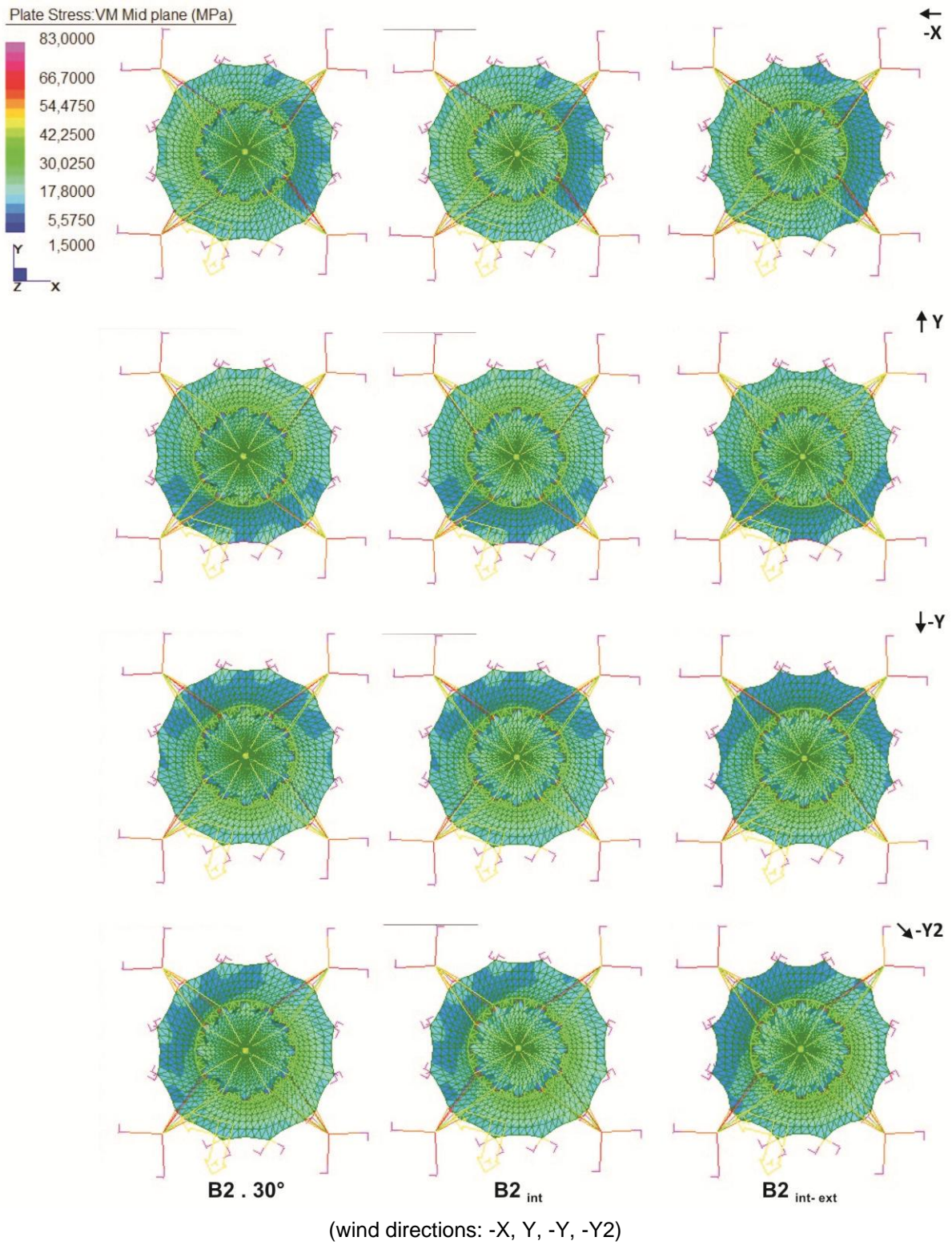
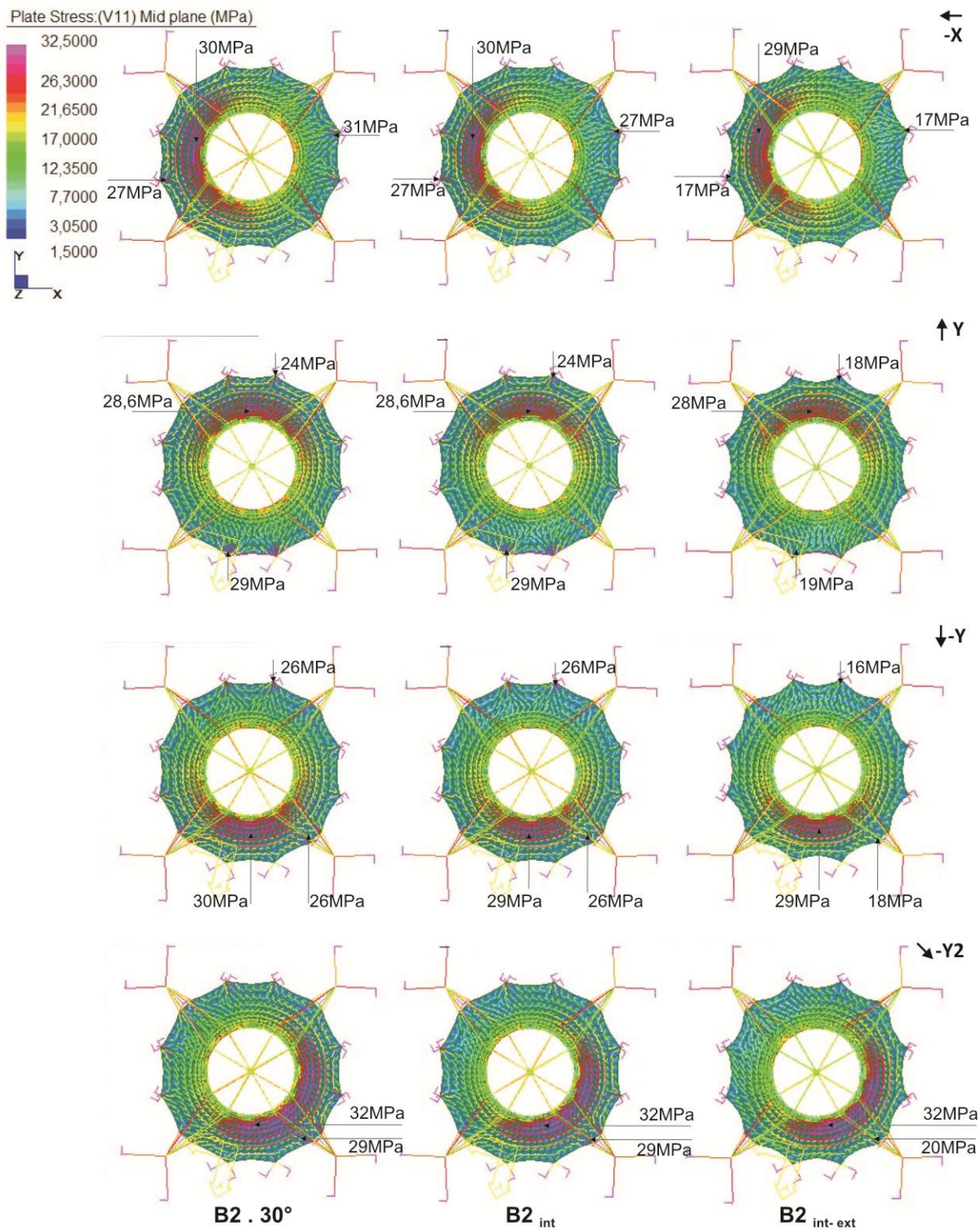


Figure 3.1-90 – Maximum stress trajectories - external surface - B2<sub>int</sub> e B2<sub>int-ext</sub> models



(wind directions: -X, Y, -Y, -Y2)

Figure 3.1-91 – Minimum stress trajectories - external surface - B2<sub>int</sub> e B2<sub>int-ext</sub> models

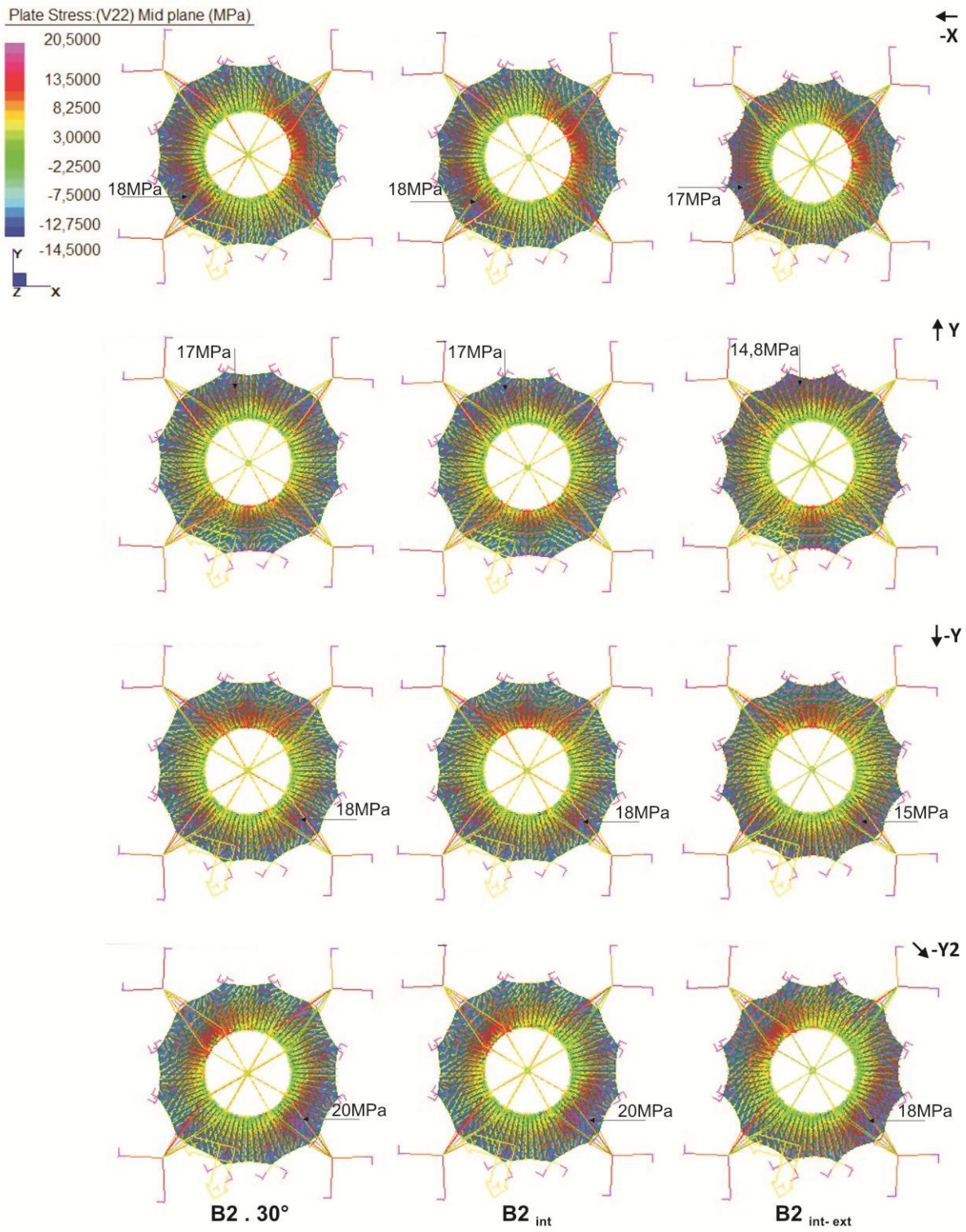
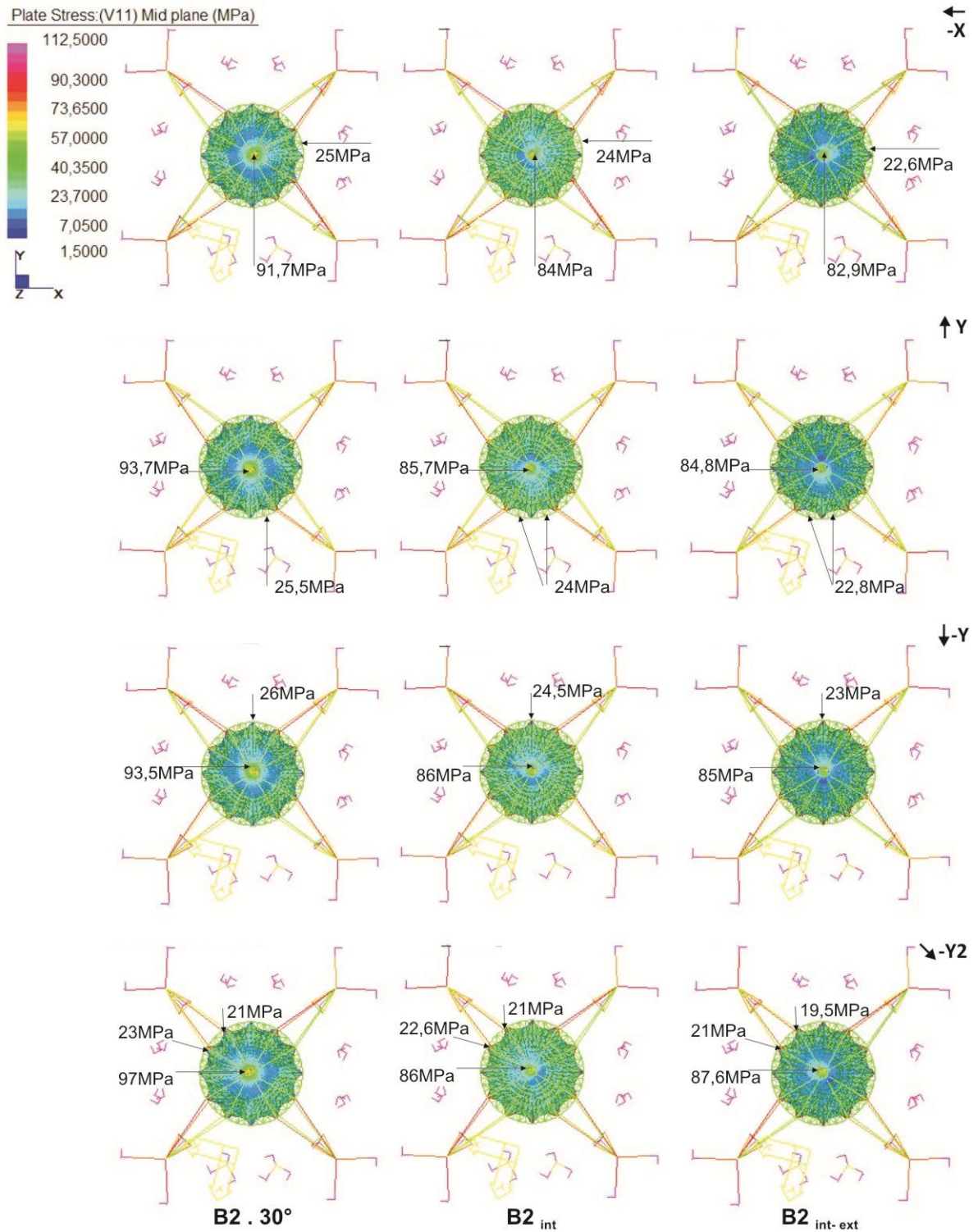


Figure 3.1-92 – Maximum stress trajectories - internal surface - B2<sub>int</sub> e B2<sub>int-ext</sub> models



(wind directions: -X, Y, -Y, -Y2)

Figure 3.1-93 – Minimum stress trajectories - internal surface - B2<sub>int</sub> e B2<sub>int-ext</sub> models

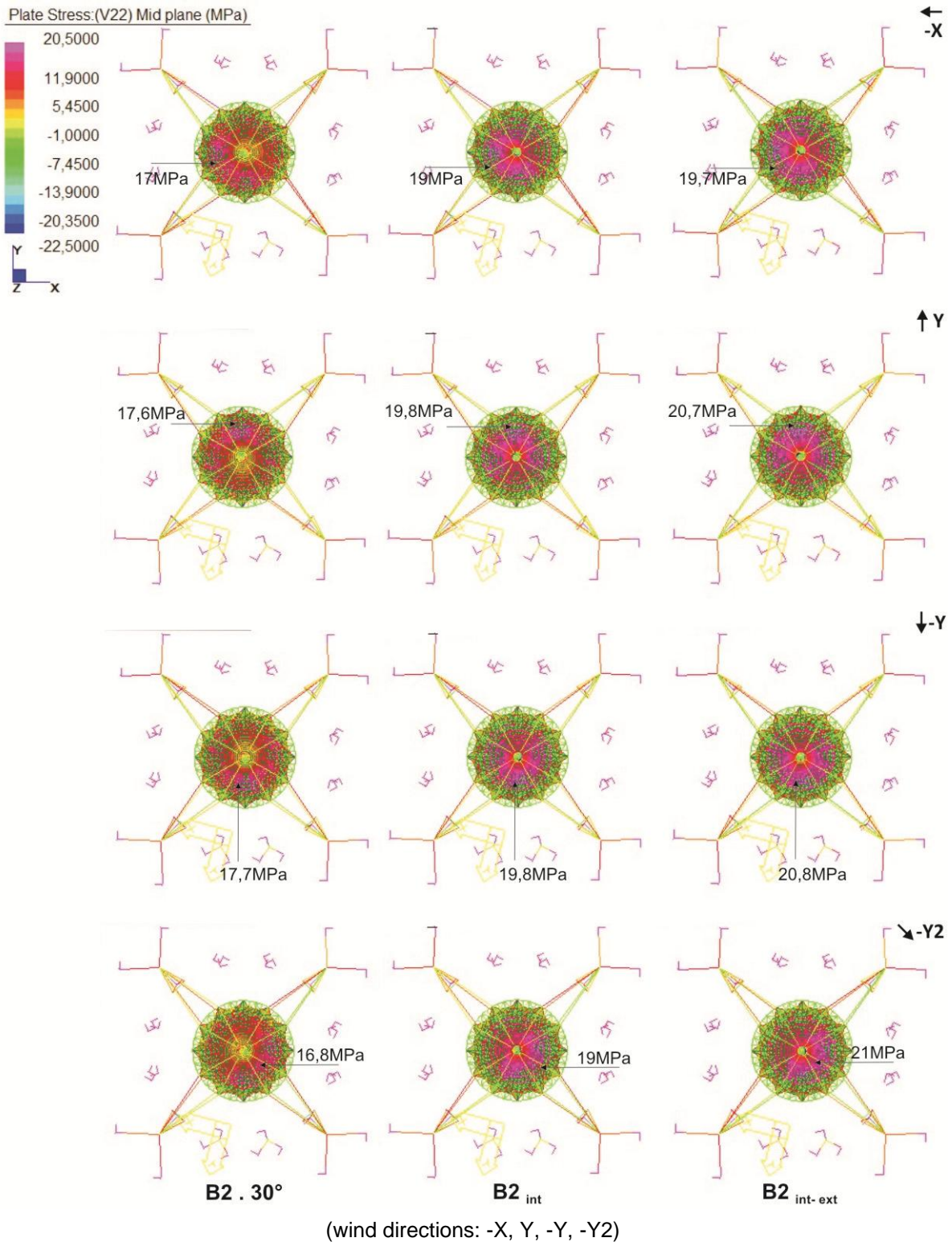


Figure 3.1-94 – Support system displacements – B2<sub>int</sub> e B2<sub>int-ext</sub> models

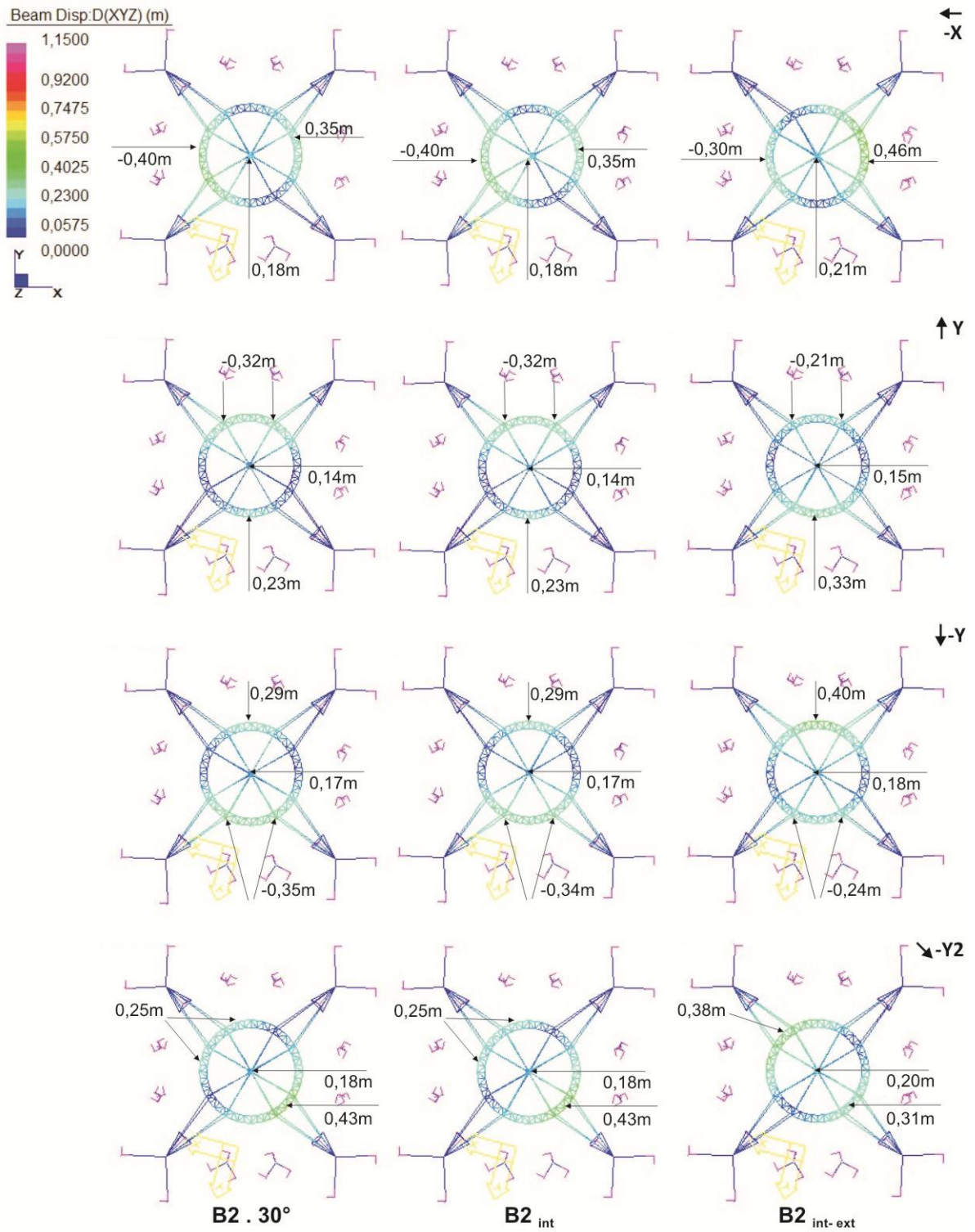


Figure 3.1-95 – External surface displacements - B2<sub>int</sub> e B2<sub>int-ext</sub> models

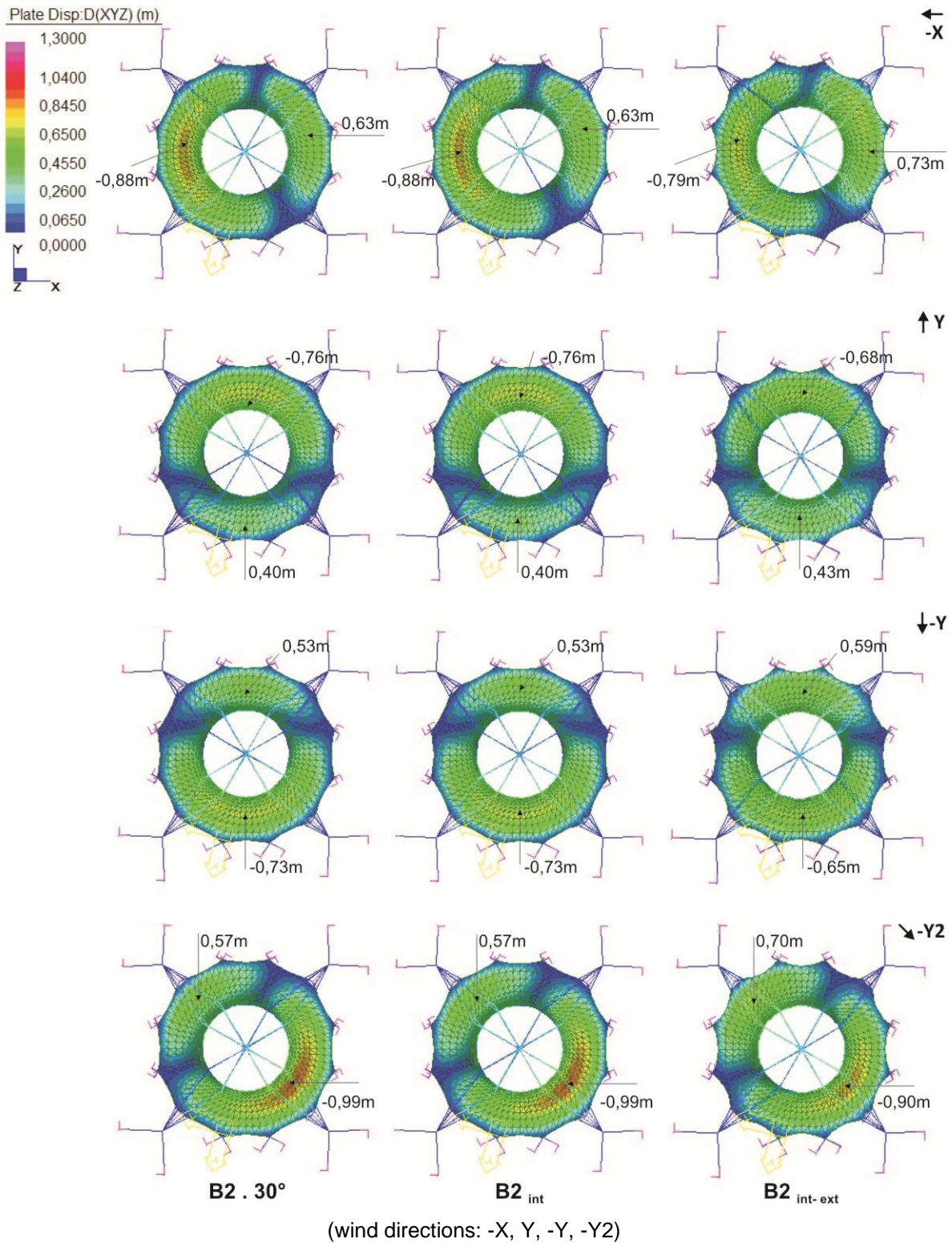
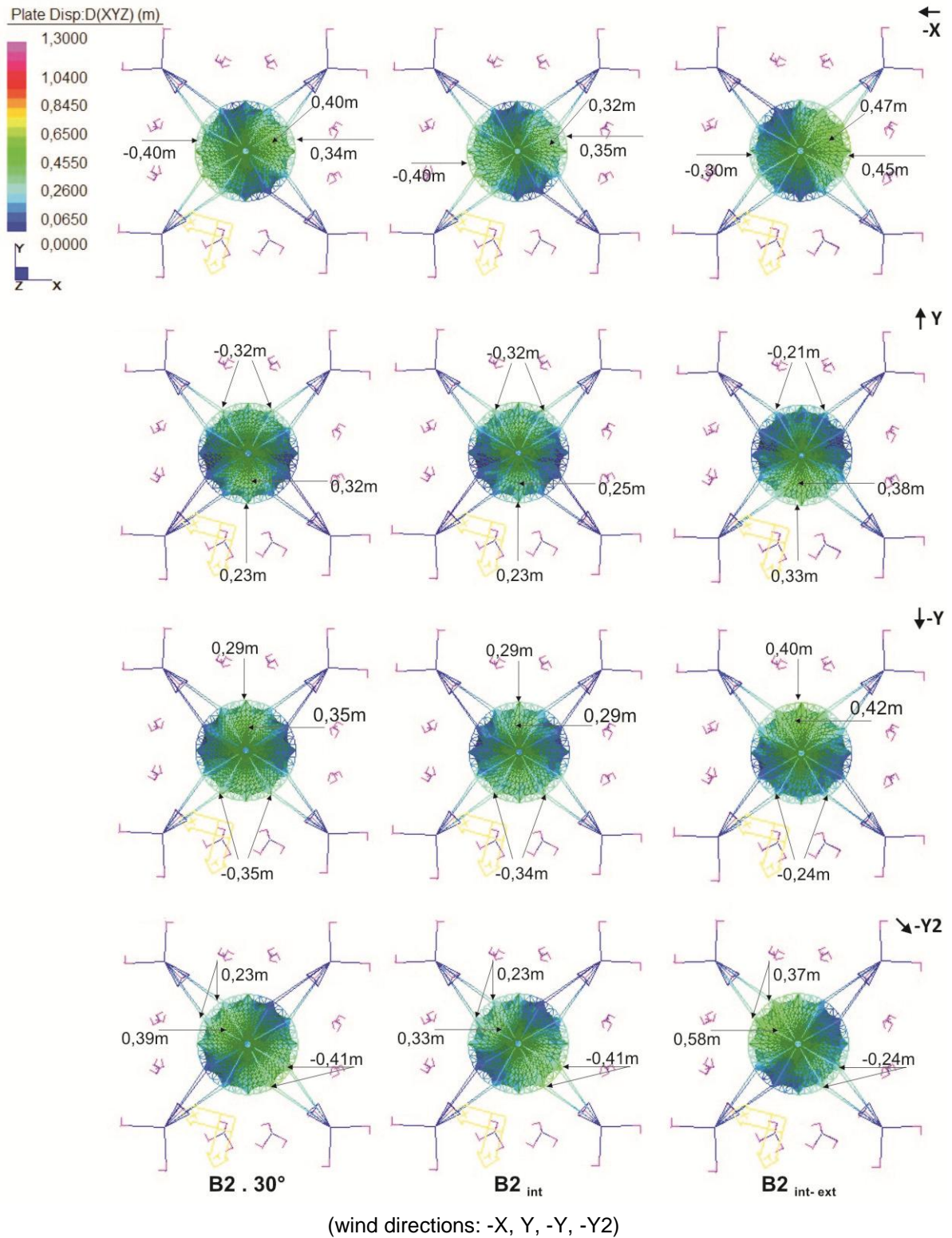


Figure 3.1-96 – Internal surface displacements - B2<sub>int</sub> e B2<sub>int-ext</sub> models



### 3.1.7 1<sup>st</sup> STAGE OF QUALITATIVE ANALYSIS - CONSIDERATIONS

Preliminary analyzes enable to predict the overall behavior of each model as a trend. The proposed variables (number of masts, cable configuration and membrane geometry) added in each case of analysis, contributed towards greater integration and joint work between components, increasing system stiffness, as well as, reducing system mass. Thus, it was verified that the path to optimal performance of the studied project benefit from the structural system arrangement (improving its three-dimensional stability) and membrane geometry (improving its stiffness).

Regarding the structural system arrangement, the system stiffness achieved by increasing the number of masts (first case) was not enough to restrict significantly the displacements of spatial support system and membranes, as observed in the first case. However, the arrangement proposed in the second case, number of masts associated with the new cable configuration enable a more integrated performance of components, creating better conditions for system global stability. The importance of the spatial arrangement of cables and the influence of angles between cables, reducing load path, were also observed.

The changes on membrane surface geometry (case 3) contributed significantly to increase membrane surface stiffness and system global stability as a consequence, enabling the reduction of pre-tension applied to the support system cables and system mass. The reduction in the magnitude and areas of stress concentration at bottom anchor points of external membrane were also verified, and thus the more homogeneous stress distribution on membrane surfaces.

Among models evaluated, C2-48° and B2<sub>int-ext</sub> showed the most favorable conditions for system equilibrium, besides having similar system mass and pre-tension magnitude applied to cables. The performance of C2-48° model was resulted of large number of masts and the new cable configuration. However, the optimal performance a B2<sub>int-ext</sub> model derives from the global stability achieved with structural system arrangement and membrane geometry. In this model, the increase of membrane stiffness enabled support system arrangement with smaller number of masts, greater integration between components and more evenly stress distribution on membranes.

### 3.2 2<sup>nd</sup> STAGE OF QUALITATIVE ANALYSIS / EXPERIMENTAL

In the first stage of qualitative analysis of the performance of a structural membrane roof project it was evaluated the effect of changes in the structural system arrangement and in the membrane geometry on system behavior and performance, taking into account system subjected to load action (Figure 3.2-1).

In this procedure it was evaluated the form of equilibrium of the membrane, i.e., a continuous three-dimensional surface whose definition does not consider the behavior of the material. However, the real form of tensile structures (formed by seam together flat panels) is influenced by material behavior and the geometric distortions of the surface patterning process.

Thus, the second stage of analysis aimed to evaluate experimentally the behavior of the material selected, considering the influence of membrane surface geometry (curvatures) and loads considered, as well as the geometry (form, dimensions) of cutting patterns (Figure 3.2 1). It also investigated the influence of the orientation of the material threads in the flat panel and between adjacent panels (in the seam), as well as the effect of temperature in seam strength, as shown in Figure 3.2-2.

This preliminary analysis aimed also to identify the parameters that should be considered in the compensation procedure of flat panels, and can also help to minimize the differences in geometry and stress distribution between the real form (real model) and form of equilibrium (theoretical model).

This investigation was guided by the experimental tests of the material (biaxial) and seam panels (uniaxial and biaxial), as well as the preliminary analysis of  $B_{2\text{int-ext}}$  model (section 3.1).

The tests were performed at Laboratory for Lightweight structures Essen, University Duisburg-Essen (UDE), Essen, Germany, using the material PES / PVC (FR1400 MEHATOP F - type IV), kindly provided by Mehler Texnologies. The samples used were kindly prepared (cutting and welding) by Carpro company.

Figure 3.2-1 – Qualitative analysis of the performance of a project: 1<sup>st</sup> e 2<sup>nd</sup> stages

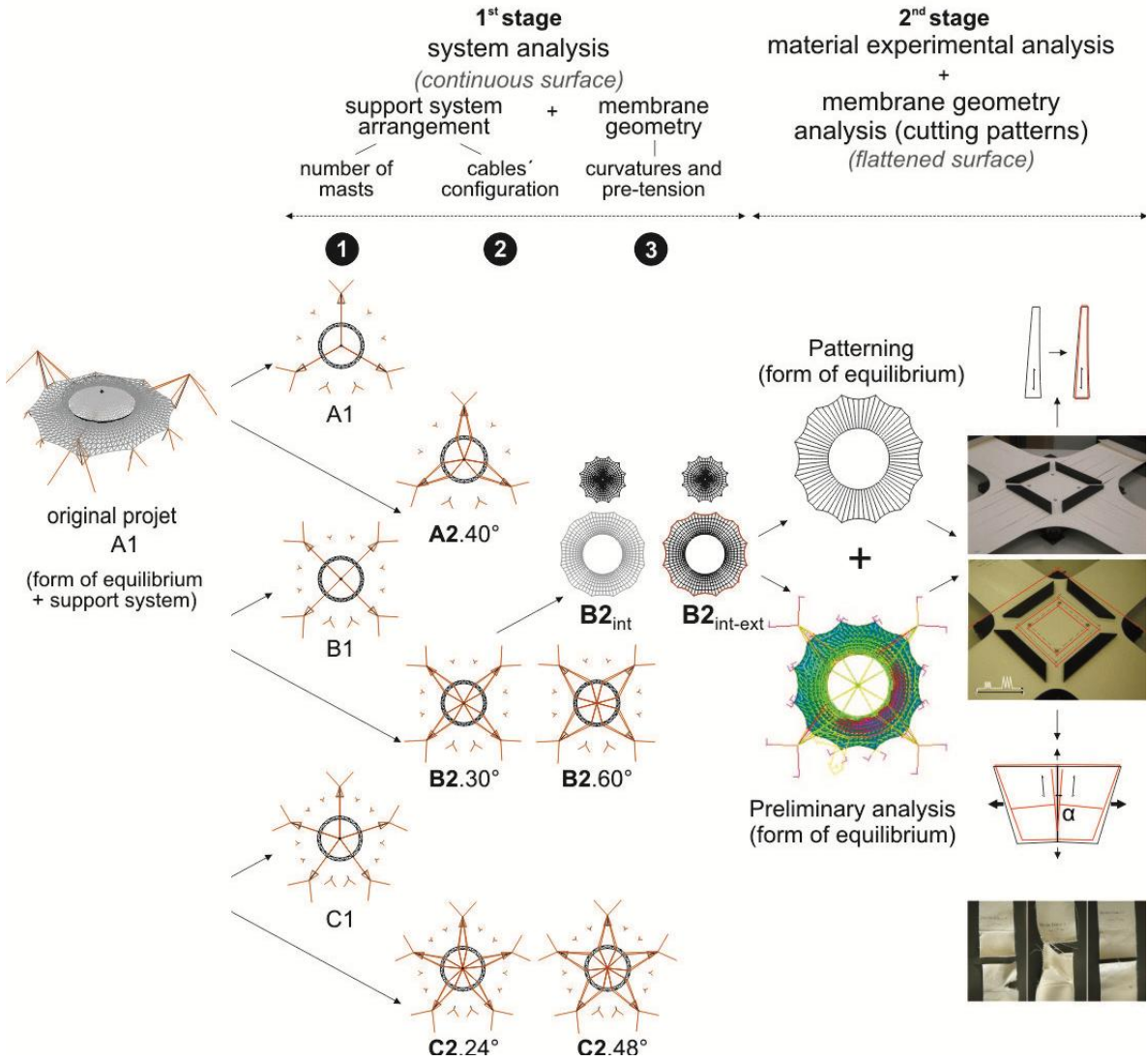
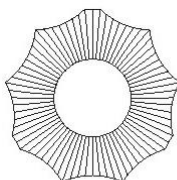
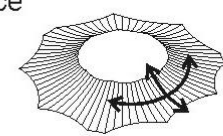
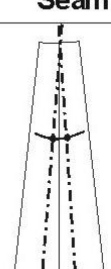


Figure 3.2-2 – Parameters and procedures evaluated in the experimental stage

Patterning	Panel		Yarn direction	Compensation		Seam
	Dimension	Quantity		material strain	% warp % weft	
	D1	Q1	surface 	panel adjustments		 angle between yarns
			panel 			

### 3.2.1 BIAXIAL TEST

The biaxial test consists of applying forces simultaneously in both specimen directions of membrane material evaluated, according to proposed load ratio (magnitude, duration and series of loads applied in warp and weft).

It aims to simulate the material behavior under loads that act in the structure, measuring stresses and strains that guide elastic constants and compensation factors evaluation.

It is performed with temperature of 23°C, with cross-shaped specimen with arms extended toward warp and weft directions. The sample arms showed cuts to ensure stress transfer equally to material (Figure 3.2-3).

Figure 3.2-3– Biaxial test; material PES/PVC

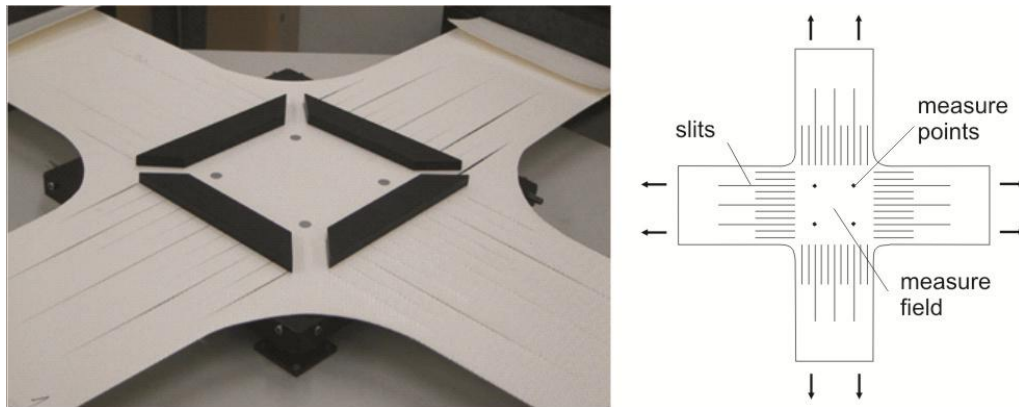
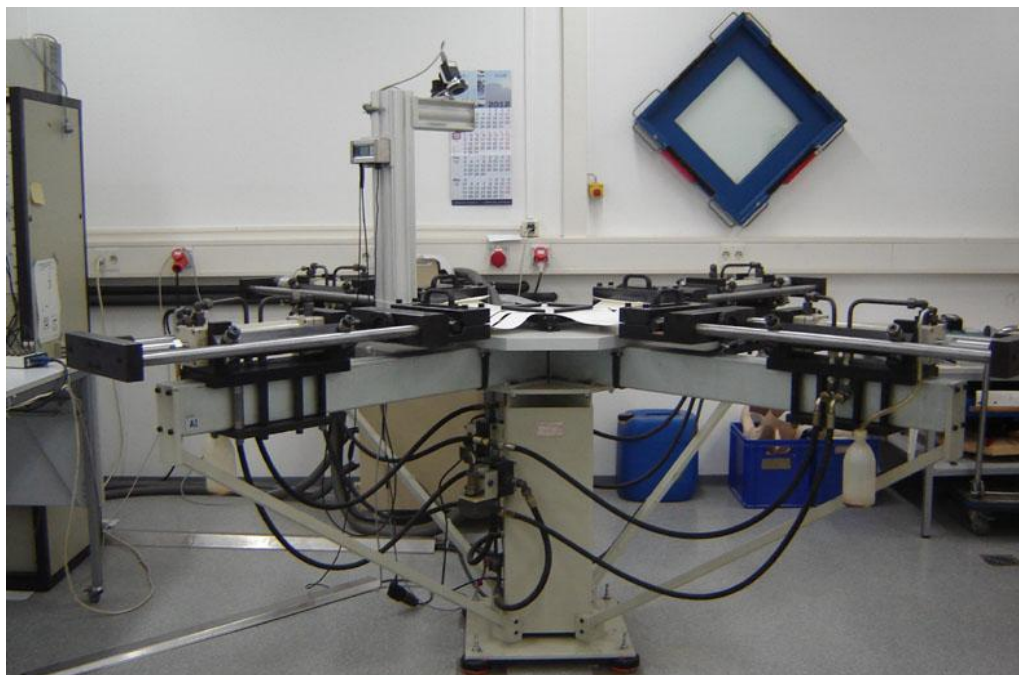


Figure 3.2-4 – Test equipment - Essen laboratory for lightweight structures, UDE



In Figure 3.2-4, it is possible to observe the equipment used for biaxial test at Essen laboratory for lightweight structures-UDE, which has optical measuring system.

The procedures for biaxial test, as well as, methods to evaluate and describe approximately the behavior of material membrane have reference to Japanese Standard MSAJ/M-02-1995 (Testing method for elastic constants of membrane material). It applies to materials type A (glass fiber / PTFE), type B (glass fiber / PVC) and type C (synthetic fiber / PVC), with plain weaving on the assumption that material has anisotropic elastic behavior (MSAJ/M-01- 1993 *apud* MSAJ/M-02-1995).

According to Uhlemann (2011), the set of elastic constants evaluated regarding the procedure described by the Japanese standard should be considered an optimized and fictitious approach, once it describes the behavior of material that includes all load combinations applied in warp and weft. However, in reality one searches the elastic constants derived from the stress field and loads ratio that act on the structure evaluated, i.e., that could represent the overall structure behavior, as material properties vary significantly in relation to each project parameters.

### 3.2.1.1 Characteristics of the structure that guides the biaxial test

This test had as precondition the investigated structure characteristics, i.e., cutting patterns (Figure 3.2-5) and stress field of external surface of  $B2_{int-ext}$  model (Figure 3.2-6, Figure 3.1-90, Figure 3.1-91).

Radial cutting patterns were proposed, aligned to surface principal curvatures. Thus, the directions of the material, warp and weft, follow radial and circumferential directions, respectively. According Wagner (2005) when the material threads are aligned to the principal curvatures, it avoids panel (strip) torsion.

Figure 3.2-5 – Cutting patterns of external and internal surfaces of  $B2_{int-ext}$  model

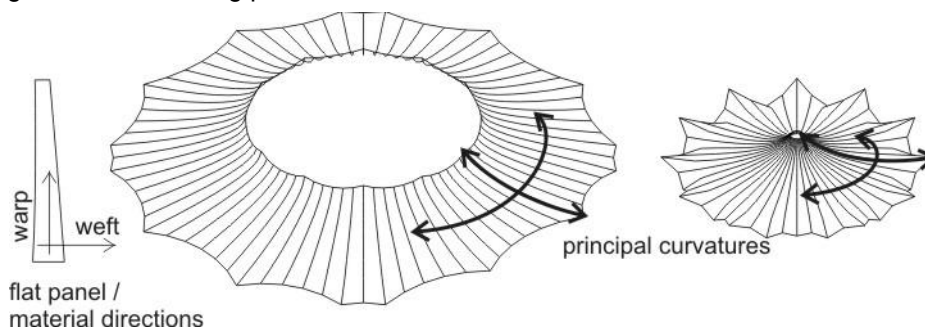
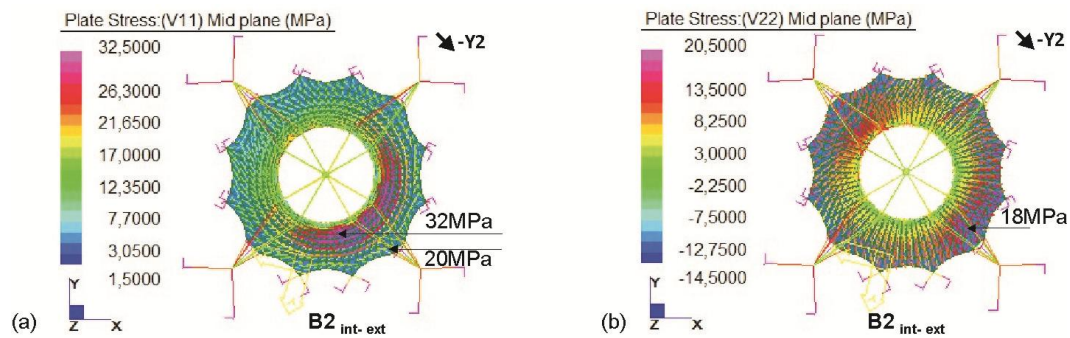


Figure 3.2-6 – Maximum stress (a) and minimum stress (b) – external membrane B2<sub>int-ext</sub> model (-Y2)



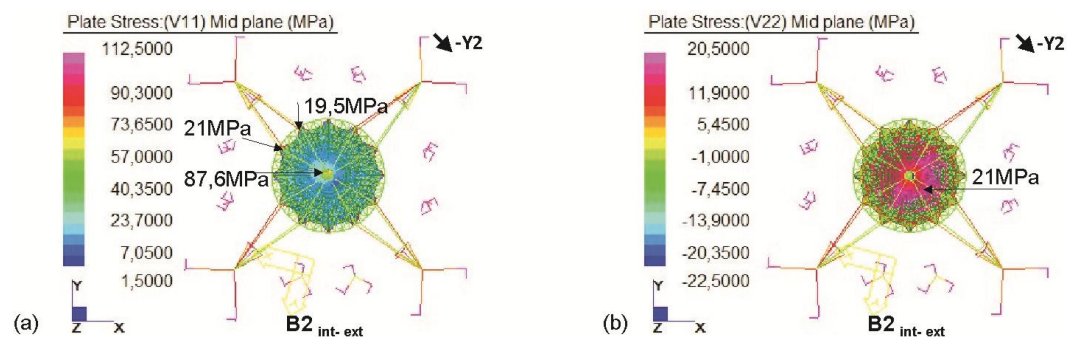
trajectories of maximum stress - circumferential direction; trajectories of minimum stress - radial direction.

In that surface the maximum stress predicted by numerical model (preliminary analysis) under critical load action (wind load) did not exceed 25% of selected material tensile strength (Figure 3.2-6a, Figure 3.1-90). The trajectories of maximum stress were observed in surface circumferential direction (32MPa) which is, in this case, the weft direction; and the trajectories of minimum stress were observed in the radial direction (18MPa) which is the warp direction (Figure 3.2-6b).

Regarding pre-tension level (5% of the selected material strength) the maximum stress predicted in the surface circumferential direction (weft) did not exceed 6.4MPa, and in surface radial direction (warp) the observed stress was 3.2MPa, as shown in Table 3.2-1.

The internal surface showed distinct characteristics of the external surface. The trajectories of maximum stress were observed in the radial direction which is, in this case, the warp direction (Figure 3.2-7, Figure 3.1-92). Thus, the evaluation of the elastic constants and compensation factors for flat panels demand a new test.

Figure 3.2-7 – Maximum stress (a) and minimum stress (b) – internal membrane B2<sub>int-ext</sub> model (-Y2)



trajectories of maximum stress - radial direction; trajectories of minimum stress - circumferential direction.

### 3.2.1.2 Definition of loads and load ratio for biaxial test

For the conducted test pre-tension loads were considered (5% of material breaking strength), as well as mean and maximum values of critical load (wind), i.e., the magnitude and duration of the loads that acts long and short term in structure, respectively.

It was observed that one of major challenges is the definition of mean load magnitude, i.e., the approximate load that predominates during structure life time. Is it fifty percent (50%) of the maximum load? Is it sixty percent (60%) of the maximum load?

It was verified that this value depends on structure characteristics, loads considered, selected material and experience of engineers and manufacturers. In this investigation, the mean load magnitude considered was fifty percent (50%) of the maximum load, i.e., influence of self-weight and pre-tension constant action and lower intensity of the wind load.

The biaxial test was performed as follows: initially the material was tensioned up to pre-tension level in both directions, maintaining this load constant. Then, the directions of warp and weft were subjected to alternated load cycles (50% and 100% of critical load). These load cycles were intercalated with steps of constant load, simulating membrane pre-tensioning.

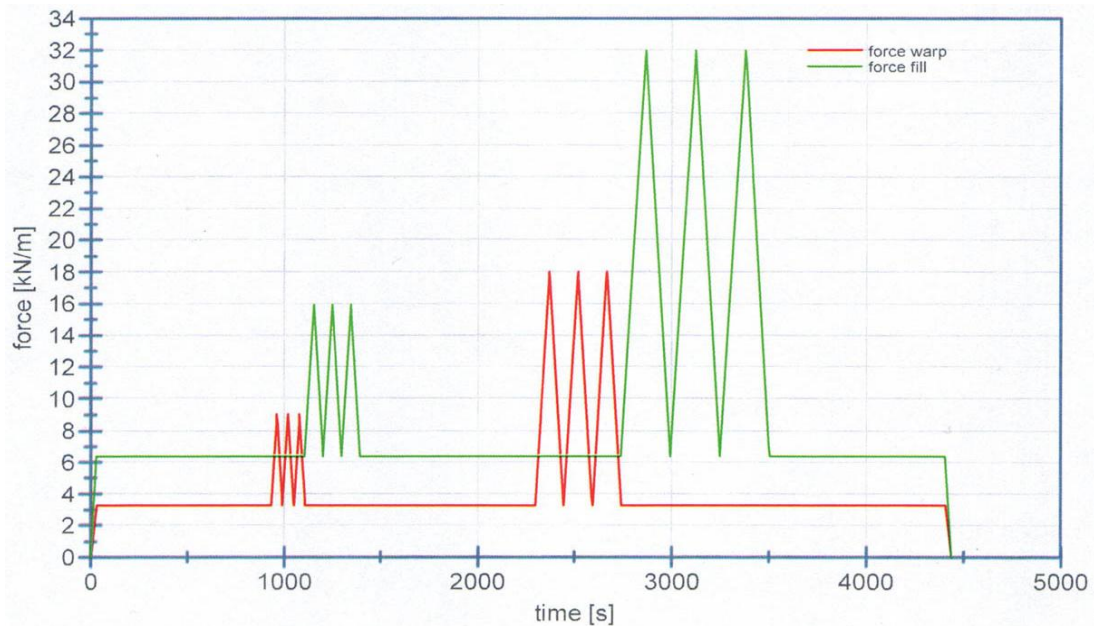
In the initial cycles, it was applied the mean value of the load. Initially, the warp direction was subjected to three cycles of load and unload, maintaining weft direction under constant tension. Then the weft direction was subjected to three cycles of load and unload, maintaining warp direction under constant tension.

The final cycles followed the same procedure, applying the maximum load in the warp and weft directions. The load ratio applied in the material directions at 0.2 (kN/m)/ s, can be seen in Table 3.2-1, Diagram 3.2-1, Appendix G.

Table 3.2-1 – Biaxial test – load ratio applied in the material directions

material directions	1° step	2° step	3° step	4° step	5° step	6° step	7° step
	constant load pre-tension [kN/m]	load cycles mean value of critical load [kN/m]		constant load pre-tension [kN/m]	load cycles maximum value of critical load [kN/m]		constant load pre-tension [kN/m]
warp	3,2	<b>9</b>	3,2	3,2	<b>18</b>	3,2	3,2
weft	6,4	6,4	<b>16</b>	6,4	6,4	<b>32</b>	6,4

Diagram 3.2-1 – Biaxial test - reference values of applied loads in the material directions (warp/ weft)



### 3.2.1.1 Biaxial test - interpretation of results

In this preliminary investigation of membrane material behavior, the stress and deformations that resulted of mean and maximum loads (predicted) that act on the evaluated structure were analyzed. These analyses guided the elastic constants and compensation factors evaluation.

The analysis and test interpretation were supported by observation, photographs, as well as information and diagrams provided by the Laboratory.

The Diagram 3.2-2, describes non linear stress-strain-paths (load-strain-paths) in the material directions (warp and weft) in relation to the applied forces in time. The Diagram 3.2-3 shows the superposition of the following information: deformations in material directions in time and the ratio of applied loads. The Diagram 3.2-4 describes deformations in material directions in time.

It was observed a large positive extension of weft and shortening of warp, according to load ratio and characteristics of the structure.

Diagram 3.2-2 – Force-time (biaxial test) in material directions: warp and weft

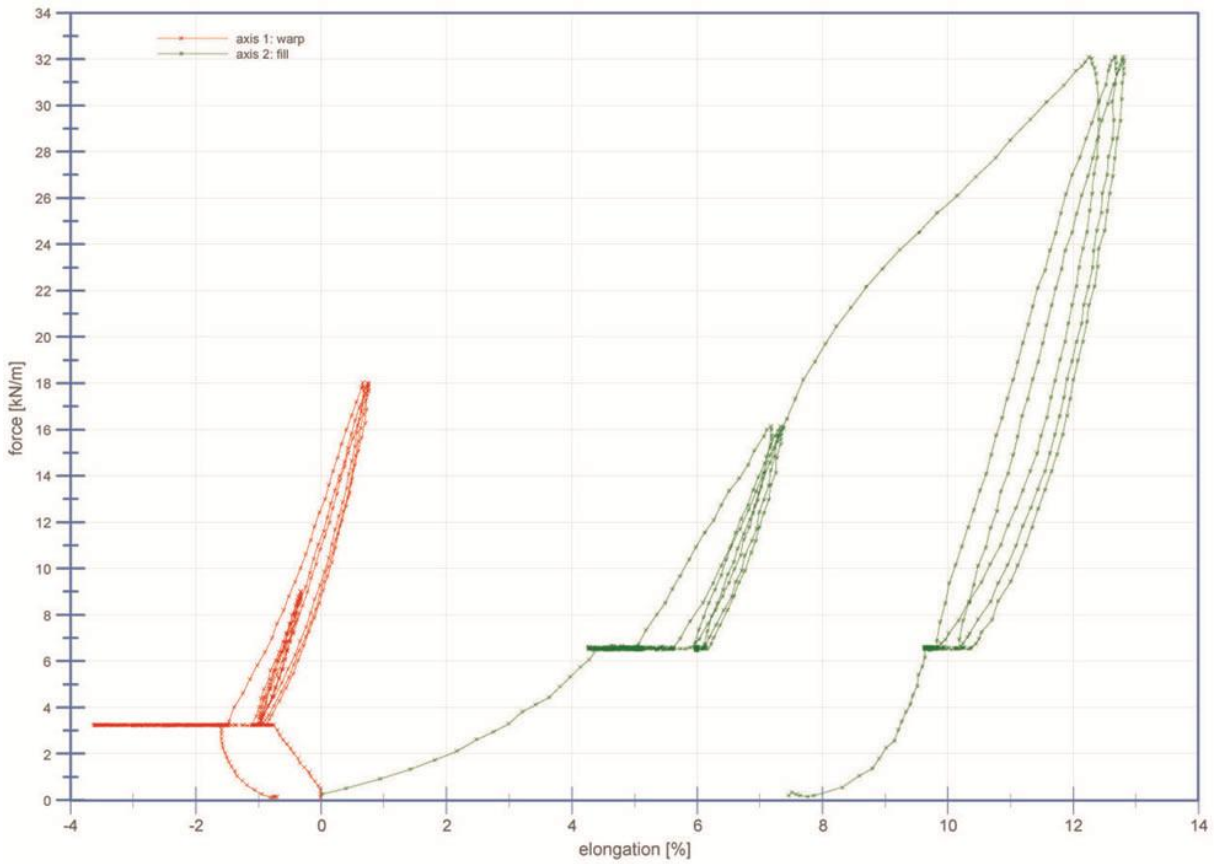
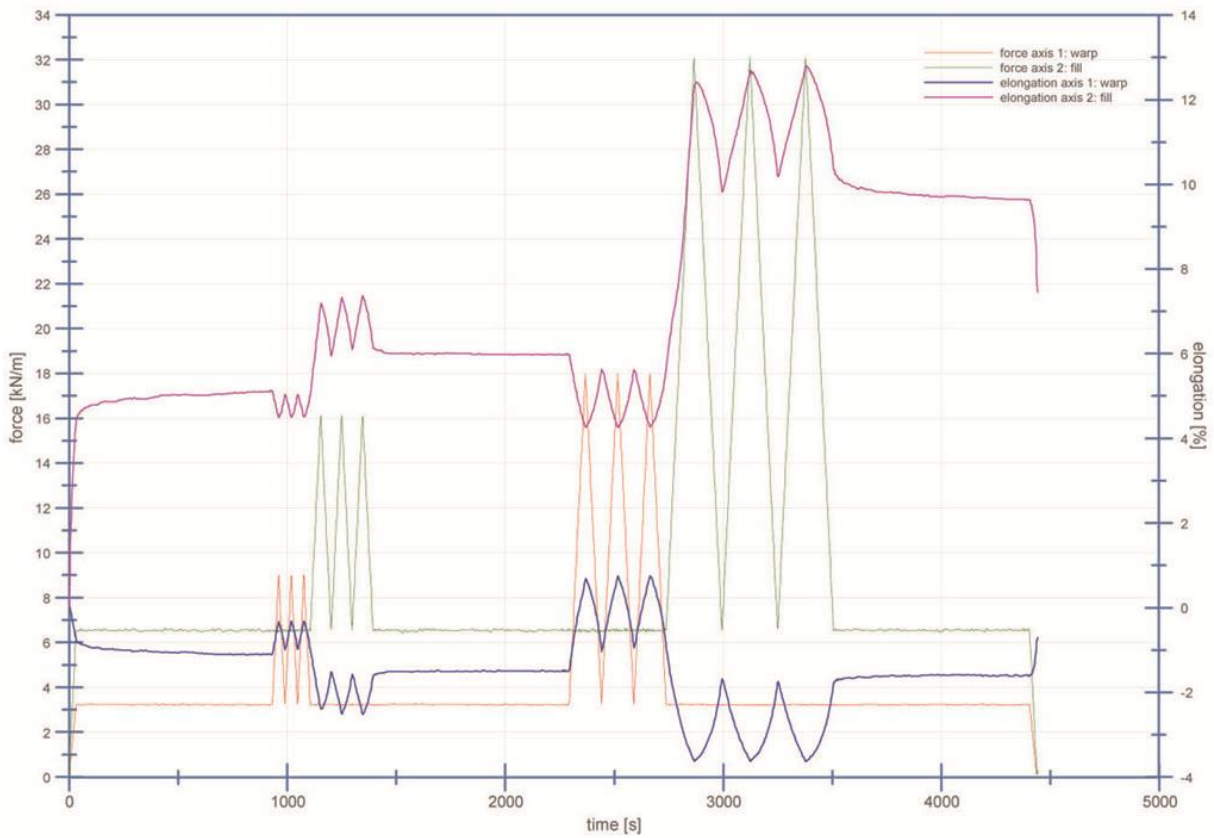


Diagram 3.2-3 – Force-elongation time (biaxial test) in material directions: warp and weft



### *Elastic constants calculation*

In this preliminary investigation, the material constants were determined by a simple linear approximation. It was done a simplified analysis that is not appropriate for cases requiring accurate evaluation of material non-linear behavior.

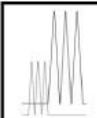
To calculate the elastic constants (elastic modulus and Poisson's ratio) of evaluated structure, it was considered the stresses and strains resulted from the maximum load or short-term load (wind) that act in the evaluated structure.

The elastic modulus or stiffness of warp direction ( $E_1$ ) and weft direction ( $E_2$ ) were obtained by linear adjustment of stress-strain longitudinal curves of the cycles of maximum load (Diagram 3.2-2). Thus, the stresses ( $\sigma$ ) and strains ( $\epsilon$ ) in the warp and weft were replaced by their range or amplitude ( $\Delta\sigma$  and  $\Delta\epsilon$ ), according Blum (2002).

The Poisson ratio ( $\nu_{21}$ ) describing the transverse deformation in the weft direction (2) caused by the load in the warp direction (1) and Poisson's ratio ( $\nu_{12}$ ) describing the transverse deformation in the warp direction (1) caused by the load in the weft direction (2) were also calculated through linear adjustment of transversal deformation curve as a function of longitudinal deformation curve, according to Alvim; Pauletti (2004).

Thus, in Table 3.2-2, it is possible to check the linear adjustment of all stress-strain curves, in the warp and weft directions, resulting of maximum load cycles.

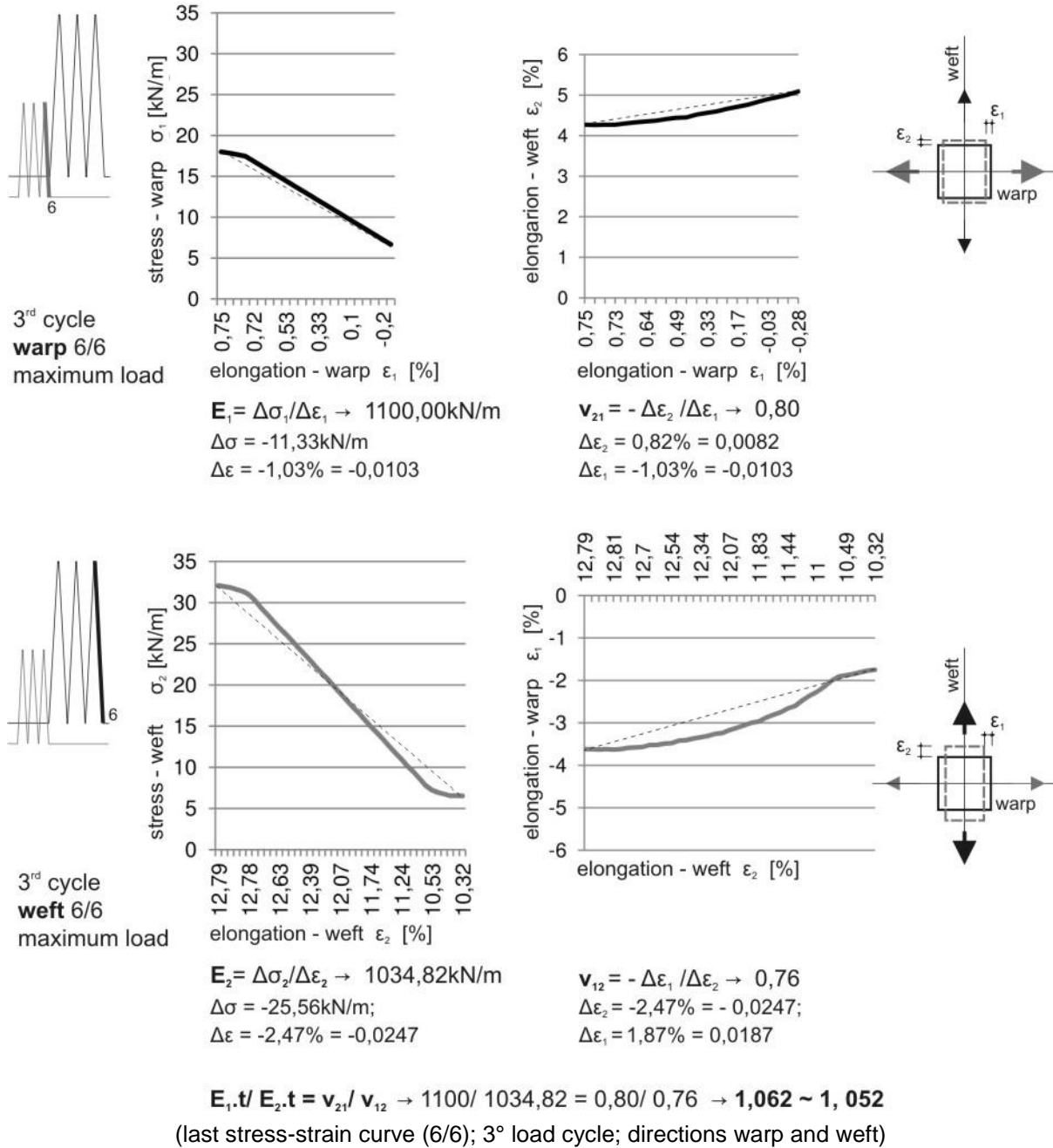
Table 3.2-2 – Evaluation of elastic constants in cycles of maximum load applied to structure

			elastic constants (maximum value)					
			cycle 1		cycle 2		cycle 3	
			1/6	2/6	3/6	4/6	5/6	6/6
warp	$E_1$	kN/m	683,33	872,78	832,77	872,19	866,47	<b>1100,00</b>
	$\nu_{21}$	%	0,78	0,80	0,77	0,80	0,79	<b>0,80</b>
weft	$E_2$	kN/m	356,84	1055,37	903,18	1036,18	983,01	<b>1034,82</b>
	$\nu_{12}$	%	0,46	0,79	0,67	0,75	0,72	<b>0,76</b>
		$E_1 \cdot t / E_2 \cdot t$	1,91	0,83	0,92	0,84	0,88	<b>1,06</b>
		$\nu_{21} / \nu_{12}$	1,70	1,01	1,15	1,07	1,10	<b>1,05</b>

It was observed that load cycles straightening threads in the direction of applied load, increasing its stiffness in each load cycle. Thus, this procedure enabled the measurement of elastic constants in the last load cycle (stress-strain curve 6/6,

3rd cycle, Figure 3.2-8) without the interference of the slacks between threads, as Commentary of Japanese standard MSAJ/M-02-1995.

Figure 3.2-8 – Calculation of elastic constants calculation



In the last stress-strain curve (6/6) of the third cycle (Figure 3.2-8, Table 3.2-2) it was also verified the reciprocal relation between tensile stiffness in the warp and weft directions and the two Poisson's ratios ( $E_{1,t} / E_{2,t} = v_{21} / v_{12}$ ), according to MSAJ/M-02-1995.

It was observed little difference between the stiffness of the warp and weft ( $E_1=1100\text{kN/m}$  and  $E_2=1034\text{kN/m}$ ), i.e., or a tendency of the material to isotropic behavior for the characteristics of investigated structure and load ratio evaluated. Moreover, these elastic modulus had lower magnitude than elastic modulus assumed in the preliminary analysis ( $E =1300\text{kN/m}$ ). So, the results of this test need to be considered in the refined final analysis.

Theoretically, Poisson's ratio for isotropic elastic materials does not exceed the value of 0.5. However, in this analysis, the calculated Poisson's ratio exceeded this value.

According to MSAJ/M-02-1995 in woven fabrics, as the membrane material that was evaluated, the elongation and shrinkage of material are associated with changes in the wave (undulation) of threads (known as crimp interchange), as Figure 3.2-9. Consequently the coefficient Poisson may eventually exceed the value of 1.0. Thus, only one fictitious Poisson's ratio is applied.

#### *Compensation of flat panels*

As described in section 2.6.3, the real shape of tensile membrane structures is influenced by material behavior and the distortions of patterning procedure (geometric procedure).

In this analysis it was evaluated only the influence of the material deformations (warp and weft directions) in the cutting patterns (two-dimensional strips/ flat panels), and to adjust (compensate) the dimension of the flat panels afterward, according to observed behavior.

Resulting deformations of mean load cycles were evaluated, i.e., deformations derived from loads that prevail during the structure life time.

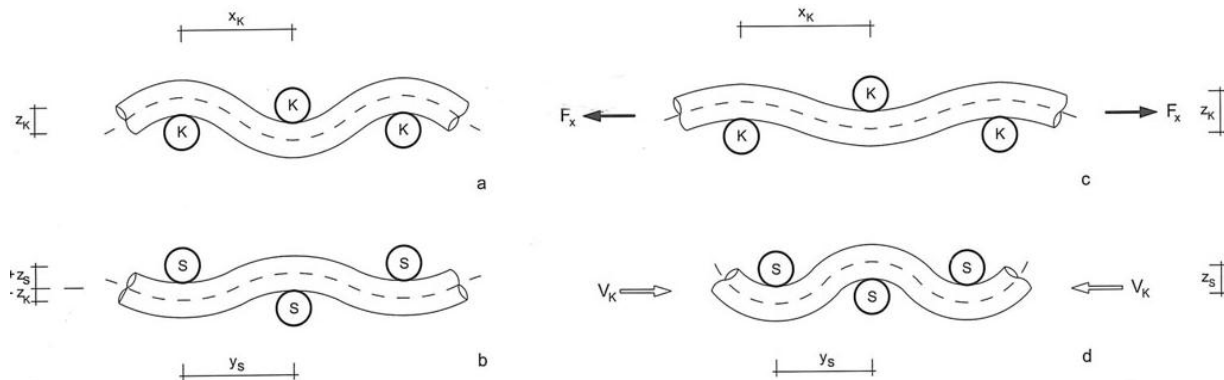
Initially, deformations in the direction of the material were observed (Diagram 3.2-4).

On the initial loading – zero load until the start of the first load step (pre-tension) –, there was a significant deformation of the material directions. It was observed a positive elongation in weft direction (+4.4%) and shrinking (transversal contraction) of warp direction (-0.76%). This behavior was interpreted as a geometric deformation caused by the change of threads curves (crimp interchange, Figure 3.2-9), since this behavior occurred before the pre-tension load and load cycles.

According to MSAJ/M-02-1995, this occurs because the fabrics used in structural membranes (woven and covered), threads and coating are not unified. When threads are tensioned, they undulate in the fabric weave. The magnitude of this wave movement depends on the stress applied to warp and weft directions during the weaving process, and generally do not have the same value.

Then, when the direction of the weft is tensioned, the warp shrinks (has a transversal contraction), and vice versa, because of the slack caused by woven threads waving (weaving wave effect), as shown in Figure 3.2-9. This effect is not an elastic deformation, but a geometric deformation known as crimp interchange, which has great influence on the mechanical properties of the material (HUNGTINGTON, 2003; MSAJ/M-02-1995).

Figure 3.2-9 – Crimp interchange



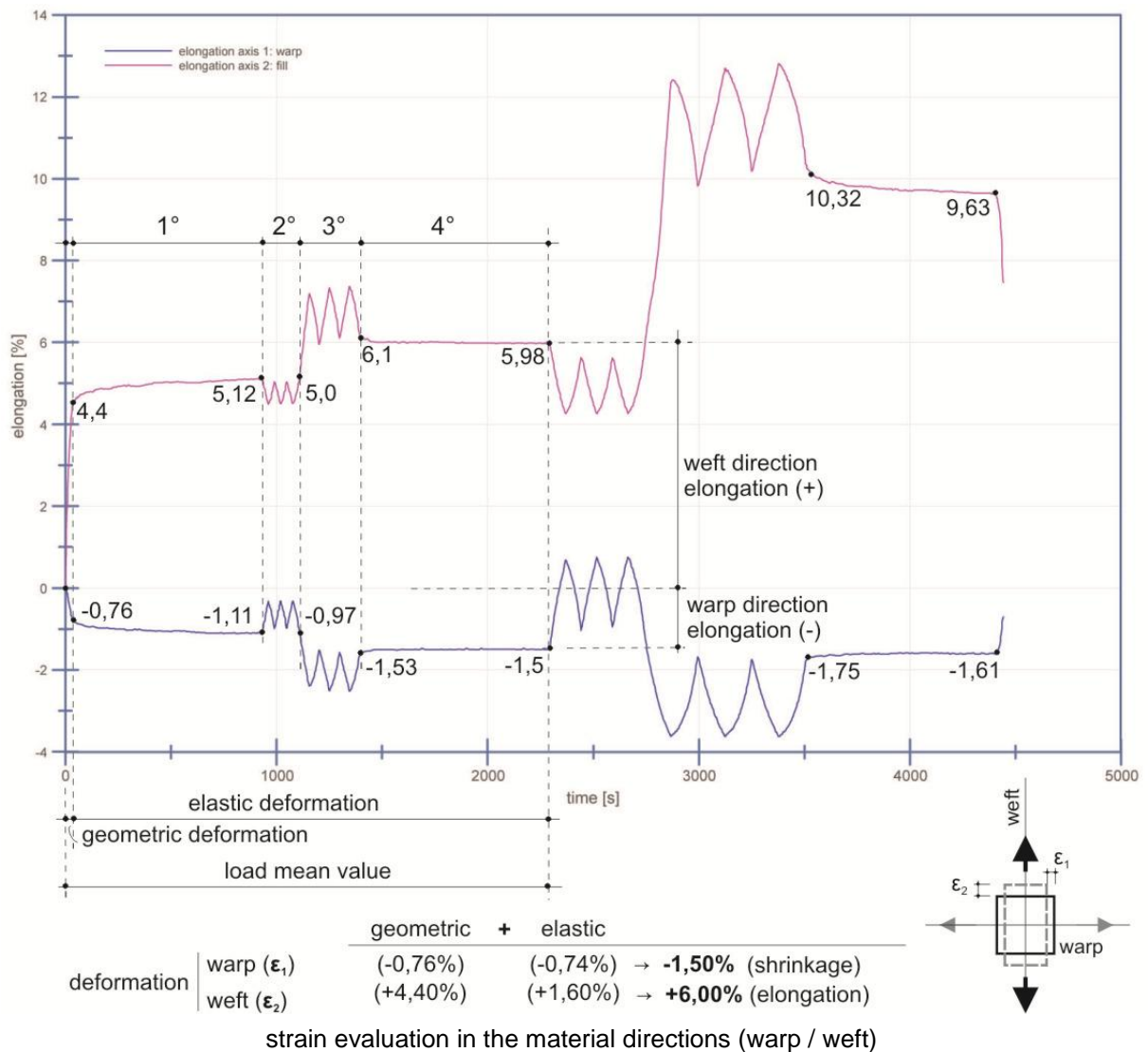
(a, b) threads not deformed, (c, d) deformed threads: tensioned weft (S); shrunk warp (K)

Source: SEIDEL, 2009, p.42.

However, after each load step applied to material – constant pre-tension ( $1^\circ$  and  $4^\circ$  load steps) and mean load cycles ( $2^\circ$  and  $3^\circ$  load steps) –, elastic deformations were observed in the material directions (Diagram 3.2-4).

Thus, the total deformation of material was considered a sum of elastic and geometric deformations observed.

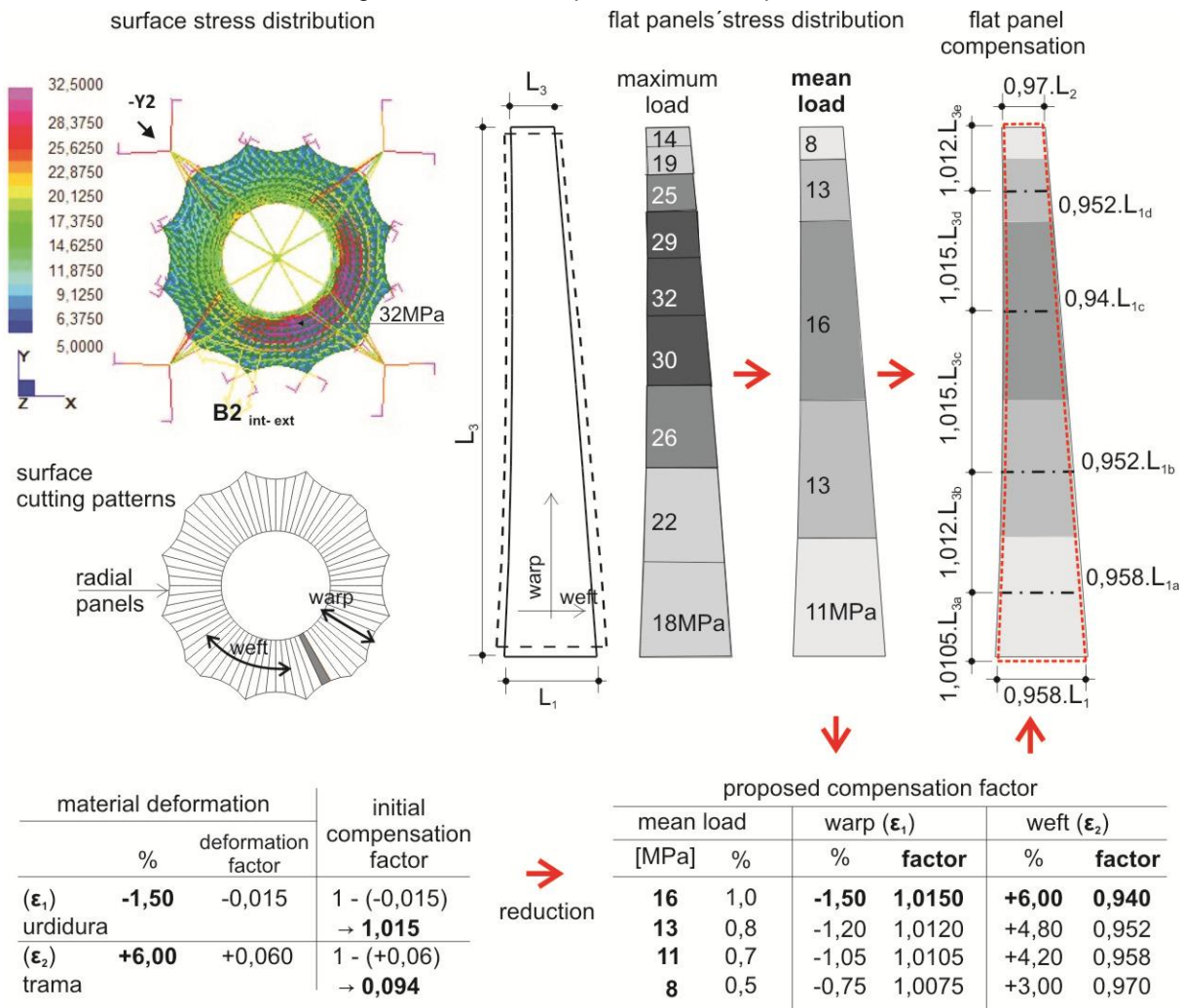
Diagram 3.2-4 – Elongation-time (biaxial test)



Then, the strains were evaluated in the material directions in relation to cutting patterns geometry and stress distribution on membrane surface. This procedure was carried out in five steps (Figure 3.2-10):

1° Step: it was observed the stresses distribution on the external surface in all directions (Figure 3.2-6, Figure 3.1-90, Figure 3.1-91). The highest stress areas were observed on leeward side, and correspond to the areas of larger displacements caused by wind suction, (Figure 3.1-95). It can be observed, for example, the stresses distribution on external surface and in the flat panel, under wind load (-Y2 direction), according to Figure 3.2-10.

Figure 3.2-10 – Compensation of flat panels



2° Step: then it was proposed the division of flat panels in five stress areas, according to stress distribution (mean load) on the surface.

3° Step: the compensation factors (reduction and or increase) of flat panels dimensions were calculated, considering only material deformation (stretching and shrinking); it was considered as a reference, an example of compensation factor calculation for pneumatic spherical buildings (OTTO *et al.*, 1983, p.77).

4° Step: it was proposed the reduction of these compensation factors in accordance with the stress distribution observed at surface and flat panels; this reduction aimed to avoid excessive cutting or addition of material, and hence regions of stress peak and or difficulties during assembly.

5° Step: to adjust the dimensions of the flat panels, reduced compensation factors were multiplied by the initial dimensions of the flat panels (two-dimensional cutting

patterns) according verified strains in the material directions (warp and weft) and proposed stress distribution.

This procedure seeks to contribute to minimize the differences between the form of equilibrium and the real shape, to prevent wrinkles caused by deformation of the material, and for the surface achieves the proposed geometry under pre-tension.

### 3.2.2 SEAM BIAXIAL TEST

At this stage it was evaluated the influence of orientation of the material, and consequently the angle between adjacent flat panels in the seam, since seam is a geometric discontinuity in the flow of forces of curved surface (SEIDEL 2009).

Firstly, it was observed the cutting patterns of the following study models: A2-40°, B2-30°, B2<sub>int-ext</sub>, C2-24°, C2-48° (where, B2-30°= B2<sub>int-ext</sub> and C2-24°= C2-48°). For these models it has been proposed radial cutting patterns, aligned to the principal curvatures of the surface (Figure 3.2-11).

The approximated angles of the cutting patterns in the external surfaces of these models are 4,8° and 5° and the internal surfaces the angles are 6°, 6.6° and 7.5°. Therefore, threads of material (warp and weft) are not parallel to the seam, but have small rotation relative to the seam.

To guide do this preliminary investigation, the external surface of B2<sub>int-ext</sub> model was chosen, evaluating the influence of the angle of 5° between panels.

In order to compare and evaluate the effect of this angle in the joint of panels by seam, biaxial tests were performed at angles of 0°, 4° and 8°. Thus, in the first test the warp direction is parallel (0°) to seam axis, and thus, the material directions are alined to the flow of forces. In the other tests the warp was rotated at 2° and 4° to seam axis (Figure 3.2-12).

In these tests, the seam of specimens was performed by hot welding with overpass of 8cm (Figure 3.2-13).

Figure 3.2-11 – Cutting patterns’ angles of external and internal surfaces (A2-40°, B2<sub>int-ext</sub> e C2-48°)

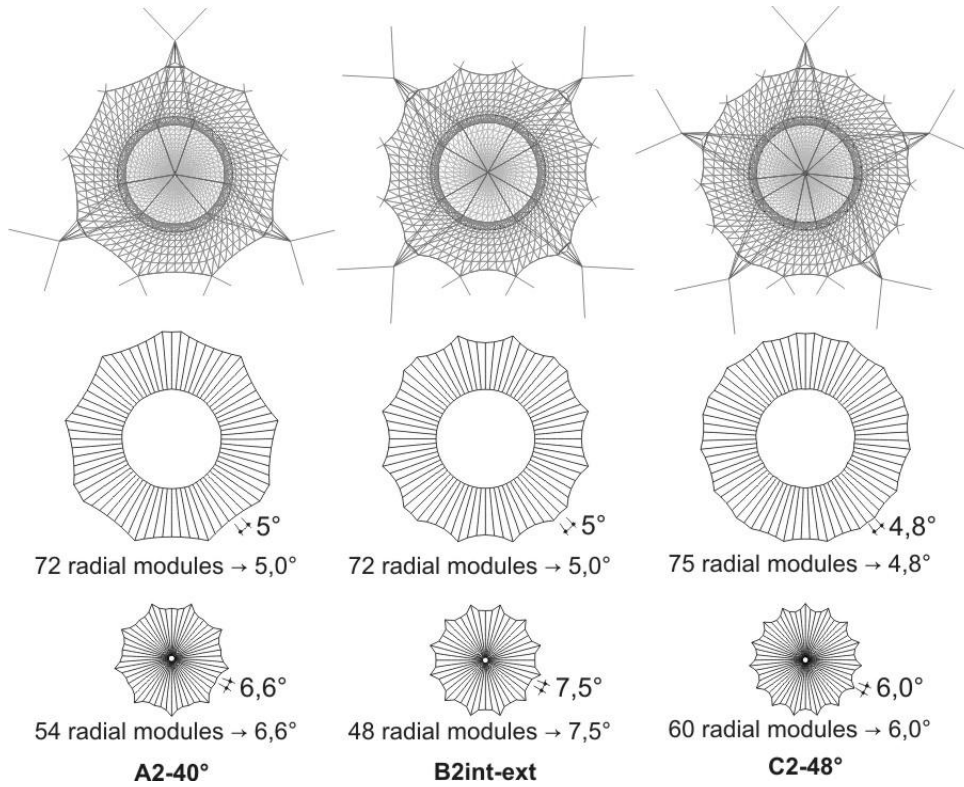
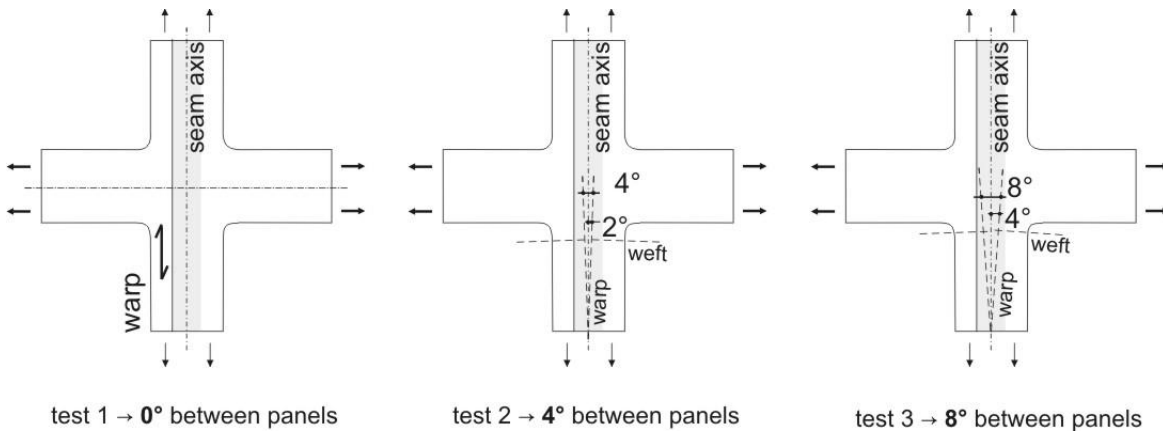


Figure 3.2-12 – Seam biaxial tests – angles between panels evaluated: 0°, 4° e 8°



3.2.2.1 Definition of loads and load ratio for biaxial seam test

In the three biaxial seam tests (angles of 0°, 4° and 8° between panels) pre-tension load, mean and maximum values of the critical load were considered.

In these tests, the material was initially tensioned at pre-tension level in both directions. The warp direction remained this constant tension throughout the test. However, the weft has been loaded in several load cycles (mean and maximum

values of critical load); these cycles were interspersed with steps of constant load (simulating membrane pre-tension). The load ratio applied to material directions at 0.2 (kN/m)/s can be seen in Table 3.2-3, Diagram 3.2-5 and Appendix G. It is possible to observe that different loads were applied in the directions of the material.

The specimens were marked with measuring points and lines, to favor material behavior observation (Figure 3.2-13).

Table 3.2-3 – Biaxial seam test – load ratio applied in material directions

material directions	1° step	2° step	3° step	4° step	5° step
	constant load pre-tension [kN/m]	load cycles mean value of critical load [kN/m]	constant load pre-tension [kN/m]	load cycles maximum value of critical load [kN/m]	constant load pre-tension [kN/m]
warp	3,2	3,2	3,2	3,2	3,2
weft	6,4	16	6,4	32	6,4

Diagram 3.2-5 – Seam biaxial test – load values applied

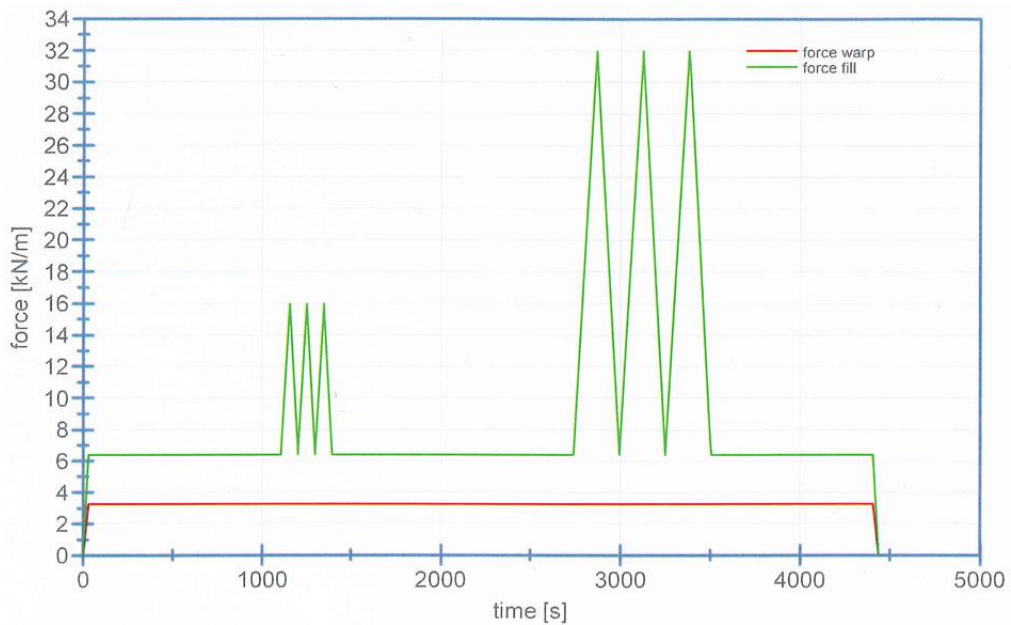
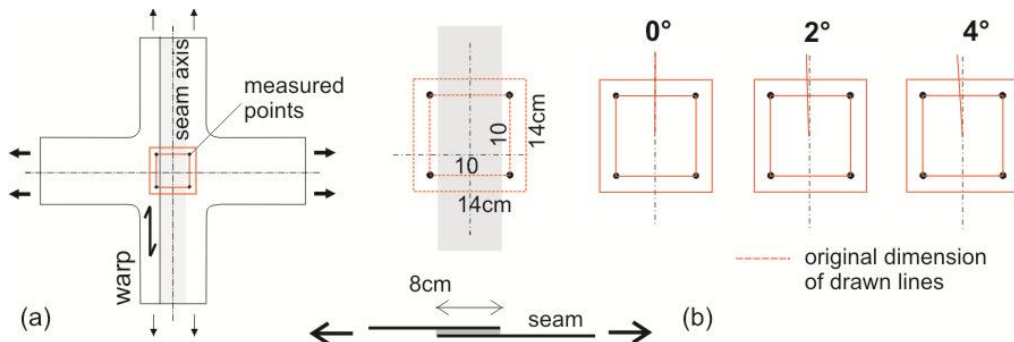


Figure 3.2-13 – (a) Reference points and lines marked in the specimen; (b) seam/ overlap of panels



3.2.2.2 Interpretation of the results of seam biaxial test

The analysis and interpretation of results were conducted based on the information and diagrams provided by the Laboratory, as well as observation and photographs of the biaxial seam tests (angles of 0°, 4° and 8° between panels).

Weft positive elongation and warp shrinkage were observed in all seam biaxial tests. The warp direction presented significant elastic deformation (approx. 70%), while in the weft direction the elastic deformation was approximately 57% (Diagram 3.2-6, Diagram 3.2-7, Diagram 3.2-8, and Table 3.2-4).

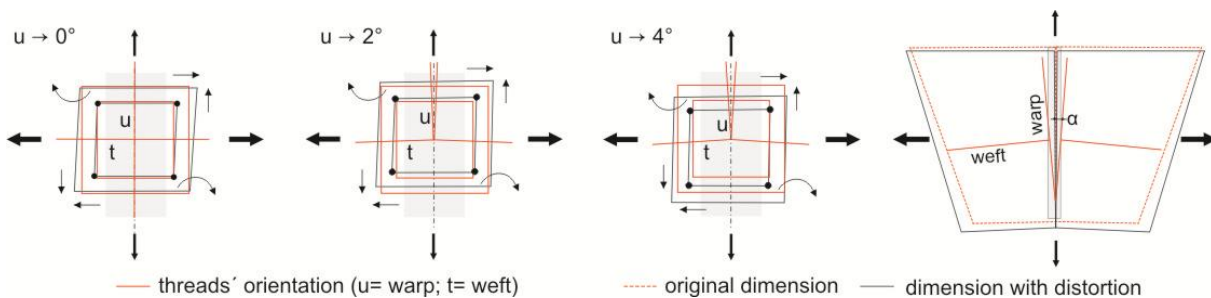
Table 3.2-4 – Seam biaxial tests - material deformation

angles between panels/ material direction		deformation (%)		
		geometric	elastic	total
0°	warp ( $\epsilon_1$ )	-0,48	-0,97	<b>-1,45</b>
	weft ( $\epsilon_2$ )	+ 2,65	+ 3,27	<b>+ 5,92</b>
4°	warp ( $\epsilon_1$ )	-0,55	-1,00	<b>-1,55</b>
	weft ( $\epsilon_2$ )	+ 2,61	+ 3,33	<b>+ 5,94</b>
8°	warp ( $\epsilon_1$ )	-0,40	-1,12	<b>-1,52</b>
	weft ( $\epsilon_2$ )	+ 2,57	+ 3,35	<b>+ 5,92</b>

The deformation magnitude of material directions (weft and warp) may be considered similar for all angles between adjacent flat panels in the seam that was evaluated, according to Diagram 3.2-9 and Table 3.2-4.

However, comparing original and distorted lines on specimens, it was observed the distortion of the material (Figure 3.2-15, Figure 3.2-16). The distortion of the material in seam tests with angles 0° and 4° (between panels) occurs in the same side and direction, but with different intensity. In the seam test with 8° between panels, the distortion in seam axis occurred in distinct side that was observed at angles 0° and 4° and with great intensity (Figure 3.2-14).

Figure 3.2-14 – Threads' direction related to seam and applied loads direction



Increasing the angle ( $\alpha$ ) between panels and the applied loads, the material distortion (or shear deformation) became more intense. This behavior results from sliding movement and rotation between warp and weft thread, and is caused by different forces acting on material directions (Table 3.2-3, Diagram 3.2-5), as well as thread orientation in relation to force direction (warp at  $0^\circ$ ,  $2^\circ$  and  $4^\circ$  to seam axis), as shown in Figure 3.2-15 and Figure 3.2-16.

According Seidel (2009) when resistance to shear strain or distortion (caused by thread movement) is small, there is little stress in material. When the threads obstruct the movement of each other, the resistance to further movements grows rapidly. As distortion between warp and weft threads can only cause small stress in the material, since woven fabrics have low shear stiffness. So, it is important to limit the angle and therefore the width of the flat panels, avoiding blockage in the rotation between threads.

This analysis allowed observing material deformations and distortions (shear) of the material. Both increased with applied intensity of the loads. However, the distortion was influenced by different forces applied in warp and weft, and principally by the increase of angle ( $\alpha$ ) between adjacent panels, i.e., orientation of the threads regarding to seam and to the direction of the applied forces.

Thus, this preliminary research confirms the importance to evaluate, in an integrate way the geometry of the panels (form and dimensions), the angle between adjacent panels, material direction in relation to the principal curvatures, as well as direction and magnitude of applied forces, aiming to reduce distortions between adjacent flat panels and in the curved surface, besides avoiding unexpected stiffness and failure.

Diagram 3.2-6 – Biaxial seam test – angle between panels: 0°

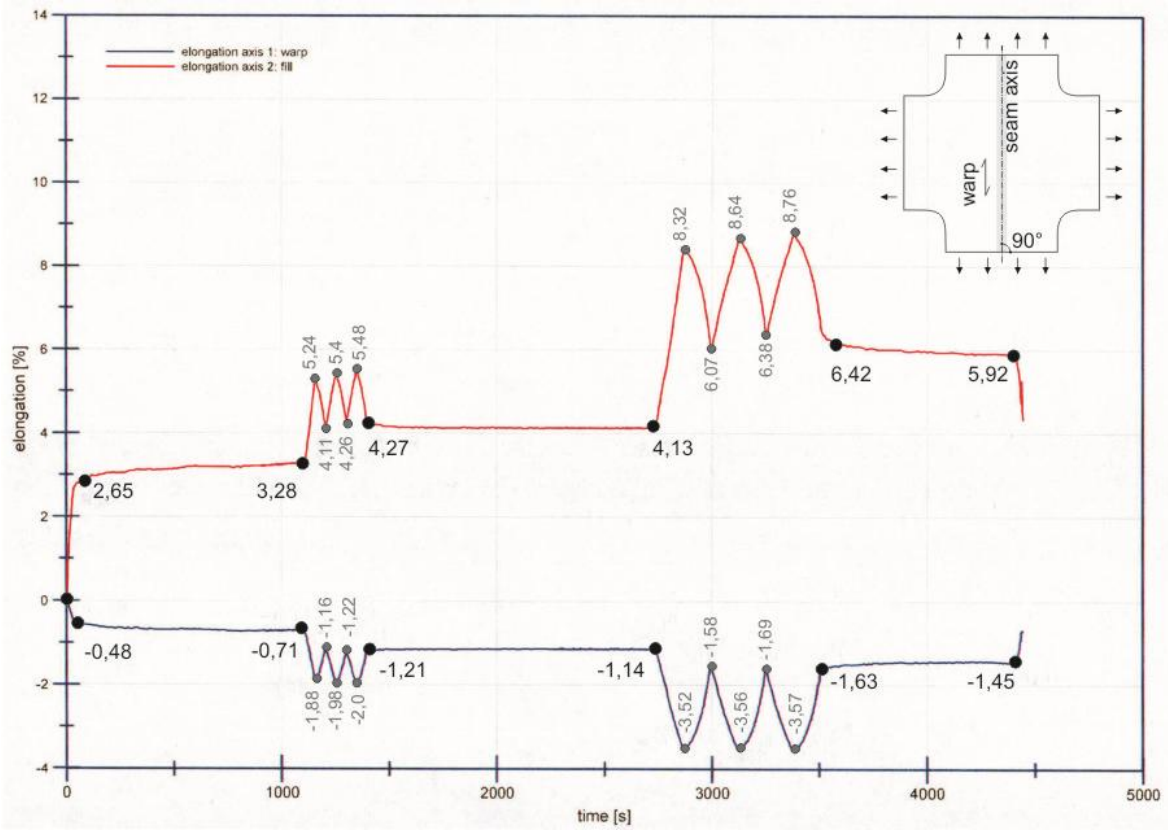


Diagram 3.2-7 – Biaxial seam test – angle between panels: 4°

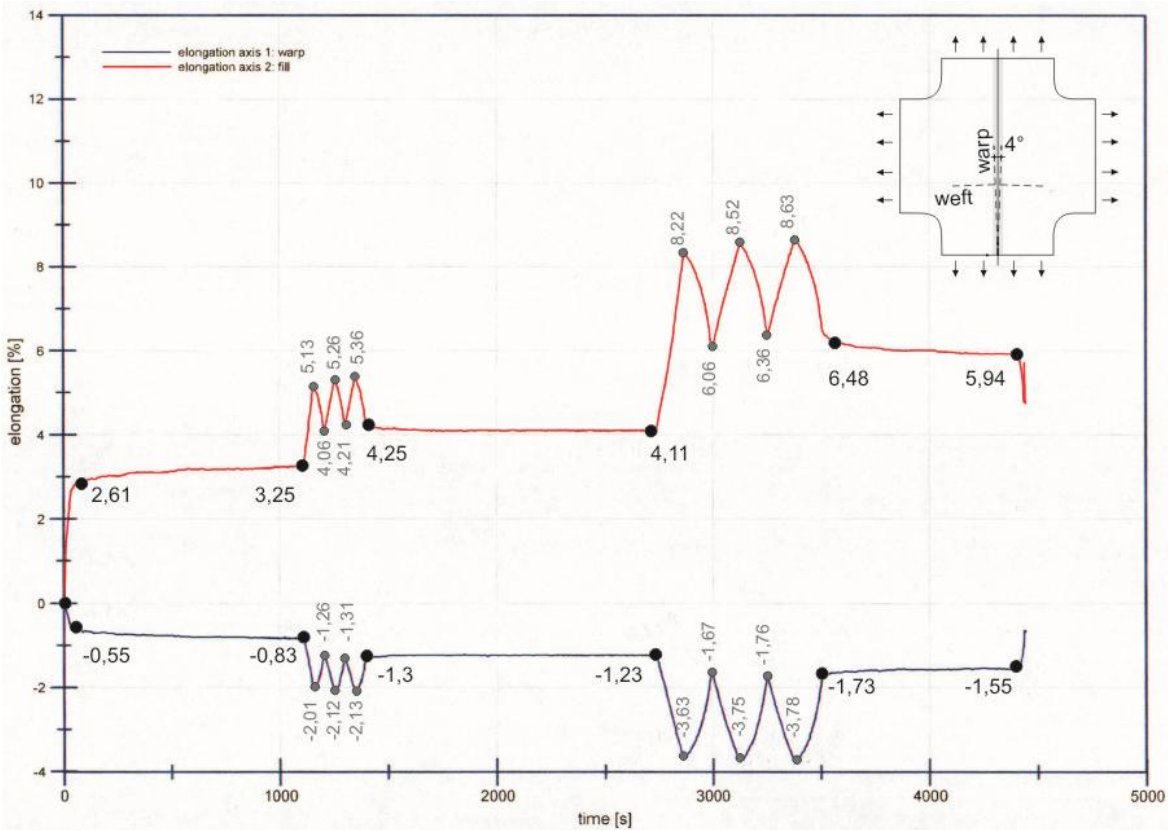


Diagram 3.2-8 – Biaxial seam test – angle between panels: 8°

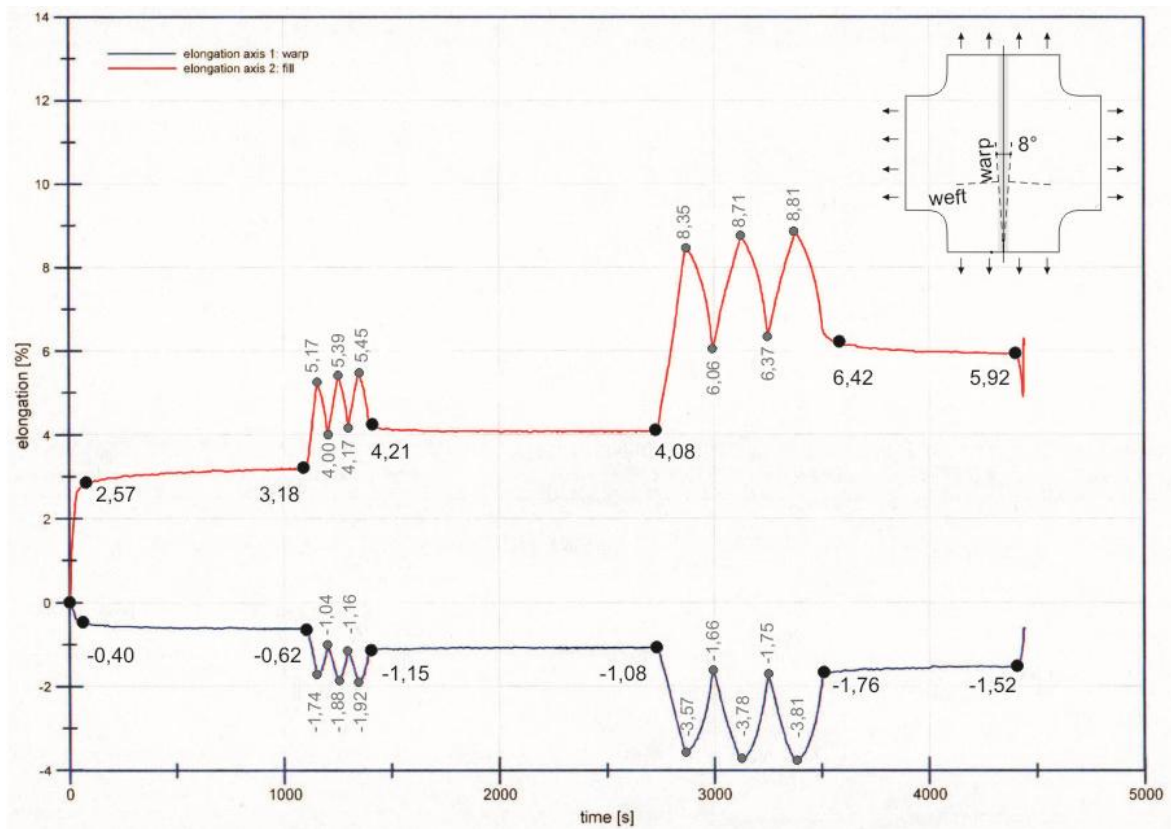


Diagram 3.2-9 – Biaxial seam test – comparison between tests

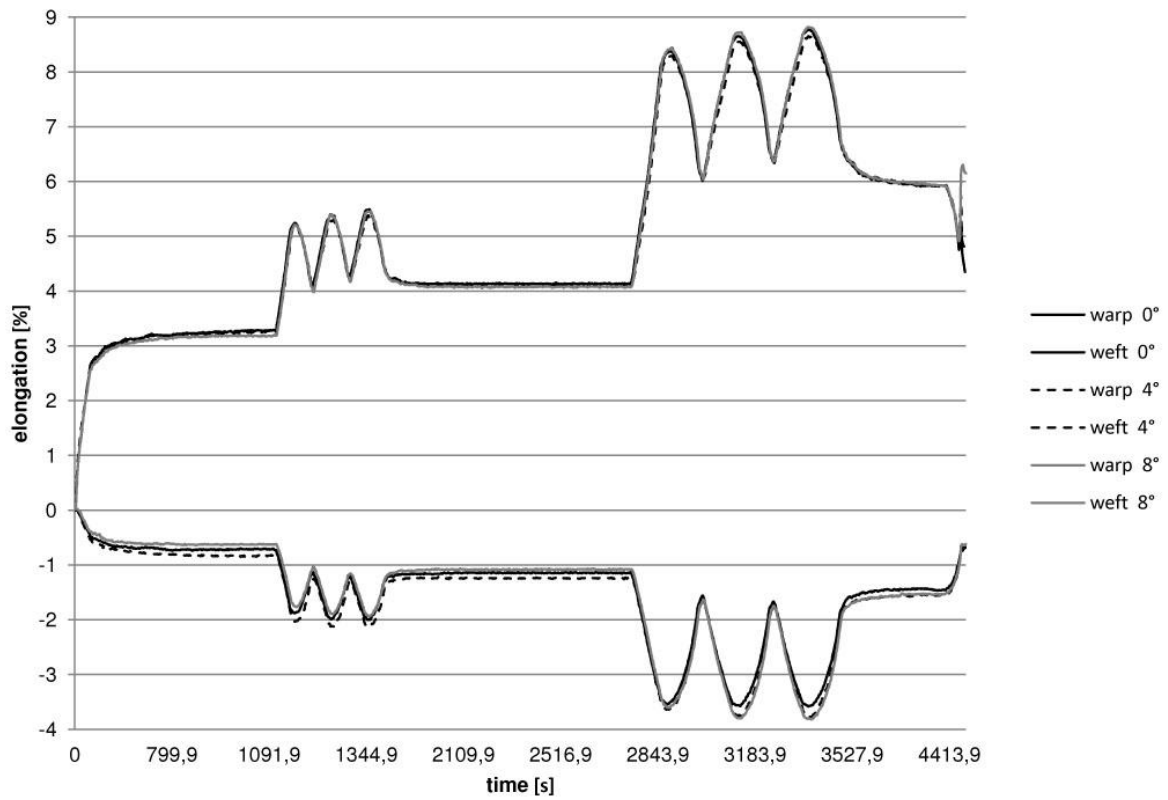


Figure 3.2-15 – Seam biaxial test - comparison of tests - angle between panels: 0°, 4°

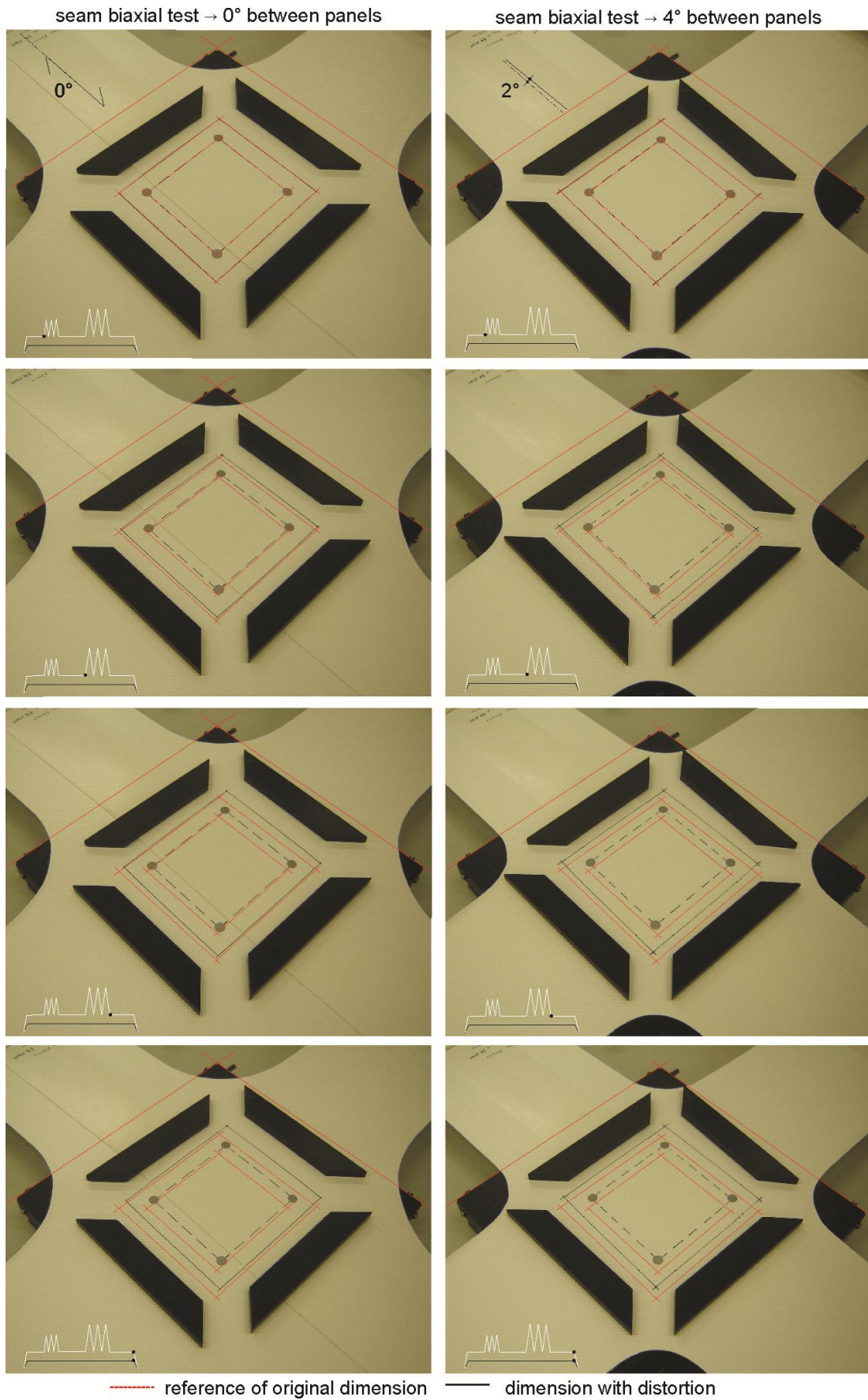
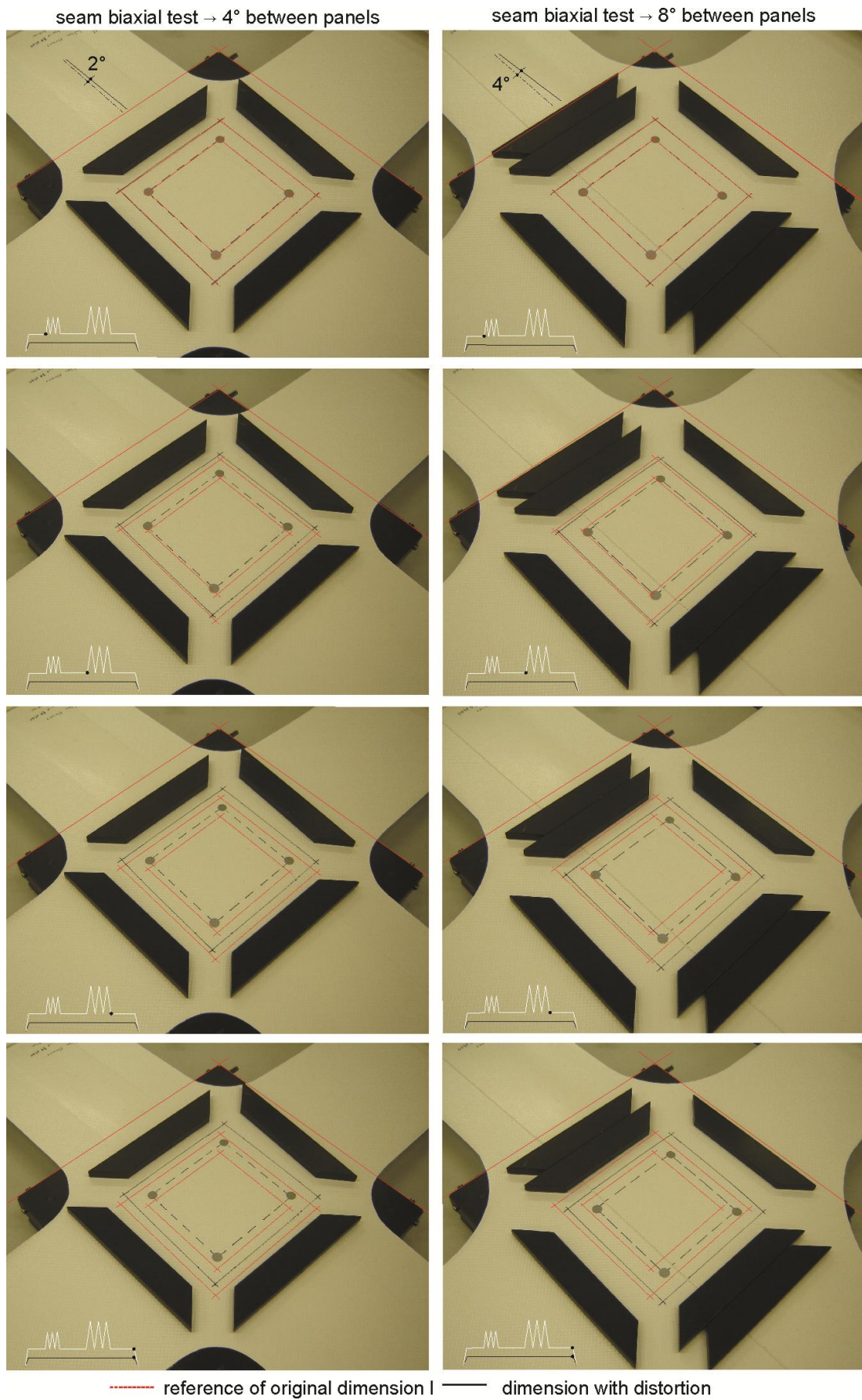


Figure 3.2-16 – Seam biaxial test - comparison of tests - angle between panels: 4°, 8°



### 3.2.3 UNIAXIAL SEAM TESTS

After evaluating the influence of the angle between adjacent flat panels in the seam, it was also verified the temperature effect in the seam performance.

According to Seidel (2009), the strength of coated fabric decreases under long term load, since material deformations increase with time (creep). These deformations are also influenced by material behavior related to temperature changes. The thermoplastic materials (synthetic polymers used in the fabric and coating manufacturing) became brittle under lower temperatures and show relative expansion of volume under high temperatures, causing the reduction of elastic module. So, in order to understand the mechanic proprieties of these materials under temperature influence it is important to acknowledge the significance of their glass transition temperature ( $T_g$ ) and melting temperature ( $T_m$ ) of them.

These temperatures indicate the limits for polymer use (service condition), as well as the limits of manufacture procedures (CALLISTER, 2008). The glass transition ( $T_g$ ) represents the temperature in which the polymer transforms from stiff to viscoelastic state (when the amorphous regions of molecular chains present mobility reducing material stiffness); the melting temperature ( $T_m$ ) indicates the temperature in which the polymer is completely fluid (when ordered regions of polymers disintegrated and melt), (KNIPPERS *et al.*, 2011; MANO, 2007).

Minte (1981) when researching the mechanic behavior of membrane material observed that coating adhesion to fabric has great influence in seam behavior, and at 70°C there is a significant reduction of material strength in seam. Moreover, Huntington (2003) highlights that service temperature of fabrics with dark colors directly under sunlight (high temperatures) rises to a 65°C.

So, uniaxial tests are carried out to evaluated seam strength observing its behavior generally at 23°C, -20°C and 70°C.

According Minte (1981), the choice of uniaxial tests for seam strength evaluation can be explained by the fact that in uniaxial test, the seam strength is lower than in biaxial seam test of similar seams, enabling seam dimensioning with security. In the uniaxial seam test, warp and weft are completely stretched. However, in the biaxial seam test, this does not occur. The loads are applied simultaneously in both fabric directions, so threads work together and constrain deformations of each other (ALVIM, 2004).

### 3.2.3.1 Characteristics of seam uniaxial test

As it was noted similarity of the material deformation relative to angles evaluated, the uniaxial seam tests were performed at angle of  $0^\circ$  between panels (warp parallel to seam). Seam uniaxial tests were performed at the following temperatures:  $-10^\circ\text{C}$ ,  $23^\circ\text{C}$  and  $70^\circ\text{C}$  (since it was not necessary to evaluate the influence of  $-20^\circ\text{C}$  to the site of the researched structure).

The seam strength was evaluated through the analysis of five specimens, considering load applied transverse seam, in the weft direction (test standart: DIN EN ISO1421 mod./ Guideline DIBt). These tests used specimens of 10cm in width and seam overlap of 8cm (Figure 3.2-17, Figure 3.2-18).

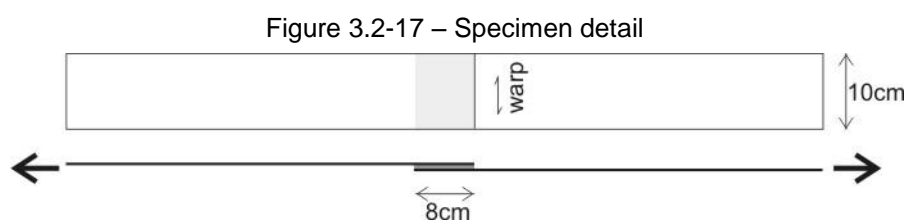
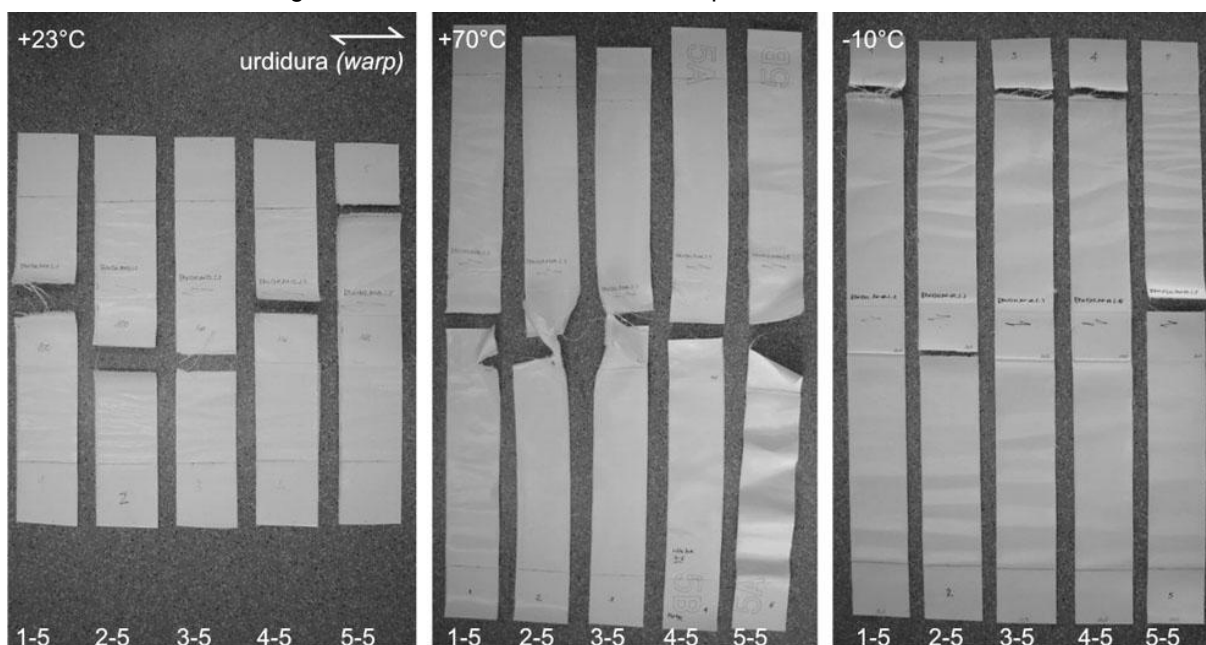


Figure 3.2-18 – Uniaxial seam test - specimens after tests



### 3.2.3.2 Interpretation of the results of uniaxial seam test

In uniaxial seam tests with temperature of 23°C (Figure 3.2-19, Diagram 3.2-10), the seam breaking strength showed a percentile value of 135.3 kN/m (5% *fractile*<sup>23</sup>).

This value is 4% higher than material tensile strength, considering weft direction strength (130kN/m) of material type IV, which guided the preliminary analysis of the external surface of the model (Table 3.1-7). According to preliminary analysis, the maximum stress observed on the external surface of B2<sub>int-ext</sub> model, was in the weft direction 32MPa (32kN/m, considering material thickness equal 1mm), i.e., 25% of material strength (Figure 3.2-6, Figure 3.1-90).

Diagram 3.2-10 – Uniaxial seam test, temperature: +23°C

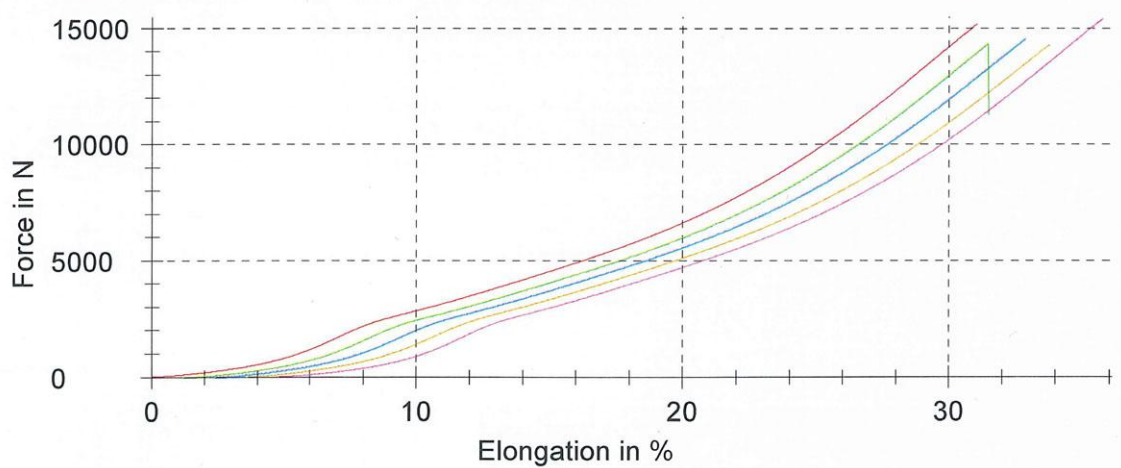
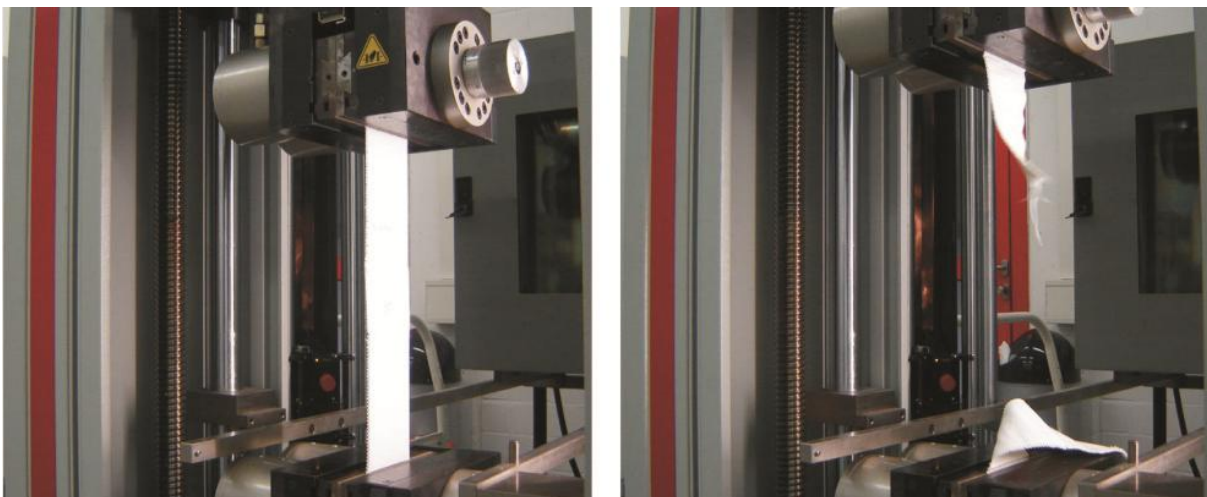


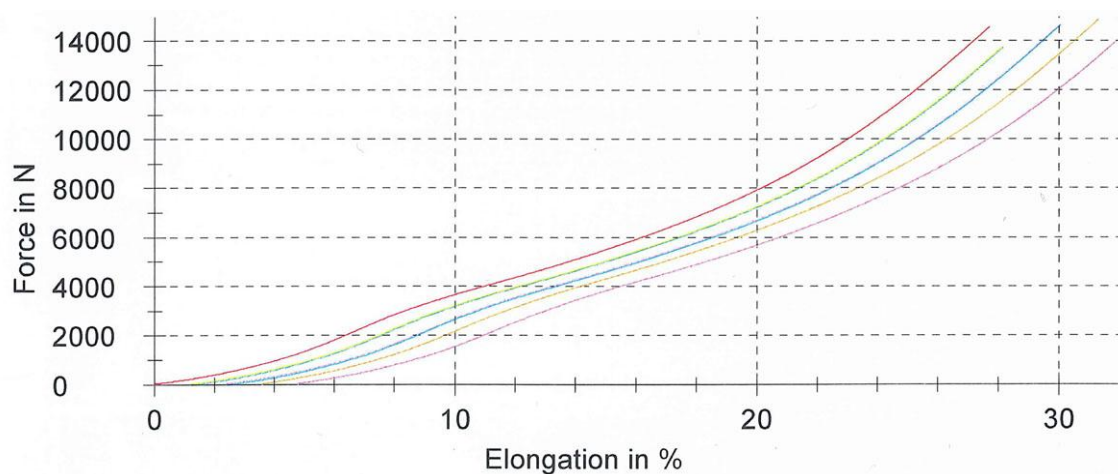
Figure 3.2-19 – Uniaxial seam test, temperature: + 23°C



<sup>23</sup> O valor 5% fractile é usado como fator de redução para a falta de homogeneidade no tecido (FOSTER, 2004).

In uniaxial seam tests with temperature of  $-10^{\circ}\text{C}$  (Diagram 3.2-11, Figure 3.2-20b), the seam breaking strength showed a percentile value of  $130.0\text{ kN/m}$  (5% fractile). Due to temperature reduction, there was a decrease in seam strength (average value) approximately 22% comparing to test at  $23^{\circ}\text{C}$ . However, this value is similar the strength of the material do material typo IV in the weft direction.

Diagram 3.2-11 – Uniaxial seam test, temperature:  $-10^{\circ}\text{C}$



In the uniaxial tests with temperature of  $70^{\circ}\text{C}$  (Diagram 3.2-12, Figure 3.2-20a), the seam breaking strength showed a percentile value of  $64.2\text{ kN/m}$  (5% *fractile*). Increasing temperature, there was a significant reduction in the seam performance (approx. 50% strength material). However, this reduction is reversible with the decrease of temperature.

Diagram 3.2-12 – Uniaxial seam test, temperature:  $+70^{\circ}\text{C}$

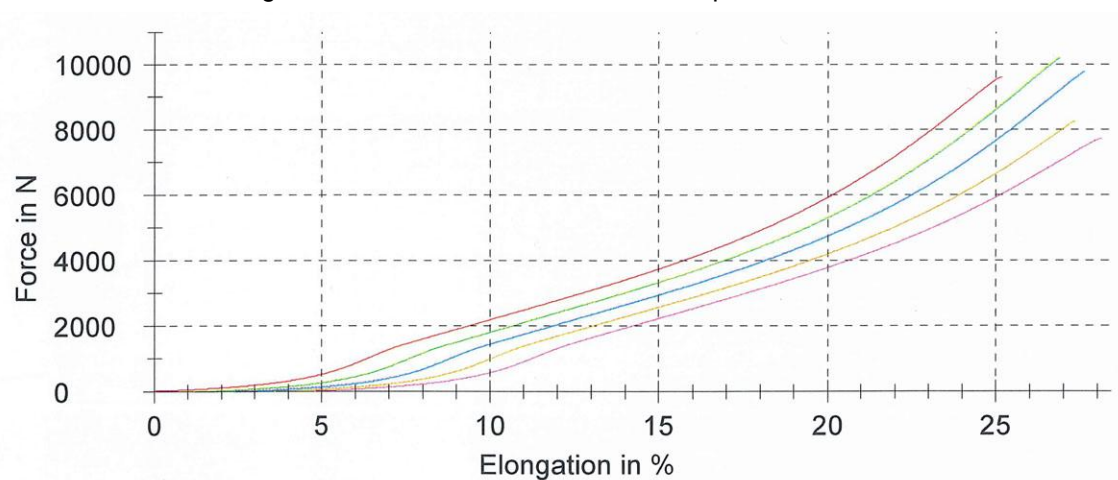
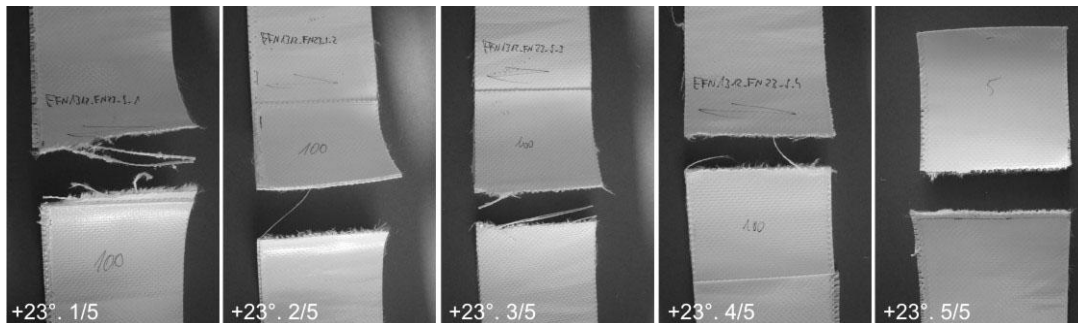


Figure 3.2-20 – Uniaxial seam test, temperatures: (a) +70°C; (b) -10°C



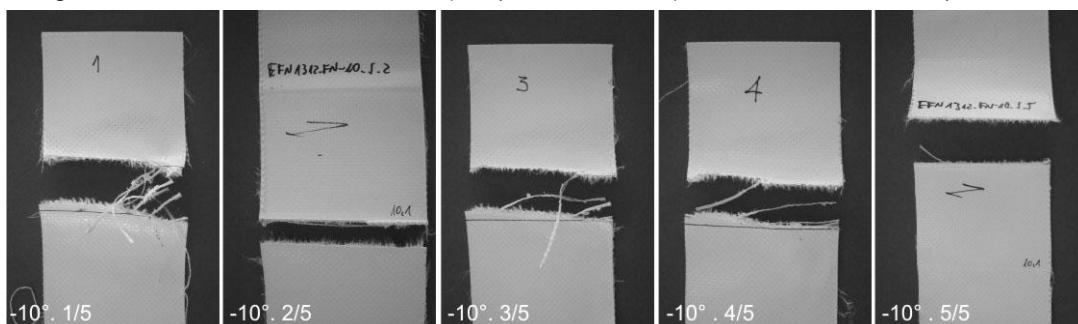
In tests at 23°C failures at the end of the seam (transition between fabric and seam) prevailed with fabric breaking parallel to seam, which reveals high strength of seam (Figure 3.2-18, Figure 3.2-21).

Figure 3.2-21 – Uniaxial seam test (temperature +23°C) - failure detail of the specimens



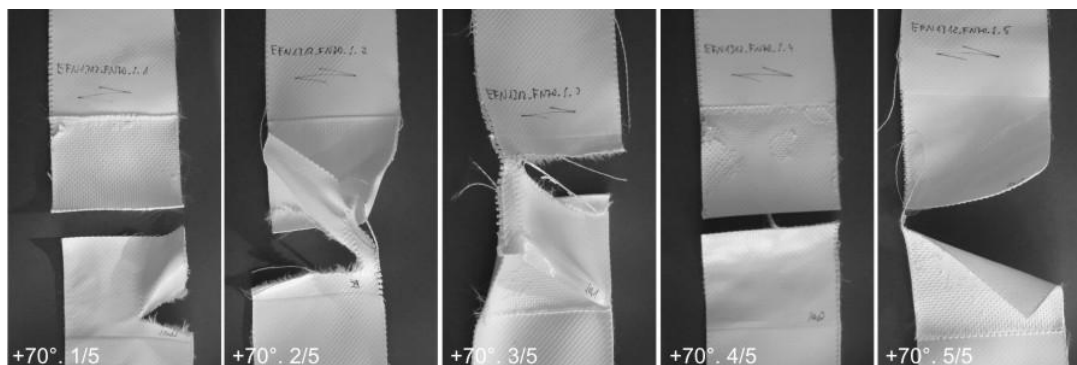
In tests at -10°C, it was observed that material was brittle, reducing the average strength of the seam (approx. 22% comparing to test at 23°C). Failures at the edge of the material prevailed, as in Figure 3.2-22.

Figure 3.2-22 – Uniaxial seam test (temperature -10°C) - failure detail of the specimens



In tests at 70°C it was observed that PVC coating softened, reducing adhesion, and therefore, separation (lost adhesion) between the coating and fabric as shown in Figure 3.2-23.

Figure 3.2-23 – Uniaxial seam test (temperature +70° C) - failure detail of the specimens



The results of uniaxial tests with temperature of 70°C lead a new analysis of membrane stress. In this new preliminary analysis it was consider the loading factored approach Summer storm, proposed by Germany standard DIN 4134:  $1n_g + 1,1n_p + 0,7n_w$ ; where:  $n_g$  =gravity;  $n_p$  = pre-tension;  $n_w$  =wind (KOENEN, 2012). This approach considers the reduction of wind action under increasing temperature.

In this new preliminary analysis, the maximum stress observed was also in external surface in the weft direction 28,88MPa (28,88kN/m, considering material thickness equal 1mm).

Then, it was calculated the allowable strength of the material ( $N_\theta$ ) considering reduction factor for high temperatures PES/PVC, based in the dissertation of Minte (1981), (KOENEN, 2012):  $N_\theta = f_{u,k} / 3,02 = 64,2 / 3,02 = 21,96$  kN/m.

It was observed that allowable strength of the material under high temperature (21,96 kN/m) was smaller than the maximum stress observed in external surface at weft direction (28.88 kN/m).

This result confirmed the importance of seam strength evaluation (seam width and weld manufacturing process) and behavior evaluation of the material (under temperature action), especially in tropical regions such as Brazil. So, in refined and final analysis, it is suggested to investigate whether safety factors adopted in this preliminary evaluation are appropriate to the climatic characteristics of the region where the structure is located.

### 3.2.4 CONSIDERATIONS OF 2<sup>nd</sup> STAGE OF QUALITATIVE ANALYSIS

These analyzes showed that membrane material is a flexible structure, which withstand forces by movement (rotating; sliding) and or deformation of threads. This behavior is influenced by weaving process and threads stiffness (warp and weft), by the orientation of threads related to panel seam and direction of forces, as well as load magnitude, time and temperature.

Consequently, the membrane surface geometry is influenced by the flexible behavior of the material and joints of the panels (linear load-bearing elements) that disturb the behavior of the curved membrane surface (SEIDEL, 2009).

Thus, to minimize the differences between the theoretical model and the real form and to ensure that the membrane can adopt the predicted form in time, it is necessary to analyze the material behavior in relation to the structure context, since preparation of the tests.

The analysis of stress and deformation of material that resulted of maximum load (biaxial test) allowed evaluation of elastic constants of the material directions.

The analysis of deformations of material that resulted of loads that predominate in membrane life time (biaxial test), considering the surface geometry and stress distribution, allowed to calculate and to propose adjustments to the compensation factors used to adjust the dimensions of flat panels, seeking to prevent stress peaks or new steps of pre-tension during structure life time.

The analysis of the angle between adjacent panels (seam biaxial test) allowed to observe deformations and distortions of material caused by movement of fabric threads under force action, since woven fabric and coating are not unified. It was also verified that distortions of material are influenced by the orientation of the threads relating to seam, directions and magnitude of applied loads; and thus, smaller angles between panels help to reduce distortions of the membrane curved surface.

The welding seam analysis considering temperature influence (seam uniaxial test) made it possible to observe coating behavior and its influence in seam strength. This analysis confirmed the importance of evaluating seam width and seam manufacturing process mainly in tropical regions.

## 4 FINAL CONSIDERATIONS

This study investigated qualitatively the performance of structural membranes considering structural and design procedure aspects.

The basic knowledge to set off this investigation included a literature review, analysis of lightweight structure buildings and design and constructive work of membrane roofs, in order to integrate theoretical knowledge and critical analysis of the study object.

The analysis of lightweight structure buildings enabled the acknowledgement of strategies used by architects and engineers for these structures to achieve great performance. Moreover, it allowed a qualitative evaluation of the performance of the structural membrane in the context of the lightweight structures.

This investigation comprised observation and analysis of structural concept of selected buildings, i.e., how the structural system was organized, which components were used and how geometry and arrangement of components helped to achieve stiffness and global stability of the system with lower mass.

Among the investigated structures, the structural membrane roofs stand out. They are both structure and roof (enclose building), working together with the supporting system. In other investigated structures (e.g. wood and grid shell, steel structure) tiles, glass, membrane have only a covering function.

It was observed that the optimum performance of membranes is associated to the spatial stability and low mass of the structural system, as well as to the high resistance of materials used (e.g., synthetic fibers and steel). According to strategies identified, this performance results from:

- structural system spatial organization and joined work of all components (membrane and system support) under pre-tension;
- membrane three-dimensional geometry in tautness state;
- use of fabric compound of synthetic fibers that withstand high stress with lower density;
- spatial arrangement of the supporting system which results of combination of systems and or three-dimensional organization of linear components mainly under axial forces (e.g. masts with cables), as well as the form of transverse section of components appropriated to the acting forces, allowing the reduction of system mass for the same volume (density).

The analysis of design and constructive work membrane roofs showed that membrane behavior is also influenced by organization, shape and dimensions of flat panels (flattened surface geometry), as well as material behavior.

It demonstrated that uncertainties regarding material behavior reduce design stage accuracy and constructive performance. Moreover, the strategies used by engineers, in constructive stage, to handle material deformations and constructive inaccuracies that may occur (e.g. connections with major adjusting) cannot always cover all uncertainties. Thus, errors or changes in the membrane geometry disturb the flow of forces, causing distortions that can be observed and cannot be disguised.

Thus, this study confirmed the importance of membrane material behavior evaluation, the knowledge of system constructive procedures (manufacture and assembly), detailing (with more accuracy) and checking components, and especially the cooperative work of architects, engineers and builders, contributing with their knowledge and experience.

These investigations conducted towards the qualitative analysis of the performance of a structural membrane roof project carried out in two stages.

In the first stage of this qualitative analysis it was evaluated the influence of the structural system arrangement and membrane geometry in the system performance. It was investigated a set of variables that generated changes in the project (original model). These changes originated models with different geometries, whose behavior and performance were investigated under load action. The analysis and comparison of these models enabled to identify which variables contributed to an optimal system performance, and which one had better result.

In the performance evaluation of structural system, it was verified that stiffness and global stability of the system are not only associated with masts addition. The cable configuration associated with increased number of masts enable a better and integrated work between support system components and contributed significantly to reduce the displacements of the support system and membranes, increasing the three-dimensional stability of the structural system.

Subsequently, the influence of changes in the geometry of membrane surfaces was assessed. An increase in the stiffness of membrane surfaces was verified, i.e., they need lower forces to be stabilized and bear loads. The reduction in the magnitude and areas of stress concentration in the membrane surfaces were

observed, and thus, a more homogeneous stress distribution in membranes was verified. A decrease in the pre-tension and global mass of system was also verified.

The analyzes showed that system performance has benefited from the flexible spatial arrangement of support system, stiffness of three-dimensional membrane surface, and the spatial organization and cooperation of all components in tautness state as verified in  $B2_{\text{int-ext}}$  model.

In the second stage of this qualitative analysis it was evaluated the geometry of the flattened membrane under the influence of material behavior.

This analysis showed that membrane material also has a flexible structure, i.e., it withstands forces by movement and or deformation of threads. This behavior is influenced by fabric weaving, orientation and stiffness of material threads, as well as magnitude and duration of loads, time and temperature. Thus, it demonstrated the importance of evaluation of material behavior considering membrane geometry and stress distribution in the membrane surface, and climate conditions of the place where the structure is located.

This evaluation enabled to investigate initially, the material behavior (stiffness, deformations) in the structure context. Then, geometry differences between theoretical model (continuous form of equilibrium whose definition disregards material behavior) and real form (formed by flat panels) were verified. Dimension adjustments of flat panels regarding material deformations were proposed. It was also verified the importance of reduction of the angle between adjacent panels, aiming to minimize surface distortions. These adjustments confirm that appropriate geometry of flat panels contributed towards a final membrane surface shape that reveals not only the best force path, but also the best use of material.

So, it is necessary to control the movements of materials and components under load action in the membrane structure. These movements can be observed in the deformation and or distortion of material, in the displacements of support system components and membrane surface so that the equilibrium can be achieved.

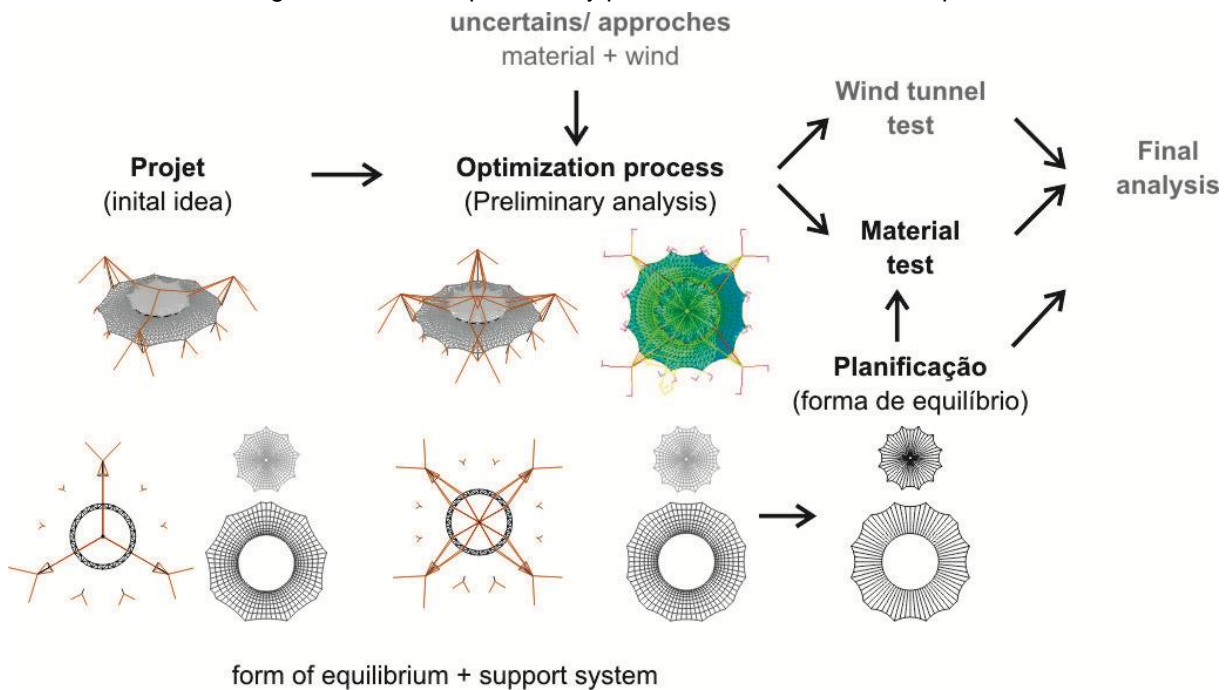
These analyzes demonstrated that the way to deal with these movements and to achieve system performance comes from evaluation of support system arrangement and system components (membrane and support system), as well as flattened membrane geometry evaluation, as proposed hypothesis.

In other words, the performance of membrane roofs is the result of an optimization process that involves the analysis of structural system spatial stability

(investigating arrangement of components), of the membrane stiffness and its load bearing capacity (evaluating surface geometry), as well as the analysis of surface cutting patterns (evaluating the influence of material behavior).

Investigations, analysis performed and working procedure adopted in the preliminary qualitative analysis allowed to extend the comprehension and evaluation of this system. They also suggest strategies to improve system performance and minimize flaws in this preliminary stage of work (Figure 4-1). It is up to architects, engineers and builders to evaluate together these procedures and possibilities for each project in particular.

Figure 4-1 – Work preliminary procedure and new work steps



### *Suggestions for designing process*

Membrane structures fall in the border area between architecture and engineering, as it was observed. So, the designing process is accomplished by bringing closer both areas and work teams.

The first stage of this procedure aims to elaborate the concept and the guidelines of the proposed building. In other words, it seeks to define the uses and activities that will be enhanced, to identify the qualities and characteristics of the place where the building will be sited, as well as the interaction of the proposed building with the environment (views, sunlight, wind, topography, and neighborhood). It also assesses the local legislation. These guidelines will conduct the development of spaces and solutions – architectural and structural – that enhance the activities and human relationships, as well as providing integration of the building and landscape (NUNES, 2008).

In the second stage, the three-dimensional configuration (arrangement of the structural system) of the proposed building is developed. It comprises the development of physical and or computational models integrating architecture and engineering actions.

The development of physical models can be considered as the first step of form finding, investigating membrane geometry and structural set. They also enable to explore and analyze qualitatively the geometry and arrangement of components (supporting system and membrane) in a tensile state, allowing intuitive understanding of the system behavior and the spontaneous development of the structural system. Moreover, they allow investigating the proposed building in landscape, as well as its manufacture and assembly process, which cannot be possible only considering the Cartesian viewpoint (plants, sections). The physical models can be made by stretch fabrics, soap film, paper, and using nails, wooden sticks, wires, cotton and lines as support.

Simultaneously, computer models of the proposed configuration are developed, allowing a more refined investigation of the form of equilibrium of the membrane and structural system arrangement. It is used, as example, the Force Density Method to define the three-dimensional shape of the membrane under pre-tension and a graphical platform for modeling the whole structure.

Subsequently, it is evaluated the global stability and behavior of the initial configuration (membrane + support system) under load action. This preliminary

analysis is guided by security factors and or adopted standards. Then, the optimization process of the proposed configuration is developed, investigating its structural (e.g. system stiffness, ability of the membrane to withstand loads, system weight) and building performance. This process involves adjustments in the geometry and arrangement of components and can be defined as a step-by-step to find the best configuration of the system.

This preliminary analysis is also the basis of the experimental tests of material and wind loads. The analysis of membrane material makes possible evaluating and refining the geometry of membrane cutting patterns, bringing closer theoretical and real models. The wind tunnel tests of the study model allow quantifying loads, avoiding the oversize of structures and increasing their safety.

The preliminary analysis and tests guide the refined analyses, increasing the quality of simulation of the structure and contributing to the appropriated dimensioning and detailing (with more accuracy) of components, and thus, to the performance of constructive work and the quality of membrane structure during its life time.

#### *Suggestions for future work*

This work points towards new evaluations guided by the refinement of membrane surface mesh and cutting patterns, as well as wind tunnel test of the study model, in order to evaluate and quantify load uncertainties increasing simulation and structure performance.

It is also suggested:

- evaluation of safety factors adopted in membrane structures performance analysis;
- material behavior and seam strength examination, especially in tropical regions such as Brazil;
- development of software that enables integration of design procedures (form finding, cutting patterns, structural analysis).

## 5 REFERENCES

ADDIS, William. Design Revolutions in the History of Tension Structures. *Structural Engineering Review*. Oxford, v.6, n.1, p.1-10. Feb. 1994.

ALVIM, Rosana de Albuquerque Arléo. *Avaliação experimental de propriedades mecânicas dos tecidos estruturais*. 2003. 134f. Dissertação (Mestrado) Escola Politécnica da Universidade de São Paulo. Departamento de Engenharia de Estruturas e Fundações. São Paulo, 2003.

ALVIM, Rosana de Albuquerque Arléo; PAULETTI, Ruy Marcelo de Oliveira. Avaliação experimental de propriedades mecânicas dos tecidos estruturais. In: JORNADAS SUD-AMERICANAS DE INGENIERIA ESTRUCTURAL, Mendonza, mai., 2004.

AMERICAN INSTITUTE OF STEEL CONSTRUCTION, Inc. AISC. *Specification for structural steel buildings*. jun., 22, 2010.

AMERICAN INSTITUTE OF STEEL CONSTRUCTION, Inc. AISC. *Load and resistance factor design specification for steel hollow structural sections*. nov., 10, 2000.

ASSOCIAÇÃO BRASILEIRA DE NORMAS TÉCNICAS. *NBR 6123: Forças devidas ao vento em edificações*. Rio de Janeiro, 1988.

AZEVEDO, Álvaro F. M. *Método dos elementos finitos*. Porto: Faculdade de Engenharia do Porto, 2003.

BAIER, Bernd. Technical characteristics and requirements of textiles used for building and construction. In: TEXTILES, POLYMERS AND COMPOSITES FOR BUILDINGS. The Textile Institute – Woodhead publishing. Cambridge. Edited by Goeran Pohl. 2010. p.49-68.

BAIER, Bernd: Leichtbau mit Membranen – Neue Entwicklungen, Materialien, Konstruktionen. In: ESSENER UNIKATE 23, BERICHT AUS FORSCHUNG UND LEHRE, INGENIEURWISSENSCHAFT. Essen: Universität Duisburg-Essen, 2004. p.86-97 *apud* BAIER, Bernd. Technical characteristics and requirements of textiles used for building and construction. In: TEXTILES, POLYMERS AND COMPOSITES FOR BUILDINGS. The Textile Institute – Woodhead publishing. Cambridge. Edited by Goeran Pohl. 2010. p.49-68.

BALDWIN, J. *Bucky Works: Buckminster Fuller's ideas for today's*. New York: John Wiley, 1996, 243p.

BARNES, Michael. Form and stress: engineering of tension structures. *Structural Engineering Review*. Oxford, v.6, n.3-4, p.175-202. aug.-nov. 1994.

BÖGNER-BALZ, H.; BLUM, R. Materials. In: MASTER PROGRAM FOR MEMBRANE STRUCTURES. Dessau: [s.n], 2008. CD-ROM do material de trabalho - divulgação restrita.

BLUM, R. Material properties of coated fabrics for textile architecture. In: THE DESIGN OF MEMBRANE AND LIGHTWEIGHT STRUCTURES - PROCEEDINGS OF THE SYMPOSIUM AT THE VRIJE UNIVERSITY BRUSSEL. Sep. 2000. Brussel. p.63-88.

BLUM, Rainer. Evaluation method for the elastic moduli. *Tensinews*, Brussels, Newsletter n.3, p.3, sep. 2002.

BUBNER, Ewald. *Membrankonstruktionen - Verbindungstechniken /Membrane construction - connection details*. Essen: Druckerei Wehlmann GmbH, 2005. p323.

CALLISTER, William D. *Fundamentos da Ciência e Engenharia de Materiais: uma abordagem integrada*. Tradução de Sérgio Murilo Stamile Soares. Revisão técnica de Paulo Emílio Valadão de Miranda. 2ª Ed. Rio de Janeiro: LTC, 2006. 720p.

CHILTON, John; BLUM, Rainer; DEVULDER, Thibau; RUTHERFORD, Peter. Thermal Environment. In: *European design guide for tensile surface structures*. Brussel: Tensinet, 2004. p.98-122.

CIMAF Cabos S/A. Cabos de Responsabilidade. *Catálogo de produtos*. Osasco, 2002.

D'ARCY THOMSON, W. On growth and form. Cambridge University Press. 1917 *apud* LEWIS, Wanda J. *Tension structures: form and behavior*. London: Thomas Telford Publishing. 2003. 201p.

DIAS JUNIOR, Urubatan de Souza. Determinação de padrões de corte *em estruturas de membrana por linhas geodésicas*. 2006. 110f. Dissertação (Mestrado) Escola Politécnica da Universidade de São Paulo. Departamento de Engenharia de Estruturas e Fundações. São Paulo, 2006.

DEUTSCHE NORM. *DIN 4134: Tragluftbauten, Berechnung, Ausführung und Betrieb*.1983.

DREW, Philip. *Frei Otto: Form and structure*. London: Crosby Lockwood Staples, 1976 *apud* PAULETTI, Ruy Marcelo de Oliveira. *História, análise e Projeto das Estruturas Retesadas*. Tese de Livre docência. Escola Politécnica da Universidade de São Paulo. São Paulo, 2003.

Experiences, ideas and new ways with architecture fabrics. *Sefar architecture*. Sefar Ag: Heiden. n. 1, p.10-11, nov. 2011.

FOSTER, Brian. Cable and membrane roofs – a historical survey. *Structural Engineering Review*. Oxford, v.6, n.3-4, p.145-174. aug-nov. 1994.

FOSTER, Brian; MOLLAERT, Marijke. *European Design Guide for Tensile Surface Structures*. Brussel: Tensinet, 2004. 354p.

GÓMES JÁUREGUI, Valentin. *Tensigridad: estruturas tensegráficas em ciência y arte*. Santander: Serviço de Publicaciones de La Universidad de Cantabria, 2007. 199p.

GONÇALVES, Roberto Martins; SALES, José Jairo de; MALITE, Maximiliano; MUNAIAR NETO, Jorge. *Ação do vento nas edificações: teoria e exemplos*. São Carlos: SET/EESC/USP, 2004. 124p.

GOSLING, P.D.; ZHANG, L. A non-safety factor approach to the design of membrane structures. In: TENSINET SYMPOSIUM 2010 – Tensile Architecture: connecting past and future. sep. 2010, Sofia.p.13-22.

GRÜNDIG, L.; MONCRIEFF, E.; STRÖBEL, P. A history of the principal developments and applications of the force density method in Germany 1970-1999. In: IASS-IACM 2000. FOURTH INTERNATIONAL COLLOQUIUM ON COMPUTATION OF SHELL & SPATIAL STRUCTURES. June 5-7, 2000. Chania-Crete, Greece. Disponível em: <[www.google.com.br/search?hl=pt-BR&q=density2.pdf&btnG=Pesquisar&meta=>](http://www.google.com.br/search?hl=pt-BR&q=density2.pdf&btnG=Pesquisar&meta=>)>. Acesso em 26/09/2007.

HUNTINGTON, Craig G. *The Tensioned Fabric Roof*. Reston: Asce Press, 2003. 203p.

INFORMATIONSDIENST HOLZ. *Holzbaupreis Nordrhein-Westfalen 1996*. Arbeitsgemeinschaft Holz e V. Dusseldorf, 1996. p.13.

JOTA, Fabiano de Oliveira; PORTO, Cláudia Estrela. *Evolução das Estruturas de Membrana*, 2003. Disponível em: < [www.unb.br/fau/pos\\_graduacao/paranoa/edicao2004/evolucao\\_estruturas\\_membrana.pdf](http://www.unb.br/fau/pos_graduacao/paranoa/edicao2004/evolucao_estruturas_membrana.pdf) >. Acesso em 18/06/2008.

KNIPPERS, Jan; CREMERS, Jan; GABLER, Markus; LIENHARD, Julian. *Construction Manual for Polymers + Membranes*. Basel: Birkhäuser. 2011. 296p.

KOCH, Klaus-Michael. *Membrane Structures: innovative building with film and fabric*. Munich: Prestel Verlag, 2004.

KOENEN, Reinhold. *Skript Leichtbau*. Institut für Metall-und Leichtbau. Universität Duisburg Essen. Ed.: Dipl.-Ing. Jan Peter Hartmann. Reviewed and broaden in 2009: Dr.- Ing Reinhold Koenen. 11/13/2009: Design of lightweight shell structures – Master course, elective module, out.2011 - fev.2012.38p. Lecture handout and notes.

KROSCWITZ, Jacqueline I. *Concise Encyclopedia and Polymer Science and Engineering*. New York: Wiley.1990. 1341p.

LEWIS, Wanda J. Lightweight tension membranes: an overview. In: PROCEEDINGS OF THE INSTITUTION OF CIVIL ENGINEERS. Civil Engineering. v.126, n.4, p.171-181. Aug. 1998.

LEWIS, Wanda J. *Tension structures: form and behavior*. London: Thomas Telford Publishing. 2003. 201p.

LINKWITZ, Klaus. About formfinding of double-curved structures. *Engineering Structures*. v. 21, issue 8, p. 709-718, aug. 1999. Disponível em: <[www.sciencedirect.com/science?\\_ob=ArticleURL&\\_udi=B6V2Y-3VWFYVR-6&\\_user=686449&\\_rdoc=1&\\_fmt=&\\_orig=search&\\_sort=d&view=c&\\_acct=C000037578&\\_version=1&\\_urlVersion=0&\\_userid=686449&md5=f2fd4e74e01fb4a7bd803394f076a946#b2](http://www.sciencedirect.com/science?_ob=ArticleURL&_udi=B6V2Y-3VWFYVR-6&_user=686449&_rdoc=1&_fmt=&_orig=search&_sort=d&view=c&_acct=C000037578&_version=1&_urlVersion=0&_userid=686449&md5=f2fd4e74e01fb4a7bd803394f076a946#b2)>. Acesso 31/01/08.

MANO, Eloisa Biasotto; MENDES, Luis Cláudio. *Polímeros como materiais de engenharia*. São Paulo: Editora Edgard Blücher Ltda, 1991. 198p.

MATTHECK, C. Why they grow, how they grow: the mechanics of trees´. *Arboricultural Journal*, 14, 1-17. 1990 apud LEWIS, Wanda J. *Tension structures: form and behavior*. London: Thomas Telford Publishing. 2003. 201p.

MEEß-OLSOHN, Lars: *Textegrity - Textiles and tensegrity* Textegrity. Dissertation. Universität Essen, 2004.150p.

MEHLER Technologies. Valmex structures. *Catálogo de produtos*. V314/ 03/ 2008.

MILWICH, M. Types and production of textiles used for building and construction. In: *TEXTILES, POLYMERS AND COMPOSITES FOR BUILDINGS*.. The Textile Institute – Woodhead publishing. Cambridge. Edited by Goeran Pohl. 2010. p.13-48.

MINTE, Jörg. *Das Mechanische Verhalten Von Verbindungen Beschichteter Chemiefasergewebe*. 1981. 117p. Thesis (PhD) Facultät für Maschinenwesen der Rheinisch-Westfälischen Technischen Hochschule Aachen. Aachen, 1981.

MOLLAERT, Marijke; HEBBELINK, Sven; HAASE, Jürgen. The design of membrane and lightweight structures -from concept to execution. *Proceedings of the symposium at the Vrije Universiteit Brussel*, sep. 2000. Brussels: VUB Brussels University Press, 2002. 315p.

MEMBRANE STRUCTURES ASSOCIATION OF JAPAN. *MSAJ/M-02-1995*: testing method for elastic constants of membrane materials.1995.

NUNES, Eliana Ferreira. *Tensoestruturas: elementos e cabos associados a membranas*. 2008. 169f. Dissertação (Mestrado). Universidade Federal de Ouro Preto (UFOP), Ouro Preto, 2008.

OLIVEIRA, Maria Betânia. *Estudo das Estruturas de membrana: uma abordagem integrada do sistema construtivo, do processo de projetar e dos métodos de análise*. 2001. 165f. Tese (Doutorado). Escola de Engenharia de São Carlos, USP, São Carlos, 2001.

OLIVEIRA, Vinícius Maia Barreto de. *Análise e projeto de tenso-estruturas têxteis para coberturas*. 2003. 139f. Tese (Doutorado). Universidade Federal do Rio de Janeiro, COPPE/ UFRJ. Rio de Janeiro, 2003.

OTTO, Frei; TROSTEL, Rudolf. *Tensile Structures: Volume 1: Pneumatic structures*. Cambridge: The M.I.T. Press, 1967.

OTTO, Frei; TROSTEL, Rudolf. *Tensile Structures: Volume 2: Basic Concepts and Survey of Tensile Structures*. Cambridge: The M.I.T. Press, 1969.

OTTO, Frei et al. *Convertible roofs - IL 5*. Stuttgart: Information of the Institute for Lightweight Structures, 1972.

OTTO, Frei et al. *Air hall handbook* - IL15. Stuttgart: Information of the Institute for Lightweight Structures, 1983.

OTTO, Frei et al. *Experiments* - IL25. Stuttgart: Information of the Institute for Lightweight Structures, 1990.

OTTO, Frei et al. *Lightweight principle* - IL24. Stuttgart: Information of the Institute for Lightweight Structures, 1997.

PAULETTI, Ruy Marcelo de Oliveira. *História, análise e Projeto das Estruturas Retesadas*. Tese de Livre docência. Escola Politécnica da Universidade de São Paulo. São Paulo, 2003.

PAULETTI, Ruy Marcelo de Oliveira. *Sistemas Estruturais Leves – PEF 5750 – EPUSP-PEF 2007 – Disciplina do Mestrado, jun - set 2007*. Notas de aulas.

REBELLO, Yopanan Conrado Pereira. *A concepção estrutural e a arquitetura*. São Paulo: Zigurate editora, 2003. 272p.

ROLAND, Conrad. *Frei Otto: Estruturas - estudios y trabajos sobre la construccion ligera*. Barcelona: Gustavo Gili, 1973. 171p.

SAITOH, Masao. Recent development of tension structures: aesthetics and technology of the strings. In: PROCEEDINGS OF IASS COLLOQUIUM – CURRENT AND EMERGING TECHNOLOGIES OF SHELL AND SPATIAL STRUCTURES. apr. 1997, Madrid.

SCHLAICH, Jörg; BERGERMANN, Rudolf. *Leicht weit - Light structures*. Munich: Prestel Verlag e Frankfurt am Main: Deutsches Achitektur Museum (DAM), 2003. 328p.

SEIDEL, Michael. *Tensile Surface structures*. Berlin: Ernst& Sohn. 2009. 229p.

SCHIEMANN, L.; MORITZ, K. Polymer foils used in construction. In: TEXTILES, POLYMERS AND COMPOSITES FOR BUILDINGS. The Textile Institute – Woodhead publishing. Cambridge . Edited by Goeran Pohl. 2010. p.189-226.

STEGMAIER, T; SCHNEIDER, P.; VOHRER, A.; PLANK, H.; BLUM, R.; BÖGNER-BALZ, H. Developing and testing textiles and coatings for tensioned membrane structures. In: TEXTILES, POLYMERS AND COMPOSITES FOR BUILDINGS. The Textile Institute – Woodhead publishing. Cambridge . Edited by Goeran Pohl. 2010. p.129-188.

SHUKHOV\_TOWER. Disponível...[http://en.wikipedia.org/wiki/Shukhov\\_Tower](http://en.wikipedia.org/wiki/Shukhov_Tower). Acesso em: 13 set. 2010.

RODRÍGUEZ, Nelson. *Diseño de estructura transformable por deformación de una malla plana em su aplicación a un refugio de rápido montaje*. 2005. 297f. Tese (Doutorado) Universidad Politécnica da Catalunya – Escola Técnica Superior de Arquitectura de Barcelona – Escuela Técnica Superior de Arquitectura del Valle. Departamento de Construcciones Arquitectónicas 1. Barcelona, 2005.

UHLEMANN, Jörg; STRANGHÖNER, Natalie; SCHMIDT, Herbert; SAXE, Klaus. Effects on elastic constants of technical membranes applying the evaluation methods of MSAJ/M-02-1995. In: INTERNATIONAL CONFERENCE ON TEXTILE COMPOSITES AND INFLATABLE STRUCTURES – STRUCTURAL MEMBRANES 2011. Barcelona, 2011.

VILELA, C.A.B.S. Ação estática do vento em tensoestruturas. 2011. 149p. Tese de doutorado em Construção civil, Departamento de Engenharia Civil e Ambiental. Universidade de Brasília, Brasília, 2011.

V&M do Brasil. Tubos Estruturais de seção circular (MSH): dimensões, propriedades geométricas e materiais. *Informações técnicas Vallourec & Mannesmann Tubes*. Edição set. 2000 – VMB – BR0001P – 1ª Edição.

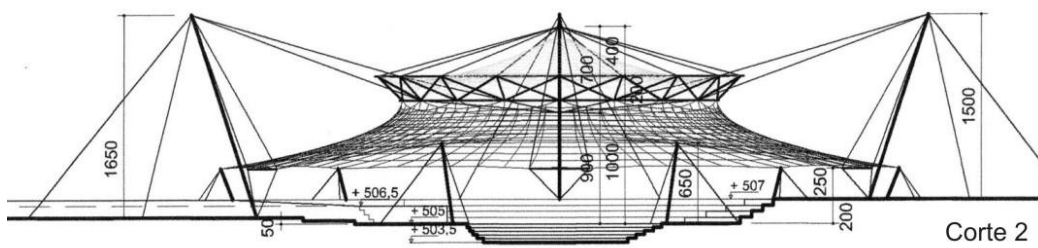
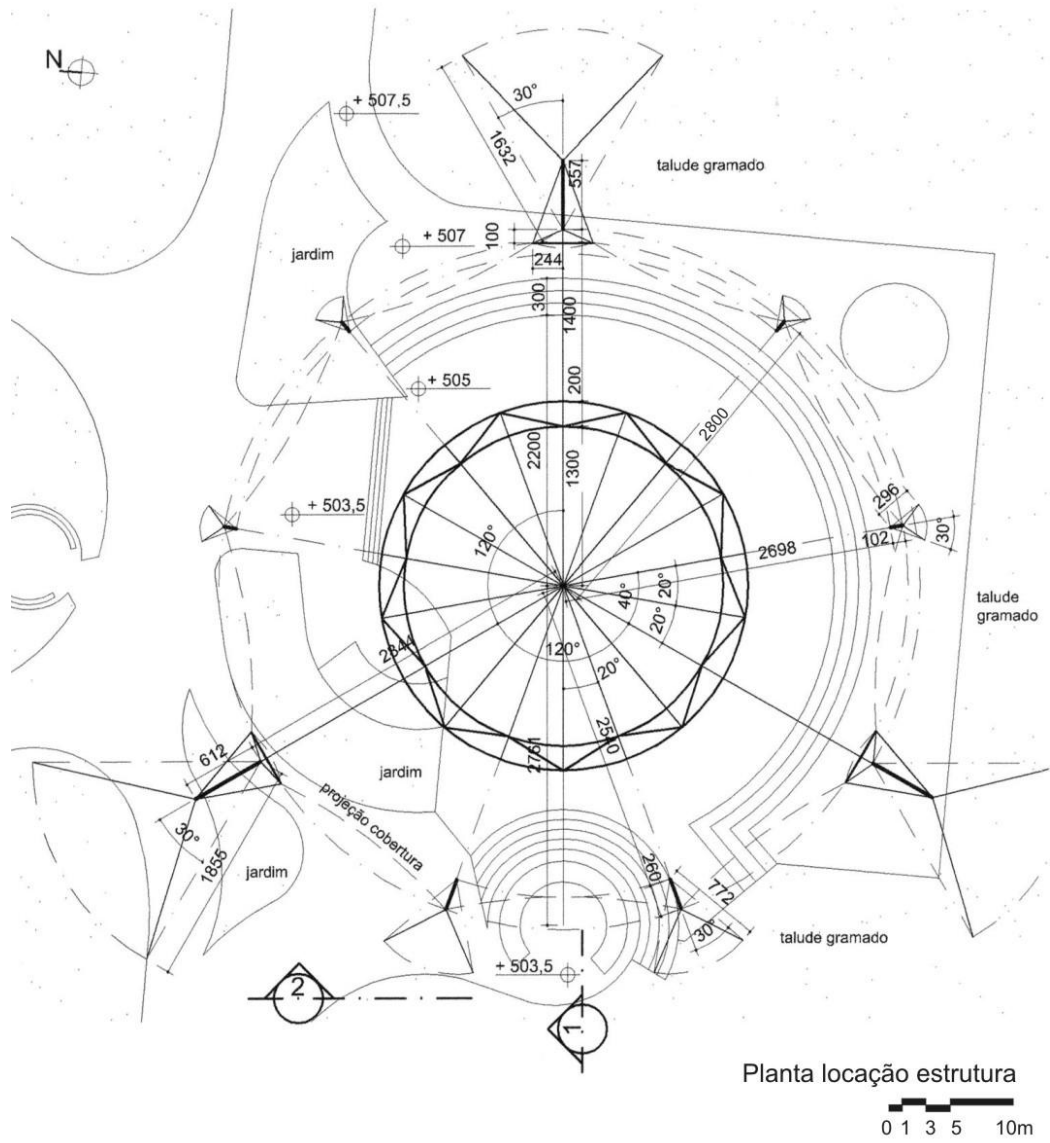
WAGNER, Rosemarie. On the design process of tensile structures. In: OÑATE, E.; KRÖPLIN, B. (eds). *Textile Composites and Inflatable Structures*. Netherlands: Springer, 2005. p.1-16.

WAGNER, Rosemarie. Kinematics in tensioned structures. In: OÑATE, E.; KRÖPLIN, B. (eds). *Textile Composites and Inflatable Structures II*. Netherlands: Springer, 2008. p.85-97.

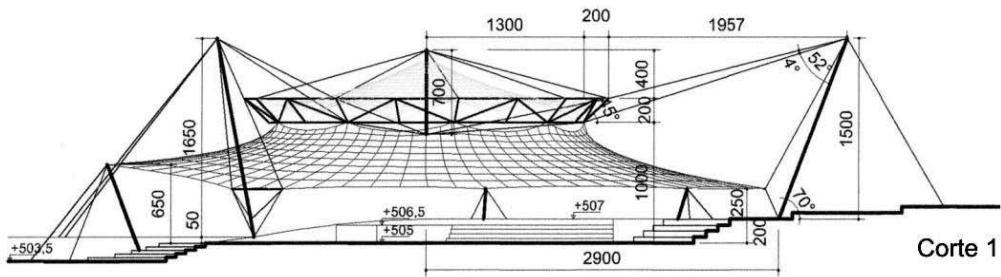
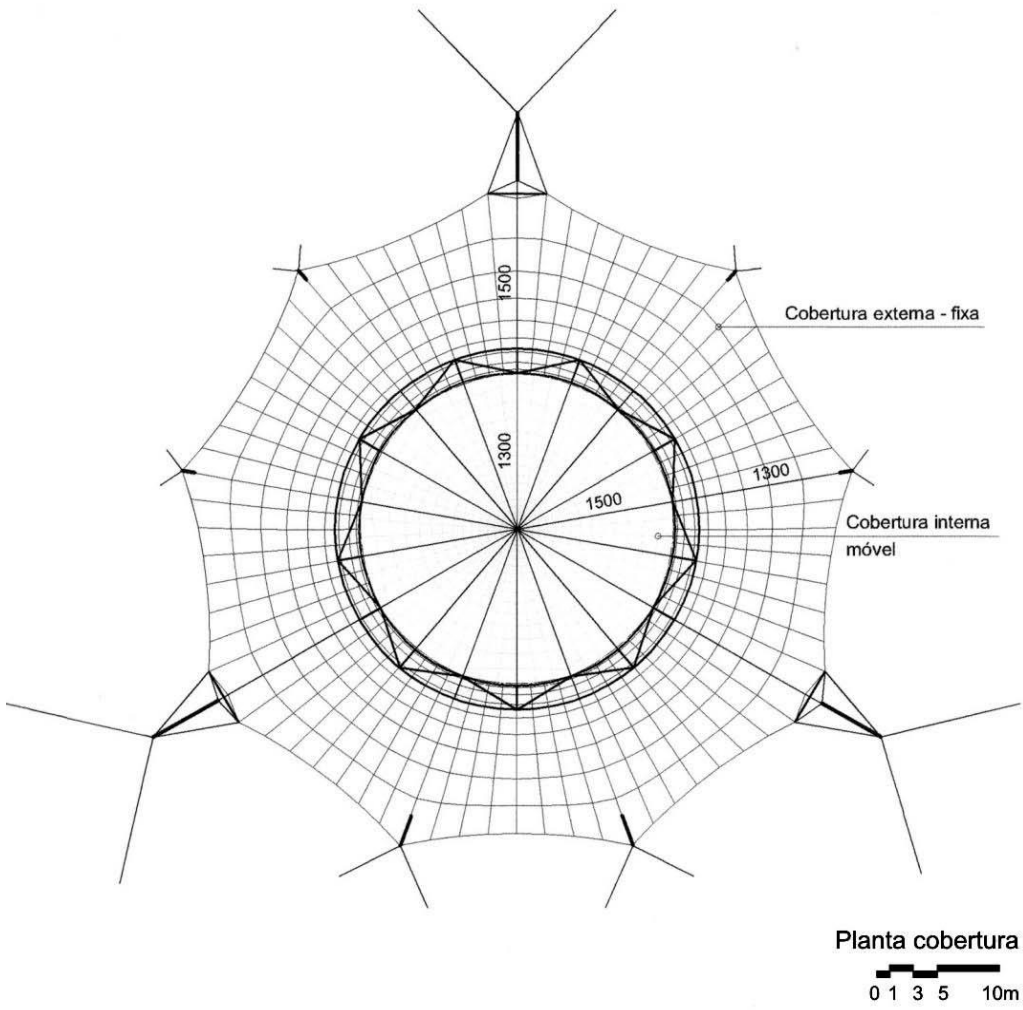
YU, Xiaobing. Bamboo: structure and culture. 2012. 178f. Thesis dissertation. Fachbereich Kunst und Design der Universität Duisburg-Essen. 2012.

ZANETTINI, Siegbert; GARCIA, José Wagner. Centro de pesquisas Petrobrás-CENPES. *Arcoweb*, 2006. (Tecnologia). Disponível em: [http://www.arcoweb.com.br/tecnologia/siegbert-zanettini-e-jose-wagner-garcia-09-04-2008.html#Scene\\_1](http://www.arcoweb.com.br/tecnologia/siegbert-zanettini-e-jose-wagner-garcia-09-04-2008.html#Scene_1)>. Acesso 5/julho 2009.

## APPENDIX A – Project information



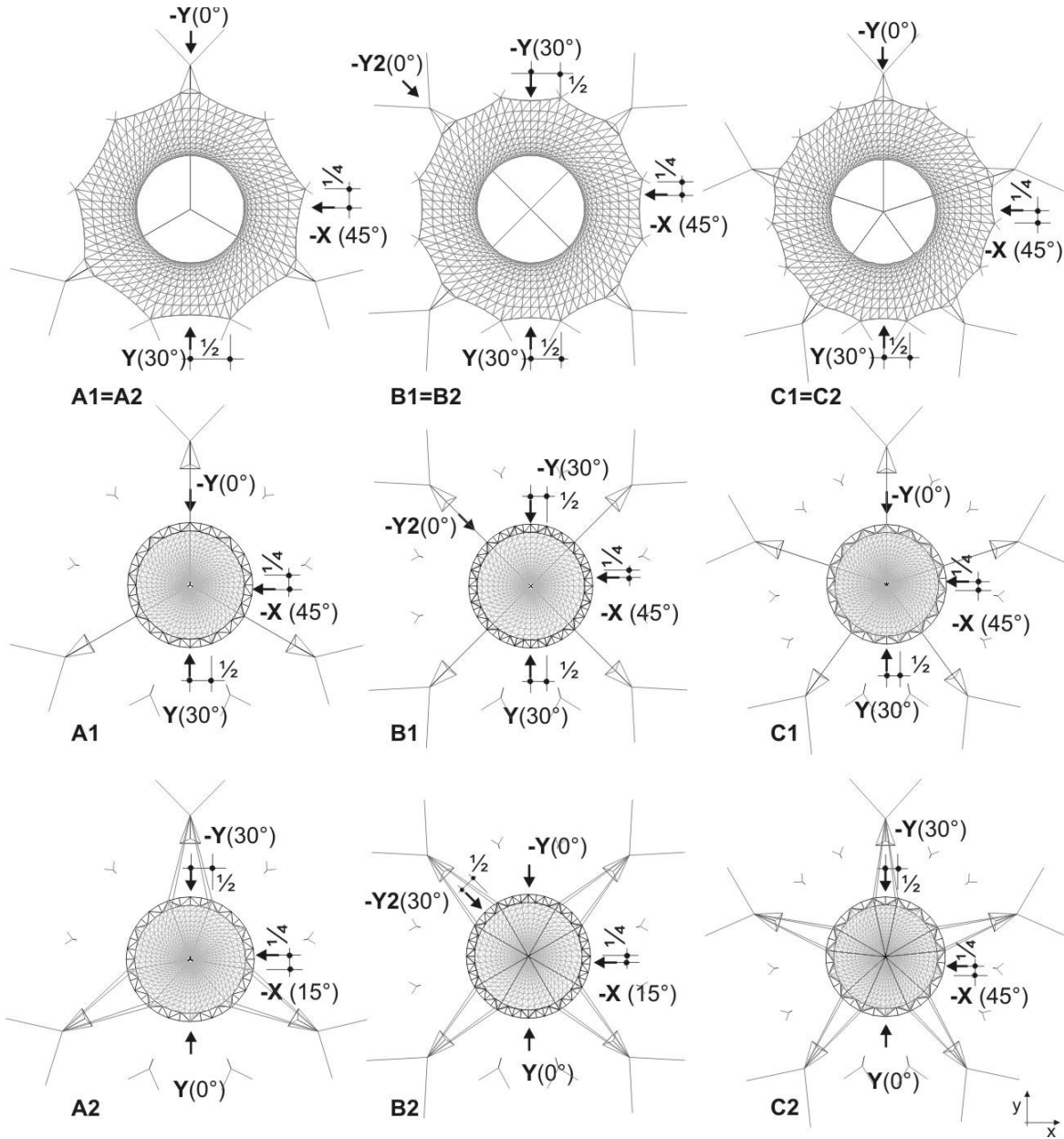
Fonte: Nunes, 2008, p.149..



Fonte: Nunes, 2008, p.150.

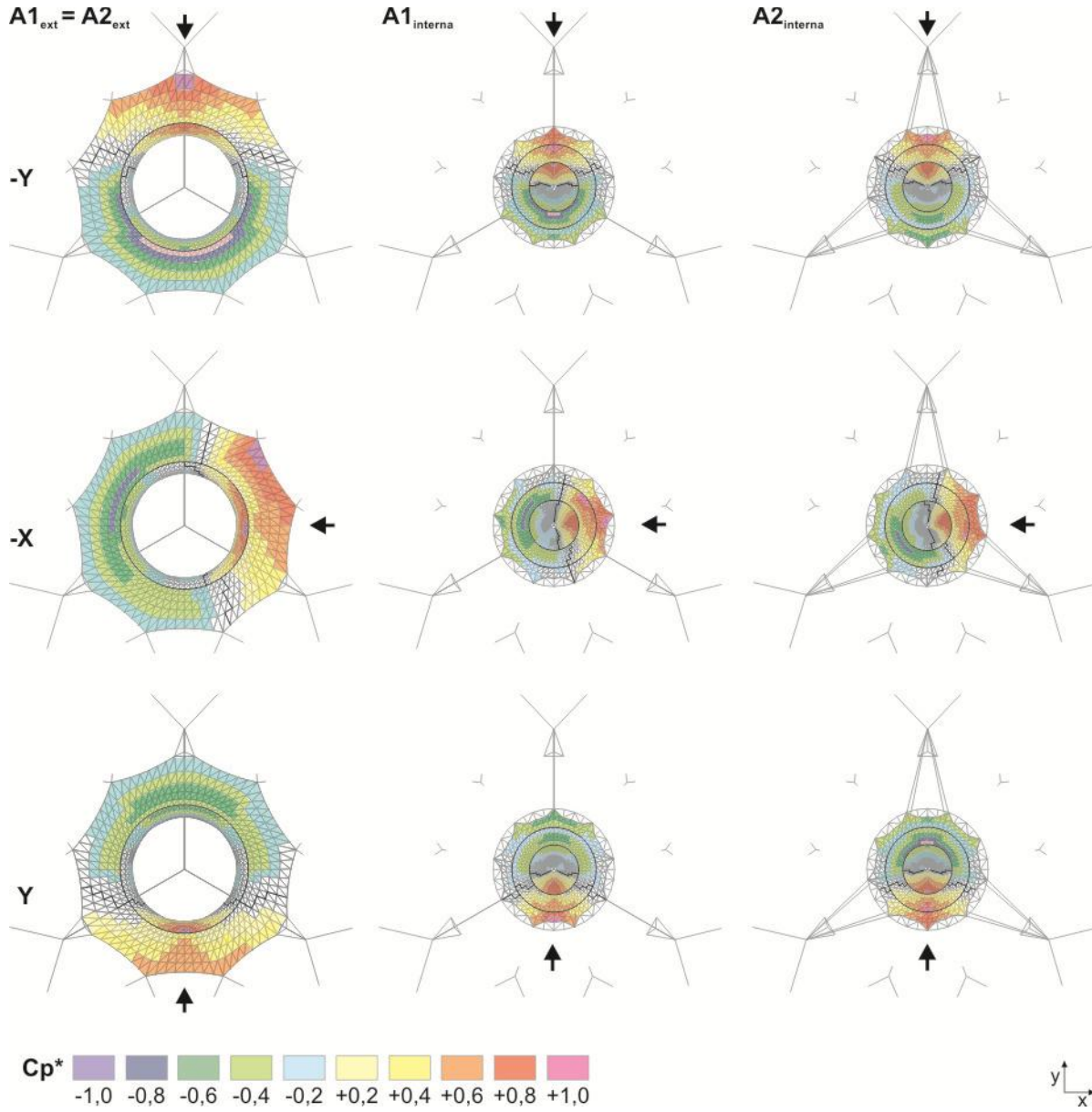
APPENDIX B – Wind directions

Wind directions – external and internal surfaces: A1, B1, C1, A1, B2, C2 models

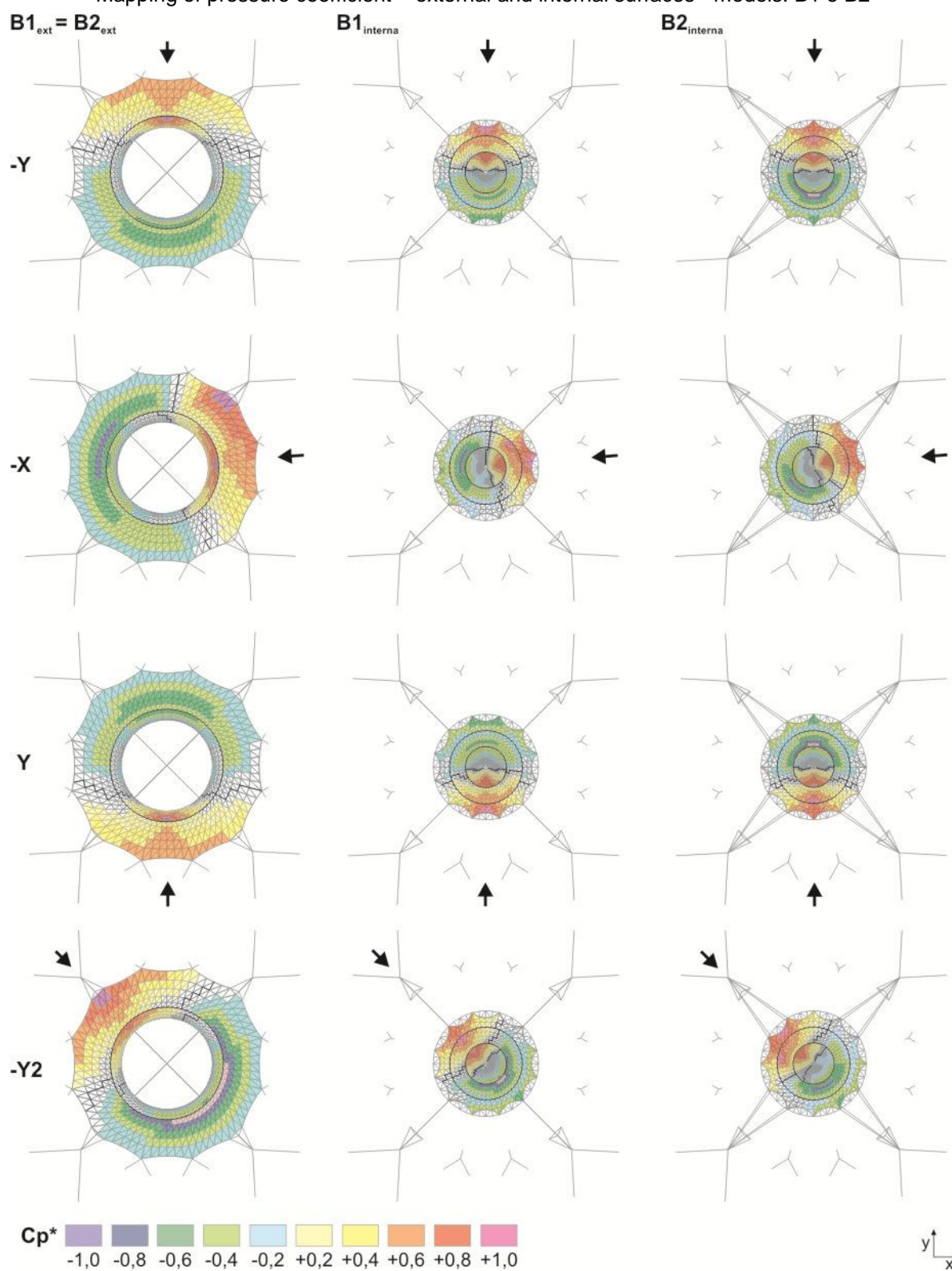


### APPENDIX C – Mapping of pressure coefficients

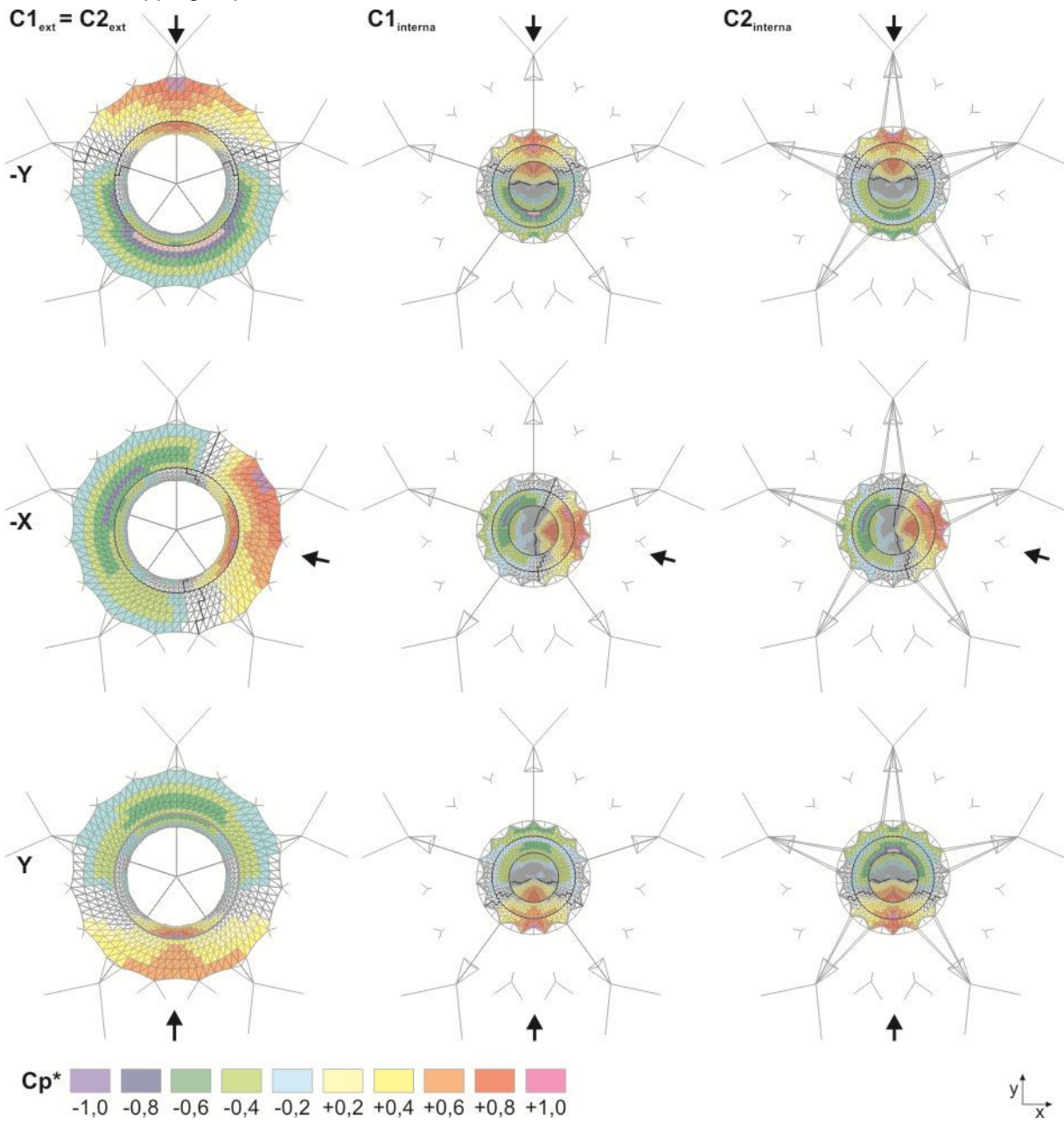
Mapping of pressure coefficient – external and internal surfaces - models: A1 e A2



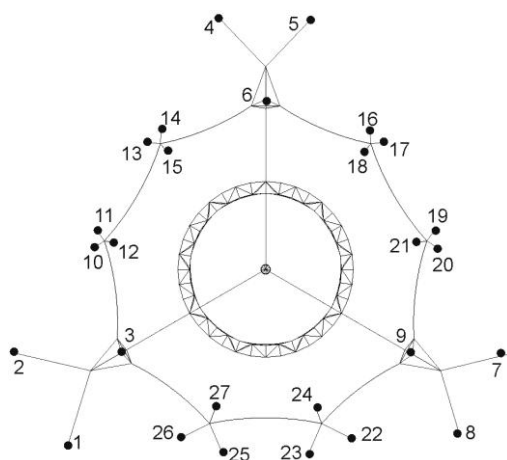
Mapping of pressure coefficient – external and internal surfaces - models: B1 e B2



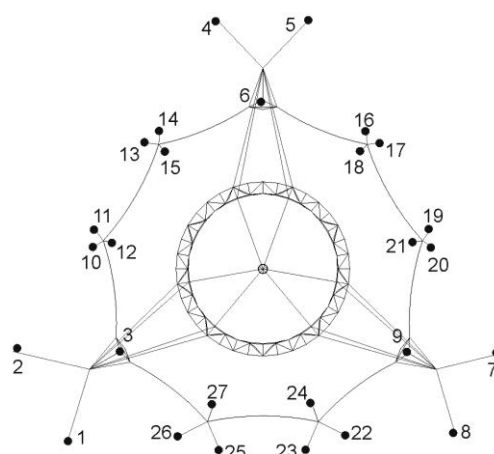
Mapping of pressure coefficient – external and internal surfaces - models: C1, C2



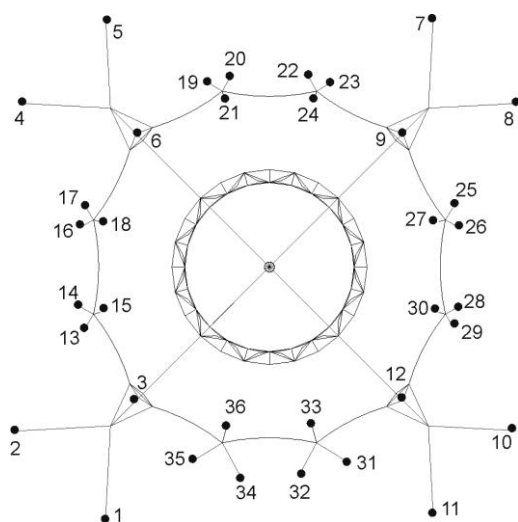
## APPENDIX D – Anchor points of models



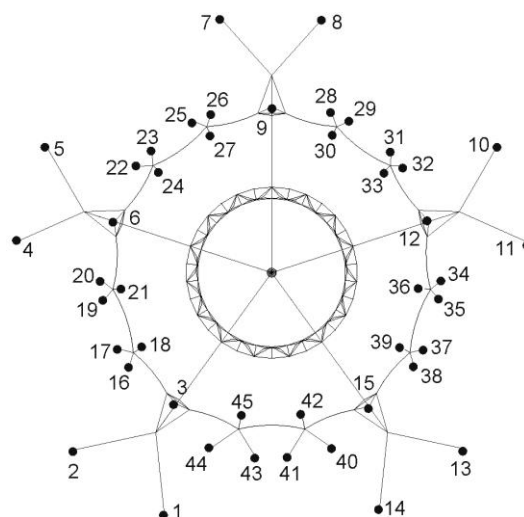
Modelo A1



Modelo A2



Modelo B1/B2

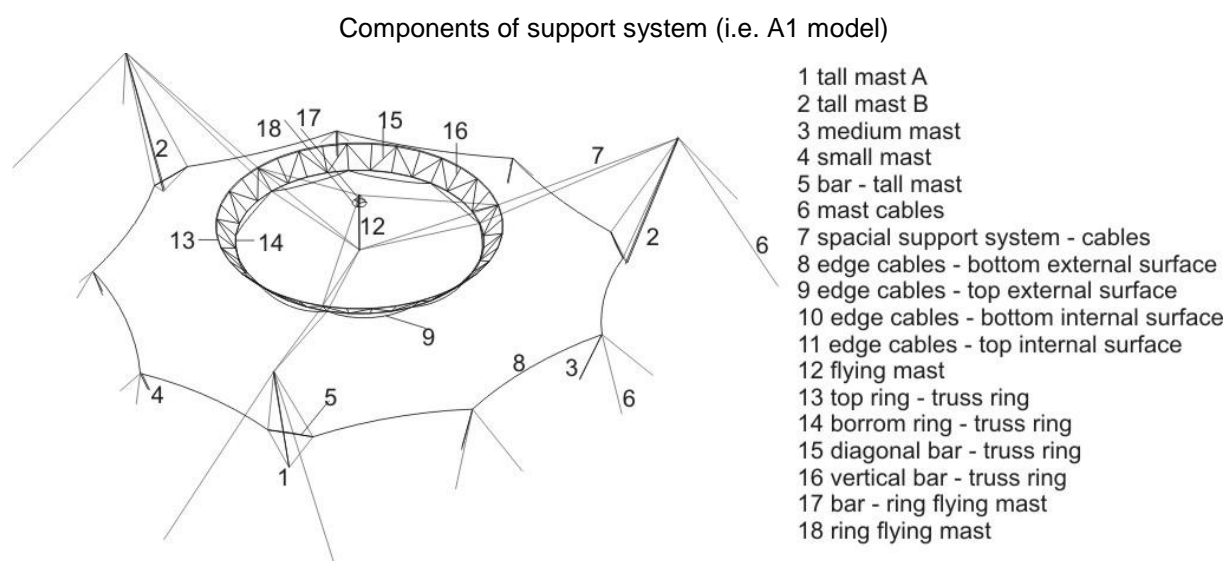


Modelo C1/C2

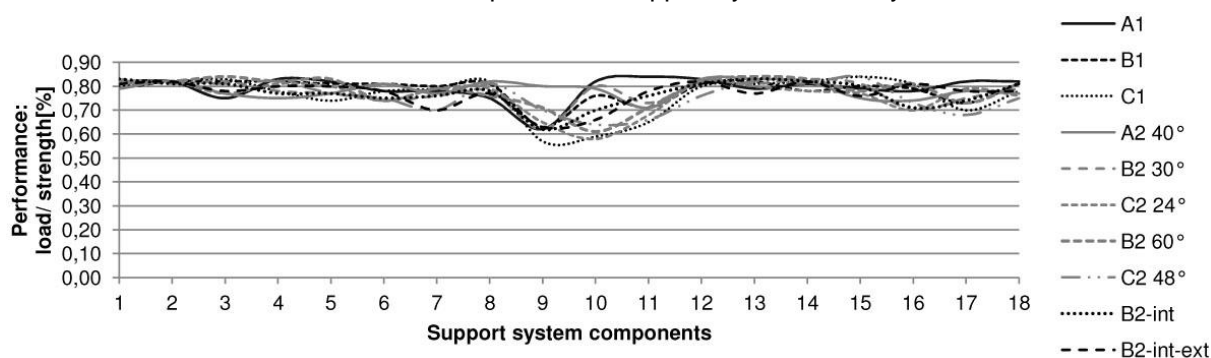
## APPENDIX E – Dimensions of support system components

support system components		A1	B1	C1	A2 40°	B2 30°	C2 24°	B2 60°	C2 48°	B2 <sub>int</sub>	B2 <sub>int-ext</sub>	
												
1	tall mast A	Diameter [m]	0,4600	0,4300	0,4270	0,5050	0,4280	0,4000	0,4540	0,4230	0,4280	0,4150
		Thickness [m]	0,0111	0,0103	0,0071	0,0127	0,0111	0,0079	0,0111	0,0084	0,0111	0,0103
		Performance [%]	0,82	0,79	0,80	0,79	0,83	0,82	0,81	0,81	0,83	0,81
2	tall mast B	Diameter [m]	0,4600	0,4300	0,4270	0,5050	0,4280	0,4000	0,4540	0,4230	0,4280	0,4150
		Thickness [m]	0,0086	0,0082	0,0066	0,0111	0,0103	0,0079	0,0103	0,0082	0,0103	0,0095
		Performance [%]	0,82	0,82	0,82	0,82	0,81	0,82	0,82	0,82	0,81	0,82
3	medium mast	Diameter [m]	0,1683	0,1683	0,1683	0,1683	0,1683	0,1683	0,1683	0,1683	0,1683	0,1683
		Thickness [m]	0,0127	0,0087	0,0071	0,0143	0,0095	0,0079	0,0095	0,0079	0,0095	0,0087
		Performance [%]	0,75	0,82	0,83	0,77	0,82	0,77	0,84	0,81	0,81	0,78
4	small mast	Diameter [m]	0,1683	0,1143	0,1143	0,1683	0,1143	0,1143	0,1143	0,1143	0,1143	0,1143
		Thickness [m]	0,0052	0,0060	0,0048	0,0064	0,0071	0,0048	0,0071	0,0052	0,0071	0,0060
		Performance [%]	0,83	0,82	0,78	0,75	0,78	0,81	0,82	0,82	0,77	0,80
5	bar tall mast	Diameter [m]	0,1413	0,1413	0,1413	0,1413	0,1413	0,1413	0,1413	0,1413	0,1413	0,1413
		Thickness [m]	0,0071	0,0071	0,0066	0,0066	0,0066	0,0056	0,0056	0,0056	0,0066	0,0066
		Performance [%]	0,82	0,81	0,74	0,77	0,77	0,80	0,83	0,77	0,77	0,80
6	cables mast	Diameter [m]	0,0380	0,0350	0,0320	0,0480	0,0380	0,0320	0,0450	0,0350	0,0380	0,0350
		Performance [%]	0,78	0,81	0,78	0,81	0,74	0,74	0,74	0,75	0,75	0,78
7	cables spatial syst	Diameter [m]	0,0380	0,0350	0,0350	0,0380	0,0320	0,0260	0,0320	0,0290	0,0320	0,0320
		Performance [%]	0,78	0,80	0,79	0,77	0,76	0,79	0,79	0,70	0,76	0,70
8	edge cable 1a	Diameter [m]	0,0320	0,0290	0,0260	0,0320	0,0290	0,0260	0,0290	0,0260	0,0290	0,0260
		Performance [%]	0,75	0,81	0,82	0,82	0,78	0,79	0,76	0,81	0,78	0,77
9	edge cable 1b	Diameter [m]	0,0220	0,0220	0,0190	0,0220	0,0220	0,0190	0,0220	0,0190	0,0220	0,0220
		Performance [%]	0,62	0,63	0,57	0,80	0,62	0,65	0,71	0,70	0,62	0,63
10	edge cable 2a	Diameter [m]	0,0190	0,0190	0,0190	0,0190	0,0190	0,0190	0,0220	0,0190	0,0190	0,0190
		Performance [%]	0,82	0,76	0,59	0,79	0,80	0,58	0,61	0,64	0,70	0,66
11	edge cable 2b	Diameter [m]	0,0095	0,0095	0,0095	0,0095	0,0095	0,0095	0,0095	0,0095	0,0095	0,0095
		Performance [%]	0,84	0,71	0,65	0,71	0,73	0,68	0,71	0,66	0,76	0,78
12	flying mast	Diameter [m]	0,1683	0,1683	0,1683	0,1683	0,1683	0,1413	0,1683	0,1413	0,1683	0,1143
		Thickness [m]	0,0143	0,0079	0,0064	0,0087	0,0079	0,0079	0,0079	0,0066	0,0064	0,0052
		Performance [%]	0,83	0,81	0,80	0,83	0,82	0,82	0,82	0,76	0,81	0,82
13	top ring - truss ring	Diameter [m]	0,2191	0,2191	0,1683	0,3556	0,3238	0,1683	0,3238	0,1683	0,3238	0,2730
		Thickness [m]	0,0103	0,0082	0,0079	0,0222	0,0103	0,0079	0,0143	0,0110	0,0103	0,0087
		Performance [%]	0,79	0,82	0,81	0,83	0,81	0,80	0,84	0,82	0,83	0,77
14	botton ring - truss ring	Diameter [m]	0,2191	0,1683	0,2191	0,3238	0,3238	0,2191	0,3238	0,2730	0,3238	0,3238
		Thickness [m]	0,0082	0,0079	0,0127	0,0222	0,0127	0,0095	0,0238	0,0143	0,0127	0,0087
		Performance [%]	0,81	0,78	0,82	0,82	0,83	0,78	0,83	0,81	0,82	0,82
15	diagonal - truss ring	Diameter [m]	0,1016	0,0889	0,0730	0,0889	0,0889	0,0889	0,0889	0,0730	0,0889	0,0889
		Thickness [m]	0,0057	0,0111	0,0064	0,0044	0,0055	0,0044	0,0064	0,0055	0,0055	0,0055
		Performance [%]	0,79	0,80	0,84	0,75	0,81	0,77	0,78	0,84	0,80	0,76
16	vertical - triss ring	Diameter [m]	0,1143	0,1016	0,1413	0,1143	0,0603	0,0730	0,0334	0,1413	0,0603	0,0603
		Thickness [m]	0,0079	0,0044	0,0095	0,0040	0,0040	0,0048	0,0034	0,0056	0,0040	0,0044
		Performance [%]	0,78	0,79	0,81	0,74	0,70	0,70	0,81	0,73	0,71	0,81
17	bars - flying mast	Diameter [m]	0,0730	0,0603	0,0422	0,0603	0,0603	0,0381	0,0603	0,0422	0,0483	0,0483
		Thickness [m]	0,0048	0,0036	0,0049	0,0044	0,0036	0,0050	0,0036	0,0049	0,0037	0,0037
		Performance [%]	0,82	0,73	0,70	0,78	0,75	0,79	0,73	0,68	0,74	0,78
18	ring - flying mast	Diameter [m]	0,1016	0,1143	0,1016	0,1413	0,1143	0,1016	0,1143	0,1016	0,1143	0,1143
		Thickness [m]	0,0048	0,0064	0,0057	0,0066	0,0064	0,0057	0,0060	0,0057	0,0044	0,0048
		Performance [%]	0,82	0,81	0,78	0,77	0,79	0,76	0,81	0,75	0,81	0,78

## APPENDIX F – Preliminary evaluation of support system components



Performance factor of components of support system of analyzed models



Calculations performed aimed a preliminary specification and dimensioning of support system components (masts, truss ring, cables) of each study model for comparison, so they are not strictly accurate. They result from preliminary analysis, considering combination of loads, which had reference to the American standard AISC (2010), American Institute of Steel Construction. In this evaluation, the performance factor (load / resistance) estimated for system components, was approximately 80%.

It was taken as reference, the dimensions of steel structural tubes of circular cross section - MSH (V&M, 2000), except for large masts, as well as the dimension and breaking tensile strength of cables IPS (Improved Plow Steel), provided by Cimaf (2002).

### *Conducted analyses*

The evaluation of the elements under axial tensile strength (cables) was performed in three steps.

- a. Initially, it was evaluated the tensile strength of the elements considering the gross area or total cross section area ( $P_n = F_y A_g$ ), and it was checked the tensile breaking strength, considering section net area ( $P_n = F_u A_e$ ), according CIMAF catalog. It was considered as nominal tensile strength, the lowest value obtained, which in this case was tensile rupture (net section) of elements ( $P_n = F_u A_e$ ). The design tensile strength ( $\Phi_c P_n$ ), considered tensile reduction factor ( $\Phi_t = 0.9$ ).
- b. It was measured tensile strength ( $P_u$ ) required for elements, according numerical model (preliminary analysis).
- c. It was evaluated the element performance, i.e., its load / resistance ( $P_u / \Phi_c P_n$ ).

The evaluation of the elements (masts) under axial compressive force (uniform) involved stability (buckling) analysis, as follows:

- a. It was evaluated the elastic buckling stress ( $F_e = \pi^2 E / (KL/r)^2$ ), then the critical buckling stress of the elements, considering:  
 when:  $kL/r \leq 4.71 \sqrt{E/F_y}$  >> critical stress:  $F_{cr} = [0.658 F_y / F_e] F_y$   
 when:  $kL/r > 4.71 \sqrt{E/F_y}$  >> critical stress:  $F_{cr} = 0.877 F_e$
- b. This analysis guided the evaluating the nominal compressive strength of elements ( $P_n = F_{cr} A_g$ ), and then design compressive strength ( $\Phi_c P_n$ ), considering compression reduction factor ( $\Phi_c = 0.9$ ).
- c. It was measured the required compressive strength to elements ( $P_u$ ) according numerical model (preliminary analysis).
- d. It was evaluated the element performance, i.e., its load / resistance ( $P_u / \Phi_c P_n$ ).

The evaluation of the elements under the combined forces: flexure-compression (truss ring components and flying mast) involved stability (buckling) and flexural strength analysis (elements of hollow circular cross section), and interaction of flexure and axial force.

It was initially evaluated, the nominal compressive strength of elements ( $P_n = F_{cr}A_g$ ), as described previously, and then design compressive strength ( $\Phi_c P_n$ ), considering compression reduction factor ( $\Phi_c = 0.9$ ).

Then, it was evaluated the nominal flexural strength ( $M_n$ ). This analysis included the limit state of yielding (Y) and local buckling (LB) for elements with circular sections having wall slenderness ratio:  $\lambda = D/t \leq 0,45E/F_y$ .

→ Evaluation of limit state of yielding (Y):

$M_n = M_p = F_y Z$ , where:

Plastic section modulus  $> Z = 4/3(r_2^3 - r_1^3)$ ;  $\lambda_p = 0.0448E/F_y$  (compact section)

→ Evaluation of limit states for local buckling (LB), considering:

- (LB) for noncompact sections:  $M_n = (0.021E/(D/t) + F_y)S$

- (LB) for sections with slender wall:  $M_n = F_{cr}S = (0.33E/D/t)S$

Where:

Elastic modulus section  $\gg S = W_1 = W_2 = I/y$ ;

$I = \pi(R-t/2)^3t$  and  $y/2 = \text{radius} = h/2$

$\lambda_p = 0,0714E/F_y$ , se  $\lambda \leq \lambda_p$  (section compact);

$\lambda_r = 0.309E/F_y$ , se  $\lambda \leq \lambda_r$  (noncompact section)

( $\lambda_p$  e  $\lambda_r$  : tabela 2.21, p.4, AISC/2001)

It was considered as the nominal flexural strength ( $M_n$ ), the lowest value obtained according to the limit states of yielding (Y) and local buckling (LB sections: noncompact and with slender walls). Then it was determined the nominal flexural strength ( $\Phi_b M_n$ ), considering strength reduction factor ( $\Phi_b = 0.9$ ).

After that, it was measured forces ( $P_r$ ) and flexural strength ( $M_1$ ) and ( $M_2$ ) required by elements according numerical model (preliminary analysis).

The final analysis comprised the combination of forces (flexural and axial force), or interaction between applied and resistant efforts. Whereas:

$$\text{Se } P_u/\Phi P_n \geq 0.2... (M_{n_x} = M_{n_y}) \gg P_r/\Phi P_n + 8/9(M_1/\Phi_b M_{n_x} + M_2/\Phi_b M_{n_y}) \leq 1$$

$$\text{Se } P_u/\Phi P_n < 0.2... (M_{n_x} = M_{n_y}) \gg P_r/2\Phi P_n + (M_1/\Phi_b M_{n_x} + M_2/\Phi_b M_{n_y}) \leq 1$$

There is as example A1 model analysis.

A1 model / Elements under compression forces			1 -Tall mast A	2 - Tall mast B	3 - Medium mast	4 - Small mast	5 - Bar of tall mast	
Characteristics	Modulus of elasticity of steel (E)	MPa	200000	200000	200000	200000	200000	
		kN/m <sup>2</sup>	200000000	200000000	200000000	200000000	200000000	
	Diameter (d)	m	<b>0,46</b>	<b>0,46</b>	<b>0,1683</b>	<b>0,1683</b>	<b>0,1413</b>	
	Thickness (t)	m	<b>0,0111</b>	<b>0,0086</b>	<b>0,0127</b>	<b>0,0052</b>	<b>0,0071</b>	
	Moment of inertia (I)	m <sup>4</sup>	0,000394	0,000311	0,000019	0,000009	0,00000674	
	Cross sectional area (A)	m <sup>2</sup>	0,0160	0,0124	0,0067	0,0027	0,00315	
	y/2	m	0,2300	0,2300	0,0842	0,0842	0,07065	
	Elastic section modulus (S)	m <sup>3</sup>	0,0017	0,0014	0,0002	0,0001	0,0001	
	Density (ρ)	kg/m <sup>3</sup>	7850,00	7850,00	7850,00	7850,00	7850,00	
	Length of the member (l)	m	<b>17,60</b>	<b>16,00</b>	<b>7,00</b>	<b>2,70</b>	<b>4,88</b>	
	Radius of gyration (r)	m	0,157	0,158	0,053	0,057	0,046	
	Specified minimum yield stress - Fy	MPa	250,00	250,00	250,00	250,00	250,00	
	reference (V&M, 2000), except tall mast data	kN/m <sup>2</sup>	250000,00	250000,00	250000,00	250000,00	250000,00	
	Effective length factor (k)		1	1	1	1	1	
Wall slenderness (λ)		112,26	101,20	132,33	47,56	105,54		
Design strength: φRu (compressive) Rn ≤ φRu - LRDF (AISC, 2010)	<b>Flexural buckling of members without slender elements</b>							
	$4.71 \sqrt{E/Fy}$	MPa	133,22	133,22	133,22	133,22	133,22	
	Elastic buckling stress $F_e = \pi^2 E / (KL/r)^2$	MPa	156,64	192,72	112,72	872,55	177,22	
	Fy/Fe	MPa	1,60	1,30	2,22	0,29	1,41	
	when... $kL/r \leq 4.71 \sqrt{E/Fy}$ ... >> Critical stress (flexural buckling stress) : $F_{cr} = [0.658 Fy / Fe] Fy$							
	<b>Critical stress</b> $F_{cr} = (0.658 Fy / Fe) Fy$	MPa	<b>128,18</b>	<b>145,26</b>	<b>98,80</b>	<b>221,75</b>	<b>138,52</b>	
		kN/m <sup>2</sup>	128182,10	145257,69	98803,93	221747,47	138521,53	
	<b>Nominal compressive strength .... &gt;&gt; Pn= FcrAg</b>							
	Resistance factor <b>φc</b> (compressive)		0,9	0,9	0,9	0,9	0,9	
	Nominal compressive strength (Pn)	kN	2056,17	1805,28	663,46	609,67	436,58	
	<b>Design compressive strength</b> (φcPn)	kN	<b>1850,55</b>	<b>1624,75</b>	<b>597,11</b>	<b>548,70</b>	<b>392,93</b>	
	Required compression strength* (Pu)	kN	-1525,55	-1328,23	-446,60	-456,14	-323,46	
	<b>Pu/φcPn</b> (performance factor)		<b>0,82</b>	<b>0,82</b>	<b>0,75</b>	<b>0,83</b>	<b>0,82</b>	

(\*) PU - measure values, according preliminary analysis

A1 model / Elements under tensile forces			6 - Mast cables	7 - Spatial system cables	8-Membrane edge cable 1a	9-Membrane edge cable 1b	10-Membrane edge cable 2a	11-Membrane edge cable 2b
Characteristics	Modulus of elasticity of wire rope ** (E)	kgf/mm <sup>2</sup>	9500	9500	9500	9500	9500	9500
		kN/m <sup>2</sup>	95000000	95000000	95000000	95000000	95000000	95000000
		MPa	95000	95000	95000	95000	95000	95000
	Diameter (d)	m	<b>0,038</b>	<b>0,038</b>	<b>0,032</b>	<b>0,022</b>	<b>0,019</b>	<b>0,0095</b>
		inches	1.1/2"	1.1/2"	1.1/4"	7/8"	3/4"	3/8"
	Mass (m)	kg/m	6,19	6,19	4,30	2,11	1,55	0,38
	Cross sectional area (Ag)	m <sup>2</sup>	0,00113	0,00113	0,00080	0,00038	0,00028	0,00007
	Density (ρ)	kg/m <sup>3</sup>	5458,00	5458,00	5346,61	5550,69	5466,82	5389,22
	Nominal tensile stress of the wire rope** (Fy)	kgf/mm <sup>2</sup>	180,00	180,00	180,00	180,00	180,00	180,00
		kN/m <sup>2</sup>	1800000,00	1800000,00	1800000,00	1800000,00	1800000,00	1800000,00
		MPa	1800,00	1800,00	1800,00	1800,00	1800,00	1800,00
	Specified minimum breaking load ** (Pn)	tf	89,70	89,70	63,00	31,40	23,20	5,94
		kN	897,00	897,00	630,00	314,00	232,00	59,40
	Design strength φRu (tensile) Rn ≤ φRu - LRDF (AISC /2010)	<b>Nominal tensile strength (for tensile yielding).... &gt;&gt; Pn= FyAg</b>						
Resistance factor (tensile yielding) <b>φt</b>			0,90	0,90	0,90	0,90	0,90	0,90
Nominal tensile yielding strength (Pn)		kN	2041,41	2041,41	1447,65	684,24	510,35	127,59
<b>Design tensile yielding strength</b> (φtPn)		kN	<b>1837,27</b>	<b>1837,27</b>	<b>1302,88</b>	<b>615,81</b>	<b>459,32</b>	<b>114,83</b>
<b>Nominal tensile strength (for tensile rupture).... &gt;&gt; Pn= FuAe = Specified minimum breaking load *</b>								
Resistance factor (tensile rupture) <b>φt</b>			0,75	0,75	0,75	0,75	0,75	0,75
<b>Design tensile rupture strength</b> (φtPn)		kN	<b>672,75</b>	<b>672,75</b>	<b>472,50</b>	<b>235,50</b>	<b>174,00</b>	<b>44,55</b>
Required tensile strength*** (Pu)		kN	521,56	525,00	352,25	146,44	141,99	37,62
<b>Pu/φtPn</b>	%	<b>0,78</b>	<b>0,78</b>	<b>0,75</b>	<b>0,62</b>	<b>0,82</b>	<b>0,84</b>	

(\*) Class wire rope - fiber core (CIMAF, 2002); (6 legs with 27 to 49 wires each) - 6x37

(\*\*) wire rope: IPS (Improved Plow Steel) - (CIMAF, 2002) (\*\*\*) PU - measure values, according preliminary analysis

A1 model - Elements under combined forces (flexure + axial force)		12- Flying mast	12- Flying mast	13- Top ring - truss	14- Bottom ring - truss	15-Diagonal bar - truss	16- Vertical bar - truss	17- Truss - flying mast	18- Ring - flying mast	
Characteristics	Modulus of elasticity (E)	MPa	200000	200000	200000	200000	200000	200000	200000	
		kN/m <sup>2</sup>	200000000	200000000	200000000	200000000	200000000	200000000	200000000	
	Diameter	m	<b>0,1683</b>	<b>0,1683</b>	<b>0,2191</b>	<b>0,2191</b>	<b>0,1016</b>	<b>0,1143</b>	<b>0,073</b>	<b>0,1016</b>
	Thickness	m	<b>0,0143</b>	<b>0,0143</b>	<b>0,0103</b>	<b>0,0082</b>	<b>0,0057</b>	<b>0,0079</b>	<b>0,0048</b>	<b>0,0048</b>
	Internal section radius (R1 )	m	0,06985	0,06985	0,09925	0,10135	0,0451	0,04925	0,0317	0,046
	External section radius (R2)	m	0,08415	0,08415	0,10955	0,10955	0,0508	0,05715	0,0365	0,0508
	Moment of inertia (I)	m <sup>4</sup>	0,00002051	0,00002051	0,000037	0,000030	0,000002	0,000004	0,00000060	0,00000171
	Cross sectional area (A)	m <sup>2</sup>	0,00756	0,00756	0,0071	0,0056	0,0018	0,0028	0,00110	0,00153
	y/2	m	0,08415	0,08415	0,1096	0,1096	0,0508	0,0572	0,03650	0,05080
	Elastic section modulus (S)	m <sup>3</sup>	0,0002	0,0002	0,0003	0,0003	0,0000	0,0001	0,00002	0,00003
	Plastic section modulus (Z)	m <sup>3</sup>	0,0003	0,0003	0,0004	0,0004	0,0001	0,0001	0,0000	0,0000
	Density (ρ)	kg/m <sup>3</sup>	7850,00	7850,00	7850,00	7850,00	7850,00	7850,00	7850,00	7850,00
	Length of the member (L)	m	<b>1,00</b>	<b>6,00</b>	<b>2,61</b>	<b>2,26</b>	<b>3,73</b>	<b>2,8284</b>	<b>1,25</b>	<b>0,26</b>
	Radius of gyration (r )	m	0,052	0,052	0,072	0,073	0,033	0,036	0,023	0,033
	Specified minimum yield stress (Fy) *	MPa	250,00	250,00	250,00	250,00	250,00	250,00	250,00	250,00
		kN/m <sup>2</sup>	250000,00	250000,00	250000,00	250000,00	250000,00	250000,00	250000,00	250000,00
	Effective length factor (k )		0,5	0,5	0,5	0,5	0,5	0,5	0,5	0,5
Wall slenderness (λ)		9,60	57,60	18,14	15,43	56,64	38,96	26,82	3,90	
<b>Flexural buckling of members without slender elements</b>										
4.71√(E/Fy)	MPa	133,22	133,22	133,22	133,22	133,22	133,22	133,22	133,22	
Elastic buckling stress (Fe)	MPa	21417,94	594,94	5997,98	8292,21	615,28	1300,16	2744,80	129842,44	
Fy/Fe	MPa	0,01	0,42	0,04	0,03	0,41	0,19	0,09	0,00	
when.... $kL/r \leq 4.71\sqrt{E/Fy}$ .... >> Critical stress (flexural buckling stresses) : $F_{cr}=[0.658^{Fy/Fe}]Fy$										
<b>Critical stress (Fcr)</b>	MPa	<b>248,78</b>	<b>209,68</b>	<b>245,68</b>	<b>246,87</b>	<b>210,90</b>	<b>230,67</b>	<b>240,65</b>	<b>249,80</b>	
	kN/m <sup>2</sup>	248781,60	209680,00	245676,46	246865,12	210902,41	230668,21	240648,83	249798,61	
Nominal compressive strength .... >> <b>Pn= FcrAg</b>										
Resistance factor <b>Φc</b> (compressive)		0,90	0,90	0,90	0,90	0,90	0,90	0,90	0,90	
(Pn)	kN	1881,00	1585,36	1741,78	1393,37	383,71	654,35	264,91	382,71	
<b>(ΦcPn)</b>	kN	<b>1692,90</b>	<b>1426,82</b>	<b>1567,60</b>	<b>1254,03</b>	<b>345,34</b>	<b>588,92</b>	<b>238,42</b>	<b>344,44</b>	
Nominal flexure strength .... >> <b>Mn</b> .... >> applied to round HSS having D/t ratios: $D/t \leq 0,45E/Fy$										
0,448E/Fy		358,40	358,40	358,40	358,40	358,40	358,40	358,40	358,40	
Wall slenderness $\lambda = D/t$		11,77	11,77	21,27	26,72	17,82	14,47	15,21	21,17	
Limit states of yielding or plastic moment (Y) - wall slenderness for compression members (table 2.21 - p4 - AISC/2001)										
$\lambda_p = 0,0448E/Fy$ (compact section)		35,84	35,84	35,84	35,84	35,84	35,84	35,84	35,84	
Limit states of local buckling (LB) - wall slenderness for compression members (table 2.21 - p4 - AISC/2001)										
$\lambda_r = 0,0714E/Fy$ , $se \lambda \leq \lambda_p$		57,12	57,12	57,12	57,12	57,12	57,12	57,12	57,12	
$\lambda_r = 0,309E/Fy$ , $se \lambda \leq \lambda_r$		247,20	247,20	247,20	247,20	247,20	247,20	247,20	247,20	
Nominal flexure strength .... >> <b>Mn</b> - the lower value obtained according to the limit states of yielding (Y) and local buckling (LB)										
1- (Y) $Mn=M_p=F_yZ$	kNm	<b>85,03</b>	<b>85,03</b>	<b>112,35</b>	<b>91,23</b>	<b>13,12</b>	<b>22,40</b>	<b>5,59</b>	<b>11,25</b>	
2- (LB) non compact sections $Mn^{**}$	kNm	147,91	147,91	150,39	112,28	18,87	35,33	8,62	15,09	
3- (LB) slender wall sections $Mn^{***}$	kNm	1366,78	1366,78	1042,83	681,09	143,90	298,28	71,09	104,94	
Resistance factor $\Phi_b=0,9$		0,90	0,90	0,90	0,90	0,90	0,90	0,90	0,90	
<b>(ΦbMn)</b>	kNm	<b>76,53</b>	<b>76,53</b>	<b>101,12</b>	<b>82,10</b>	<b>11,81</b>	<b>20,16</b>	<b>5,03</b>	<b>10,13</b>	
<b>Required forces and stress</b> (measuar values, according preliminary analysis)										
Required axial strenght (Pr)	kN	-186,26	-197,17	-241,70	-263,58	-187,75	-36,68	-38,550	16,98	
Required flexural strenght (M1)	kNm	-39,21	-40,56	38,62	40,30	-2,15	-15,37	-1,350	14,03	
Required flexural strenght (M2)	kNm	-18,10	-19,31	49,49	34,81	-1,06	0,18	-2,360	-6,00	
<b>Required forces and stress</b> (measuar values, according preliminary analysis)										
Pr/ΦPn.... $\Phi_c=0,90$ e $\Phi_t=0,90$		-0,11	-0,14	-0,15	-0,21	-0,54	-0,06	-0,16	0,05	
Pr/2ΦPn.... $\Phi=0,90$ e $\Phi_t=0,90$		-0,06	-0,07	-0,08	-0,11	-0,27	-0,03	-0,08	0,02	
M1/ ΦbMnx.... $\Phi_b=0,9$		-0,512	-0,530	0,382	0,491	-0,182	-0,762	-0,268	1,385	
M2/ ΦbMny.... $\Phi_b=0,9$		-0,237	-0,252	0,489	0,424	-0,090	0,009	-0,469	-0,592	
For $P_u/\Phi P_n \geq 0,2$ ( $M_{nx}=M_{ny}$ )										
$P_r/\Phi P_n + 8/9(M_1/\Phi_b M_{nx} + M_2/\Phi_b M_{ny}) \leq 1$		<b>-0,78</b>	<b>-0,83</b>			<b>-0,79</b>		<b>-0,82</b>		
For $P_u/\Phi P_n < 0,2$ ( $M_{nx}=M_{ny}$ )										
$P_r/2\Phi P_n + (M_1/\Phi_b M_{nx} + M_2/\Phi_b M_{ny}) \leq 1$				<b>0,79</b>	<b>0,81</b>			<b>-0,78</b>	<b>0,82</b>	

(\*) Fy - reference (V&M, 2000) except tall mast ; (\*\*) non compact sections  $M_n=(0.021E/(D/t)+F_y)S$ ; (\*\*\*) slender wall sections  $M_n= F_{cr}S=$

$F_e=\pi^2E/(KL/r)^2$ ;  $F_{cr}= (0,658 F_y/F_e)F_y$ ;

## APPENDIX G – Information of experimental tests

Biaxial test - loads (reference values)

	time [s]	applied load [kN/m]	
		warp	weft
	0:00:00	0,1	0,1
00:00:32	0:00:32	3,2	6,4
<b>pre-tension constant</b> 0:15:00 (900s)	0:15:32	3,2	6,4
<b>3 cycles: warp</b> 0:02:54 (29s x 6= 174s)	0:16:01	9,0	6,4
	0:16:30	3,2	6,4
	0:16:59	9,0	6,4
	0:17:28	3,2	6,4
	0:17:57	9,0	6,4
	0:18:26	3,2	6,4
<b>3 cycles: weft</b> 0:04:48 (48s x 6= 288s)	0:19:14	3,2	16,0
	0:20:02	3,2	6,4
	0:20:50	3,2	16,0
	0:21:38	3,2	6,4
	0:22:26	3,2	16,0
	0:23:14	3,2	6,4
<b>pre-tension constant</b> 0:15:00 (900s)	0:38:14	3,2	6,4
<b>3 cycles: warp</b> 0:07:24 (74s x 6= 444s)	0:39:28	18,0	6,4
	0:40:42	3,2	6,4
	0:41:56	18,0	6,4
	0:43:10	3,2	6,4
	0:44:24	18,0	6,4
	0:45:38	3,2	6,4
<b>3 cycles: weft</b> 0:12:48 (128s x 6= 768s)	0:47:46	3,2	32,0
	0:49:54	3,2	6,4
	0:52:02	3,2	32,0
	0:54:10	3,2	6,4
	0:56:18	3,2	32,0
	0:58:26	3,2	6,4
<b>pre-tension constant</b> 0:15:00 (900s)	1:13:26	3,2	6,4
	1:13:58	0,0	0,0

applied load rate : 0,2 (kN/m) /s; test temperature: 23° C

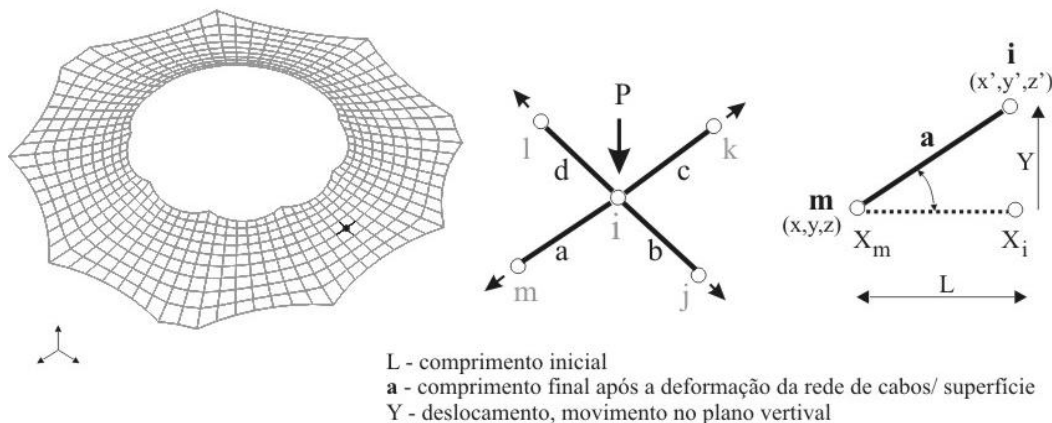
Seam biaxial test - loads (reference values)

	time [s]	applied load	
		warp	weft
	00:00:00	0,1	0,1
00:00:32	00:00:32	3,2	6,4
<b>pre-tension constant</b> 0:15:00 (900s)	00:15:32	3,2	6,4
<b>3 cycles: weft</b> 0:04:48 (48s x 6= 288s)	00:16:20	3,2	16
	00:17:08	3,2	6,4
	00:17:56	3,2	16
	00:18:44	3,2	6,4
	00:19:32	3,2	16
	00:20:20	3,2	6,4
<b>pre-tension constant</b> 0:15:00 (900s)	00:35:20	3,2	6,4
<b>3 cycles: weft</b> 0:12:48 (128s x 6= 768s)	00:37:28	3,2	32
	00:39:36	3,2	6,4
	00:41:44	3,2	32
	00:43:52	3,2	6,4
	00:46:00	3,2	32
	00:48:08	3,2	6,4
<b>pre-tension constant</b> 0:15:00 (900s)	01:03:08	3,2	6,4
00:00:32	01:03:40	0	0

applied load rate : 0,2 (kN/m) /s; test temperature: 23° C

## APPENDIX H – Method Density Force (equations)

Behavior of the bar element as part of a cable net



Source: adapted of GRÜNDIG *et al.*, 2000, p.4.

System of non-linear equations, according to Gründig (2000):

$$S_a \cos(a, x) + S_b \cos(b, x) + S_c \cos(c, x) + S_d \cos(d, x) = p_x$$

$$S_a \cos(a, y) + S_b \cos(b, y) + S_c \cos(c, y) + S_d \cos(d, y) = p_y$$

$$S_a \cos(a, z) + S_b \cos(b, z) + S_c \cos(c, z) + S_d \cos(d, z) = p_z$$

$S_a, S_b, S_c, S_d$  = internal forces in the bar elements;  $p_x, p_y, p_z$  = external forces

a, b, c, d = non-linear length - function of coordinates XYZ

$(x_m + x_i)$ , = projection length of cables (axis x);

$$\cos(a, x) = \frac{(x_m + x_i)}{a}$$

$$\frac{S_a}{a} (x_m + x_i) + \frac{S_b}{b} (x_j + x_i) + \frac{S_c}{c} (x_k + x_i) + \frac{S_d}{d} (x_l + x_i) = p_x$$

$$\frac{S_a}{a} (y_m + y_i) + \frac{S_b}{b} (y_j + y_i) + \frac{S_c}{c} (y_k + y_i) + \frac{S_d}{d} (y_l + y_i) = p_y$$

$$\frac{S_a}{a} (z_m + z_i) + \frac{S_b}{b} (z_j + z_i) + \frac{S_c}{c} (z_k + z_i) + \frac{S_d}{d} (z_l + z_i) = p_z$$

Definition of a constant parameter – density force:(q):

$$\frac{S_a}{a} = q_a, \quad q = \frac{\text{force}}{\text{tensile length}}$$

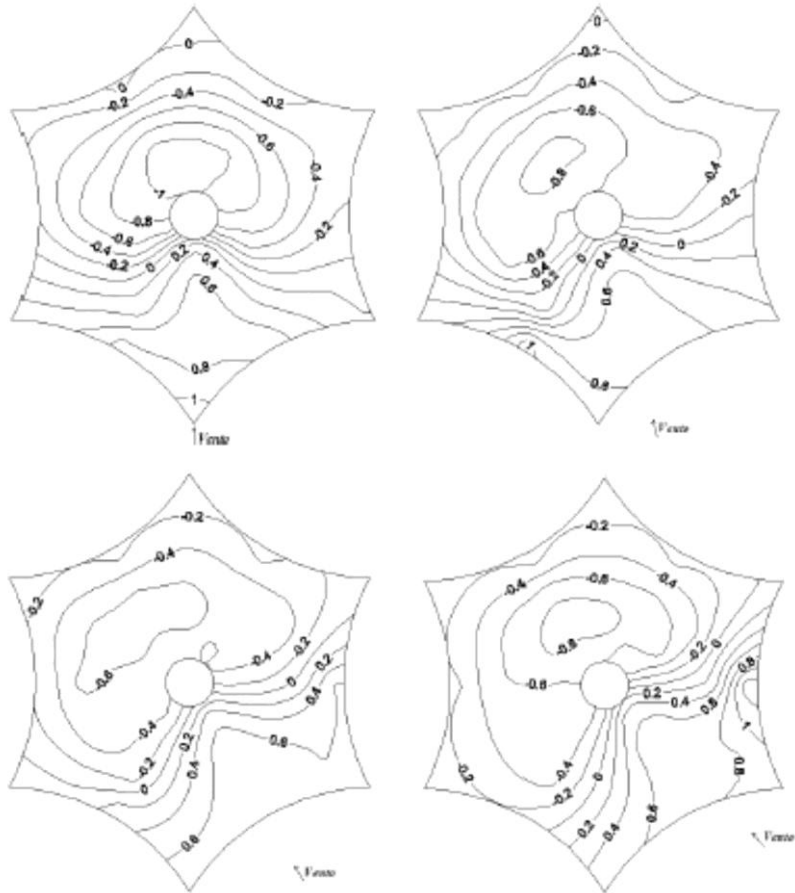
Replacing values, there are a System of linear equations:

$$q_a (x_m + x_i) + q_b (x_j + x_i) + q_c (x_k + x_i) + q_d (x_l + x_i) = p_x$$

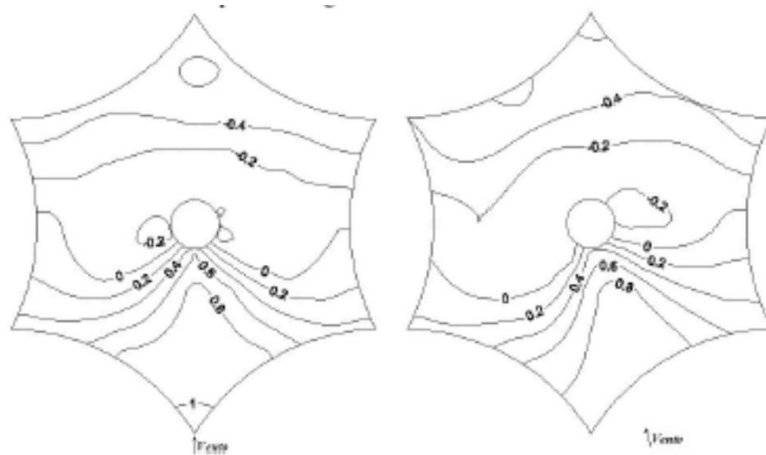
$$q_a (y_m + y_i) + q_b (y_j + y_i) + q_c (y_k + y_i) + q_d (y_l + y_i) = p_y$$

$$q_a (z_m + z_i) + q_b (z_j + z_i) + q_c (z_k + z_i) + q_d (z_l + z_i) = p_z$$

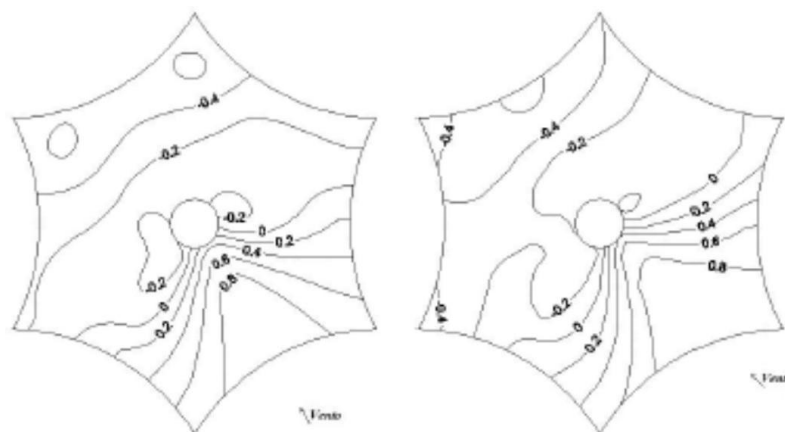
## APPENDIX I – Isobar lines of $C_p$ , tested models



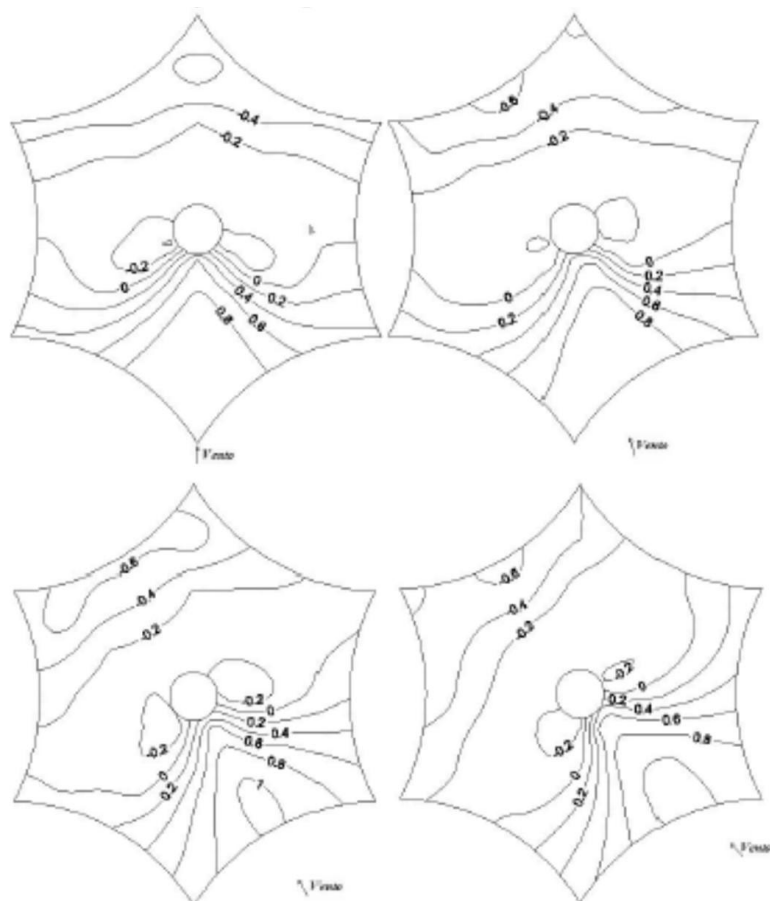
Superior view: isobar lines of pressure coefficient – resulting pressure average ( $C_p^*$ ) of model R215 for wind directions:  $0^\circ$ ,  $15^\circ$ ,  $30^\circ$  e  $45^\circ$ .  
Source: VILELA, 2011, p.91.



Superior view: isobar lines of pressure coefficient – resulting pressure average ( $C_p^*$ ) of model R390 for wind directions:  $0^\circ$ ,  $15^\circ$ .  
Source: VILELA, 2011, p.94.



Superior view: isobar lines of pressure coefficient – resulting pressure average ( $C_p^*$ ) of model R390 for wind directions: 30° e 45°. Source: VILELA, 2011, p.94.



Superior view: isobar lines of pressure coefficient – resulting pressure average ( $C_p^*$ ) of model R390 for wind directions: 0°, 15°, 30° e 45°. Source: VILELA, 2011, p.95 e 96.